http://researchcommons.waikato.ac.nz/

Research Commons at the University of Waikato

Copyright Statement:

The digital copy of this thesis is protected by the Copyright Act 1994 (New Zealand).

The thesis may be consulted by you, provided you comply with the provisions of the Act and the following conditions of use:

- Any use you make of these documents or images must be for research or private study purposes only, and you may not make them available to any other person.
- Authors control the copyright of their thesis. You will recognise the author's right to be identified as the author of the thesis, and due acknowledgement will be made to the author where appropriate.
- You will obtain the author's permission before publishing any material from the thesis.

Site characterisation of the Hamilton Basin using surface wave methods

A thesis

submitted in fulfilment

of the requirements for the degree

of

Master of Science in Earth Science

at

The University of Waikato

by

Ashley Cave

THE UNIVERSITY OF
WAIKATO
Te Whare Wānanga o Waikato

2020

Abstract

Observed amplification and reverberation of ground motions in the Heathcote Valley during the 2010-2011 Canterbury Earthquake Sequence highlighted the lack of data on the subsurface velocity structure of sedimentary basins across New Zealand. A similar lack of data applies to the Hamilton Basin, a deep, predominantly alluvial, basin in the Waikato Region. In response, 13 deep shear wave velocity profiles have been measured in this study. Dispersion data obtained through active and passive methods were inverted with fundamental frequencies deduced from the horizontal-to-vertical spectral ratio method and a suite of layering ratios in the absence of detailed geological information. Potential for amplification is inferred from the large impedance contrasts at the soil-basement interface in the developed V_s profiles. The fundamental site period is over 5s in the Te Rapa and Gordonton depressions in the northern basin, where basement rock is up to 1400m deep. As basement shallows towards the south, fundamental periods shorten. Complex wave propagation occurs towards the southeastern basin influenced by ignimbrite deposition interspersed within the alluvial sediments of the Tauranga Group. Despite the variation in basement structure, velocities associated with lithology changes tend to be relatively consistent, allowing for the use of a four-unit velocity structure to represent basin deposits. The peat bogs which dominate the surficial landscape have significantly low shear wave velocities (28-38m/s), which presented unique difficulties in near surface velocity resolution. The soft near surface soil deposits across the basin have V_{s30} values ranging from 166-234m/s and four class E sites have been identified. Based on the new V_s profiles, a refined fundamental frequency-depth correlation was developed for the region. The results in this thesis are intended to inform site response analysis and seismic risk assessment.

Acknowledgements

I have the upmost gratitude to everyone who contributed to this thesis in one form or another.

Firstly, thank you to my supervisor Dr. Vicki Moon for your invaluable guidance, patience and candid discussions. To my supervisor Dr. Seokho Jeong and also to Dr. Andrew Stolte from Canterbury University for assisting with fieldwork and lending your time and expertise to steer me through this research. Also to Dr. Liam Wotherspoon from Auckland University for your feedback. Thank you to QuakeCoRE for providing the funding for this project and to Canterbury University for loaning the necessary equipment.

I wish to thank everyone who pitched in with field-testing over the summer, Tom Robertson, Ellena Cauldwell and Amir Mohammad, all of your help was much appreciated. To all the farmers and land owners who approved land access and co-ordinated with the fieldwork, thank you, this research would evidently not have been possible without somewhere to research.

Beyond grateful to my colleagues, George, Tori, Tom, Francesca and Anya; your support, humour and general distractions were immeasurable.

To my partner Finley, I am deeply grateful for your motivation and love. For brightening my days, my confidence and encouraging me to work harder. Thank you for standing by me. Lastly a loving thank you to my close family; my mother Debi and father Robert, my grandparents Ray and Robyn. None of this would have been possible without all of you and your unwavering support.

Glossary

Active surface waves

Generated from un-natural sources (sledgehammer, drop-weight, vibrating trucks

A' priori

A latin word meaning 'from before' which when applied in this study means existing geological knowledge 'from before'

Basin effects

Amplification of ground motions based on basin structure

Dispersion curve

The relationship between frequency and wavelength of a wave, which can be presented in many domains (commonly a scale of frequency and wavenumber)

Dynamic characteristics

*Primarily shear wave velocity (V_s) and shear modulus (*G)

Ellipticity

The deviation of an ellipse from a circle

Engineering bedrock

Rock with a shear wave velocity of >1100m/s (Walling et al., 2008)

Fundamental mode

A wave mode with the lowest frequency

Ground Vibration

Movement of energy through a medium, which creates oscillations

HRFK

High Resolution Frequency-Wavenumber (processing method, see p.44)

HVSR|H/V

Horizontal to Vertical Ratio (A ratio of horizontal to vertical ground motion). See p.43.

Impedance contrast

Contrast of velocity multiplied by density associated with soil/rock layers. Also termed acoustic or seismic impedance.

Inversion

A statistical technique for retrieving below ground level information from geophysical data

Local site effects

Is a term for the influence of local geology on ground motion propagation

MAM

Microtremor Array Method (acquisition method, see p.39)

MASW

Multichannel Analysis of Surface Waves (acquisition method, see p.38)

Microtremor

A form of seismic noise, which is termed ambient vibration in seismology. Typically >1Hz

Misfit

Difference between the experimental dispersion curve and the theoretical dispersion

MSPAC

Modified Spatial Auto Correlation (processing method, see p.44)

Passive surface waves

Generated from microtremors (cultural noise (cars, building) and microseisms (natural noise (ocean, wind)

Rayleigh waves

A surface wave, which travels elliptically along the earth's surface

Seismic bedrock

Upper interface of the earth's crust (typically has a velocity of >3000m/s)

Shear wave velocity

A mechanical soil property representing elastic wave speed

Site response

How the soil of a site will respond to seismic wave propagation

Surface waves

A seismic wave, which travels parallel to the earth's surface

Table of Contents

List of Figures

List of Tables

Chapter 1

Thesis introduction

1.1 Background

Characterising the influence of local geology on seismic motions (penned as local site effects by (Aki, 1993)) is an essential component in seismic response analysis at both local and regional scales. It is well established that seismic motions are amplified in soft sediment; this is compounded in basins when the thickness of the soil layer increases with increasing depth to basement rock. This phenomenon known as "basin effects", has been attributed to increased damage in several historic earthquakes including those in Mexico, Italy and the 2010-2011 Canterbury earthquake sequence (Jeong & Bradley, 2017; Kaiser et al., 2014; Piatti et al, 2013). Shear wave velocity (V_s) in particular is a key control in ground motion amplification (Bard et al., 2010) and an important parameter for resolving dynamic site properties. In the last 20 years retrieving the subsurface shear wave velocity structure by use of surface wave methods has become increasingly popular across the disciplines of seismology, geotechnical engineering and earthquake engineering (Socco et al., 2010). This is due to the non-invasive, cost effective appeal of the methods compounded by increased literature surrounding solutions for the non-linear, ill-posed, solution non-uniqueness limitations of surface wave inversion (Foti et al., 2017). Surface waves are geometrically dispersed in the subsurface meaning waves of different frequencies have proportionately different wavelengths and penetration depths. The vertical component of Rayleigh waves (a type of surface wave) is commonly utilised in site response studies as these waves travel with an elliptical motion and retain 1/3 of the seismic source energy making them easy to generate and measure (Socco et al., 2010). The 1D shear wave velocity profile can be solved through an inversion solution; assuming vertically homogeneous layering (increasing thickness and V_s with increasing depth) (Socco et al., 2010; Foti et al., 2017). Diligent parameterisation of the inversion is essential in selecting realistic profiles, particularly where there is a lack of geological information.

The Hamilton Basin in particular (within the study area outlined in figure 1.1) is characterised by soft sedimentary layers (Kear & Schofield, 1964; Schofield, 1967). This likely increases the regional seismic hazard.

Figure 1.1 *- Cartographic shaded relief map of New Zealand and surrounds, with the study area for this research outlined in a black dashed rectangle. © Esri basemaps*

Geophysical and geological studies carried out after the Canterbury earthquakes reported previously undiscovered faults, frequency-dependent site amplification effects, and highlighted the lack of data on the velocity structure of the Canterbury region and subsequently all regions

across New Zealand (Teague et al., 2018). Velocity structure studies have since been conducted extensively in the Canterbury region and are underway in many sedimentary basins across of the rest of New Zealand. This includes but is not limited to basins in Nelson, Manukau, Wellington, Hauraki and Napier (Dawson et al., 2015; Deschenes et al., 2018; Jeong, 2019; Mcmahon & Wotherspoon, 2017; Wotherspoon et al., 2015). The concern in sedimentary basins, is the potential for trapping and amplification of seismic waves (basin effect) and generation of localized surface waves within the basin (local site effects). These effects are well known to contribute to increased damage in the event of an earthquake. Recent work by (Jeong, 2019) into the fundamental site period distribution across the Hamilton Basin concluded that there are areas of long site periods (>5s) in Te Rapa and Gordonton and that most of the basin has site periods of >0.6s. This indicates increased depth to basement rock in areas with long site periods, which translates to areas of increased shaking duration in an earthquake. These findings are compounded by recent fault zone discoveries with undetermined activity status (Moon & de Lange, 2017), the potential for localized liquefaction in the surficial Hinuera Formation (Kleyburg et al., 2013) and the close proximity of the Keripehi Fault (closest rupture segment is ~38km from Hamilton CBD (as per the GNS New Zealand active faults database). Despite the relatively low seismicity in the Waikato Region, a rupture on the Keripehi Fault could produce a Mw5.5-7.4 earthquake (Persaud et al., 2016) and early research suggests that the Hamilton Basin is subject to long duration shaking. Thus, the earthquake risk for the Hamilton Basin may be higher than previously thought. Given the population of the Hamilton Basin is ~455,241 with the Waikato region home to 482,100, the Waipa region home to 53,241 and Hamilton city home to 160,911 (Stats NZ, 2018). Determining the subsurface velocity structure is needed to further refine the dynamic properties within the Basin, in particular determining the spatial variability of ground motions and refining site class E sites as per the NZS1170.5 for seismic design. Fully characterising the velocity structure will also inform site specific ground motion analysis and simulation (Graves & Pitarka, 2010).

1.2 Aims and Objectives

The intended outcome of this research is to provide deep shear wave velocity profiles in the Hamilton Basin that will determine spatial variability in ground motions and aid seismic response analysis and seismic risk assessment. This will be achieved by utilising surface wave methods across 15 sites, specifically, by jointly inverting Hortizontal-to-Vertical Spectral Ratio

(HVSR) with Rayleigh wave dispersion curves obtained through a combination of Multichannel Analysis of Surface Waves and (MASW) and Microtremor Array Measurements (MAM). There are three main objectives of this research:

1. Obtaining fundamental site period data throughout the Hamilton Basin using the single station horizontal-vertical (H/V) ratio method
2. Obtaining dispersion data through both the active source method (MASW) and the passive source method (MAM) and
3. Producing shear wave velocity profiles throughout the Hamilton Basin and determining geological relationships for some dynamic characteristics

The results from this research will help to characterise local site dynamics on a regional scale study through the development of deep shear wave velocity profiles. This is a part of QuakeCoRE's flagship programme 1: ground motion simulation and validation: seismic velocity model development.

1.3 Thesis outline

This thesis presents the design and analysis undertaken for dynamic site characterisation of the Hamilton Basin as well as the findings and interpretations. The presentation is split into six chapters encompassing the literature review, acquisition methodology, analysis and interpretation of the components in this research. A more detailed outline is given below for each chapter:

Chapter 2 ~ Surface wave methods, applications & the geology of the Hamilton Basin

Presents a comprehensive review of the geophysical literature and geological literature relevant to this thesis. Including why surface waves are used, how the methodology has been applied in New Zealand and locally in the Hamilton Basin. Then subsurface structure, geological formation distribution and composition.

Chapter 3 ~ Surface wave methodology for the Hamilton Basin

Details the methods used to obtain the shear wave velocity results for the Hamilton Basin and any limitations they may have.

Chapter 4 ~ Shear wave velocity profiles for the Hamilton Basin

Displays the results of the project relative to each of the 15 sites surveyed. In particular, shear wave velocity profiles.

Chapter 5 ~ Result validity and implications for seismic design and site response

Discusses these results in terms of how they relate to the local geology, any complications in the results and what this may mean for site response in the Hamilton Basin.

Chapter 6 ~ Research summary

Concludes the thesis and summarises the findings of this work as well as providing recommendations for further research.

Chapter 2

Surface wave methods and the geology of the Hamilton Basin

2.1 Chapter brief

This chapter includes a review of both the geophysical and the geological literature relevant to this thesis. Sections 2.2 will introduce surface waves and methods of analysis in regards to earthquake engineering research and site characterisation. This is in order to review what surface waves are and what the current analysis methods are in the science. Section 2.3 introduces applications of surface waves in regards to site effects and site characterisation. Section 2.4 reviews the current and historic seismic hazard in the Hamilton Basin as well as surface wave analysis of the basin to date. A review of the literature around the geology of the Hamilton Basin is presented in the second half of this chapter. Section 2.5 looks at the structure of the basin revealed by cross sections, maps and geophysical analysis. Section 2.6 describes the geological groups of the basin, with depth, distribution and lithological data.

2.2 Surface wave methods and analysis

Energy released from earthquakes travels by large in the form of long period surface waves, these waves make up most of a seismic signal at large distances from the earthquake epicentre. Surface waves have been studied since the 1920's with practical use of these waves becoming widespread in the 60's and 70's as utilisation methods developed. Surface wave methods utilise surface waves to reconstruct the dispersive properties at a site and resolve the subsurface properties through an inverse solution. Over the last decade surface wave methods have been developed for both the geotechnical and geophysical fields, in particular, for earthquake research (Socco et al., 2010; Foti et al., 2011; Foti et al., 2017). How dispersion works, is in vertically homogenous media the amplitude of a surface wave decreases exponentially with depth whereby most of the energy is retained within the wavelength (Socco et al., 2010; Foti

et al., 2017). This dispersive nature in surface waves means the subsurface structure and properties can be derived through an inverse solution. One of these properties is shear wave velocity which is an important control on site amplification (Bard et al., 2010). While the concept itself is consistent throughout the literature, there are many different methods and processing techniques that use these waves to the same end, for example (Nakumara, 1989; Park et al., 2002; Wathelet, 2008) to cite a small number. The lack of an official standard procedure makes sifting through all the methods available time consuming, however, thanks to the collaborative efforts of organisations across the globe, particularly in Europe, there are broad guidelines for surface wave methods, their appropriate applications and their drawbacks. In particular (Foti et al., 2017) developed the most recent guidelines resulting from the InterPACIFIC project (Intercomparison of methods for site parameter and velocity profile characterization). These guidelines followed on from (Bard et al., 2010) who detailed current standard practice in 2010 that resulted from research from 2005-2010 and (Foti, 2005) who detailed surface wave use for the geotechnical field from prior research. Surface wave measurements are comparatively reliable to other methods, outputting results within ±10% of results from more invasive methods such as cross-hole and downhole (Bard et al., 2010). Surface wave methods have been deemed cost effective and non-invasive, as well as being an arguably faster means to deducing subsurface properties when compared to these more invasive methods (Foti, 2005). Results from surface wave methods are also more representative of earthquake behaviour due to the 'more appropriate' frequency range used (Bard et al., 2010).

There are three main procedural steps repeated throughout the literature independent of method; acquisition, processing and inversion as detailed in figure 2.1 below.

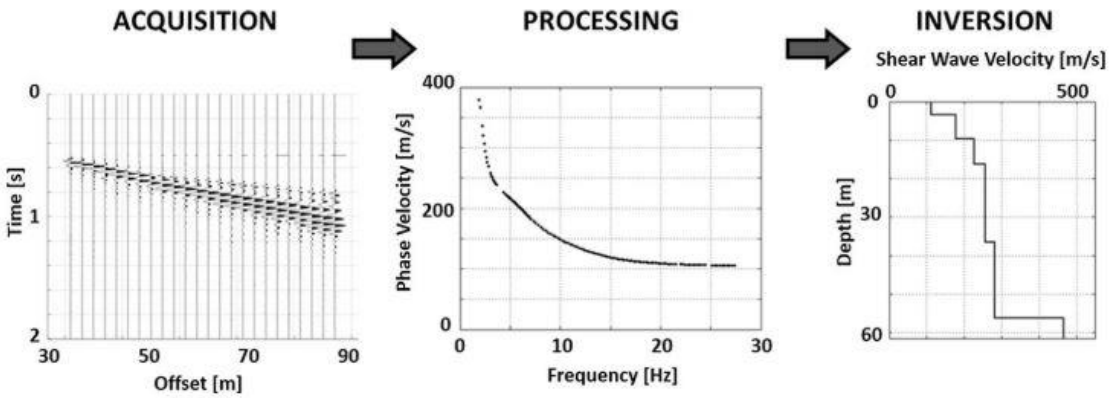

Figure 2.1 *Flow diagram of the three-step surface wave testing procedure; a) raw data, b) dispersion curve and c) shear wave velocity profile. Reprinted from Guidelines for the good practice of surface wave analysis: a product of the InterPACIFIC project (p.5), by Foti et al., 2017, Bulletin of earthquake engineering. Copyright (Foti,2017).*

Raw data are retrieved in the time domain and more commonly processed in the frequency domain to produce a dispersion curve which describes propagation speed as a function of frequency. This dispersion curve is then inverted to a profile of shear wave velocity (V_s) versus depth. Rayleigh waves are commonly analysed in this process as these surface waves exist in homogeneous and heterogeneous media, although *a priori* information is required for the latter (Foti et al., 2017).

2.2.1 Acquisition

The way in which surface wave data are acquired varies depending on site factors and the intended outcome of the investigation. At a basic level there are two methods; active and passive, whereby active surveys measure artificially generated waves and passive surveys measure ambient waves. Active methods typically involve high frequency data which results in shallow resolvable depths, this is because short wavelength Rayleigh waves propagate close to the surface and the energy generated during an active test is high frequency short wavelength waves, which are captured by geophones (Foti, 2017).

Passive methods are the opposite and have a low resolution at shallow depths with a larger resolvable depth. This is because seismometers are typically used to measure low frequency long wavelength waves (ambient waves) occurring from natural sources. These long wavelength waves resolve deeper subsurface. As a result, it is recommended for deeper investigation (i.e for earthquake research) to use a combination of the two techniques in order to develop a better-defined model. For a geotechnical investigation it is best to use an active method, since the investigation focus is typically the upper 30m (Foti et al., 2017). In the review by (Socco et al., 2010) 64% of the literature the author surveyed involved testing using active methods, however of the literature reviewed, 64% was weighted toward shallow investigation depths and 36% to deeper investigation. In case studies from three regions across New Zealand, referred to in table 2.1, depths <30m were characterised using active linear array methods and depths >30m where characterised using passive methods, in all cases. Table 2.1 also includes the processing and inversion methods, which will be discussed in detail in chapter three. Multichannel analysis of surface waves (MASW) (Park et al., 1999; Xia et al., 1999) is the predominant active testing method used in New Zealand with spectral analysis of surface waves (SASW) (Stokoe et al. 1994), used in the Manukau lowlands only. Varying geometries and diameters of the Microtremor array method (Aki, 1957; Okada, 2003).

Table 2.1 *Comparison of investigation, processing and inversion methods as well as target depths and geology between three New Zealand studies for dynamic site characterisation; Nelson by (Mcmahon & Wotherspoon, 2017), Christchurch by* (Deschenes, Wood, Wotherspoon, Bradley, & Thomson, 2018) *and the Manukau lowlands by* (Dawson, Wotherspoon, Nelis, & Fraser, 2015).

Site	Depth	Acquisition Method	Geology	Processing	Inversion
Manukau lowlands	<30m	Active: MASW[*] (Park et al., 1999) 24 geophones, 2m spacing & SASW[†] (Stokoe et al. 1994)); 6kg sledgehammer and 90kgdropweight (sources)	Interbedded sandstone, mudstone and alluvial deposits with interwoven deposits of basalt and tuff. Some areas of peat	FDBF[‡] (Zywicki,1999), Phase unwrapping method (Cox and Wood 2011)	Neighbourhood algorithm (Watheelet,2008)
Nelson	<30m	Active: MASW[*] (Park et al., 1999) 24 geophones, 2m spacing; 6kg sledgehammer (source)	Takaka terrane overlain by a thick dense gravel basin (Port Hills gravels & Moutere gravels) which is overlain by Holocene alluvial deposits in places. Sedimentary rock and igneous rock surfaces to the east and west.	FDBF[‡] (Zywicki,1999), HRFK[§] (Capon, 1969) & MSPAC[¶] (Bettig et al. 2001)	Neighbourhood algorithm (Watheelet,2008), Joint HVSR[#] (Parolai et al., 2005)
	>30m	Passive: MAM[**] (Aki, 1957) L shape array of 24, 5m spaced geophones as well as circular 50-200m diameter circular shape arrays		FDBF[‡] (Zywicki,1999), HRFK[§] (Capon, 1969) & MSPAC[¶] (Bettig et al. 2001)	
Christchurch	<30m	Active: MASW[*] (Park et al., 1999) 24,2m spaced horizontal geophones for Rayleigh waves and 24-48, 2m vertical geophones for love waves; 5.4kg sledgehammer (source)	Waipapa-composite terrane overlain by alluvial soils and gravels to the west and interbedded (increasing eastward) terrestrial gravel and fine-grained marine sediments sand silt clay and peat	FDBF[‡] (Zywicki,1999), MSOT[‡‡] (Cox and Wood 2011), HRFK[§] (Capon, 1969) & MSPAC[¶] (Bettig et al. 2001)	Neighbourhood algorithm (Watheelet,2008), Joint HVSR[#] (Parolai et al., 2005)
	>30m	Passive: MAM[**] (Aki, 1957) 50, 200, 500 and 1000m diameter circular shape arrays			

[*]Multichannel Analysis of Surface Waves [**]Microtremor array method [†]Spectral Analysis of Surface Waves [‡]Frequency Domain Beam-Former method [‡‡]Multiple-Source Offset Technique [§]High Resolution Frequency-Wavenumber transformation [¶]Modified Spatial Auto-Correlation method # Horizontal to Vertical Spectral Ratio

were used as the passive acquisition method in all cases. These methods look to be used independently of geology with highly varied geology between the three locations not affecting the acquisition method. The Neighbourhood algorithm (Wathelet, 2008) is the primary inversion method for all sites; this algorithm is imbedded in the Geopsy.org platform. Geopsy.org is an open source software for geophysical research, particularly for site characterisation from ambient vibrations with input from the 2005 SESAME project and in particular (Wathelet, 2004, 2005, 2008). The Frequency Domain Beam-Former method, High Resolution Frequency-Wavenumber transformation and Modified Spatial Auto-Correlation method were the primary processing methods used at the Christchurch and Nelson sites.

2.2.1.1 Active methods

Artificially generated waves in active surveys can vary in source from vibroseis to drop weight with the most common source being a sledgehammer, which is struck on a metal plate. These waves are measured by geophones in varying methods/arrangements. Spectral analysis of surface waves (SASW) was developed in the 1980's by (Nazarian & Stokoe, 1983) where the source is either in line with the receivers or in a rotational array where source and receivers rotate around an imaginary centreline based on recommendations by (Heisey et al., 1982), in either case the number of receivers is two. The slow test rate combined with low resolution led to the development of multistation analysis of surface waves (MASW) popularized by (Park et al., 2002). This method uses more than twelve equally spaced receivers in line with the source (a linear array). The variations in both methods are depicted in figure 2.2, with the setup for SASW in 2A and MASW in 2B from (Park et al., 1999).

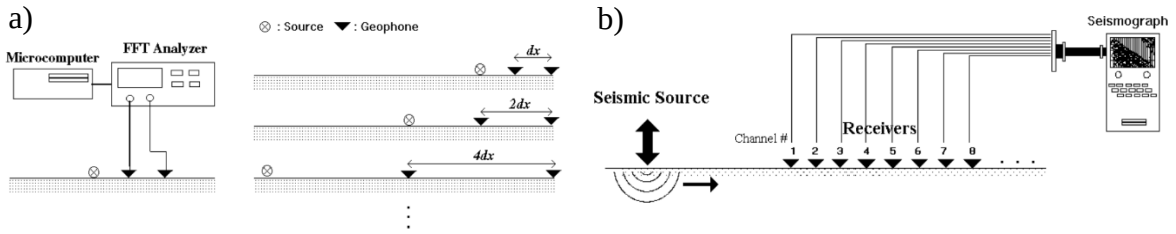

***Figure 2.2**- A) Schematised set-up for spectral analysis of surface waves (SASW) with only two geophones and B) Multi-channel analysis of surface waves (MASW) with many receivers. Both images are reprinted from Multichannel Analysis of Surface Waves (MASW) (p.15), by Park et al., 1999, Geophsyics. Copyright (Park et al., 1999).*

The MASW method has been built upon over the last decade with recommendations from various authors. Receiver spacing has been topical due to the relationship between spacing and penetration depth being two times the wavelength. Due to this, one of the main issues is the length of the array being limited by the available receivers and therefore by the spacing of receivers which has implications for resolution and penetration depth. While one meter spacing has a high resolution it also has a shallower penetration depth due to the reduced array length, and while three meter spacing has a deeper penetration depth resolution is lost at shallower depths. Recommendations by (Foti, 2005) included having forward and reverse shots as well as having at a minimum 24 receivers with two tests done at one and three meter spacings; these were also repeated by (Bard et al., 2010). While these suggestions increased test time and cost, comparatively this outweighs SASW in resolution, cost and time (Foti, 2005). Additions in the guidelines by (Foti et al., 2017) suggest array length should be at least twice the investigation depth, and receiver spacing should be 0.5-4m depending on the minimum expected wavelength at each site. The number of receivers suggested is 24-28 based on far field effects with too many receivers and aliasing with too few. Near field effects which distort the velocity in the low frequency range are still a common issue as well as lateral variations in the subsurface; to address this it is suggested that shots at 2, 5, 10 and 20m are taken either side of the linear array (Foti et al., 2017).

2.2.1.2 Passive methods

Passive surveys involve the measurement of ambient waves both human induced and natural with a 2D array. Array geometry is commonly circular or triangular to allow for multidirectional analysis, other geometries such as T and L shapes however, require verification of the array response and directional sources (Foti et al., 2017). (Bard et al., 2010) recommended a layout of eight stations for a typical site with a wavelength range of 10-1000m with (Foti et al., 2017) recommending 1 Hz, 5 Hz and 30 Hz seismometers for deep investigation. (Foti, 2005) suggested that recording ambient noise at a site can aid dispersion curve development in noisy environments such as roadways and townships. This is due to the high level of noise obscuring the Rayleigh wave signal in the record. Microtremor array measurements (MAM) are a passive survey which was developed on the basis that surface waves exist in microtremors and therefore phase velocity can be used to determine subsurface structures and velocity (Aki, 1957). (Okoda, 2003) developed the method specifically for

resolving the subsurface velocity structure to significant depths in earthquake engineering studies with advancements in acquisition technology. Below is an illustration from (Cho & Iwata, 2019) of the general MAM theory, which includes data processing and inversion (figure 2.3). The seismic sensor is generally a seismometer with a low natural period capable of detecting low frequency microtremors (~0.5-2Hz) as well as frequencies up to ~30Hz. A vertical component seismometer can analyse the Rayleigh wave signal while 3-component seismometers are needed for analysis of the horizontal to vertical ratio (HVSR) (Foti et al., 2017). Array geometry which is (circular in figure 2.3) can also be linear however, selection is site dependant.

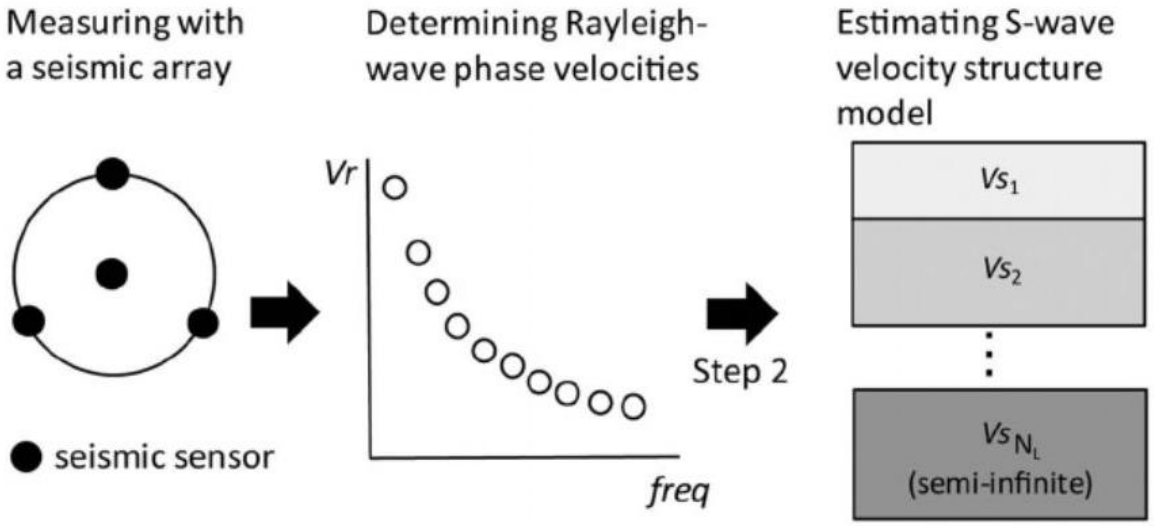

Figure 2.3 *Illustration of the mircrotremor array method. Reprinted from A Bayesian approach to Microtremor array methods for estimating shallow S wave velocity structures: Identifying structural singularities, (p.528), by Cho & Iwata, 2019, JGR. Copyright (Cho & Iwata, 2019).*

2.2.2 Processing and inverting surface wave data

Processing involves extracting a dispersion curve of phase velocity V_s frequency from the acquired surface wave data (Foti et al., 2011). Geopsy software developed for processing and inversion was originally a side project of SESAME (Site EffectS assessment using AMbient Excitations) and has since been further developed with the NERIES (Network of Research Infrastructures for European Seismology) project (Bard et al., 2010). The online availability of the software was part of the participating researchers' efforts to help reduce the cost of surface wave techniques by creating a free platform with all standard surface wave testing modules embedded. Traditional coding methods whereby the same methods are performed script by script on a software such as Python also perform these calculations to the same end, with less

ease. (Foti et al., 2017) outline that active data are most commonly processed in the frequency wavenumber domain using a frequency wavenumber technique (FK) or high resolution FK (HRFK) developed by (Capon, 1969), while spatial auto-correlation (SPAC) developed by (Aki, 1957) is commonly used for passive data. This review also suggested that a combination of these two techniques be used in processing passive data. (Aki, 1957) developed SPatial AutoCorrelation (SPAC), a technique for processing ambient vibrations based on the "stochastic regression of theoretical functionals of wave propagation" (Socco et al., 2010). The technique is widely used for surface wave analysis and has been developed with derivatives such as (ESAC (extended spatial autocorrelation) & MSPAC (modified spatial auto correlation)) (Foti et al., 2017; Socco et al., 2010). FK processing transforms the raw data from the time versus space domain into the frequency to wavenumber domain to be worked with. HRFK built on SPAC to estimate concentrated phase velocities (Horike, 1967). However, both methods have different assumptions and therefore different limitations so are therefore best used simultaneously in analysis for more evaluated results (Foti et al., 2017). Uncertainty still ranges from 5-20% (Garofalo et al., 2017).

There are various methods of inversion, all of which fit the best velocity model to the experimental data using the derived dispersion. Inversions often assume a layered earth model with linear elastic layers. Each layer is parametrised with a fixed soil density (ρ), compressional-wave velocity (Vp), shear-wave velocity (V_s), and thickness (depth range) (Wathelet et al., 2004). There are two types of algorithms; global search methods which explore many solutions to find the lowest misfit between the theoretical and experimental dispersion curves , and local search methods which search for the lowest misfit and work forwards from there (Socco et al., 2010). The neighbourhood algorithm, which is imbedded in the Geopsy platform, is a local search method algorithm capable of generating solutions within irregular boundaries where Vp, V_s and depth can be altered, ρ is fixed and multimodal inversions are possible (Wathelet, 2008). Enabling multimodal inversions helps to retrieve reliable velocity profiles where the dispersion dataset may not be entirely fundamental mode. Mode selection is influential in final model results and identification of higher modes is essential to obtaining reliable results (Foti et al., 2011; Foti et al., 2017). The algorithm can run any number of models set by the user, however computational efficiency must be considered along with adequate exploration of the parameter space (Wathelet et al., 2004). Surface wave inversion is however, ill-posed, and there can be markedly different velocity profiles which all best fit the experimental dispersion. This is influenced by parameter selection, especially in the absence of subsurface geological data, which is termed a blind analysis and highly prone to solution non-uniqueness. (Cox & Teague, 2016) introduced a solution to blind parameterisation with a

layering ratio (multiplier) method. This multiplier works by increasing the potential thickness of a layer dependant on the potential thickness of the overlying layer; common ratios are 1.2, 1.5, 2.0, 4.0 and 5.0. It is recommended to run inversions with different multipliers in order to evaluate which best suits the site conditions. An illustration of the method is given in figure 2.4. This method is for parametrisation only and works with exploration algorithms such as the neighbourhood algorithm to constrain model selection in order to select profiles that are more realistic. In any case profile uncertainty needs to be represented with surface wave inversion results as the solution non-uniqueness limitation cannot be eliminated. This is commonly represented by displaying a set of model results (generally the lowest misfit models) which can also be represented with standard deviation (Cox & Teague, 2016; Foti et al., 2017; Wathelet et al., 2004).

.

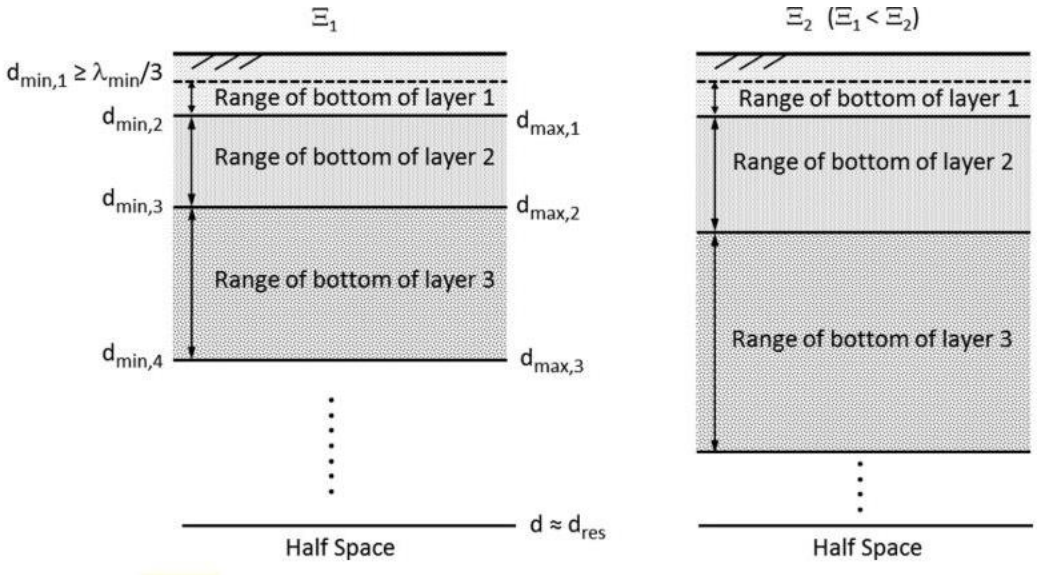

Figure 2.4 *Illustration of the layering ratio inversion method, which aids parameter selection for the layered earth model when geological information is not available. Reprinted from Layering ratios: a systematic approach to the inversion of surface wave data in the absence of a priori information, (p.423), by Cox & Teague, 2016, Geophysics, Copyright (Cox & Teague, 2016).*

A method for a joint inversion with horizontal to vertical ratio curves (H/V) has also been developed by (Parolai et al., 2005). The fundamental peak in an H/V curve provides additional information on the subsurface velocity structure and helps to resolve large impedance contrasts in the inversion. Abundant literature on the technique and its effectiveness has been published since 1970, and guidelines from (Bard et al., 2004; Parolai et al., 2005) propose a joint inversion of dispersion data and H/V ratio curves to produce a more constrained final model. This method is included in (Foti et al., 2017) as a viable method to reduce final model uncertainty. The

SESAME project involved rigorous testing of the H/V ratio method and it's applications; resulting guidelines were published in 2004 (Bard et al., 2004).

2.3 The applications of surface wave methods

2.3.1 Site characterisation

Since the 1920's surface wave methods have been a focus of research, however, they have only gained popularity since advancements in technology over the last thirty years have made the method more viable (Foti, 2011). They are a particularly useful geophysical tool as they enable non-invasive subsurface investigation with relatively the same reliability as invasive methods (Garofalo et al., 2017). The dispersive nature of surface waves enables characterisation of the subsurface; this is more commonly used in the shallow region (less than thirty meters) but can also be performed up to depths of more than one kilometre (Socco, 2010). Depending on the analysis used, the measurement of surface waves can reveal several subsurface properties and this is termed site characterisation.

Site characterisation does tend to refer more commonly to the determination of the shear wave velocity at a site. Most of the literature discusses site characterisation in terms of classifying the shear wave velocity of a soil to 30m deep; termed the V_{s30}, a parameter that is common in seismic design (Foti, 2011). However, the technique can also be used to determine shear wave velocities to depths exceeding 1km and scales from specific sites to basin level (Piatti et al., 2013; Wotherspoon et al., 2015). These data are useful in seismic hazard analysis (Foti, 2011). Each site is unique and at present, no standardised guidelines exist on how to classify a site using surface wave methods. Published research such as (Socco et al., 2010) and guidelines provided by the InterPACIFIC project, outline basic principles and suggestions for common situations as well as comparing effectiveness of common methods and any concerning limitations (Foti et al., 2017).

All the surveyed published research reiterates that site characterisation using surface waves is a three step process involving acquisition, followed by processing, followed by inversion (Foti et al., 2011; Garofalo et al., 2017; Socco et al., 2010). While straightforward in its simplest form there are many possible complications in the process, the main one being the solution

non-uniqueness (Foti et al., 2017). When fitted to the dispersion curve, many shear wave velocity solutions can be given. Approaches to the design of the survey as well as the methods chosen for data acquisition, processing and inversion must be tailored to each other and the survey goal. Having a well-defined subsurface velocity structure available is integral in understanding the spatial variability of ground motions. The velocity structure can be used to determine the potential vibration of foundations and vibration transmission in soils as well as seismic response analysis.

2.3.2 Dynamic site characterisation in New Zealand

Internationally, literature surrounding the use of surface wave methods and the H/V ratio method to characterise the subsurface velocity structure is abundant. However, in New Zealand the technique is still in its infancy. First used in the Canterbury region in 2015 (Wotherspoon et al., 2015) surface wave methods have since been used in the Manukau lowlands (Dawson et al., 2015) and the Nelson-Tasman region (Mcmahon & Wotherspoon, 2017) to characterise the subsurface velocity structure in the near surface. Active and passive surface wave methods were used in a 2018 Canterbury region study to resolve shear wave velocity to depths of up to 2km (Deschenes et al., 2018). The consequences of the 2011 Canterbury Earthquake Sequence were the motivations for these studies spotlighting the lack of dynamic subsurface data in regions across New Zealand. Characterising the shear wave velocity structure is influential to broadband ground motion simulations and seismic analysis (Eberhart-Phillips et al., 2010; Graves & Pitarka, 2010; Tarbali et al., 2019). Adequate characterisation is key to forward and reverse ground motion simulations that accurately reflect local and regional response.

The Manukau lowlands geology contains some similarities to the Hamilton Basin geology, the shear wave velocity results from this study are reprinted from (Dawson et al., 2015) in table 2.2.

Table 2.2 *Shear wave velocity ranges for several deposits in the Manukau lowlands; similar to deposits in the Hamilton basin. Reprinted from (Dawson et al., 2015).*

Deposit	Shear wave velocity (m/s)
Peaty silt	65-90
Tauranga Group Alluvium	115-130
Puketoka Formation	150-300

2.3.3 Current site characterisation research for the Waikato Basin

Near surface shear wave velocity measurements (V_{s30}) have been made in the Hamilton Basin, unfortunately however, such measurements are not readily available in literature form. Instead, these results have been resolved using cone penetration testing (CPT) in geotechnical investigations often undertaken by consulting firms for private use. In one case, shear wave velocity results were obtained for liquefaction assessment using cross hole and downhole methods for the Waikato Expressway development, on a scale of <30m (Clayton et al., 2017). There is also a geology and terrain based V_{s30} model from (Foster et al., 2019) for the basin, developed as a part of a national scale study with a 100m resolution. The North Island section of the model in map form is given in figure 2.5 with the velocity scale for reference; showing the Hamilton Basin is expected to have a V_{s30} of <300m/s.

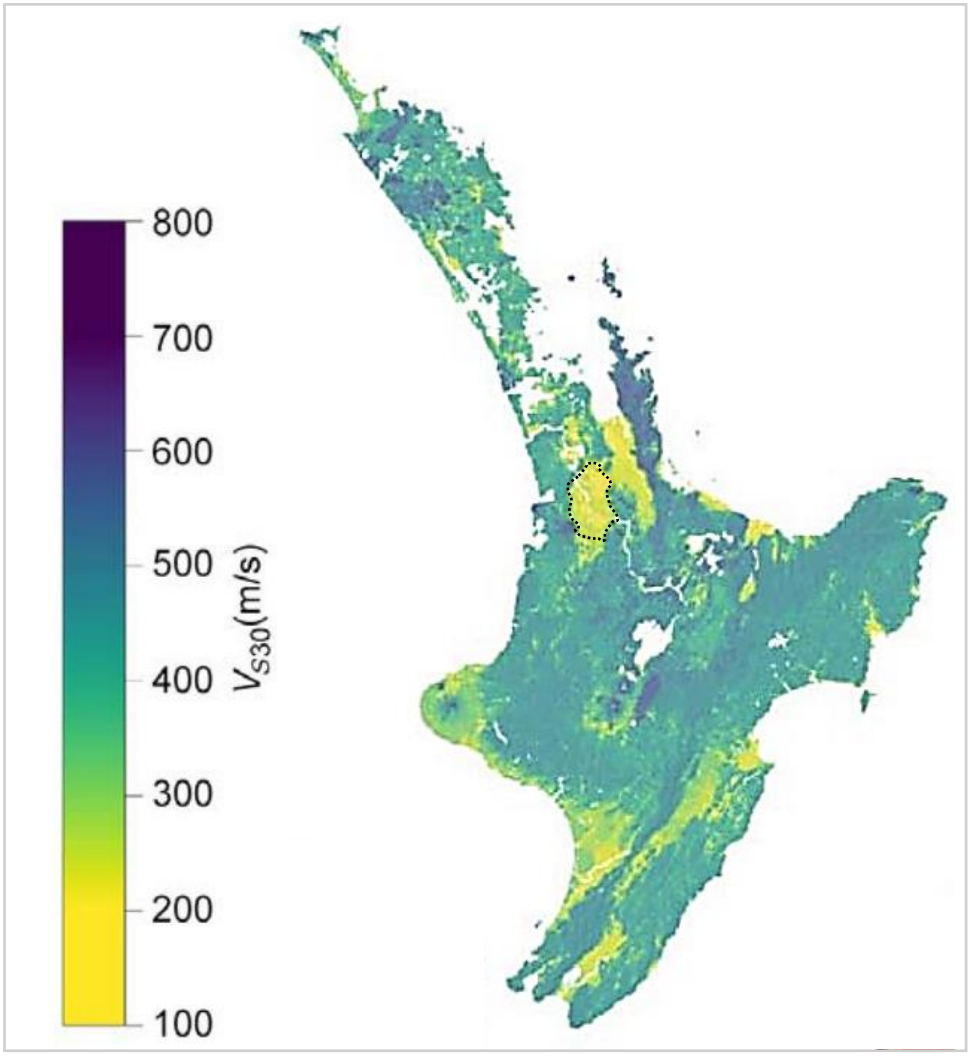

Figure 2.5 *V_{s30} model of the North Island developed from statistically weighted geological and terrain data. A dashed black line defines the extent of the Hamilton Basin. Reprinted from (Foster et al., 2019).*

The fundamental period has been deduced from H/V testing using surface wave methods (Jeong, 2019). The horizontal to vertical spectral ratio method, first introduced by (Nogoshi & Igarashi, 1970) and revised by (Nakumara, 1989), analyses microtremor as a ratio of the horizontal spectra to vertical spectra in order to characterise surface sediments. The spectral peak output from the H/V method is often the same frequency as the fundamental site period (f_0), which directly relates to layer thickness (Parolai et al, 2005) and can be used to estimate the shear wave velocity (V_s) (Rosenblad & Goetz, 2010). This study by (Jeong, 2019) found that the fundamental period was generally more than five seconds in the north-west of Hamilton indicating a deep soft basin with high potential for amplification in this area (Macau et al., 2015). South of this, the site period was generally less than three seconds towards Cambridge indicating a shallower basement, but the amplification potential in this fundamental period range is still high. There was evidence of complex layering near Gordonton and Te Awamutu with multiple peaks indicating multiple impedance contrasts. It was also noted that the results were limited by a lack of information on the spatial variability of shear wave velocities within the basin, particularly near the basin edge. No attempt to date has been made to characterise the subsurface shear wave velocity structure in the Hamilton Basin on a regional scale to depths of up to 2km.

2.4 Current seismic hazard in the Waikato region

The National Seismic Hazard Model (NSHM) for New Zealand was last updated in 2010, underpinned by probabilistic seismic hazard analysis models (PSHA) developed by (Cornell, 1968). The model relies on geological data and historical earthquake data as well as results from a set of ground motion prediction equations (GMPEs) to determine the seismic risk of a region (Stirling et al., 2012). These GMPEs characterise ground motions using the response spectra of acceleration from the predicted source, adjusting it for site characteristics and presenting this as peak ground acceleration (PGA), an index of motion. The 2010 NSHM estimated the hazard in the Waikato in terms of PGA as low, (0.1-0.3g), for both 475yr, and 2500yr, return periods. The higher hazard areas defined by this model are centred in areas with dense, large or active faults. At the time of writing, this is still the current assessment.

Recent probabilistic seismic hazard analysis (PSHA) models by (Tarbali et al., 2019) use physics based ground motion simulations for seismic hazard analysis (Cybershake NZ v18.5) rather than empirically based models that form the NSHM. Fault data from (Stirling et al., 2012)

was used in addition to the hybrid broadband ground motion simulation method (Graves & Pitarka, 2010). The research emphasises among other components the need for accurate representation of subsurface soil behaviour and higher resolution velocity models to model the influence of local site conditions on ground motions. This was highlighted through the Christchurch analysis whereby basin depth modelling and enhanced velocity modelling significantly influenced the ground motion results compared to the empirical approach.

A smaller regional scaled (1:50,000) seismic hazard assessment by the Waikato Regional Council (WRC) published in 2003, groups risk zones depending on the geology. Holocene material is deemed high risk and basement rocks, low risk (figure 2.6). Overall, the majority of the Hamilton Basin is mapped as low risk with higher risk areas in the far west (Waikato Regional Council, 2003).

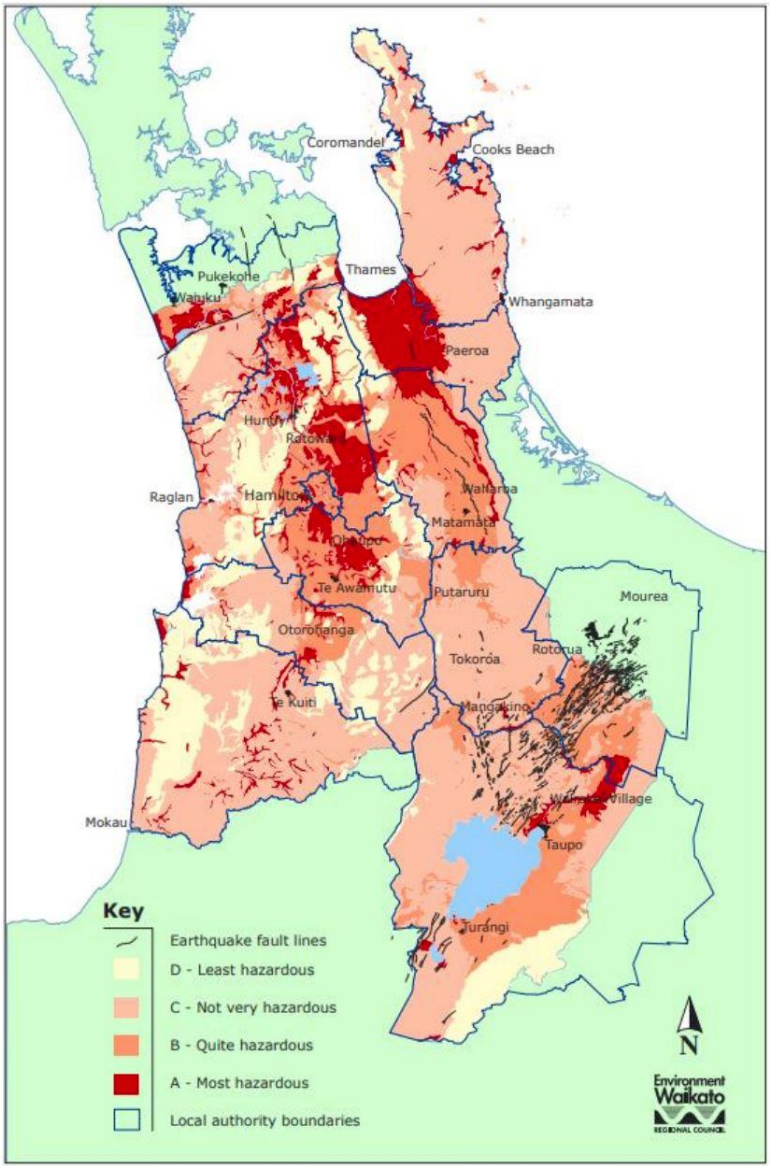

Figure 2.6 *A map of fault lines and earthquake hazard zones in the Waikato Region. Reprinted from Environment Waikato (Waikato Regional Council, 2003)*

2.5 Structure of the Hamilton Basin: Cross sections, fault maps and subsurface data

Located in the Central North Island, New Zealand, the Hamilton Basin (figure 2.7) is a horst and graben structure formed during the Kaikoura Orogeny (24 Ma to the present) due to strain on the Pacific crust leading to faulting and uplift in the basement terranes across New Zealand (Lowe, 2010). Hamilton City, New Zealand's fourth largest city with a population of 160,911 (Stats NZ, 2018), lies along the Waikato river in the middle of this basin. Spanning ~80km north south from Taupiri to Tokanui and ~40km east west from Karamu to Cambridge, the extent of the Hamilton Basin is illustrated by the thick brown line in figure 2.7 (Kamp & Lowe., 1981; Selby & Lowe., 1992).

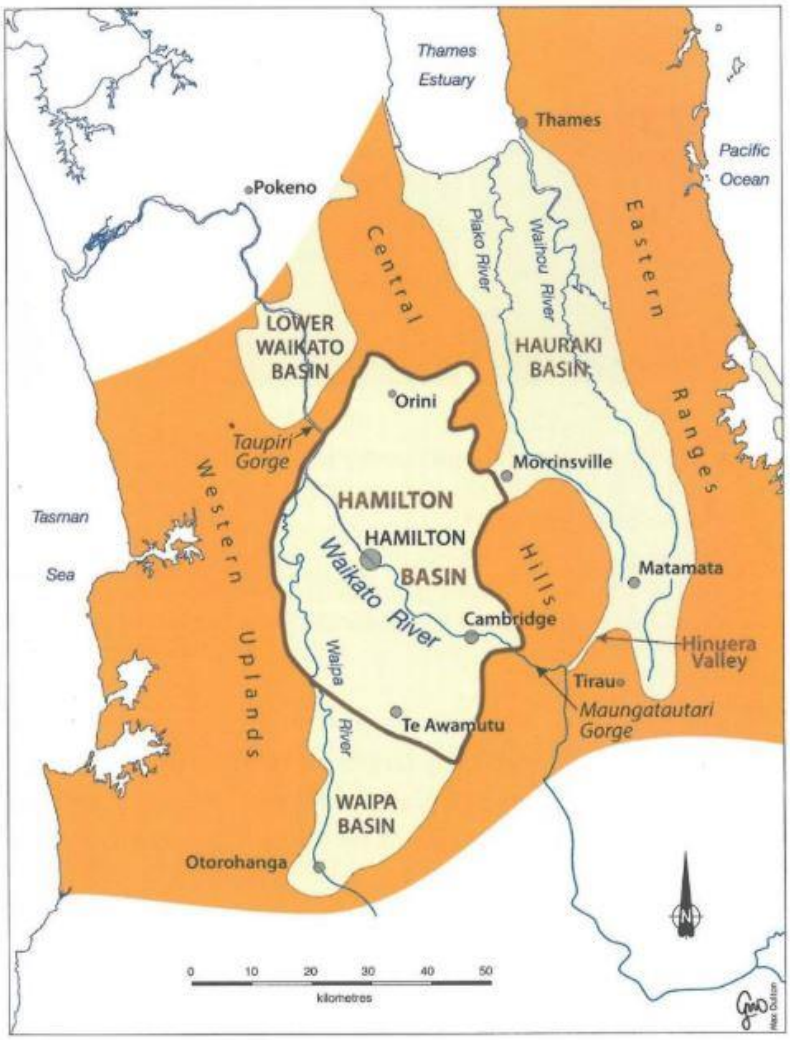

Figure 2.7 General landscape and extent of the Hamilton Basin (brown line) and surrounding basins, hills and uplands. Reprinted from (McCraw, 2011).

The basin represents the graben structure and the surrounding hills and ranges represent the horst structure in the basement terranes. Over the last 24 million years, sea level change and the redirection of the Waikato River at approximately 22ka (Lowe, 2010) has infilled the basin with various formations. Overlying the Waipapa Composite Terrane is the limestone dominated Te Kuiti Group, overlain by the sandstone dominated Waitemata Group and lastly the alluvial dominated Tauranga Group. Presently, bogs, alluvial plains and low hills dominate the surficial landscape (Lowe, 2010). Separating the ranges and uplands from the basin is the NNE trending Waipa Fault in the west, the Taupiri Fault in the north and an inferred fault in the west (Edbrooke, 2005). New research suggests that the low hills in the surficial landscape are fault-bounded structures in themselves (Moon & de Lange 2017).

2.5.1 Cross sections and contour maps

The most recent cross section of the Hamilton Basin by Edbrooke in 2005 is based on the interpolation of data from exploration well logs, made available in the search for economic resources within the Waikato Basin during the 1970's and 1980's. (Edbrooke,2005) schematises the existence of three basement terranes; with the Murihiku terrane in the far west, surtured to the Dun Mountain – Matai Terrane (Ydw) through the Waipa Fault which is connected through an inferred fault to the Waipapa Composite Terrane (Jm) to the east. Jm comprises most of the basement rock that underlies the basin and dips to the west, outcropping in the ranges east of the basin. Faulting on the basement rock in the cross section extends into the overlying sediment, although it does not outcrop (figure 2.8a). The Te Kuiti Group (Mw) is depicted as being thickest in the west with decreasing elevation eastward. The Walton Subgroup follows this same pattern, however extending further eastward where it directly overlies the basement terrane. Contour maps exist exclusively for the Hinuera Surface (surface of the Hinuera Formation described in a later subsection) and the basement rocks in the Waikato region. Contours on the Hinuera Surface produced by (Schofield, 1965) in 2.8c show a decrease in elevation towards the north by 1 m every 1 km (Lowe, 2010). It has been suggested that this is due in part to the northward decrease in elevation on the basement rock (Edbrooke et al 2005). As per figure 2.8d, the basement rock sits at -200 m between Cambridge and Hamilton and deepens to -1000 m north of Te Rapa. The basement map is based on recordings from the same well logs as (Edbrooke, 2005) while the Hinuera Surface map is based on recordings by (Schofield, 1965) during field mapping.

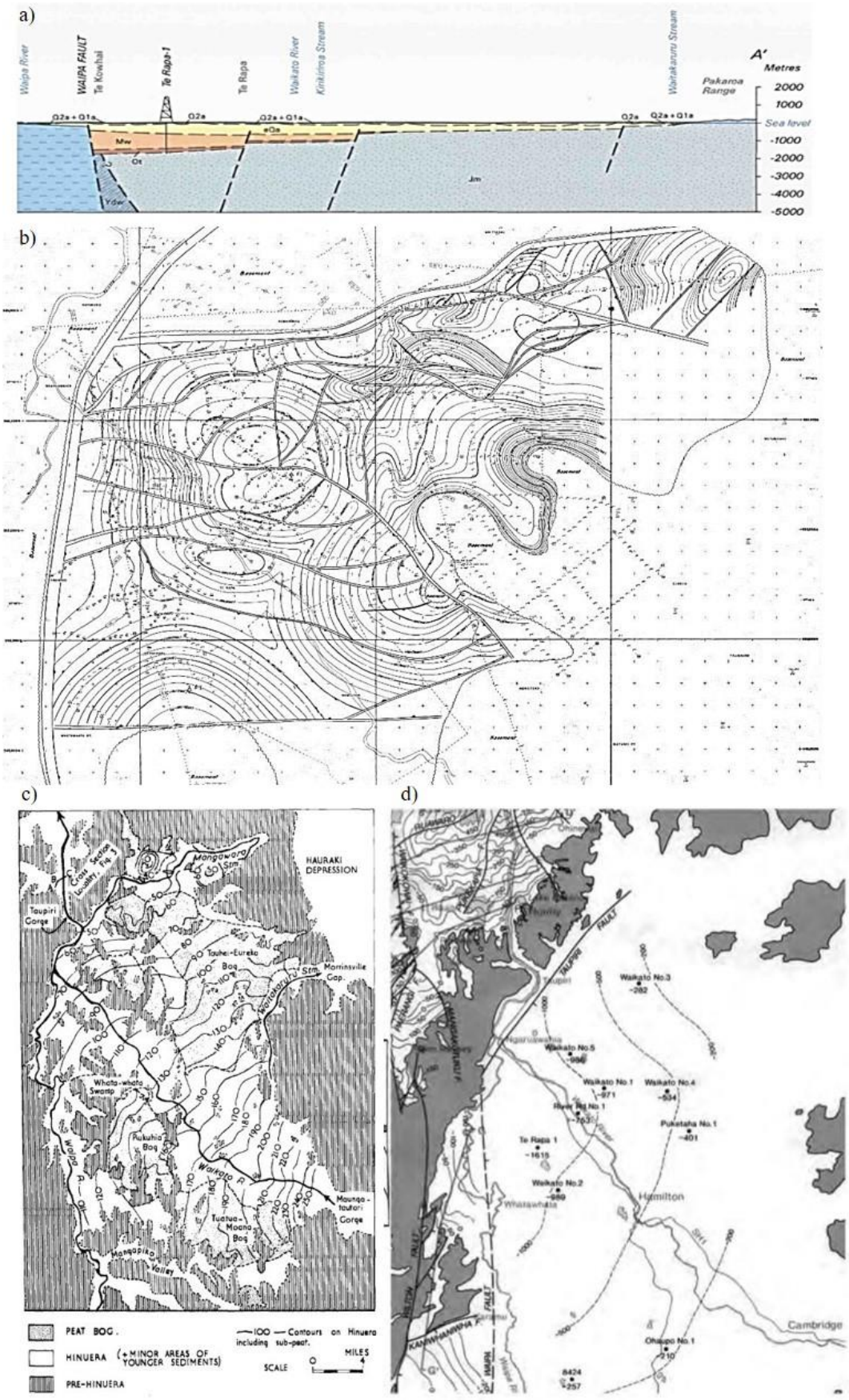

Figure 2.8 *Cross-sections of the Waikato Basin from 1966-2005. A) Cross section from (Edbrooke, 2005). B) Shotpoint maps with lines shot and horizon maps of the base Miocene-Top Oligocene of the Waikato Basin map (NZ Petroleum mineral database, 1971). C) Hinuera surface contour map in feet reprinted from (Schofield, 1965). D) Basement contour map (Edbrooke, 2005)*

The seismic line horizon maps were developed based on the seismic survey lines from petroleum exploration in the 1970's and represent contours on age-based horizons interpolated between shot points. There are two maps in existance, of which the Oligocene-Miocene horizon is shown in figure 2.8b. The other map illustrates the Miocene-Pliocene horizon and both are more legible in raw format. Both maps are on the NZ Petroleum and Minerals database and were authored by Liles, V.E. With no accompanying report map limitations are left to be inferred by the user, however the seismic lines are confined to the north-west of the Hamilton Basin. What each map does show is areas predicted to have shallower extent to basement and areas with a deeper extent. This looks to be a general shallowing towards the south, particularly to the south-east and a deepening toward the north-west. The basement contours from (Edbrooke, 2005) closely align with the Oligocene-Miocene contours in figure 2.8.

2.5.2 Basement level geophysical investigations

Gravity anomaly maps are used to show subsurface structure based off gravity anomalies which pick up changes in density (typically basement depth). A fundamental period map shows period (s) of the fundamental frequency (Hz) of a site (which can be correlated with depth). Figure 2.9 shows the results of both surveys and the similarities between the 2011 FrOG Tech gravity map and the 2019 interpolated fundamental period (T_0) map for the Hamilton Basin. The gravity anomaly map (figure 2.9a) is read as blue is low and pink is high whereas the fundamental period map (figure 2.9b) is read as yellow is a long period (correlated with deeper topography) and purple is a short period (correlated with shallower topography). (Jeong, 2019) found that the fundamental site periods in Te Rapa and Gordonton were longer than 5s correlating this to the depth of the basement rock in these locations. This is in agreement with the gravity anomaly map where the same zones were predicted to be depressions. The T_0 period trend in the depressions extends further than the area of extent of the depressions shown in the gravity anomaly survey. These two depression structures lie north of Hamilton City, the deeper depression covers a larger area in Te Rapa and the slightly shallower depression a smaller area in Gordonton. The two depressions, are separated by a ridge of higher topography running approximately NE-SW. This was inferred to be due, to the western side being downthrown by the Taupiri Fault (Moon & de Lange, 2017). These maps highlight the shallowing of the basin

which occurs southward, attributed to the slope of the basement rock which daylights in the ranges to the south (Moon & de Lange, 2017)(Jeong, 2019).

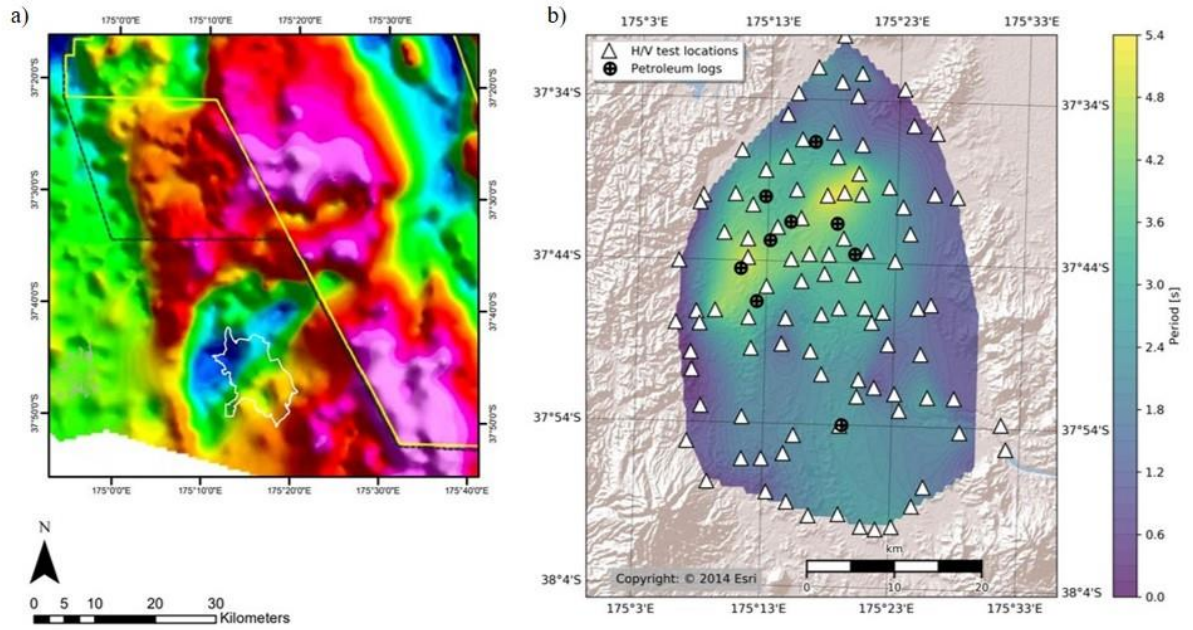

Figure 2.9 *A) Isostatic Residual Bouguer Anomaly map with Hamilton city outlined, FrOG Tech (2011). From (FrOG Tech, 2011, as cited in Moon & de Lange 2017). B) Interpolated map of T_0 across the Waikato basin with H/V test sites and the locations of petroleum boreholes marked, (Jeong, 2019).*

2.5.3 Faulting

The Hamilton Basin is bound in the west by the Waipa Fault and in the north by the inferred Taupiri Fault; these faults have been mapped by surficial geomorphology since 1960. Both faults are inactive, and it was assumed until 2015 that there were no other faults active or otherwise, within the basin. In 2015 work on the expressway local subdivision unearthed evidence of faulting in the Quaternary sediment (Moon & de Lange, 2017). As a result there has been a significant amount of research on faults in the Hamilton Basin in the last five years and the discovery of potentially active fault traces has led to the planned reassessment of the seismic hazard for the Waikato Basin (Spinardi, 2017). (Moon & de Lange, 2017) detail the findings of this research, which resulted in the discovery of six possible fault zones within the Hamilton Basin, which run approximately NE-SW within the Hamilton Basin (Figure 2.10). A high-resolution CHIRP seismic reflection survey was undertaken along the Waikato River and resistivity surveys conducted across suspected fault zones. These data, as well as existing data on boreholes, test pits and CPT tests were analysed to determine faults and fault zones. This resulted in confirmation with high confidence of, five faults, and ten faults with moderate

confidence. Evidence of faulting is confined to the western basin with limited data available in the east (Moon & de Lange, 2017). A lack of data in the east may be why faults appear to terminate along a ridge. These faults are potentially listric and form half grabens which could be responsible for the 'Hamilton Hills' otherwise known as the Walton Sub-Group (Moon & de Lange, 2017). Previous suggestions have been that the Walton Sub-group is not readily erodible and therefore erosion is responsible for the outcropping hills (Shofield, 1965). The change in faulting toward the south is also attributed to the Waipa Fault and the lack of faulting in the east is attributed to both the lack of available data and the extent of the Komakorau Swamp submersing any geomorphological indicators and inhibiting surveys.

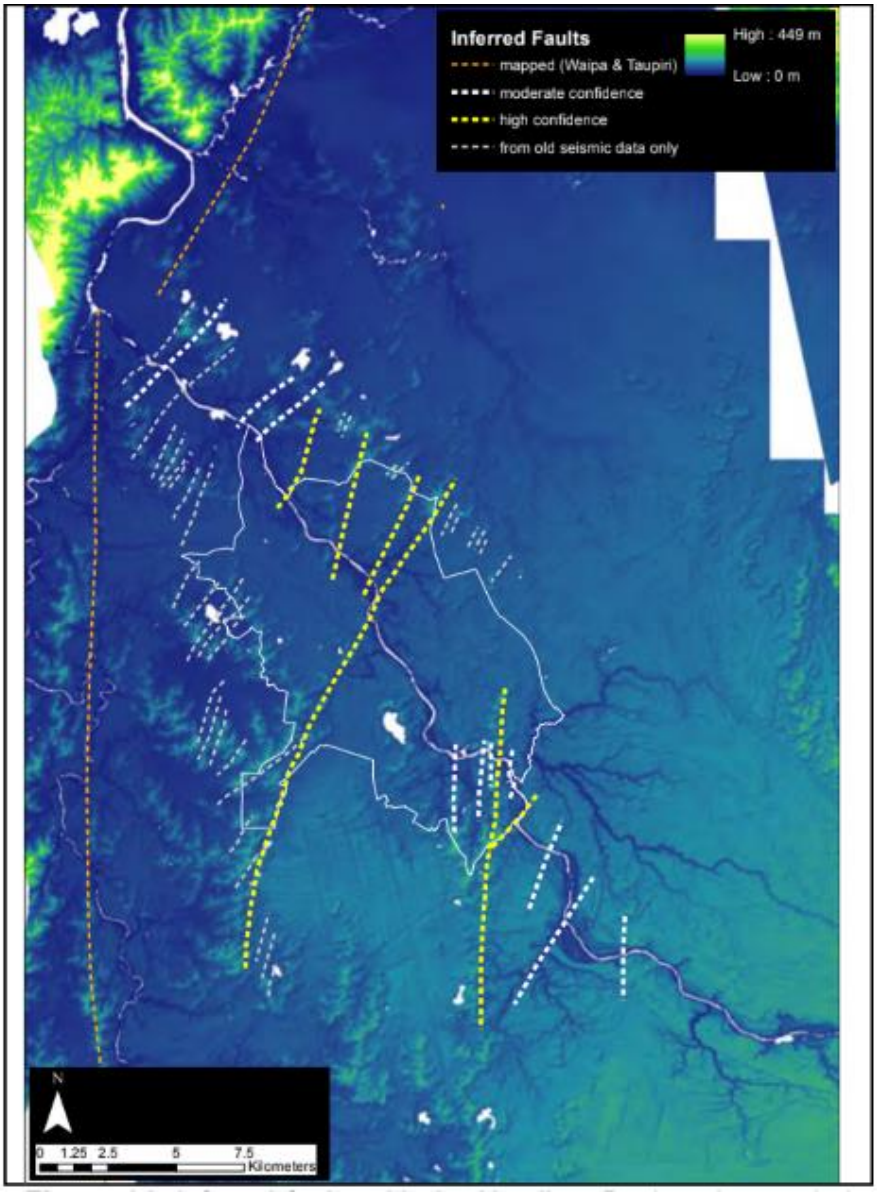

Figure 2.10 *Map of faults in the Waikato Basin with confidence levels colour coded as yellow (high) and thick white (moderate), mapped faults are in orange while faults from old seismic data are represented by thin white dashed lines. Reprinted from (Moon & de Lange 2017).*

2.6 Geological groups and basement terranes of the Hamilton Basin

In order to increase the reliability of the acquired shear wave velocity models it is suggested that the inversion process is constrained by geological knowledge (Foti et al., 2017). Lithology, age and other geological properties influence shear wave velocity propagation by controlling density. There are estimates of shear wave velocity for typical 'geomaterials' such as rock, clay, sand and gravel (Foti et al., 2017). Shear wave velocity structure will be site specific and the velocities of geological formations and groups will be unique. Engineering bedrock is defined internationally (BSSC, 2015) as having a V_s>760m/s, and this differs to seismic bedrock which typically has a V_s >3500m/s, both differ from basement rock which varies depending on study area. This section will cover the depths, compositions and distributions of the main geological groups and basement terranes within the Hamilton Basin.

2.6.1 Permian – Cretaceous basement terranes

The oldest rocks in New Zealand are termed 'basement rocks' as they are the base of the geology throughout New Zealand. Basement rock is distinguishable due to being 10 km or more thick and it's division into terranes is dependent on origin and suturing sequence (Ballance, 2009). The Hamilton Basin is underlain by three terranes discussed in the structure section of this review and represented in figure 2.8a. The Waipapa Composite Terrane is tilted west-east to surface in the east and in the far west this terrane is connected to the older Dun Mountain terrane through an inferred fault which is connected to the younger Murihiku Terrane.

The Dun Mountain Terrane (DMT), a Permian ophiolite sequence, is obducted oceanic crust mantle rock overlain by volcanics. The terrane is an accretionary deposit formed through the deposition of oceanic crust and volcanics in a trench within a subduction zone and is 285-275 myr old. Although the terrane does not outcrop in the basin it's presence below the surface is distinguishable via it's unique geophysical signature, a magnetic anomaly (Ballance, 2009). Defined in the QMAP by (Edbrooke, 2005) the steeply dipping terrane is comprised of Wairere serpentinite, part of the Dun Mountain Ultramafics Group. This is a "sheared, serpentinised hazburgite with xenoliths of metasomatised gabbro" (Edbrooke, 2005). The DMT is denoted by number 5 in figure 2.11 and follows the dashed line in the North Island and the thick black line in the South Island.

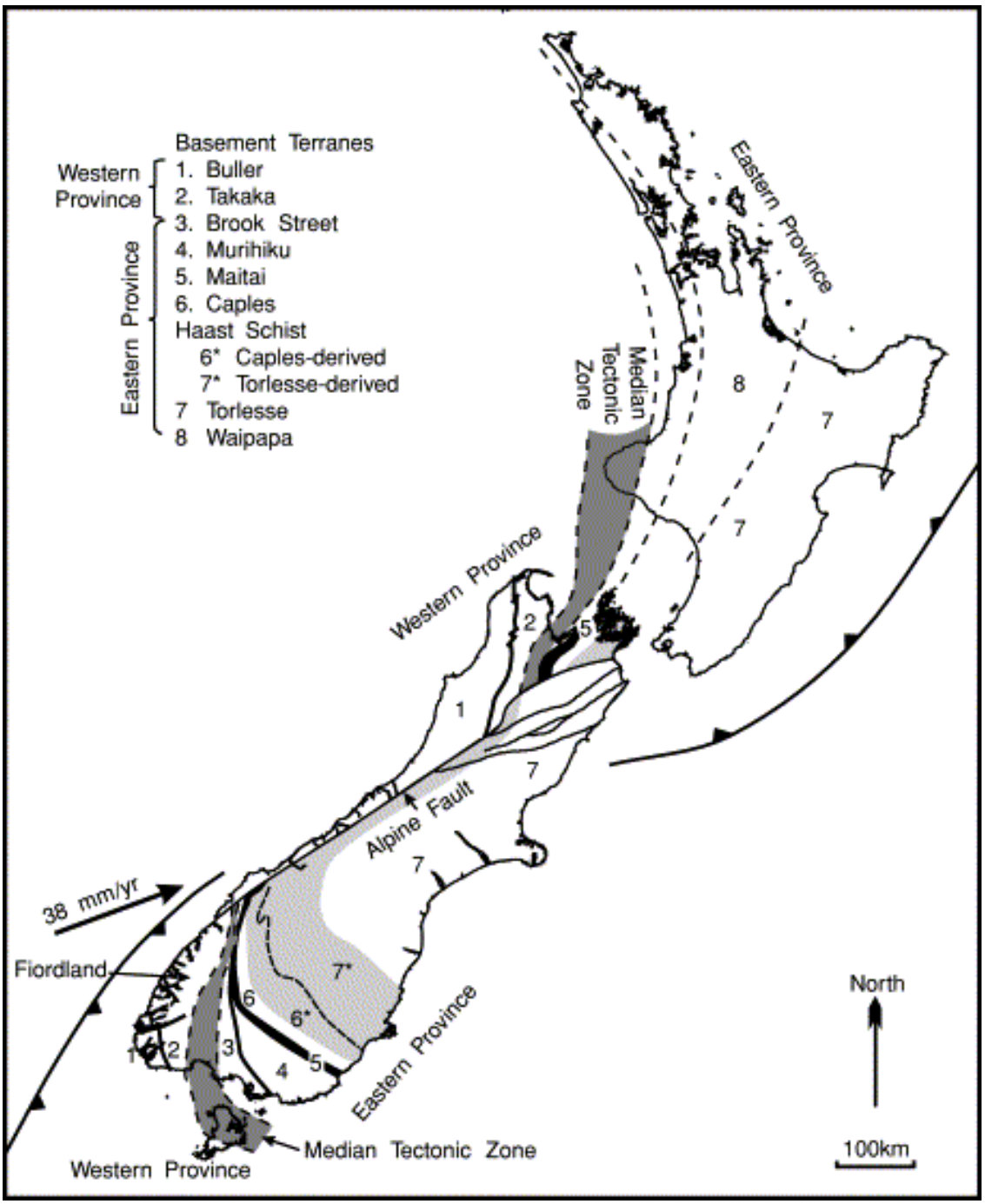

Figure 2.11 *Basement Terranes of New Zealand with the Maitai Terrane (5) following the thick line in the South Island and the dashed line in the North. Reprinted from (Sutherland, 1999).*

The 250-100 myr old Waipapa Composite Terrane (WCT) is comprised of greywacke, characteristic of a deep sea trench deposit (Ballance, 2009). This terrane predominantly underlies most of the Hamilton Basin and is comprised of the Morinsville Facies, specifically the Manaia Hill Group. Edbrooke (2005) defines the Manaia Hill Group as "massive to poorly bedded, fine to medium grained sandstone with interbedded thin siltstone and conglomerate; some alternating sandstone and siltstone. Sheared locally with common quartz veins"

(Edbrooke, 2005). The WCT is present in both the North and South Islands as shown in figure 2.11 denoted by the number 8 key. The Murihiku Terrane is denoted by the number 4 key in figure 2.9 and lies west of the WCT. Classified into six stratigraphic groups by (Edbrooke, 2005), the Newcastle Group (NCG) specifically, is sutured to the Dun Mountain Terrane in the eastern Hamilton Basin. The NCG is siltstone dominant with fine-coarse sandstone, conglomerate, zeolite veins, tuff beds and sparse shell beds.

2.6.2 Late Eocene - Oligocene Te Kuiti Group and the Miocene Waitemata Group

The Te Kuiti Group is a transgressive deposit formed in the Eocene Epoch during active separation of Zealandia from Gondwana. Gradual submersion of modern New Zealand's basement terranes occurred as the sea floor spread, leading to shallow marine deposition. Coal seam formation began around 41.3Mya (Edbrooke,2005) 37 Ma (Hall, et al., 2006) which marks the base of the Te Kuiti Group. The Waikato Coal Measures (Edbrooke, 2005; Schofield, 1967) are a carbonaceous mudstone with shale, coal seams and rare conglomerate, typical of a shallow marine deposit. The sequence progresses upward through interbedded siltstones and sandstones of the (Mangakotuku Formation-mudstone, Glen Massey Formation- sandstone, Waingaroa Formation-siltstone, Aotea Formation-sandstone) to limestones and sandstones of the (Orahiri Limestone, Te Akatea Formation-siltstone, Waitomo Sandstone and Otorohanga Limestone). Thus the Lower Subgroup is dominated by "carbonaceous mudstone and local coal seams with calcareous siltstone and sandstone", while the Upper Subgroup is dominated by, "sandy and pure bioclastic limestone with calcareous sandstone and rare conglomerate" (Edbrooke,2005). In the upper reaches of the Te Kuiti Group an unconformity marks the base of the Waitemata Group (deposited in the Miocene). In the early Miocene (25-26Ma), the formation of a continental rift initiated block faulting and uplift across New Zealand. This led to the erosion of the Te Kuiti Group down to the Mangakotuku Siltstone in the Hamilton area and full removal in other areas (Kear, 2004; Schofield, 1967). Thicknesses from (Kear & Schofield, 1964) detail the unit thickness being up to 500m and (Hall et al., 2006) estimates similar extents, 180-600m. Specific to the Hamilton Basin, petroleum logs put the unit as 30-228m thick in the north-west.

The Waitemata Group (22-19 Ma) (Hall et al., 2006) underlies the Tauranga Group in the northwestern Hamilton Basin and appears to thin toward the northwest (Edbrooke, 2005). Composed of siltstones and sandstones; the Koheroa Siltstone, Mercer Sandstone and the

Waikawau Sandstone, the group is sandstone dominated with increasing calcareous content toward the base. There is also evidence of subduction related volcanism in the form off tuff beds (Shofield, 1967). The depositional history of the group is not well known and within the Hamilton Basin, Quaternary sediments bury the group. The thickness varies across the basin, up to 839m thick in Rotokauri and as thin as 104m in the far northwest from petroleum logs (Jeong, 2019).

2.6.3 Pliocene to Holocene Tauranga Group

The Quaternary Tauranga Group is the most recent deposit in the Hamilton Basin, with alluvially and fluvially deposited lithology. It is thought to be thickest in the North-western basin based on well logs data and is more widespread than the Late Eocene-Oligocene sedimentary rocks. The two subgroups are the Walton Sub-group and the Piako Sub-group.

2.6.3.1 Late Pliocene to Mid-Pliestocene Walton Subgroup, Ignimbrites and Ash Formations

Southward movement of the Hikurangi subduction front, initiated in Northland in the early Pliocene, led to the flare up of basaltic eruptions of the Alexandra Volcanics Group (AVG) between 2.74-1.54Ma (Briggs et al., 1989). A chain of six calcalic volcanoes, most of which border the south-southwestern boarder of the Hamilton Basin, have an almost straight northwestern alignment. This chain extends from the stratovolcanoes of Karioi (2.31Ma) and Pirongia (2.74Ma-1.6Ma), to the cones of Kakepuku (2.35Ma), Te Kawa (2.21Ma) and the small shield volcanoes in Tokanui and Waikeria (1.99Ma; Briggs et al., 1989). There are 5 corresponding formations in the AVG, Okete Volcanic Formation, Karioi Volcanic Formation, Pirongia Volcanic Formation, Kakepuku Volcanic Formation and Te Kawa Volcanic Formation; all predominantly basaltic lava and tuff (Briggs et al., 1989; Edbrooke,2005). Eruptive material is distributed varying distances from vent sources, however, does not extend into the alluvial plains of the Hamilton Basin.

The Mangakino Caldera MC was active 2.5Ma-950ka (Kear, 2004) marking the relative closure of the AVG eruptions. The MC produced the first of many large eruptions of the Taupo Volcanic Zone (TVZ). There are four distinguishable ignimbrites (Ig) from this caldera, all

classified under the early-mid Pleistocene Pakaumanu Group (figure 2.12). These include the 1.8 Ma Ngaroma Ig (Partly welded, pumice-rich), the 1.23 Ma Ongatiti Ig (variably welded, crystal-rich), the ~1.1 Ma Ahuroa Ig (Mangaokew Formation, partly welded, inverse thermal zonation) and the ~1 Ma Rocky Hill ignimbrite (Raepahu Formation, pumic-rich with inverse thermal zonation) (Edbrooke, 2005; Lowe, 2010).

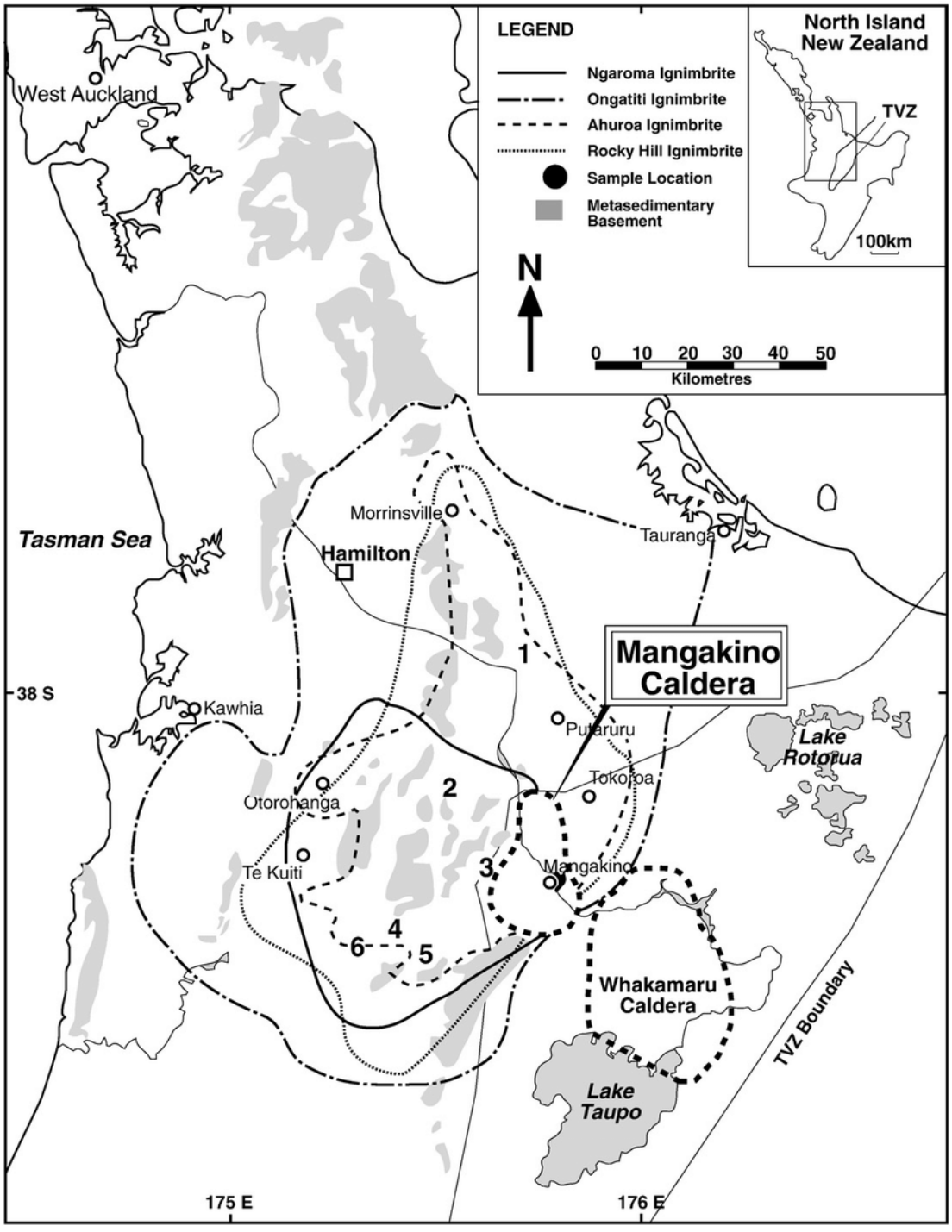

Figure 2.12 *Distribution of the Ngaroma, Ongatiti, Ahurpa and Rocky Hill Ignimbrites from the Mangakino Caldera. Reprinted from (McCormack et al., 2009) who adapted the map from (Briggs et al., 1993) to include field site numbers and sampling locations.*

The Ongatiti Ig has the largest distribution which is expected to be at least 362km in diameter (Kamp & Lowe, 1981) as shown in figure 2.12; reaching the ranges at the northernmost extent of the Hamilton Basin. The Rocky Hill ignimbrite breaches the southeastern alluvial plain of the Hamilton Basin, along the modern day Waikato River near Cambridge. The three youngest ignimbrites are up to 20m thick in the Hamilton Basin (Lowe, 2010).

The Walton Subgroup has a complex and varied stratigraphy as it was deposited during the active volcanic period of the MC so ignimbrites and tephra's are interwoven (Kamp & Lowe, 1981). The subgroup is classified into two formations. The older Puketoka Formation is described as pumice gravels and soft unconsolidated ignimbrite (specifically Ongatiti (Kamp & Lowe, 1981) by (McCraw, 1967) further defined by (Selby & Lowe, 1992) as well sorted pale grey pumiceous clays, sands, breccias and unsorted beds with distal portions of rhyolitic ignimbrite flows. (Edbrooke, 2005) defines the unit as pumiceous silt sand and gravel with interbedded peat, rhyolitic or alluvial pumice, non-welded ignimbrite and tephra. The formation is a bluff forming unit caused by either case hardening or compaction, found up to 540ftasl (164.5masl) (Kear & Schofield, 1964). It was noted by (Kear & Schofield, 1964) that the base of this formation is distinguishable due to the gradual grading into pure pumice.

The Karapiro Formation is the youngest formation in the Walton Sub-group, deposited in the mid-late Pleistocene (Kear & Schofield, 1964). It is an alluvium with weathered volcanic grits, pumiceous and rhyolitic gravelly sands (Kamp & Lowe, 1981) dominated by primary and reworked non-welded ignimbrite (Edbrooke, 2005). The Kauroa Ash Formation (c. 780 ka) interfingers with the Karapiro and Puketoka Formations and in some areas overlies or underlies both formations; in most cases it is <2m thick in the Hamilton Basin due to erosion (Kamp & Lowe, 1981; Lowe, 2010; Selby & Lowe, 1992). It is comprised of weathered, clay-rich rhyolitic tephra and paleosols (Edbrooke, 2005; Kamp & Lowe, 1981). The Hamilton Ash Formation (80-350 ka) which is the younger of the two tephra sequences, is generally 1-3m thick and overlies the Kauroa Ash with an erosional unconformity. Thus, the Hamilton Ash is also interwoven with the formations of the Walton Sub-group (Kamp & Lowe, 1981; Lowe, 2010). The Walton Sub-group outcrops at many locations standing above the Hinuera surface as mapped by (Edbrooke, 2005), and encompassing the ignimbrites and ash formations; are termed the Hamilton Hills by (Kear & Schofield, 1964; Lowe, 2010). Figure 2.8a from (Edbrooke, 2005) shows a west-east cross section through the Hamilton basin, with the Walton Sub-group depicted as being thickest in the west, not extending below ~1000mbsl.

2.6.3.2 Mid-Pliestocene - Holocene Piako Subgroup

The Hinuera Surface is the extensive alluvial plain underlain by Quaternary alluvial deposits throughout the Waikato Basin (the Hinuera Formation (HF)). Volcanogenic in origin, the Hinuera Formation is characterised by gravels, gravelly sands and silts with localised peat deposits (Hume et al., 1975; McCraw, 1967; Schofield, 1965; Schofield, 1967). Lithology varies from current bedded sand to pumiceous sand with quartz and, feldspar interbedded with rhyolitic gravel to peat deposits, pumice clays and silts; each joined with irregular erosional contacts (Hume et al., 1975; Schofield, 1965). The Hinuera Formation is fanned throughout the Hamilton lowlands, following old wandering river channels and underlying peat bogs. Finer sediment has settled in the old channels, separated by levees of coarser material. Thickness ranges from up to 90m in the southern basin, down to 10m in the north and near Walton Sub-group hills, this is due to a sourthern sediment loading source through the Hinuera Gap near Cambridge (McCraw, 2011).

Historically, the ancestral Waikato River followed a course through the Hauraki Basin, discharging into the Firth of Thames. In the late Pleistocene, this river was redirected through the Hamilton Basin, this change of course is attributed to tephra build-up and subsequent aggradation at the 'Hinuera junction' (McCraw, 1967). The 'Hinuera Surface' of which there are two, refers to an alluvial plain with an aged based differential where Hinuera-1 is older and Hinuera-2, younger. Of the two surfaces, Hinuera-2 is dominant north of the disjunction in the Hamilton lowlands (Schofield, 1965).

The distinction between the HF and the younger Taupo Pumice Alluvium (TPA) is the presence of charcoal in the TPA which is not found in the HF. Sourced from the Taupo shower material the TPA is a subaqueous Holocene deposit dominated by pumice, sand, silt, gravel and charcoal (Edbrooke, 2005; Schofield, 1965). The Melville member consists of silts and sands of pure pumice and is confined to terrace margins and lakes. The Hohapu sand member is pumiceous coarse sand and grits with charcoal fragments which is confined to the terrace centre (Kear & Schofield, 1964). North of Ngaruawahia towards Huntly the TPA buries the Hinuera-1 surface, however, in the Hamilton Basin it varies from 0-30m thick across Hinuera-1. The TPA surface decreases in elevation 0.7m per 1km from Cambridge to the Waipa river junction in Ngaruawahia.

Chapter 3

Active and passive surface wave methods

The Hamilton Basin is a deep predominantly alluvial infilled graben structure which tilts to the North- West following the dip on the underlying basement rock. The depth of the basement rock combined with the extent of the soft sediment that overlies it creates in theory, ideal conditions for site amplification (increase in ground shaking) and increased earthquake risk. One of the ways to evaluate such an effect is to characterise the subsurface velocity structure; on a regional scale this structure can be resolved by using surface wave methods which are non-invasive. The dispersive characteristics of surface waves in vertically heterogeneous media allow for the analysis of subsurface shear wave velocity profiles through an inverse solution. This chapter discusses the surface wave methods used in this research to produce a shear wave velocity model for the Hamilton Basin.

A shaded relief map of the study area and the locations of all surveyed sites is given in figure 3.1. Each site has been given a code, which will be referred to in subsequent chapters. The co-ordinates for all sites are given in table 3.1 below, along with the list of associated codes and the maximum and minimum array diameters used at each site. Site locations are in figure 3.1.

Table 3.1 *Coordinates, site codes and array diameters (d), minimum (dmin) & maximum (dmax) for all surveyed sites in the Hamilton Basin*

Site name	Site code	Latitude	Longitude	dmax (m)	dmin (m)
Kainui Road	(KN)	-37.661820	175.217135	150	50
Gordonton	(GD)	-37.658795	175.323065	1200	50
Te Rapa	(TR)	-37.749458	175.177178	1500	50
Elliot Park	(EP)	-37.783230	175.239750	150	50
Temple View	(TV)	-37.827408	175.232564	1000	5
Hamilton Boys High	(HB)	-37.785057	175.296666	200	50
Ruakura	(RK)	-37.779211	175.328247	1000	50
Kiroa Road	(KR)	-37.724053	175.369607	150	50
Tamahere	(TM)	-37.816514	175.415889	150	50
Ohaupo Road	(OP)	-37.882900	175.317122	150	50

McGregor Road	(MG)	-37.906643	175.272696	1200	50
Ngahinapouri	(NP)	-37.892493	175.212413	150	50
Ngaroto	(NO)	-37.971002	175.274903	150	50
Wallace Large	(WL)	-37.955518	175.395975	1200	50
Wallace Small	(WS)	-37.929448	175.382665	150	50
Saint Peters	(SP)	-37.888065	175.423922	600	50

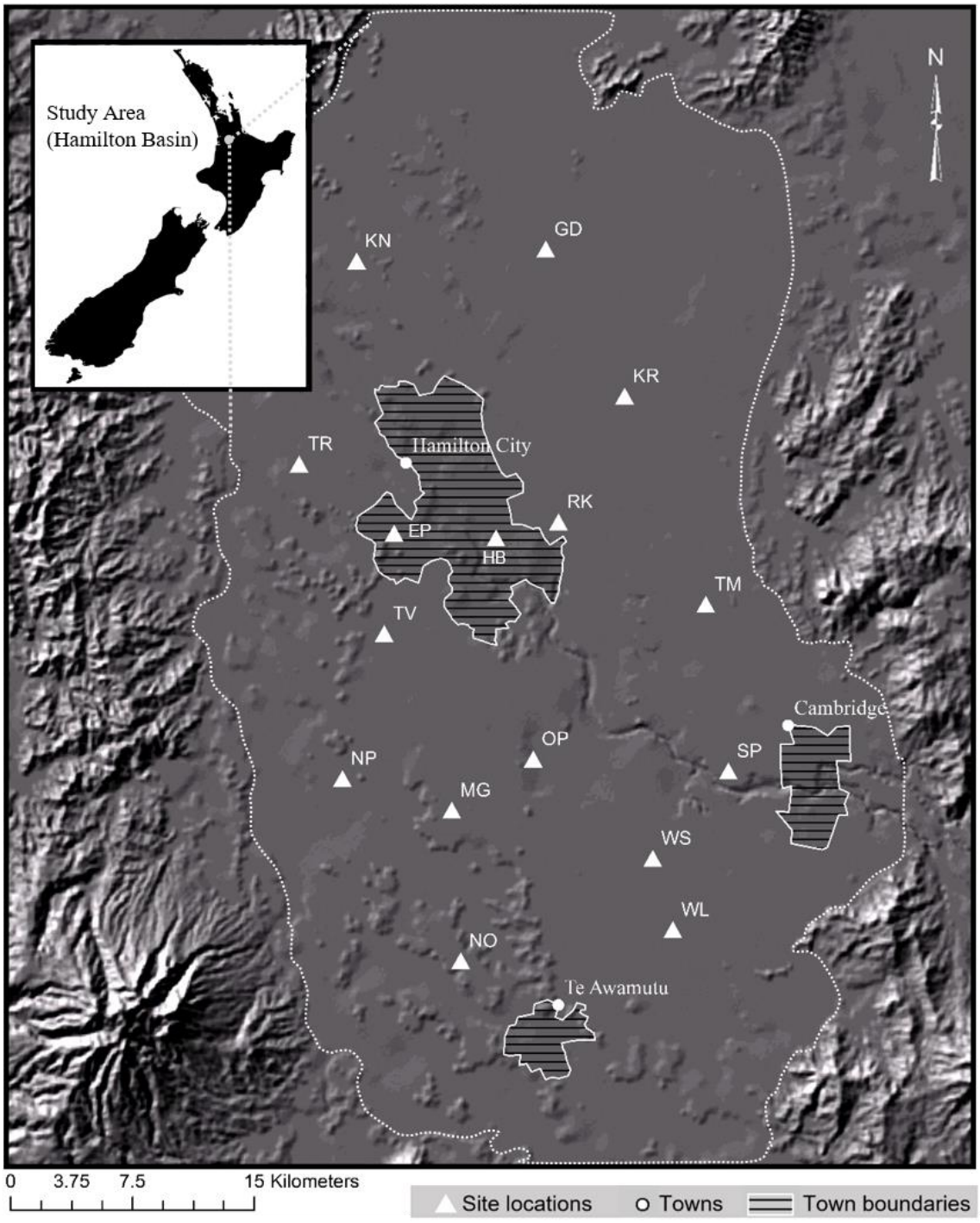

Figure 3.1 *Shaded relief map of the Hamilton Basin set within the North Island of New Zealand. Sourced from the LINZ Data Service and licensed for reuse under the CC BY 4.0 licence. Surveyed sites are denoted by triangles with town boundaries given for indication of relative position. Site codes given in this figure are elaborated on in table 3.1. The dashed line indicates the basin extent.*

Given the geometric constraints of the microtremor array layouts, site selection was limited to large land parcels and further limited by access permissions. As a result, fifteen sites were selected for analysis, some on smaller land parcels to gain near surface information for interpolation between large sites. All sites were spaced for adequate coverage of the basin, centred near densely populated areas and areas of interest. This included different surface lithologies, potential fault presence and in the case of HBHS, a strong motion station. Site planning was based on land access, farm size and time constraints.

The array layouts used at each site are given in the site maps in appendix A, all data processing figures are given in appendix B. While many methods exist for the inversion of surface waves, the theory involves three repetitive steps, acquisition, processing, and inversion. For the objectives of this research two geophysical acquisition methods were chosen, Multichannel analysis of surface waves (MASW) (Park et al., 1999; Xia et al., 1999) and Microtremor array measurements (MAM) (Aki, 1957).

3.1 Data acquisition

For all methods, ground vibration data are acquired, what differentiates active from passive is the specific way in which this data are collected. Active methods involve artificial ground motion, while passive methods rely on ambient vibration. Both active and passive methods needing suitable technical equipment, hardware and specific procedures described below. When determining the subsurface velocity structure at a regional scale, predominantly for use in ground motion simulations, it is best to combine the two methods based on expert analysis (Foti, 2017). This is due to the wider frequency range gained from combining high frequency (5-50Hz) active data with lower frequency (0.5-20Hz) passive data which allows for deeper investigation and identification of the fundamental mode (Park et al., 2005).

Acquisition advice was followed from (Foti, 2017; Socco, 2010) and depended on the site specifics including the maximum expected wavelength and geological complexity, for example, the potential for velocity reversals from soil to rock to soil layers.

3.1.1 Multichannel analysis of surface waves (MASW)

Multichannel analysis of surface waves (MASW) developed by (Park et al., 1999; Xia et al., 1999), is a commonly utilised surface wave method. This is due to the wider applicability of the method to geotechnical and earthquake engineering; compared with other methods which are more limited in application such as spectral analysis of surface waves (SASW) (Socco et al., 2010). In particular, this method is used to find V_{s30} (the shear wave velocity to the depth of 30m), a parameter widely adopted in earthquake engineering applications. For this research, a single 48m-long linear array of 24, 2m spaced geophones of 4.5Hz frequency were used to record surface wave propagation. Surface waves were generated by an impact-triggered sledgehammer, which struck a metal plate (figure 6). This acquisition set up allowed for adequate resolution of the near V_{s30}.

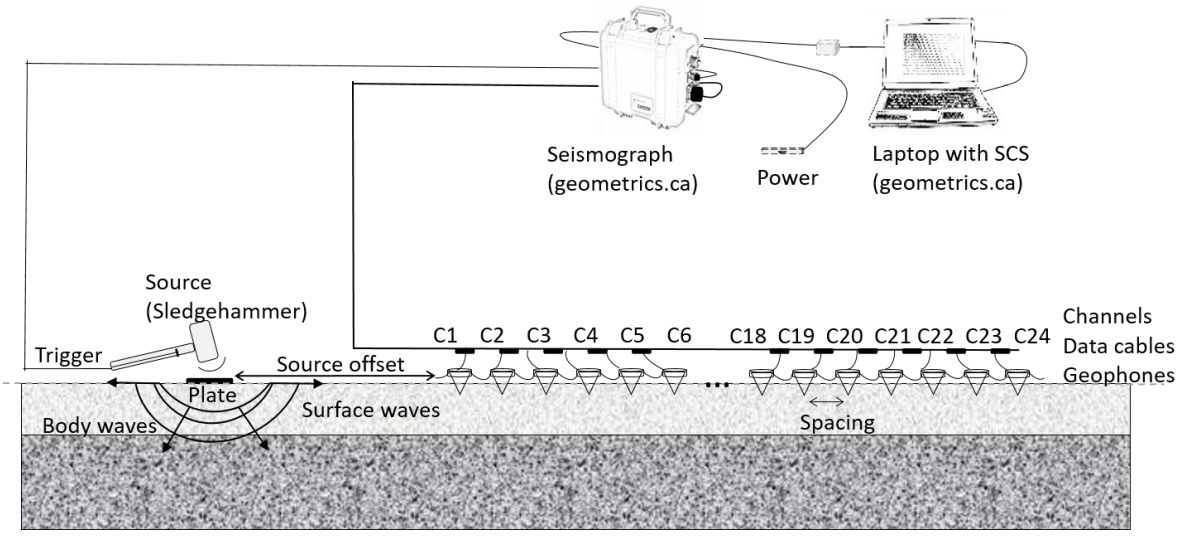

Figure 3.2 *Field testing configuration for Multichannel analysis of surface waves (MASW).*

Assuming consistent geological conditions across the Hamilton Basin, 2m spacing was used at all sites. This was the ideal spacing given the lower resolution in the near surface with larger spacing compared to the higher resolution with smaller spacing. The 48m array length was chosen due to the expected wavelength at the site being 2x the array length. As a result 24 receivers were used to satisfy the array length and spacing requirements. Reseach from (Foti et al., 2011; Foti et al., 2017; Bard et al., 2010) suggested that a minimum of 24 receivers are used. This is to minimise aliasing, which occurs when too few receivers are used. It is also to minimise far field effects, where the surface wave signal blends in with ambient noise, which occurs when too many receivers are used. Recommendations by (Foti, 2005) included having forward (from the C24 end, figure 3.2) and reverse (from the C1 end, figure 3.2) shots to reduce

the impact of near field effects and lateral variations. For this research, shots were taken at source offsets of 5, 10 and 20m either side of the array (i.e. from C1 and C24 in figure 3.2). All MASW surveys were conducted in favourable weather (low wind, no rain) away from cultural noise and when possible in between noise events (e.g. after vibrations were no longer evident from a passing car). For each offset, 10 shots were stacked to increase the signal-to-noise ratio, and geophones were always coupled to the ground (thick grass was removed from the receiver base) to ensure quality signal. Each survey was quality controlled using the geometrics seismodule controller software (SCS) (www.geometrics.com) to reduce noise in the dataset, particularly from anthropogenic sources. SCS was used to check that all receivers were recording before acquisition and that the acquired signal spanned the entire time window and was not cut off. A 2s recording time is recommended as adequate by (Foti, 2017); in this study a 3s window was used for all sites.

3.1.2 Microtremor array method (MAM)

MAM is used in site characterisation because the velocity structure can be resolved to considerable depths of 1 km or more (Socco, 2010). For this research, MAM was used as a passive surface wave method to obtain the shear wave velocity structure down to depths of 1.5 km (Aki, 1957; Foti, 2017). The term passive refers to the vibration source being ambient vibrations from sources such as wind, rain, traffic or construction, rather than user-created vibrations such as those in MASW where active input is required. To suit acquisition requirements, broadband 3-component 20s seismometers (trillium compact vault seismometers, Nanometrics.ca) were used due to the long natural period of the seismometer (20s) allowing for a deep investigation. Initial array design was programmed using Python and **Google Earth,** programmed locations were loaded into a Garmin Montana 300 680T (Garmin.com) which served as waypoints for field deployment (figure 3.4). Care was taken to deploy sensors using the prescribed method from (nanometrics.ca) whereby all sensors were powered on and waited on to sync to a GPS position before initial deployment at a site. Following this a hole was created in the soil and each sensor was levelled using the tilt bubble as per the schematic in figure 3.4. Deployment documentation outlines that a tilt error of up to 5° is acceptable but each deployment was as close to 0° as possible. Orienting the sensors magnetic north was imperative to obtaining a quality signal for analysis, commercial grade compasses were used to achieve this. Much like MASW, separating noise from the signal is important and reducing noise where possible is recommended. For all sites the seismometer was buried in line with

ground level and the surrounding soil was compacted using a trowel to ensure tight coupling between the seismometer and the soil, whereby the seismometer would not decouple with the soil when some force was applied (Foti, 2017). At all sites bar one, surveys were conducted in reasonable weather conditions, with buckets deployed over the sensors at Elliot Park in intermittent mist. Field images of the MAM setup are given in figure 3.3 below.

Figure 3.3 *Multichannel analysis of surface waves field-testing setup. a) Seismometer array deployed in the field, diameter of 5m in the image is usually a diameter of 50m+, b) Equipment used in the survey, c) Close up of seismometer installed.*

Many of the surveys were on farmland with numerous vibration source; where vibration sources such as vehicles entered the array, times were recorded and stock were ensured to be outside of the arrays. Other noise sources such as trees, busy roadways and railways were avoided where possible. 13 of the 15 surveyed sites were on flat land with minimal variation in elevation across all arrays, two sites had mildly varied topography but were within the 2m elevation change recommended by (Foti, 2017). While the handheld GPS units assisted with initial deployment, accurate sensor location recording is essential for surface wave analysis. For all sites a Leica GS16 GNSS RTK rover was used to survey seismometer positions after deployment. With RTK enabled the accuracy of these surveyed positions was 8mm+-0.03 (Leica, n.d.). The general MAM method and associated components used across all sites and described in this section are depicted in figure 3.4. Circular array geometry was used to allow for multidirectional analysis at all sites except for Te Rapa where space constraints meant that a triangular array was better suited to allow for a deeper survey; either geometry is highly suitable for MAM surveying (Foti, 2017). Array diameter is directly linked to survey depth similar to MASW, the larger the array the deeper the resolvable velocity structure is. Array diameters were selected for each site based on expected basement depth at that location and in some cases the space available. Multiple circular arrays were deployed at each site with varying

diameters, typical combinations were 50, 150 or 200, 400 or 600, 1000 or 1200 with max and min diameters given in table 3.1 for all sites. As shown in figure 3.3a and figure 3.4 in plan view, 7 seismometers were placed around the perimeter of the circle and one in the centre.

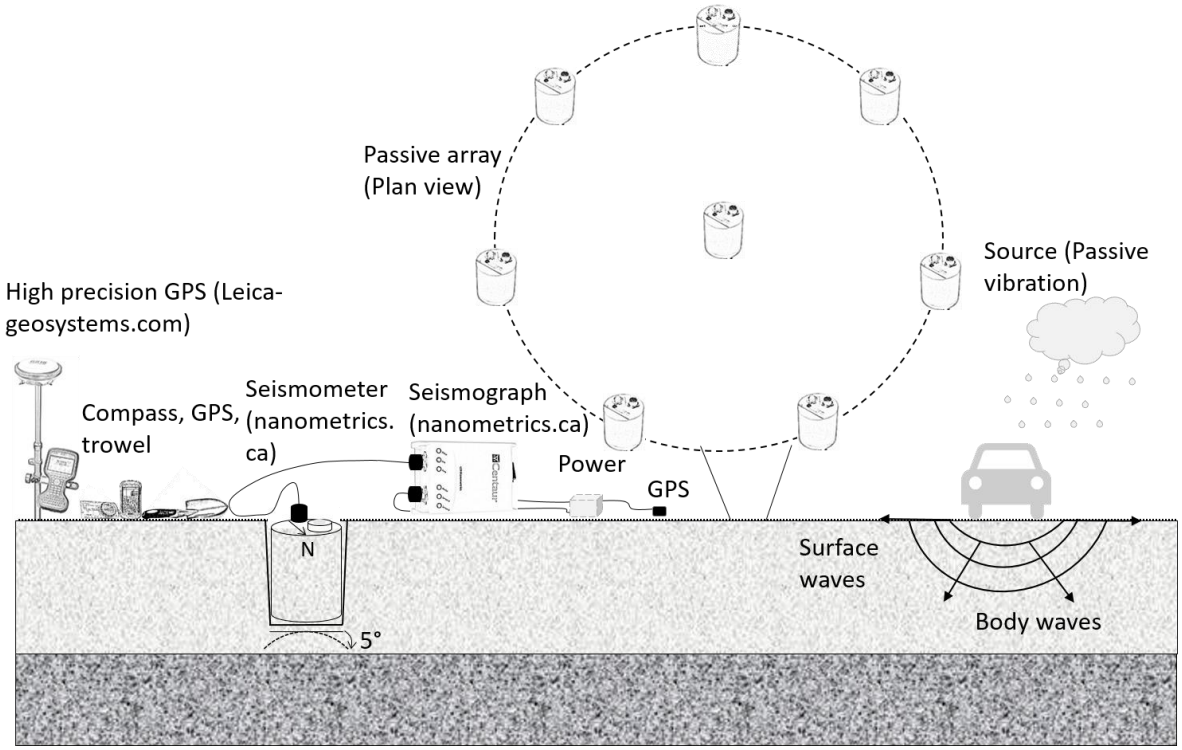

Figure 3.4 *Field testing configuration for the Microtremor array method (MAM).*

The time window for MAM is significantly longer than MASW and is related to array diameter. For this research a small 50 m array was surveyed for 60 minutes and a 1000 m array was surveyed for 180 minutes, this follows advice from (Foti, 2017) on array size and time windows. This ensures that enough signal is obtained for analysis, to account for possible noise trimming and signal cutting

3.2 Surface wave processing

3.2.1 Multichannel Analysis of Surface Waves

Dispersion data were obtained from the MASW survey using the frequency domain beamformer method from (Zywicki, 1999). Experimental dispersion data was extracted from the Rayleigh wave raw data files for each source offset, statistically analysed and then plotted

for manual analysis. Obvious outliners and inconsistent data were removed from the experimental dispersion data. Near field effects, higher modes and lateral variations were identified and removed from the dispersion where applicable.. Each stage in the analysis process is given in figure 3.5 using the MASW data acquired and analysed for the Elliot Park (EP) site. The final output is saved as a dataset of dispersion statistics and the coefficient of variation is modified before the curve is analysed with the MAM dispersion curves in Dinver (Geopsy.org).

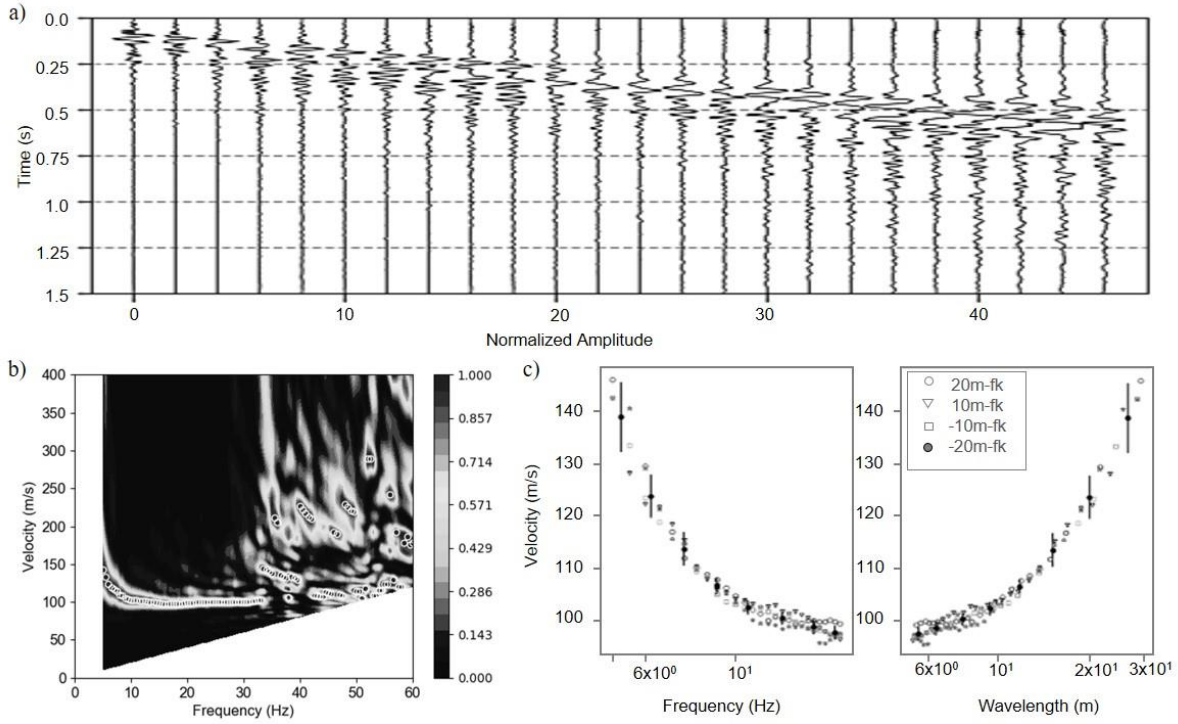

Figure 3.5 *Processing of the multichannel analysis of surface waves dataset for Elliot Park (EP) with (a) Raw data from a single acquisition/shot (b) Automatic multiple source stacking and fk dispersion curves (c) Final dispersion curve with all curves from b for each source offset*

3.2.2 Horizontal-to-Vertical Spectral Ratio processing

A ratio of horizontal to vertical movement (H/V) can be extracted from the recorded ambient vibration of the ground due to the elliptical propagation of Rayleigh waves, the H/V ratio at each site is dependent on subsurface geology. Methodology for evaluation of the H/V ratio was developed by (Nakamura, 1989) and further developed during the SESAME project in 2005 (SESAME team, 2004). Obtaining H/V curves for joint inversion with dispersion data can help to evaluate sharp impedance contrasts, increasing the reliability of the determined velocity structure (Parolai et al., 2005). Obtaining these curves is also beneficial because it indicates

possible site conditions including the expected frequency range, this is particularly useful where no a priori information is available; as was the case for all survey sites in this research except Te Rapa. H/V curves were obtained through analysis of single seismometer ambient vibrations for each site in the Geopsy platform (Geopsy.org). A 0.1-30Hz frequency band was used for analysis as well as an automatically selected 180s sampling window with 100 samples, these parameters were adjusted to suit resulting curves.

3.2.3 Microtremor Analysis of Surface Waves

Rayleigh wave data was processed in Geopsy, an open source software developed for surface wave analysis (www.geopsy.org), using the high resolution FK-transform (HFK) method developed by (Capon, 1969) and the modified spatial auto correlation method (MSPAC) from (Bettig et al., 2001). For all sites the vertical components of each signal were analysed, to do this each signal was grouped per array and field coordinates attached to each signal for HFK analysis. The processing steps are summarised in figure 3.6 below, for both methods.

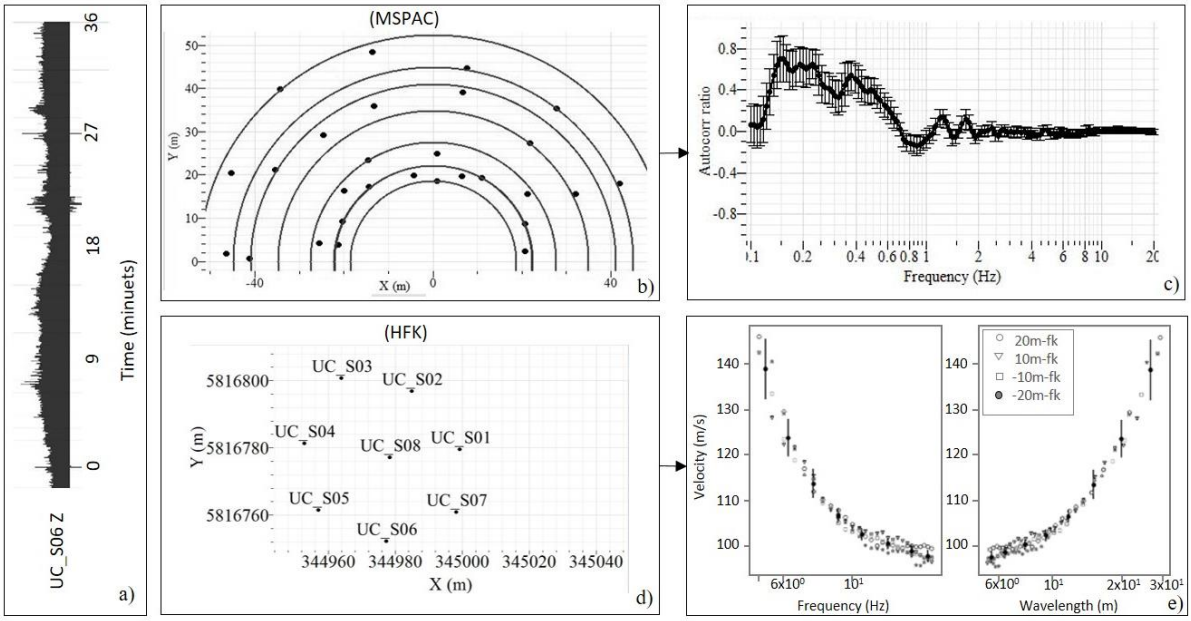

Figure 3.6 *Modified spatial autocorrelation (MSPAC) and high resolution FK-transform (HFK) processing. (a) Vertical signal used in both analyses (b) MSPAC co-array map used in developing (c) MSPAC autocorrelation curve (d) HFK seismometer array map used in developing (e) HFK dispersion curve.*

A 0.1-30Hz frequency range was used as well as either a 180s or 240s sampling window with 125 samples for the HFK analysis. These same parameters were used for the MSPAC

processing, the difference in the two methods is the requirement for setup of the co-array map which designates receiver pairs in the array and that autocorrelation curves are produced rather than typical dispersion curves. Both analysis are undertaken in Geopsy. While care is taken to identify sources of error such as outliers, higher modes and aliasing, experimental dispersion curves often include uncertainty. Modifying the co-efficient of variation post processing ensures that a curve with less uncertainty is not prioritised in the inversion.

3.3 Surface wave inversion

The final step in resolving the subsurface velocity structure is the inversion of the obtained dispersion curves. Several inversion methods exist, for this research the neighbourhood algorithm method by (Wathelet, 2008) was used. The layering ratio method (LRM) by (Cox & Teague, 2016) was used to avoid the selection of unrealistic profiles from parameterisation chosen with a lack of a priori information. Inversion curve selection is a meticulous process based on dispersion curve fit; passive and active dispersion curves are combined to create an experimental dispersion curve for a particular site. Ideally these curves should overlap in the fundamental mode, provided array diameter combinations were adequate for the given site conditions (Foti et al., 2017). Each curve for this research was resampled to 30 points between 0.1-30Hz on a logarithmic scale, reducing data points for the experimental curve in order to accelerate the inversion while still retaining accuracy (Teague & Cox, 2018). This process of resampling dispersion curve points is depicted in figure 3.7 below.

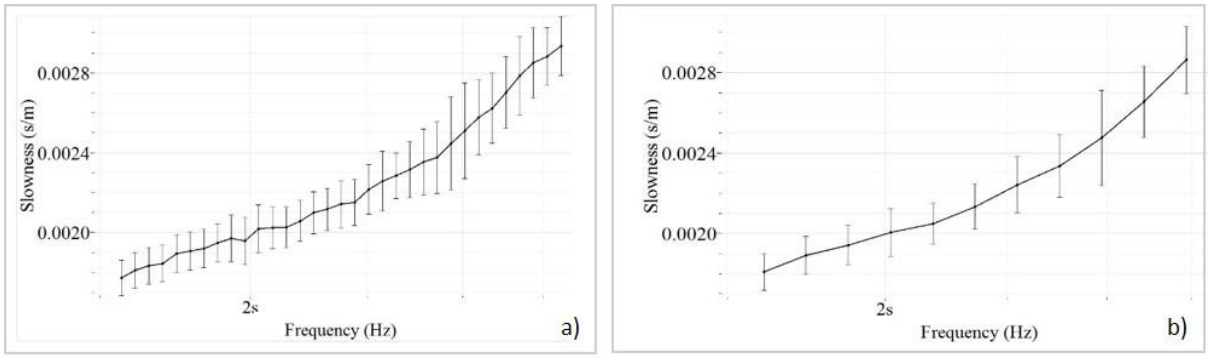

Figure 3.7 *Example of resampling of data points for a dispersion curve from a 150m passive array for the Ohaupo site. a) Un-resampled dispersion curve b) Dispersion curve resampled to 30 points between 0.1-30Hz.*

Curves with overlap in the fundamental mode were averaged for all sites; where the opposite occurred and curves were separated by a frequency band (common for all peat sites) the data range was left blank, which may decrease the reliability of the inversion for these peat sites (Foti et al., 2017). Where higher modes were identified dispersion curves were cut rather than averaged and designated a mode classification for the inversion (i.e. mode 1), these are identifiable as higher velocity regions that do not fit the overall dispersion trend. While it is important to distinguish higher modes, they are not removed because they contribute to model accuracy through being sensitive to particular parameterisations (Socco et al., 2010).

Careful parameterisation selection is critical in the inversion process because the resulting model is sensitive to the layering chosen (Cox & Teague, 2016; Foti et al., 2017; Socco et al., 2010). For this research the LRM was chosen for parameter selection to perform a blind analysis for all sites. Layering ratios are a multiplier which designate that the thickness of an underlying layer will continue to increase based on the potential thickness of the layer above it" (Cox & Teague, 2016) . Common layering ratios are 1.2, 1.5, 2.0, 4.0, 5.0 and 7.0 (Cox & Teague, 2016). The layering ratio methodology is programmed with the high and low extents of the experimental dispersion curve, to produce a suite of parameterisations. For this research layering ratios were chosen based on site conditions, commonly 1.5-7.0 at larger sites and 1.2-4.0 at smaller sites. The neighbourhood algorithm embedded in the Dinver platform creates theoretical profiles that fit the experimental data provided, constrained by the parameterisations set. For this research 1,000,000 models were created for each layering ratio to adequately explore the parameter space. The joint inversion method by (Parolai et al., 2005) was also used where the H/V curves are used in the inversion to constrain the final model and inversions were run for each layering ratio with and without the fundamental site peak. This has been shown to increase model reliability, particularly at depth (Parolai et al., 2005).

The best1000 shear wave velocity profiles with the lowest misfit (best fit between the theoretical model and the experimental dispersion curve) are obtained from the analysis. The best1000 profiles for the Ngaroto site are shown in figure 3.8(b). Presenting the final 1000 profiles is an effective way to display uncertainty from solution non-uniqueness and is commonly used in the literature (Deschenes, 2017; Foti, 2017). While the lowest misfit (LM) profiles are usually ideal in some cases the lowest misfit may not be representative of the subsurface geology due to some constraining factor such as over or under constraining within the parameterisations. The final step is to compare the velocity profiles against the parameterisations to check for over-constrained results (profile follows parameters) and under-constrained results (large variance in V_s and depth). This will determine which layering ratio

produced the most suitable velocity profiles for the site. Statistical analysis on inversion results and correlation of profiles with *a priori* information helps to reduce uncertainty and improve model reliability.

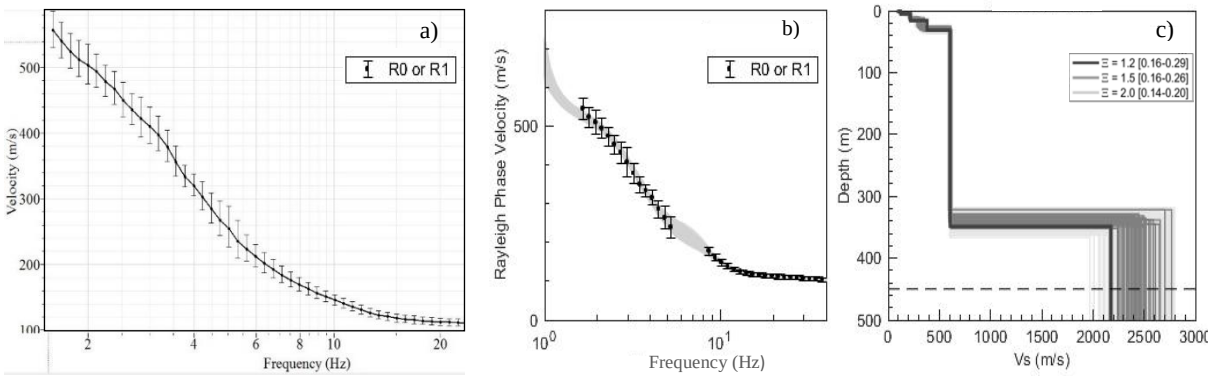

Figure 3.8 *Summarised inversion process using data from the Ngaroto site (NG) (a) Experimental dispersion curve used in the inversion, (b) Theoretical dispersion curve fit to the experimental for each layering ratio. (c) Best1000 lowest misfit profiles for each layering ratio from the inversion analysis.*

A relationship between array resolution limits, array diameter and number of stations (N) has been defined by (Jongmans et al., 2005) in table 3.2 below used to apply resolution limits to all sites in this study. Where $d_{i,j^{min}}$ is the minimum interstation distance, $d_{i,j^{max}}$ is the maximum interstation distance and r is the array radius. $\lambda^{min}$is the minimum wavelength and λ^{max} is the maximum wavelength.

Table 3.2 *Resolution limits for number of stations (N) and array diameter from the SESAME Project. Reprinted from (Jongmans et al., 2005) , table1.*

N	exact		approximate	
	$d_{i,j^{min}} - d_{i,j^{max}}$	$\lambda^{min} - \lambda^{max} - 3 * \lambda^{max}$	$d_{i,j^{min}} - d_{i,j^{max}}$	$\lambda^{min} - \lambda^{max} - 3 * \lambda^{max}$
7	0.87*r – 1.95*r	1.74*r – 1.95*r – 5.85*r	0.90*r – 2*r	1.80*r – 2*r – 6*r

The V_{s30} has been calculated by calculating the travel time through each layer (distance/velocity) to 30m in the lowest misfit profile for each site to find the average V_s in the upper 30m.. Where d_i is the thickness of layer (i) and V_{si} is the velocity of the layer (i).

The calculation is given in equation 3.1 below:

$$V_{s30} = \frac{\sum d_i}{\sum \frac{d_i}{V_{si} si}} \tag{3.1}$$

3.4 A priori Information

The Hamilton Basin has limited availability of geological data compared to other regions in New Zealand which limits the use of *a' priori* information in the surface wave inversions for the entire basin. Eight petroleum wells logged in the 1970's reach the basement rock, all of which are located in the northern end of the basin. Surface data is available in the form of groundwater stratigraphic logs from the Waikato Regional Council as well as CPT and auger data from the New Zealand Geotechnical Database.

3.4.1 Waikato Regional Council groundwater boreholes, petroleum boreholes and the New Zealand Geotechnical Database (NZGD)

Stratigraphic logs for groundwater bores in the Waikato region are publicly available through the Waikato Regional Council groundwater database. The database contains 11,600 bores, of which some do not contain stratigraphic logs and most are less than 20m in depth with only a small number exceeding 100m in depth. Of the logs that are available, all are compiled by drill loggers rather than geologists, so materials are described in a general sense as 'peat' 'clay' 'sand' rather than with lithological accuracy. To add to the limitations, not every test site had a groundwater bore on or near the array locations, so this resource was used on a 'where-available' basis and looked at with high uncertainty.

There are eight petroleum well logs in the Waikato Region, all of which are available for download on the Petroleum and Mineral Exploration Database. All logs extend to basement rock making them particularly useful for the inversion process, however, land access and site suitability drawbacks meant only the Te Rapa site was directly over one of these logs. Each log is a raw stratigraphic column with no subsequent interpretations of geological formations. It is therefore up to the interpreter to decide which stratigraphic sequence represents which formation.

The CPT and hand auger data available on the NZGD was used where applicable although the CPT data commonly goes to less than 20m and hand auger data less than 2m. These were therefore not useful for the analysis of deeper sites.

Chapter 4

Shear wave velocity profiles in the Hamilton Basin

4.1 Introduction

This section details the final inversion results for all fifteen sites within the Hamilton Basin, presenting the best-fit shear wave velocity models, resulting from the extensive analysis detailed in chapter 3. The experimental dispersion curves and H/V peaks used in the inversion are also included in this section as well as the velocity profiles for each site. The geology of the Hamilton Basin was expected to be relatively homogenous with shear wave velocity increasing with depth allowing for a simpler inversion model. However, the peat bogs, which cover a large proportion of the basin surface, presented unique difficulties in near surface resolution with markedly low shear wave velocities within a small range of frequency. It is important to note that the results in this study are intended for seismic response analysis and therefore the near surface is not studied in detail, is limited by lack of site-specific geological information and resolution limits apply. Geological units were expected to be varied across the surveyed sites with little *a'priori* information available. All field layouts can be found in appendix A, and all processing workflows and tabulated dispersion curves in appendix B.

4.2 Southern Basin

The southern basin is south of an inferred line between Tamahere and McGregor Road sites. This is useful in separating the results based on geology and highlights the contrasting results for the Northern basin in the sedimentary basins. The southern basin has limited *a' priori* information compared to the northern basin since the focus of economic interest was to the northwest.

4.2.1 Saint Peters (SP)

The processed experimental dispersion curve for Saint Peters (figure 4.1a) spans a frequency range of 0.7-24 Hz. The resampled 600m array curve, which corresponds to the low frequency high velocity curve in figure 4.1a, has notably large standard deviations, expected for dispersion curves at lower frequencies.

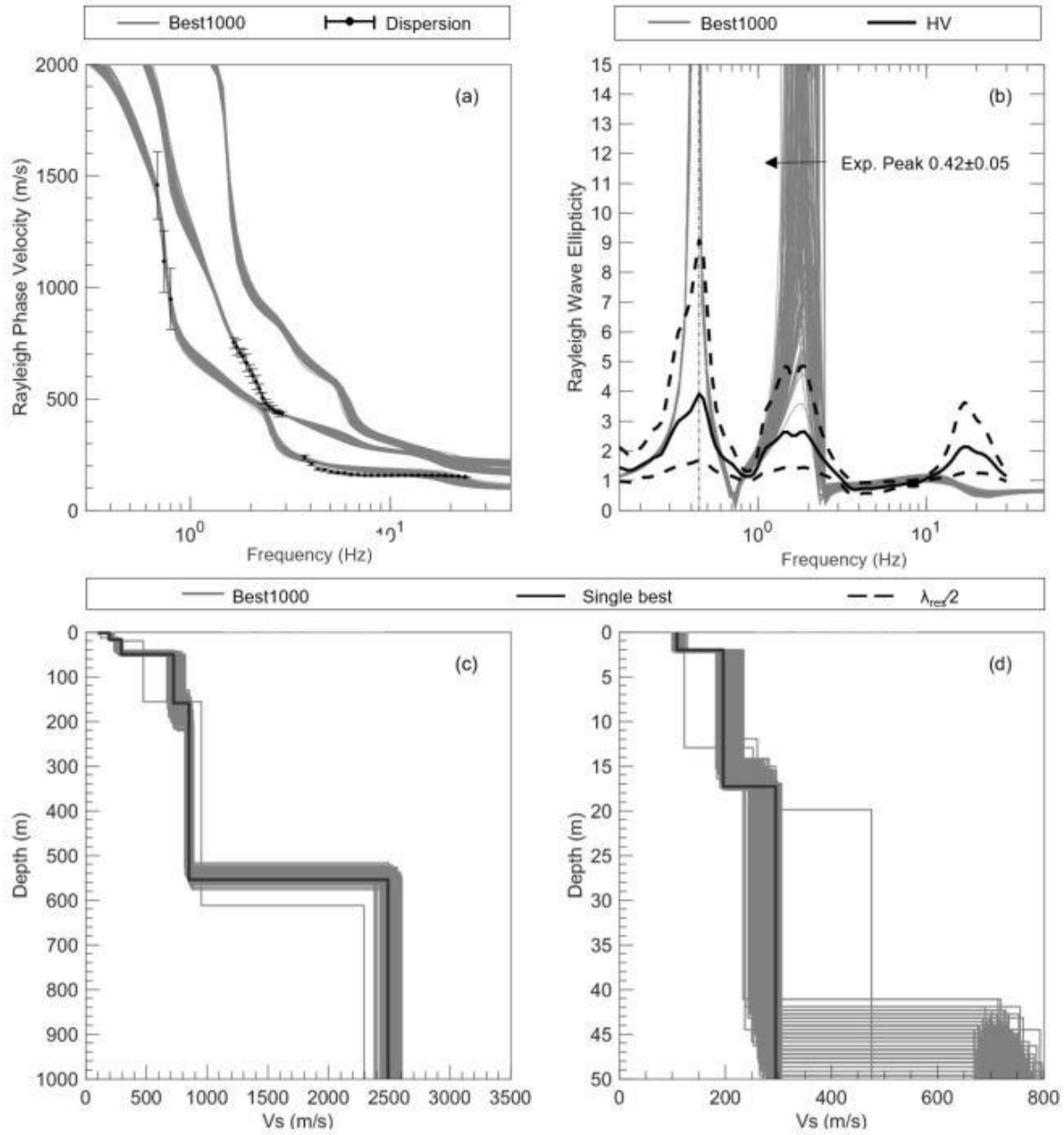

Figure 4.1 *Surface wave inversion results for Saint Peters (SP). a) Experimental and best1000 theoretical Rayleigh wave dispersion curves. b) Experimental and best1000 theoretical Rayleigh wave ellipticity curves with the fundamental frequency used in the inversion. c) Best1000 shear wave velocity (V_s) models down to basement (in grey) with the lowest misfit profile in black. A 1200m off graph resolution limit applies (approximately $\lambda_{max}/2$). d) Best1000 shear wave velocity (V_s) models for the upper 50m (in grey) with the lowest misfit profile in black*

The data from 1.2-3Hz corresponding to the 200m array was inverted as a higher mode in the final inversion, which resulted in the lowest-misfit models of shear wave velocity to the experimental dispersion curve in table 4.1 (0.226 as higher mode versus 0.69 fundamental mode) and less variability in V_s with depth. An inversion with the 200m dispersion curve removed produced a similar lowest-misfit of 0.278 (table 4.1, inversion 4) however, the resulting models were highly variable ±500m/s, 100m. The final inversion presented in figure 4.2 is with the peak, due to the lowest-misfits being significantly lower with than the inversions without (table 4.1, inversion 3).

Table 4.1 *Saint Peters inversion; misfits between the experimental dispersion and theoretical data for three different dispersion curves with and without the fundamental peak frequency.*

	1 – A fundamental mode dispersion curve inversion		2- 200m dispersion curve set as a higher mode		3- 200m dispersion curve removed from the inversion	
Layering Ratio	With Peak	No Peak	With Peak	No Peak	With Peak	No Peak
1.5	3.58	0.88	0.249	0.346	0.376	0.482
2.0	3.44	0.86	0.246	0.323	0.33	0.465
3.0	3.33	0.8	0.241	0.330	0.291	0.448
4.0	3.25	0.69	0.226	0.304	0.278	0.440
5.0	4.02	0.81	0.12	0.339	0.287	0.452

The overlap between the active and passive dispersion curves was agreeable which increases the reliability of the near surface inversion. Experimental (HVSR) peak amplitude is ~3.8 with a second lower amplitude peak at a slightly higher frequency (~1.8Hz) (figure 4.1b). The best1000 theoretical models follow the fundamental frequency at 0.42±0.05Hz with slight variation due to the influence of love and body waves on the experimental results. These theoretical models also follow the higher frequency peak near ~1.8Hz, closely in line with the experimental data.

Shear wave velocity increases from 196m/s to 295m/s at 17m and the underlying layer increases to 724m/s at 50m (figure 4.1d). The next underlying layer increases to 851m/s at 160m with basement depth at 554m, indicated by the rapid velocity increase to 2490m/s (figure 4.1c). Shear wave velocity averages to 215m/s in the upper 30m. The conditions at this site do not meet the criteria for a class B, C or E site. With a fundamental period of 2.4s and V_s>150m/s in the upper 10m, this is a class D site (NZS1170.5, 2004).

4.2.2 Ngaroto (NO)

Given the largest array diameter at this site was 150m, the resulting processed dispersion curve spans a higher frequency range (1.4-20Hz) (figure 4.2a) compared to the previous Saint Peters site.

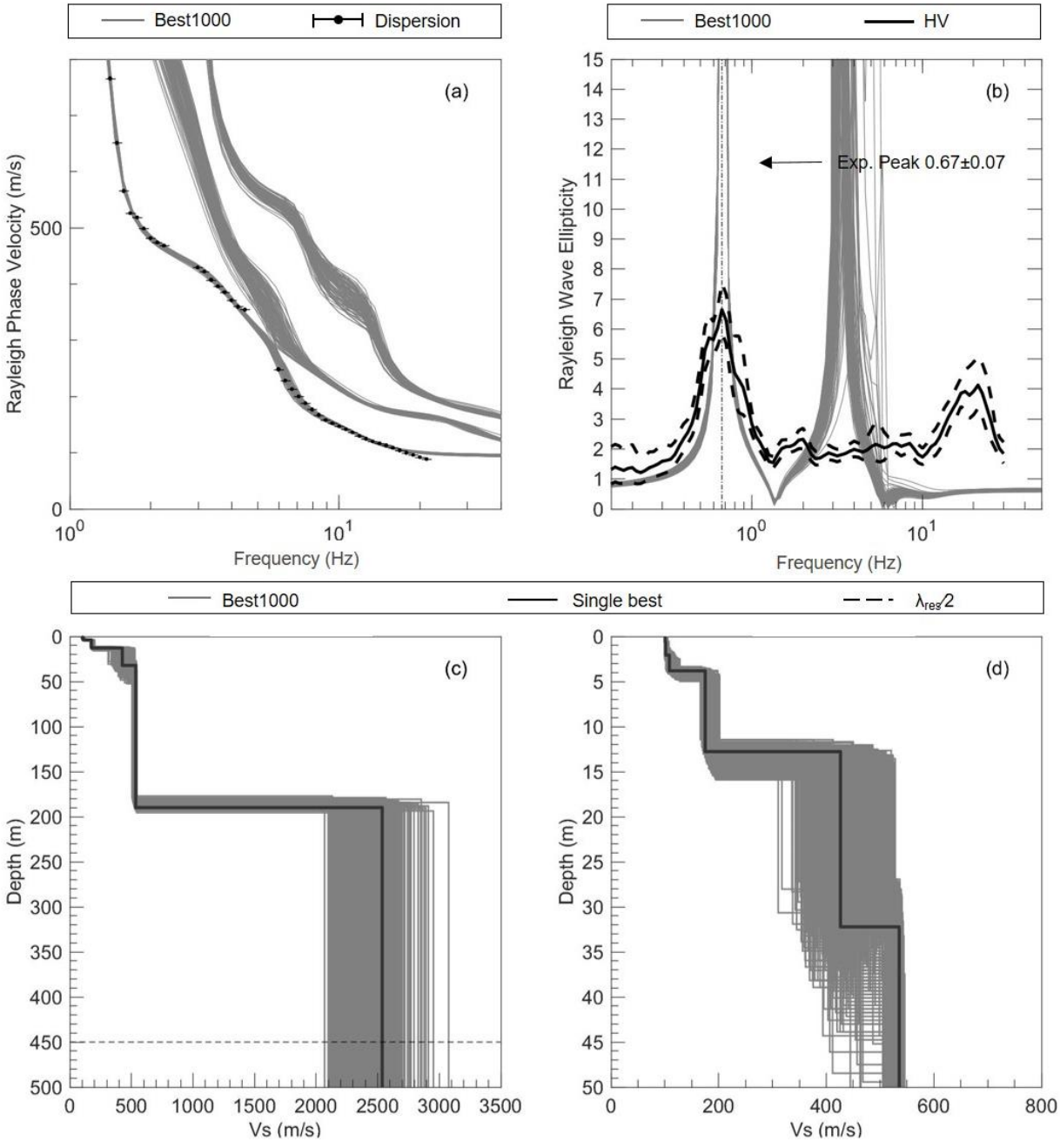

***Figure 4.2** - Surface wave inversion results for Ngaroto. a) Experimental and best1000 theoretical Rayleigh wave dispersion curves. b) Experimental and best1000 theoretical Rayleigh wave ellipticity curves with the fundamental frequency used in the inversion. c) Best1000 shear wave velocity (V_S) models down to basement (in grey) with the lowest misfit profile in black. A 450m resolution limit applies (approximately $\lambda_{max}/2$). d) Best1000 shear wave velocity (V_S) models for the upper 50m (in grey) with the lowest misfit profile in black.*

The experimental dispersion curve was assumed to be entirely fundamental mode with an agreeable overlap between the active and passive dispersion data. The fundamental peak was used in the inversion to better resolve depth to a large impedance contrast (potential basement depth) and produced lower misfits than inversions run without (0.115 versus 0.345). The resulting models from the inversions with and without the peaks were comparable in profile appearance, where V_s and depth increases were relatively consistent. The fundamental frequency from the HVSR is 0.67±0.07Hz with a HVSR peak amplitude of 6.5 (figure 4.2b). The best1000 theoretical ellipticity peaks align with this fundamental peak but appear to find a peak around 2.5Hz which is not present in the experimental data. This theoretical peak also appeared in the inversion run with no peak but where the peak for the site was still plotted with the results. The fundamental frequency from the HVSR was consistent across all 16 seismometer recordings for the site.

There is some obvious variation in the upper 50m of the velocity profile where velocity ranges from 300-500m/s across all profiles. Following the lowest misfit profile from the inversion, shear wave velocity increases from 100m/s to 430m/s in the upper 13m visually depicting four layers (figure 4.2d). This fourth underlying layer with a V_s of 535m/s begins at 32m and extends to 190m where basement is reached and V_s increases to 2536m/s (figure 4.2.c). The V_{s30} from the lowest misfit profile is 234m/s. The fundamental period is 1.5s so class C does not apply and the site does not satisfy criteria for class A, B, or E making this a class D site as per (NZS1170.5, 2004).

4.2.3 McGregor Road (MG)

The dispersion curve used in the inversion and the associated theoretical models (best1000) are given in figure 4.3a for the McGregor Road site. Fundamental mode Rayleigh wave data was determined to span 0.4 to 25Hz. There was no overlap between the active and passive dispersion data at the site with a frequency band between 1.5 and 5.5 Hz unaccounted for; this could be due to the acquisition of the active data on the Walton Sub-group hillside adjacent to the passive acquisition on the peatlands... Higher modes were present in the lower frequency band for the 50 and 200m dispersion curves. In this case, these higher modes were cut in Dinver, and removed from the inversion since reliable fundamental mode data from the larger arrays overlapped with the fundamental mode in the smaller arrays. In the theoretical dispersion curves, Rayleigh phase velocity increases rapidly in the frequency band with no experimental

data before flattening to line up with the experimental dispersion in the lower frequency range, decreasing the reliability of the inversion results within this frequency band.

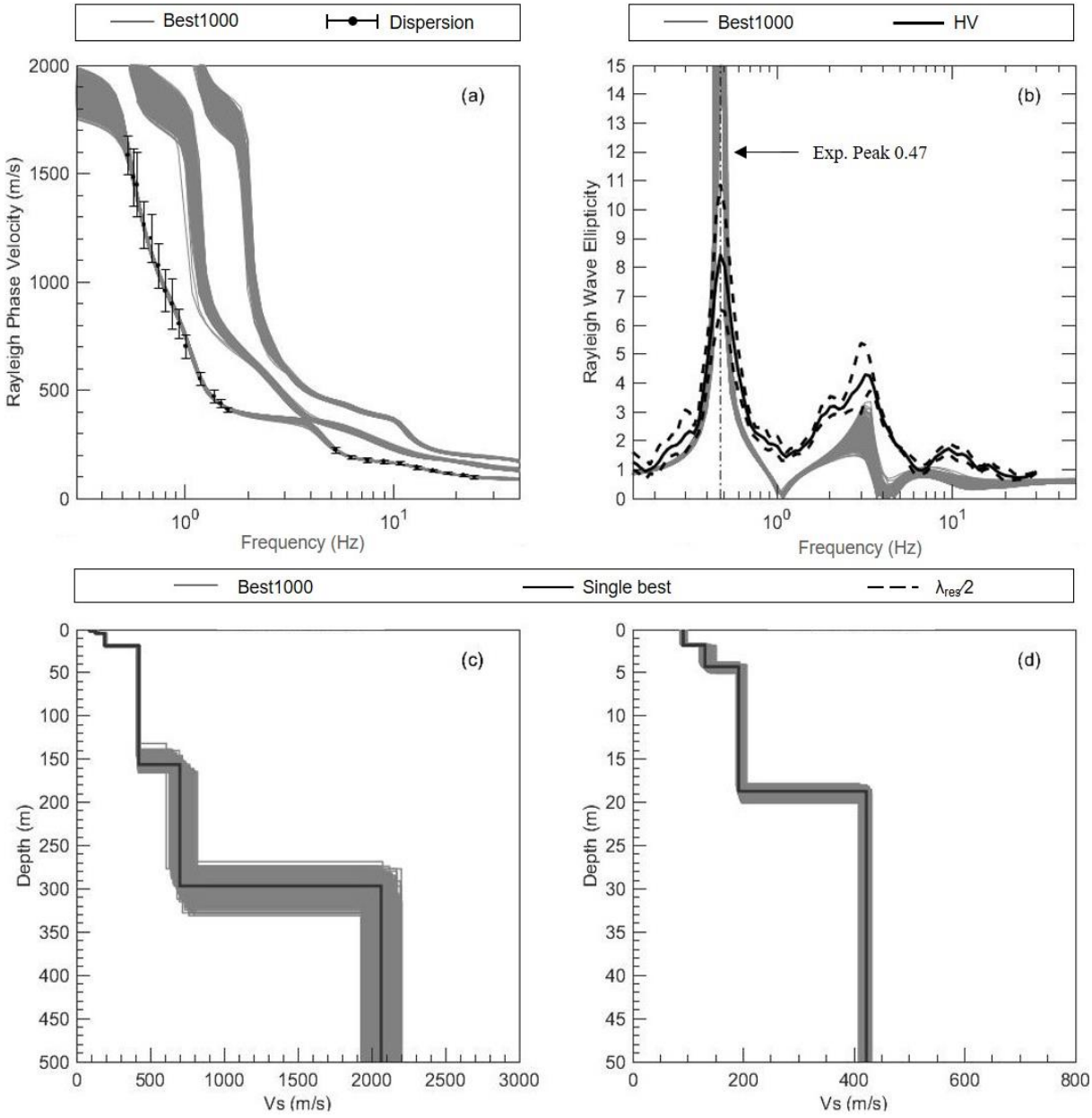

Figure 4.3 *Surface wave inversion results for McGregor road. a) Experimental and best1000 theoretical Rayleigh wave dispersion curves. b) Experimental and best1000 theoretical Rayleigh wave ellipticity curves with the fundamental frequency used in the inversion. c) Best1000 shear wave velocity (V_s) models down to basement (in grey) with the lowest misfit profile in black. A 1550m off graph resolution limit applies (approximately λ/2). d) Best1000 shear wave velocity (V_s) models for the upper 50m (in grey) with the lowest misfit profile in black.*

The fundamental frequency for the site was 0.47±0Hz with a HVSR peak amplitude of 8 (figure 4.3b), which was jointly inverted with the dispersion data resulting in a lower misfit (0.152 LR40WP versus 0.328 LR40NP) (Table 4.2).

Table 4.2 *McGregor inversion; misfits between the experimental and theoretical dispersion curves and shear wave velocity profiles for 1) a fundamental mode dispersion curve inversion*

	1) Fundamental mode dispersion curve inversion	
Layering ratio	No Peak	With peak
LR5.0	0.299	0.198
LR4.0	0.328	0.152
LR3.0	0.415	0.201
LR2.0	0.446	0.244
LR1.5	0.405	0.254

The fit of the theoretical HVSR peak frequency to the experimental HVSR peak frequency used in the inversion is suitable with some variation expected due to the influence of body and love waves on the experimental H/V ratio. The second clear peak with an amplitude of ~4 indicates a smaller shallower impedance contrast, which falls within the same frequency as the dispersion curve gap. The best1000 theoretical models for the McGregor road site, with the lowest misfit between the theoretical and experimental data, are shown in figure 4.3c.

In the upper ~19m shear wave velocity is relatively low (V_s ~91-191 m/s), increasing to 422m/s in the underlying layer to a depth off 156m and again in next underlying layer to 701m/s to a depth of ~297m where basement is reached. Basement rock; formally the Waipapa (composite terrane); is inferred by the large impedance contrast where the velocity increases from 701m/s to 2065m/s. The V_{s30} calculated from the lowest misfit profile is 213m/s, however, this does not take into account the peat layer at the site. This site has a T_0 of 2.1s and meets the criteria for class D as per NZS 1170.5. If peat is >10m in the area the site class will most certainly change to E.

4.2.4 Ohaupo (OP)

The array layout for the Ohaupo site was close to the SH1/SH23 intersection. Ohaupo-1 was 2km from the array location and while the geological information was not used in the parameterisation due to the distance from the site, it did provide an indication of the potential geology for the site. The Tauranga Group (Hinuera Formation + Walton Subgroup) is expected to overlie basement rock, which occurred at a depth of 295m in the Ohaupo-1 well log.

The obtained experimental dispersion curve covers a high frequency range of 1.6-30Hz with a lack of overlap between passive and active data at 5-8Hz due to the active data presenting as a higher mode at lower frequencies (figure 4.4a).

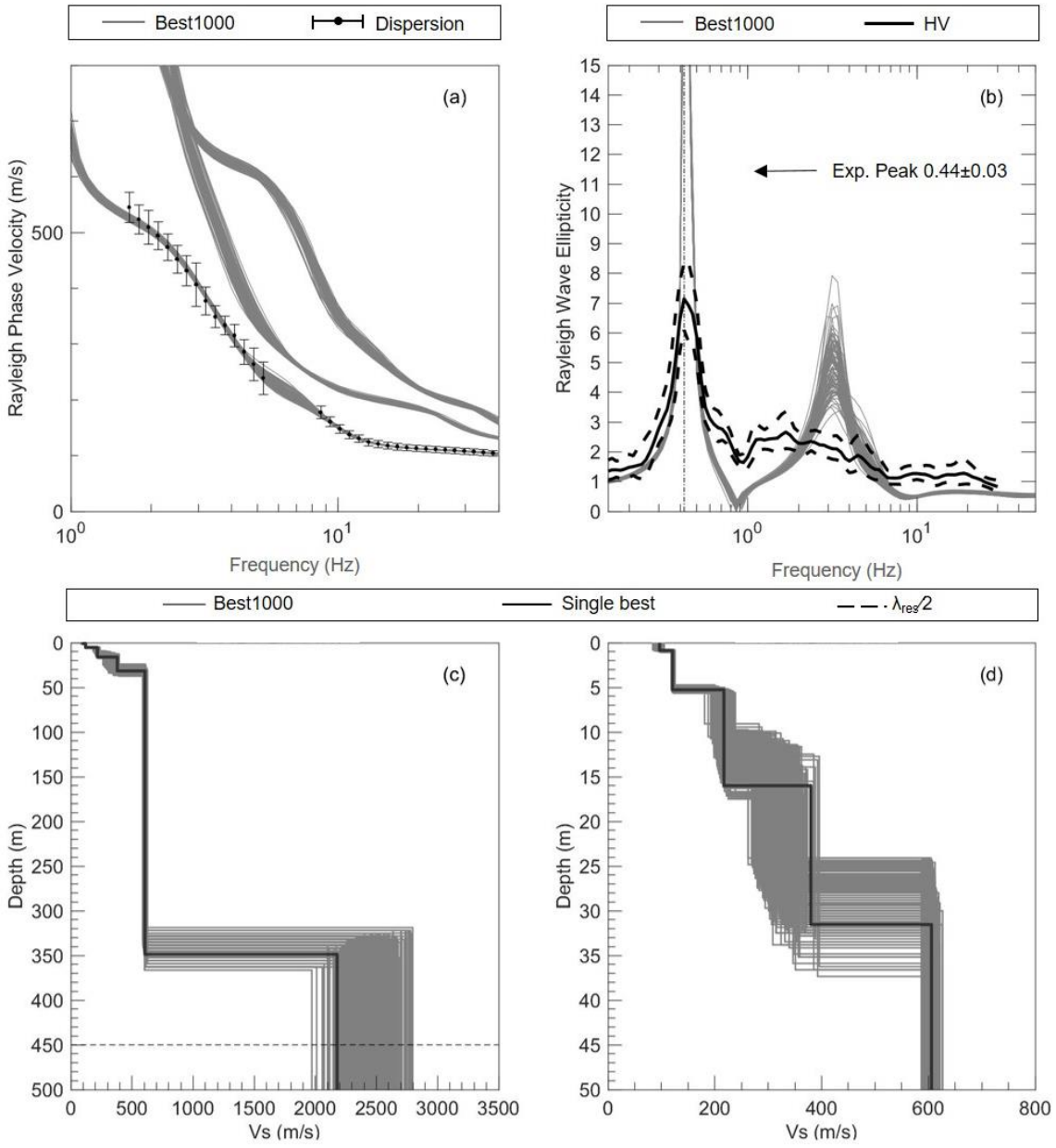

Figure 4.4 *- Surface wave inversion results for Ohaupo. a) Experimental and best1000 theoretical Rayleigh wave dispersion curves. b) Experimental and best1000 theoretical Rayleigh wave ellipticity curves with the fundamental frequency used in the inversion. c) Best1000 shear wave velocity (V_s) models down to basement (in grey) with the lowest misfit profile in black. A 450m resolution limit applies (approximately λmax/2). d) Best1000 shear wave velocity (V_s) models for the upper 50m (in grey) with the lowest misfit profile in black.*

Despite the appearance of a wider range of Rayleigh phase velocity between 5-8Hz the best1000 dispersion models (figure 4.4a) have a lowest misfit of 0.118 (table 4.3, layering ratio

4.0) suggesting a good fit between the experimental and theoretical data. Layering ratio 5.0 produced the lowest misfit result of 0.076 (table 4.3), however, the models appeared to be over constrained as per guidelines from (Foti, 2017).

Table 4.3 *Ohaupo inversion misfits between the experimental and theoretical data for each layering ratio with and without the fundamental peak frequency.*

Inversion 1 – A fundamental mode dispersion curve		
Layering Ratio	No Peak	With Peak
1.5	0.177	0.174
2.0	0.183	0.136
3.0	0.169	0.172
4.0	0.118	0.118
5.0	0.101	0.076

The HVSR peak frequency in figure 16b of 0.44±0.03Hz was used in the inversion, the lowest misfit from layering ratio 4.0 was the same with the inversion run with the peak and without the peak (table 4.3). There is only one fundamental peak for the site suggesting one large impedance contrast assumed to be soft soil overlying basement, with a HVSR peak amplitude of 7.

Following the lowest misfit profile, V_s increases from ~97m/s to ~217m/s at 5m, then to 380m/s at 16m and to 606m/s at 32m (figure 4.4d). The layer with a V_s of 606m/s extends to ~349m where velocity rapidly increases to ~2178m/s (figure 4.4c). The maximum wavelength (λ_{mac}) at this site was 345m with the largest array diameter (d_{max}) being 150m, this means the maximum resolvable depth is 450m ($\lambda_{max}/2$). The V_{s30} from the lowest misfit profile is 228m/s. The Ohaupo site did not meet the conditions for a class A, B C or E classification and had a fundamental period of 2.3s making it class D.

4.2.5 Tamahere (TM)

The Tamahere site is in the south-eastern quadrant of the surveyed area, 5km SE of the Tamahere interchange. Rayleigh phase velocity over a frequency range of 1.5-30Hz was acquired with adequate overlap between the active and passive data at the site. The best1000

theoretical dispersion curves (figure 4.5a) look to fit to the lower velocity of the standard deviation in the experimental dispersion curve at low frequencies.

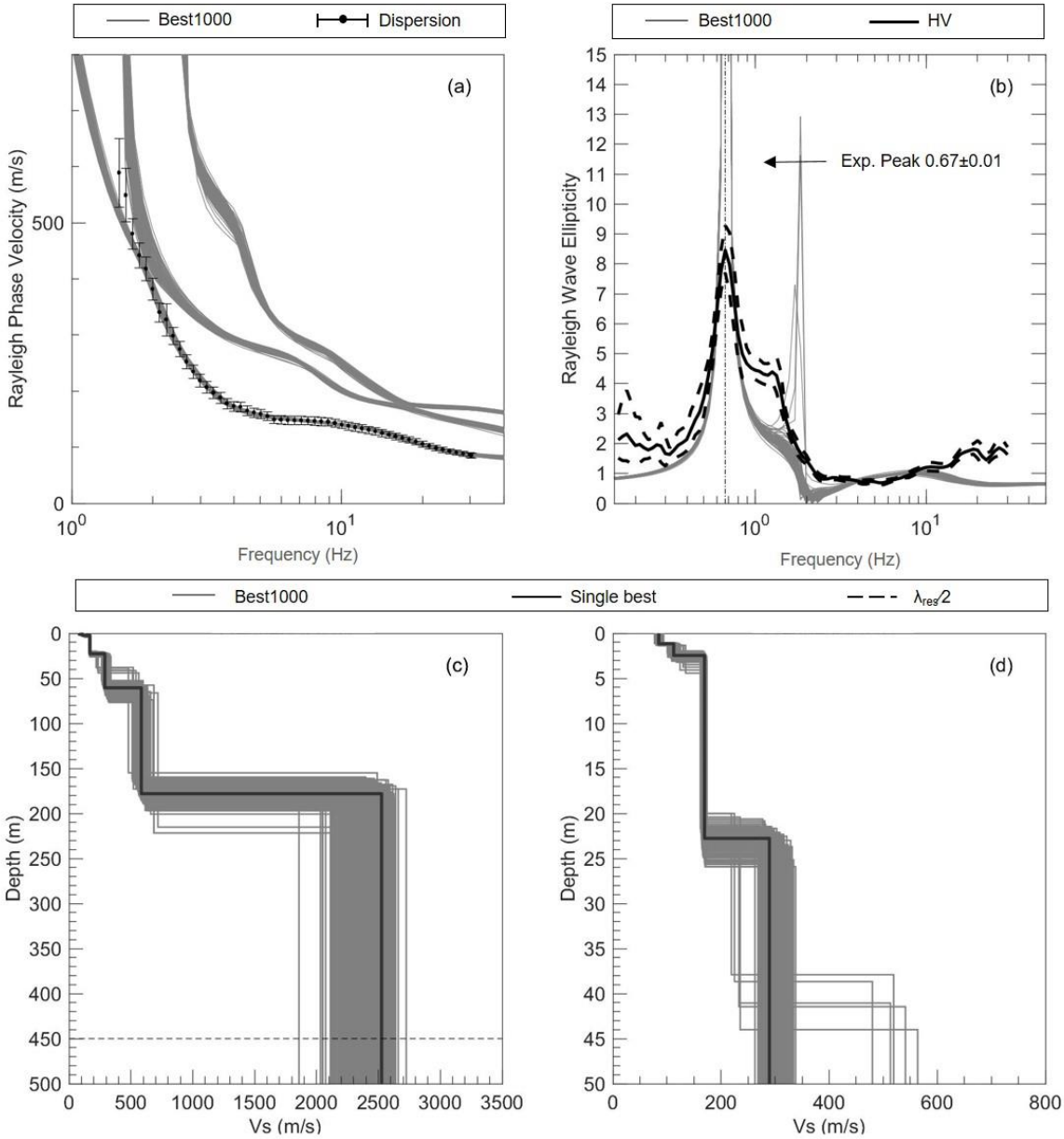

Figure 4.5 *Surface wave inversion results for Tamahere. a) Experimental and best1000 theoretical Rayleigh wave dispersion curves. b) Experimental and best1000 theoretical Rayleigh wave ellipticity curves with the fundamental frequency used in the inversion. c) Best1000 shear wave velocity (V_s) models down to basement (in grey) with the lowest misfit profile in black. A 450m resolution limit applies. d) Best1000 shear wave velocity (V_s) models for the upper 50m (in grey) with the lowest misfit profile in black.*

The fundamental H/V peak frequency for the site is 0.67±0.01Hz (figure 4.5b) which suggests that the basement depth at this site will be relatively shallow; this is supported by the Ngaroto site having an HVSR peak frequency of 0.42±0.05Hz with basement depth of ~190m. This

fundamental peak has an amplitude of 8.5 with the best1000 theoretical ellipticity curves fitting closely to the experimental HVSR peak. The shear wave velocity presented in the lowest misfit (single best) profile ranges from ~85-169m/s in the upper 23m increasing to ~289m/s until ~60m where velocity increases to 585m/s. At ~ 178m, shear wave velocity rapidly increases to ~2490m/s (figure 4.5c). The maximum wavelength (λ_{mac}) at this site was 460m with the largest array diameter (d_{max}) being 150m, this means the maximum resolvable depth is 450m. The V_{s30} calculated from the lowest misfit profile is 176m/s. The fundamental period for the Tamahere site is 1.5s which classifies this as a class D site with a fundamental period of >0.6s and a V_{s30}>150m/s in the upper 10m.

4.3 Northern Basin

The Northern basin is defined as every site north of a reference line between the Tamahere and McGregor Road sites. This has been determined for this research only.

4.3.1 Kiroa Road (KR)

Kiroa Road is the easternmost site in the surveyed area, at -37.724053, 175.369607. The largest array diameter was 150m with a maximum obtained wavelength of 455m. The resolution limit (λres) is 450m, and data is particularly reliable at depths <225m which is ($\frac{1}{2}$ λres). Rayleigh phase velocity in the dispersion curve used for the inversion (figure 4.6a) spans a frequency range of 1.4-37Hz with adequate overlap between active and passive dispersion curves. The best1000 theoretical models follow the experimental dispersion curve; however, the first higher mode models touch the experimental dispersion curve at 3.5Hz. Lower misfits were obtained using the experimental HVSR peak frequency compared to using no peak. This is shown in table 4.4 where the lowest misfit obtained with the peak was 0.18 compared to 0.31 with no peak.

Table 4.4 *Kiroa Road inversion misfits between the experimental dispersion curves and theoretical data for a fundamental mode inversion with and without the fundamental peak frequency.*

	1) Dispersion curve inverted as fundamental mode	
Layering Ratio	No Peak	With Peak
1.2	0.4	0.32

1.5	0.43	0.27
2.0	0.4	0.22
3.0	0.36	0.28
4.0	0.31	0.18
5.0	0.36	0.19

The shear wave velocity profile from layering ratio 4 with peak from table 4.4 is shown in figure 4.6c and 4.6d.

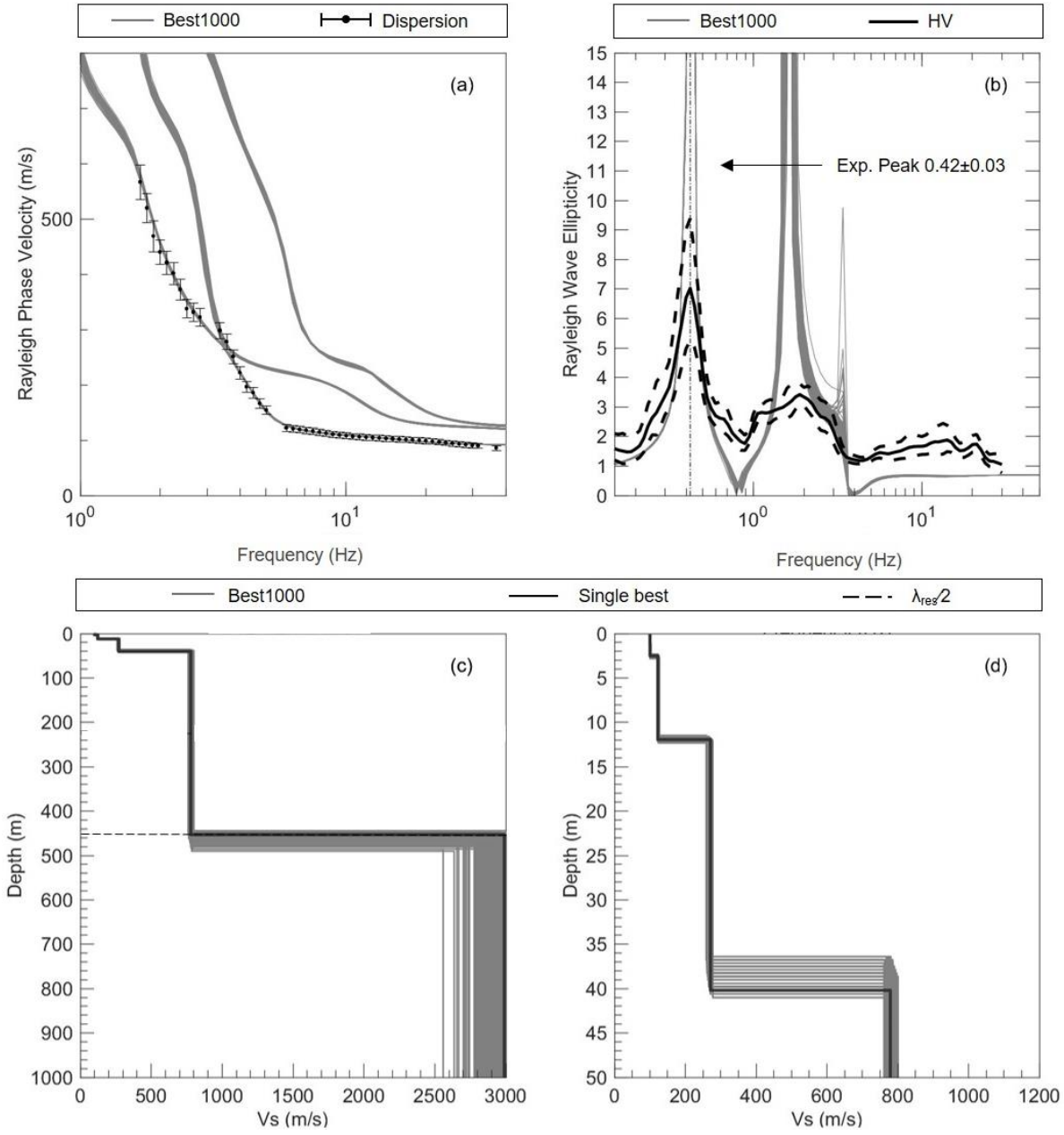

Figure 4.6 *Surface wave inversion results for Kiroa. a) Experimental and best1000 theoretical Rayleigh wave dispersion curves. b) Experimental and best1000 theoretical Rayleigh wave ellipticity curves with the fundamental frequency used in the inversion. c) Best1000 shear wave velocity (V_s) models down to basement (in grey) with the lowest misfit profile in black. A 450m resolution limit applies. d) Best1000 shear wave velocity (V_s) models for the upper 50m (in grey) with the lowest misfit profile in black.*

There is low variance in shear wave velocity and depth between the best1000 models, which is not always the best solution, however, layering ratio 3 with peak produced models with high variance (±200 m/s), and layering ratio 5 did not incorporate the fundamental peak frequency in the inversion. Following the single best profile (lowest misfit) in figure 4.6d shear wave velocity increases from ~77-244 m/s in the upper 30m increasing at ~33m to ~851 m/s. Basement depth is ~450 m as per figure 4.6c, however, this is deeper than the depth of resolution and is solely a result of the impedance contrast assumed from the fundamental HV peak. The V_{s30} calculated from the lowest misfit profile is 173m/s and T_0 is 2.4s. V_s in the upper 10m is however <150m/s (122m/s) meaning the site class will be E for this location.

4.3.2 Ruakura (RK)

HVSR analysis of the seismometer recordings for the Ruakura site showed some interesting anomalies, particularly, a large variance between fundamental Rayleigh wave ellipticity peak frequencies. Seismometer-5 is 0.9Hz, seismometer-4 is 9Hz and seismometers-3 and 6 are 0.3Hz as shown in figure 4.7.

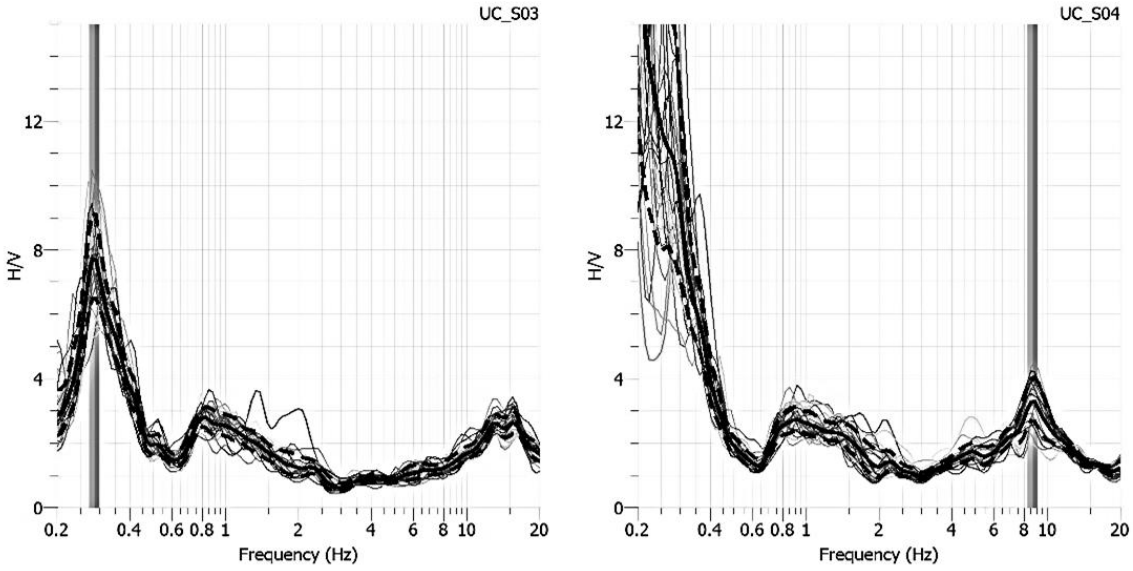

Figure 4.7 *Presented are 4 of the 24 analysed Rayleigh wave ellipticity curves (RWEC) for the Ruakura site showing the main variances in curve peak frequency between seismometers (UCS0) 3 and 4 in the 1000m array.*

This is a small sample of 2 from 24 HV curves and overall the fundamental peak of 0.28 was present in 15 of them. Therefore, a peak frequency of 0.28±0.03Hz was used in the inversion. The profiles developed with the peak used in the inversion had a lower misfit to the experimental dispersion curve, as shown in table 4.5. The lowest misfit obtained was 0.201 with the peak and 0.231 with no peak.

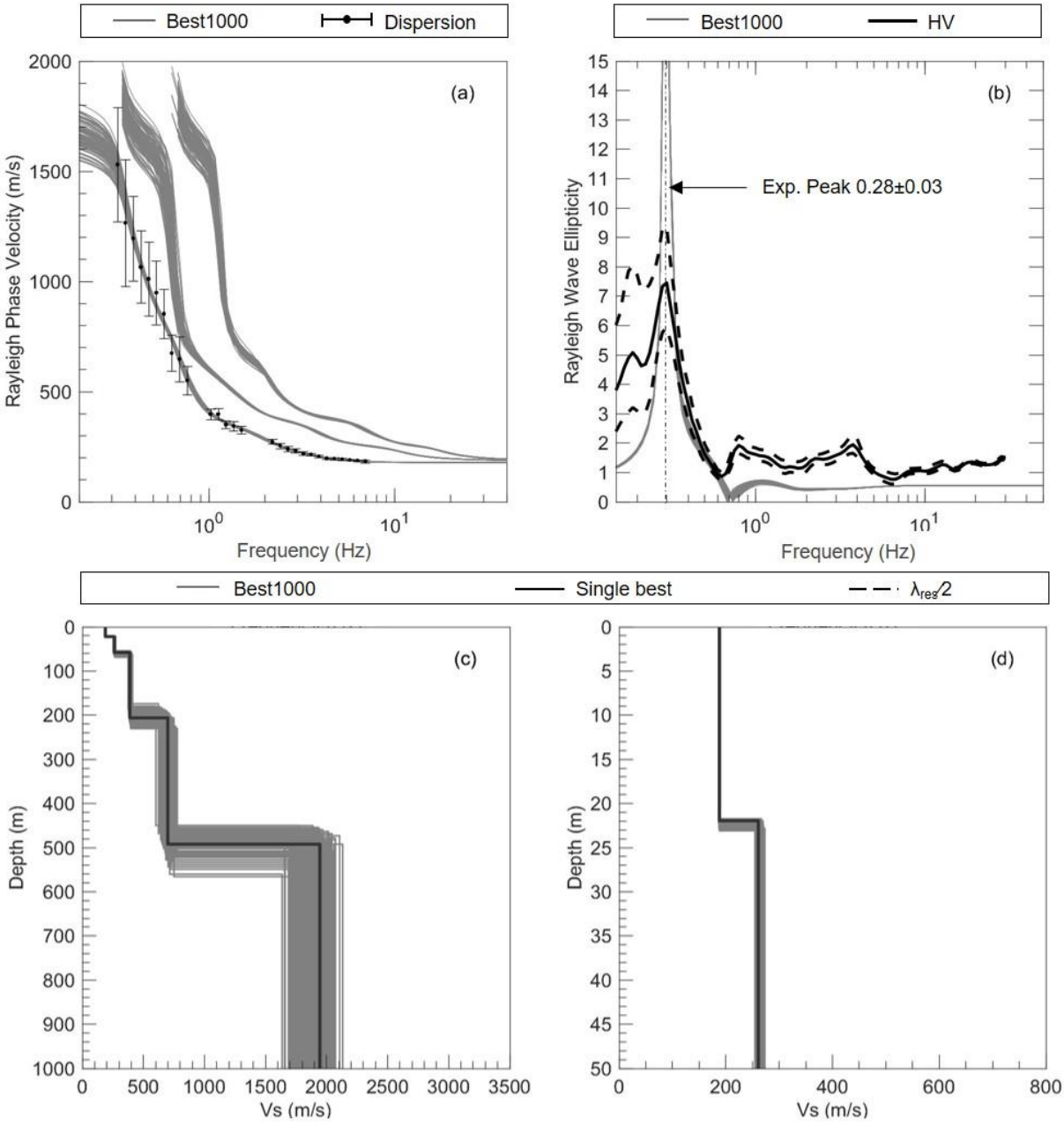

Figure 4.8 *- Surface wave inversion results for Ruakura. a) Experimental and best1000 theoretical Rayleigh wave dispersion curves. b) Experimental and best1000 theoretical Rayleigh wave ellipticity curves with the fundamental frequency used in the inversion. c) Best1000 shear wave velocity (V_s) models down to basement (in grey) with the lowest misfit profile in black. An off graph 3000m resolution limit applies. d) Best1000 shear wave velocity (V_s) models for the upper 50m (in grey) with the lowest misfit profile in black.*

The theoretical ellipticity curve from the inversion closely matches the experimental ellipticity curve (figure 4.8b). The theoretical dispersion curves also match the experimental dispersion (figure 4.8a), which has large standard deviations at low frequencies but otherwise appears as an ideal dispersion curve with adequate overlap between the active and passive data.

Table 4.5 *Misfits between the experimental dispersion curve and theoretical data for each layering ratio used for the Ruakura site; for a fundamental mode inversion with and without the fundamental peak frequency*

Layering ratio	No Peak	With Peak
5.0	0.361	0.247
4.5	0.231	0.285
4.0	0.286	0.2
3.0	0.282	0.201
2.0	0.339	0.255
1.5	0.381	0.251

The best1000 V_s profiles from the inversion are given in figure 4.8c and d, with the lowest misfit profile given in black. Shear wave velocity increases from ~188m/s to ~261m/s at ~22m, increasing to ~389m/s at 58m and ~700m/s at ~206m. Basement is indicated by the large impedance contrast at ~492m where V_s increases to ~1944m/s. The V_{s30} calculated from the lowest misfit shear wave velocity profile is 203m/s. With a fundamental period of 3.6s and a V_s>150m/s in the upper 10m the Ruakura site, is site class D (NZS1170.5).

4.3.3 Hamilton Boys High School (HB)

There was adequate overlap between the active and passive dispersion curves at this site with a frequency range of 0.6 to 16Hz acquired in terms of Rayleigh wave phase velocity. Both the experimental and the best1000 theoretical dispersion curves are given in figure 4.9a for reference. The best1000 theoretical curves from the inversion are highly compatible with the experimental dispersion, demonstrated by the 0.17 lowest misfit. The standard deviation is quite high at low frequencies compared to high frequencies in the dispersion curve; however, this is a phenomenon usually expected at low frequencies (Foti, 2017; Deschenes, 2018). The maximum wavelength at the site was 1355m with a resolution limit of 600m determined from SESAME guidelines. This resolution limit is deeper than the resolved basement depth of 396m

increasing reliability, although, V_s results below 300m ($\frac{1}{2}\lambda$res) should be considered even more reliable (Foti, 2017). Basement depth is associated with the large impedance contrast at 396m in figure 4.9c. Of the best1000 shear wave velocity profiles given, this result is taken from the lowest misfit profile and has a shear wave velocity of 3282m/s. There are several other impedance contrasts of smaller magnitude with jumps in V_s of <200m/s.

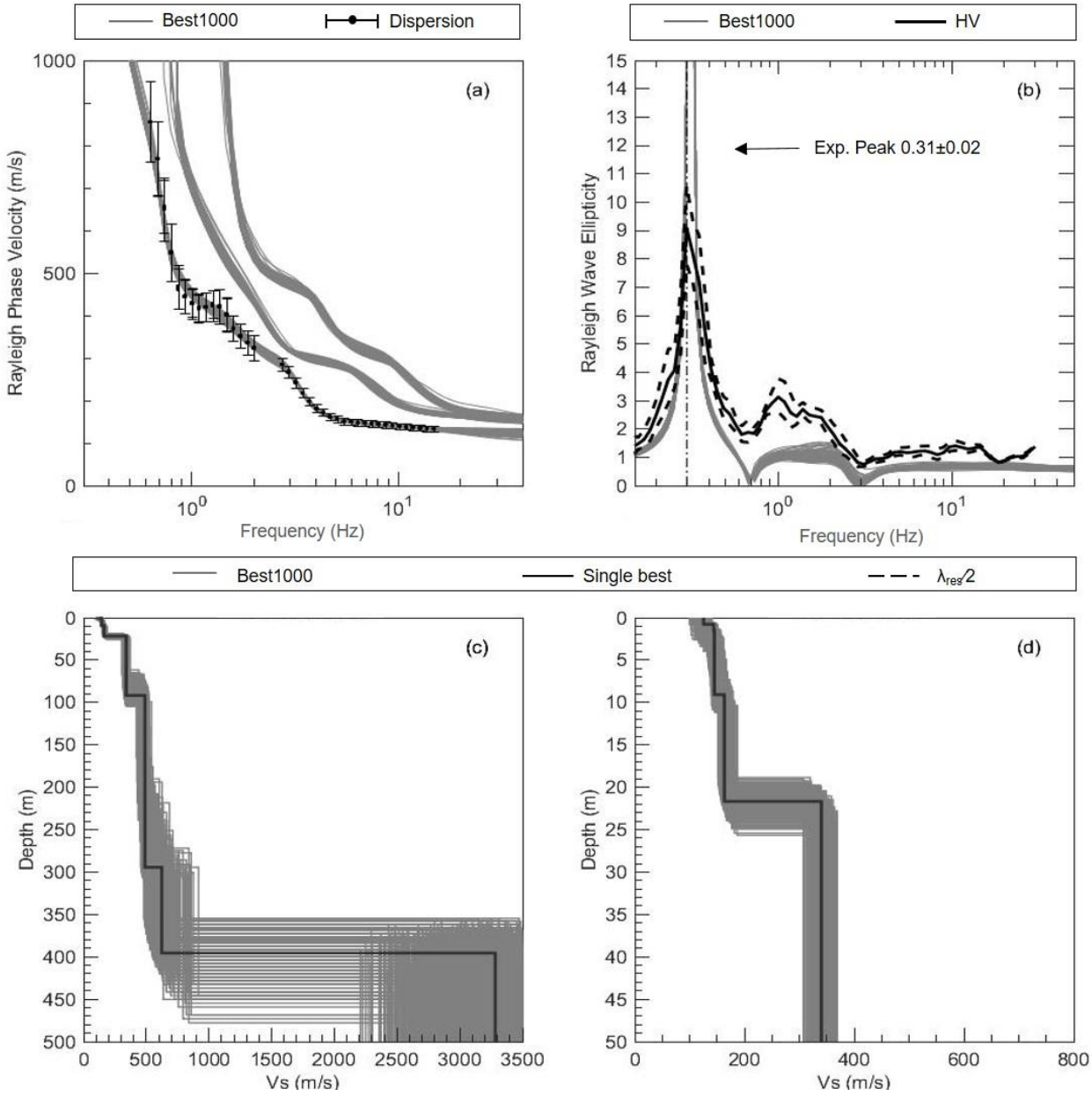

Figure 4.9 *Surface wave inversion results for Hamilton Boys High School. a) Experimental and best1000 theoretical Rayleigh wave dispersion curves. b) Experimental and best1000 theoretical Rayleigh wave ellipticity curves with the fundamental frequency used in the inversion. c) Best1000 shear wave velocity (V_s) models down to basement (in grey) with the lowest misfit profile in black. An off graph 600m resolution limit applies. d) Best1000 shear wave velocity (V_s) models for the upper 50m (in grey) with the lowest misfit profile in black*

There is one clear peak at 0.31±0.02 Hz that is the fundamental period (f_0) of the site, and one less clear peak ~1Hz in the HVSR. HVSR peak amplitude is ~9 for the experimental fundamental peak frequency, this indicates that there is a large impedance contrast at depth. This will likely lead to ground motion amplification, which is 80% likely to be >9 (SESAME, 2004). The second smaller amplitude peak indicates a smaller impedance contrast at a shallower depth likely due to a lower surface velocity. This can mean amplification is carried across a broader frequency range (SESAME, 2004). The theoretical HVSR peaks from the inversion adequately suit the theoretical ellipticity peaks with some variation due to the potential love and body wave influence on the experimental dataset (Foti, 2017). Both theoretical and experimental Rayleigh wave ellipticity curves for HB are given in figure 4.9b. The fundamental peak frequency of 0.31±0.02Hz (figure 4.9b) was jointly inverted with the dispersion data to aid in resolving this strong impedance contrast linked to basement depth.

Table 4.6 *Hamilton Boys High inversion misfits between the experimental dispersion curves and theoretical data with two different parametrisations (final depth not extended to more than the maximum wavelength at the site).*

	1) Fundamental mode dispersion with a shallow final parameter		2) Fundamental mode dispersion with extended final parameter depth	
Layering Ratio	No peak	With peak	No peak	With peak
1.5	0.297	0.188	0.309	0.179
2	0.255	0.189	0.295	0.187
3	0.26	0.184	0.291	0.19
4	0.241	0.205	0.277	0.17
5	0.239	0.152	0.278	0.169

The joint HV inversion resulted in lower misfits between the experimental and theoretical data; the resulting misfit with the peak used was 0.17 (table 4.6, inversion 2) compared to 0.27 without the peak (table 4.6, inversion 3) for the same dispersion dataset. Inversion 1 in table 4.6 presents an initial inversion with inadequate maximum depth. While misfits between inversion 1 and 2 appear similar the resulting velocity profiles have significant variation in appearance due to the over constraint on inversion 1; where profiles typically take on the appearance of the parameters (Foti, 2017). The maximum depth was extended to no more than half of the available wavelength (677m) for the second inversion, which is recommended, and produced a less varied result which was not constrained to the parameterisation (Foti, 2017).

Following the lowest misfit profile in figure 4.9c and 4.9d, shear wave velocity increases from ~125m/s to ~340m/s in the underlying layer to a depth of ~91m and to ~489m/s to a depth of ~294m. Underlying this is a layer with a shear wave velocity of ~624m/s which extends to ~396m where basement is reached (V_s ~3282m/s). There is variability in both the velocity and depth of basement rock at the site, which may be due to the higher standard deviation at lower frequencies as shown in figure 4.9a. Nonetheless, this represents the large impedance contrast in the HVSR, increasing from 624m/s to 3282m/s indicating a transition from a weathered rock to a competent rock (Foti, 2017). Shear wave velocity averages to 182m/s in the upper V_{s30}, with a fundamental period of 3.2s, classifying this soil as a class D soft soil (NZS1170.5: 2004).

4.3.4 Elliot Park (EP)

The surveyed area is 2.7km from the Waikato-2 petroleum well, which contains the Tauranga Group, Waitemata Group and Te Kuiti Group overlying basement rock at 1015m. This information was not used to constrain the inversion due to the distance of the well log from the site; however, it was useful in evaluating the sensibility of the inversion models. . The obtained HVSR for the site were all similar in structure and the fundamental peak frequency was around ~0.49Hz for all analysed seismometer recordings (figure 4.10).

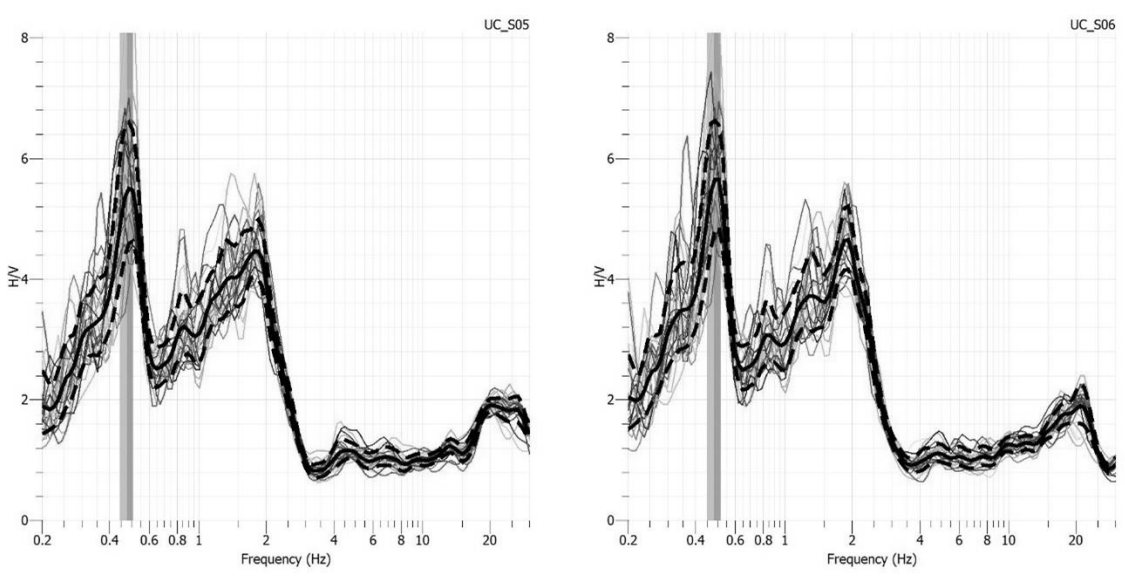

Figure 4.10 *- Presented are 2 of the 24 analysed Rayleigh wave ellipticity curves (RWEC) for the Elliot Park site showing the similar curve peak frequency between seismometers (UCS0) 4 and 5 in the 50m array.*

The dispersion curve used in the inversion spans from 1.5-15Hz, considered to be fundamental mode (figure 4.11a). There is an agreeable overlap between the active and passive data dispersion data. The results presented in figure 4.11a, do not include HVSR curves because no peak frequency was used in the corresponding inversion. Another inversion, which used the peak frequency, obtained from the site, gravely underestimated basement depth according to existing data on the local geology presented in chapter 2.

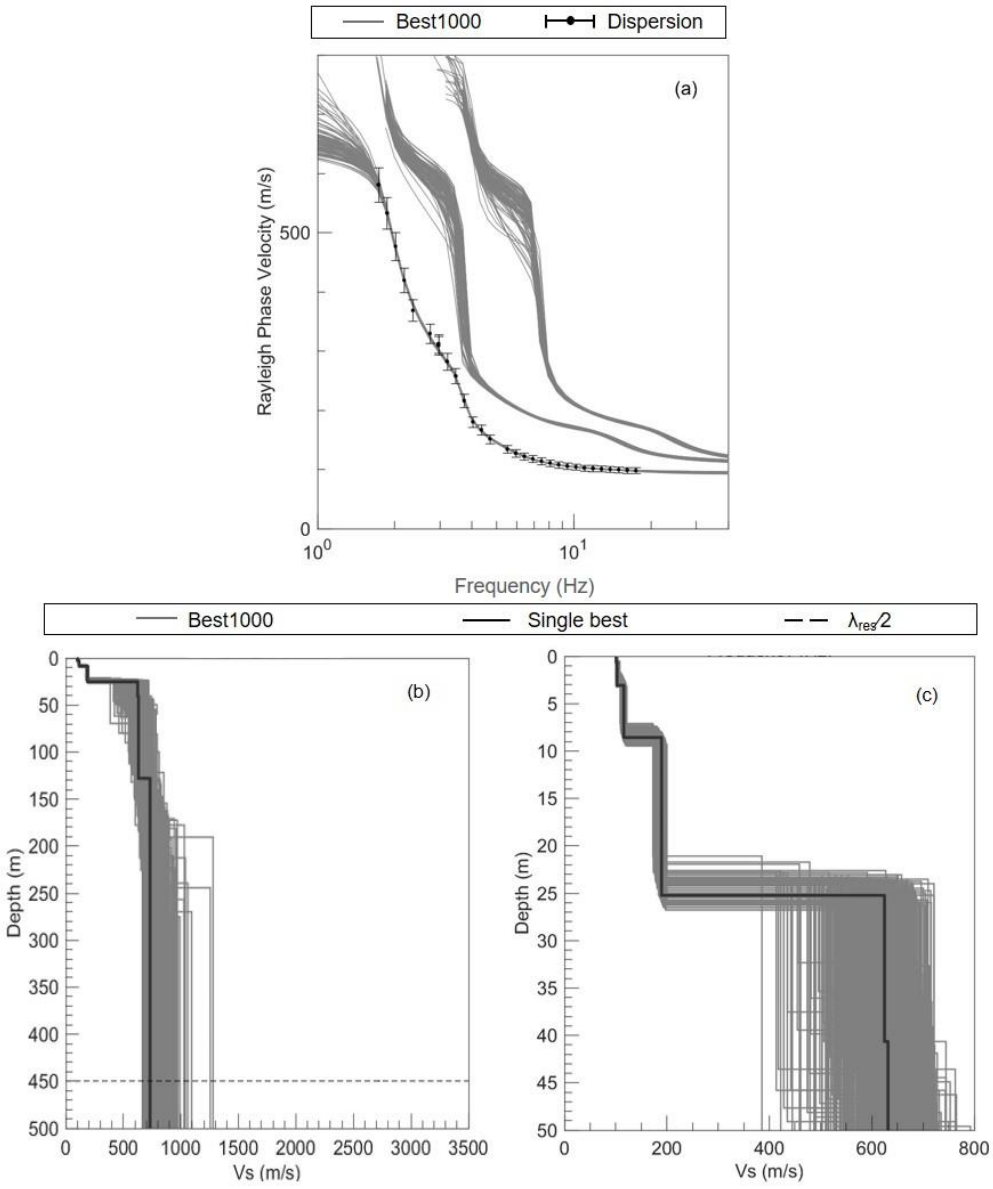

Figure 4.11 *Surface wave inversion results for Elliot Park. a) Experimental and best1000 theoretical Rayleigh wave dispersion curves. b) Best1000 shear wave velocity (V_s) models down to basement (in grey) with the lowest misfit profile in black. A 450m resolution limit applies. c) Best1000 shear wave velocity (V_s) models for the upper 50m (in grey) with the lowest misfit profile in black.*

Layering ratio 3 is presented in figures 4.11c and d, due to layering ratio 4 appearing to have over-constrained the models and high variability in layering ratio 2 suggesting under-constrained models. The misfits for the inversion including the HVSR peak frequency were variable and on average higher than the misfits obtained when no peak frequency was used in the inversion as per table 4.7.

Table 4.7 *Elliot Park misfits between the experimental dispersion curve and theoretical data for each layering ratio used for a fundamental mode inversion. With and without the fundamental peak frequency.*

	1) Fundamental mode dispersion curve	
Layering Ratio	Lowest misfits (no peak)	Lowest misfits (with peak)
1.2	0.203	0.615
1.5	0.165	0.383
2	0.131	0.456
3	0.147	0.141
4	0.131	0.094
5	0.134	2.202

The maximum wavelength at the site was not large enough to resolve basement depth at this site with results below the depth of 450m being beyond the dispersion resolution. Results are increasingly reliable at half the resolution depth (225m). Following the lowest misfit profile in figure 4.11c, shear wave velocity increases from ~101-183m/s in the upper 23m. The underlying layer increases to ~398m/s below 23m, increasing to 913m/s at 90m continuing beyond the resolution depth. Depth to basement is undetermined at this site. The V_{s30} calculated from this lowest misfit profile is 176m/s. This site is classified as site class D since V_s increases to 182m/s below 10m and the fundamental period is 2s (NZS1170.5, 2004).

4.3.5 Ngahinapouri (NP)

The active data acquired at the Ngahinapouri site spans a higher frequency range than the passive data, so there is no overlap between them. The active data also has a higher velocity than the highest frequency passive data (figure 4.12a). Given that this passive data is considered the fundamental mode and the active data is considered fundamental mode, this is an interesting result. The best1000 theoretical models have averaged out the passive and active data, following the active dispersion curve rather than the highest frequency portion of the passive curve as shown in figure 4.12a. Several inversions were run to rule out assumptions of modes for this dataset.

The higher misfits in inversion 1, table 4.8, are a result of the active data being run as a higher mode. Inversion 1 returned much higher misfits for all layering ratios compared to inversion 3, table 4.8, where the dataset was run as fundamental mode. When the low velocity passive data (~2.5-4.5Hz) was removed from the inversion; the misfits were still higher (inversion 2; table 4.8) than inversion 3. Given that the lowest misfit is not always the best fit the final dispersion curves, shear wave velocity profiles were also compared for variability and inversion 3 was considered the best result. While the lowest misfit is not always the best fit, misfits of >0.5 are generally considered unreliable. Inversions 1 and 2 both returned misfits >0.5 for all layering ratios (table 4.8).

Table 4.8 *Misfits between the experimental dispersion curve and theoretical data for each layering ratio used for the Ngahinapouri site; for three different dispersion curve settings with and without the fundamental peak frequency.*

	1) Active data set as higher mode		2) Low velocity passive data removed		3) All dispersion curves fundamental mode	
Layering Ratio	No Peak	With Peak	No Peak	With Peak	No Peak	With Peak
1.2	0.91	0.67	0.62	0.83	0.61	0.23
1.5	0.86	0.70	0.58	0.70	0.57	0.22
2.0	0.83	1.00	0.53	0.99	0.54	0.21
3.0	0.67	0.89	0.53	0.86	0.54	0.16
4.0	0.65	0.41	0.59	0.44	0.55	0.13
5.0	0.89	1.67	0.90	1.92	0.66	0.20

Inversion 3 also returned misfits >0.5 when the HV peak was not used, while misfit were all comparatively lower than 0.22 when the peak was used. The inversion presented in figure 4.12 is inversion 3, layering ratio 4, with peak which returned a lowest misfit of 0.13.

The HVSR peak frequency is 0.47±0.02Hz with the best1000 theoretical ellipticity curves largely following the experimental HVSR peak (figure 4.12b). Some of the experimental ellipticity profiles have also peaked at a smaller, non-significant peak. This seems to have influenced the resulting V_s profile in figure 4.12c and d. Some of the best1000 V_s profiles vary in V_s at the same depth and some vary with depth at the same V_s, with no profiles fit in between. In any case, a V_s or depth change of ±50 is not significant, particularly with increasing depth.

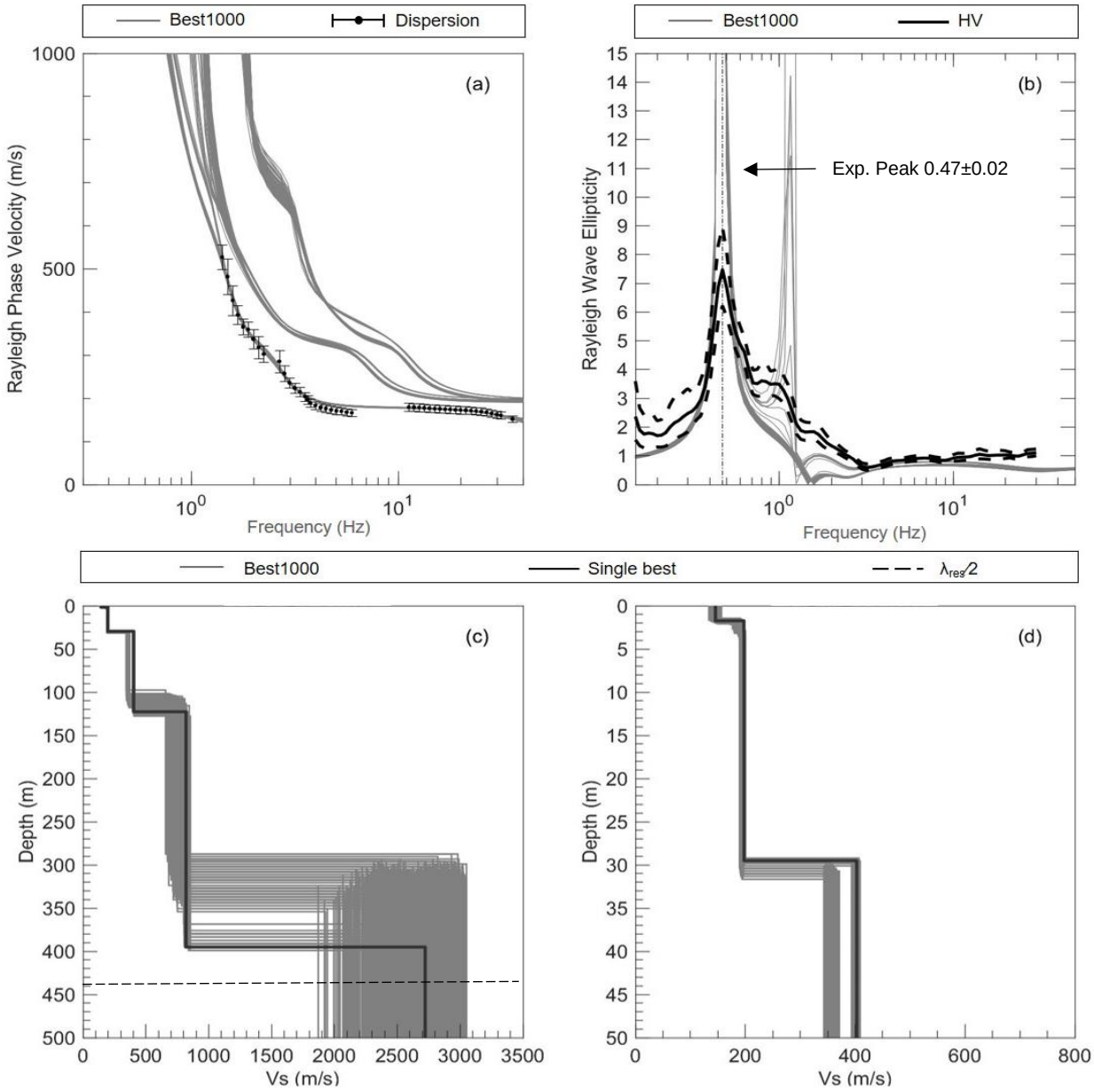

Figure 4.12 *Surface wave inversion results for Ngahinapouri. a) Experimental and best1000 theoretical Rayleigh wave dispersion curves. b) Experimental and best1000 theoretical Rayleigh wave ellipticity curves with the fundamental frequency used in the inversion. c) Best1000 shear wave velocity (V_s) models down to basement (in grey) with the lowest misfit profile in black. A 450m resolution limit applies. d) Best1000 shear wave velocity (V_s) models for the upper 50m (in grey) with the lowest misfit profile in black.*

The lowest misfit profile in figure 4.12c and d shear wave velocity increases from ~146-198m/s in the upper 30m, below this V_s increases to ~403m/s and at ~123m increases to ~819m/s. Basement depth is inferred as 395m from the increase in V_s to ~2722m/s. The V_{s30} calculated from the lowest misfit profile is 195m/s. The site does not meet the conditions for class A, B or E and has a low amplitude period 2.1s, so is site class D.

4.3.6 Te Rapa (TR)

The Te Rapa site is the northern most site in the study area, with the array surveys 700m from the Te Rapa-1 petroleum well log. As per the well log data, the greywacke basement is 1660m deep with the overlying Te Kuiti Group spanning between this and 1190m, the overlying Waitemata Group from 1190m to 650m and the overlying Tauranga Group from 650-0m. The V_s profile measured for the site is in figure 4.13 below.

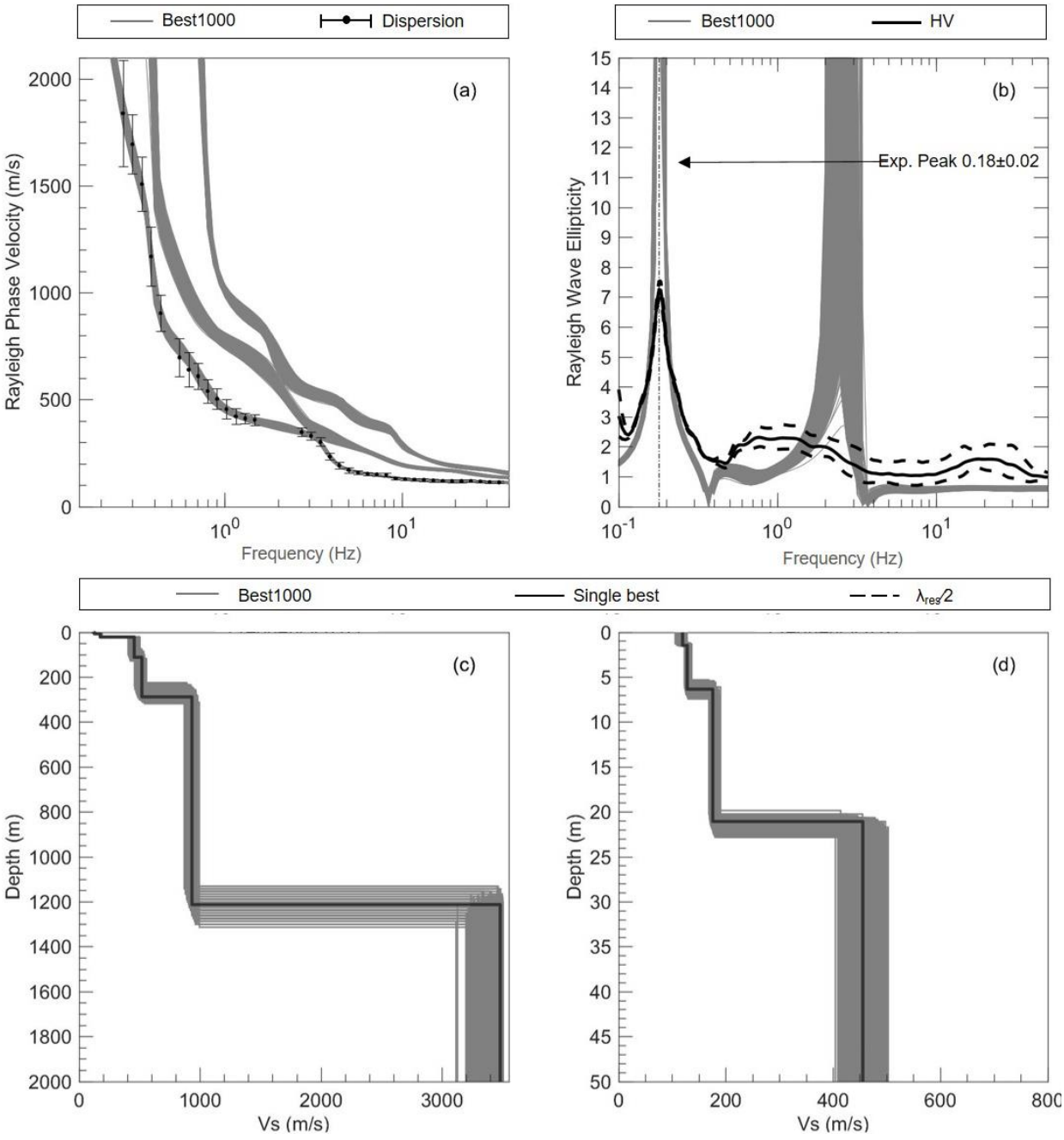

Figure 4.13 *Surface wave inversion results for Te Rapa. a) Experimental and best1000 theoretical Rayleigh wave dispersion curves. b) Experimental and best1000 theoretical Rayleigh wave ellipticity curves with the fundamental frequency used in the inversion. c) Best1000 shear wave velocity (V_s) models down to basement (in grey) with the lowest misfit profile in black. A 3000m off graph resolution limit applies. d) Best1000 shear wave velocity (V_s) models for the upper 50m (in grey) with the lowest misfit profile in black.*

This information was not used to constrain the parameters in the inversion but rather to check that the results were similar to the known geology. The dispersion curve used in the inversion spans a frequency range of 0.2-35Hz (figure 4.13a). The fundamental frequency used in the inversion was 0.18±0.02Hz suggesting a significantly deeper impedance contrast compared to all previously mentioned sites with peak frequencies >0.27Hz. The experimental HVSR in figure 4.13b has one clear peak frequency which is closely followed the theoretical HVSR peak frequency.

As per the lowest misfit profile in figure 4.13c and d; V_s increases from ~120m/s to ~175m/s in the upper ~21m. Below 21m, V_s increases to 455m/s until ~111m where V_s increases to ~518m/s. At 287m V_s increases to 932m/s until 1212m where basement is inferred from the increase in V_s to 3479m/s. The V_{s30} calculated from this lowest misfit profile is 195m/s and V_s is more than 150m/s in the upper 10m. With a fundamental period (T_0) of 5.5s, this is a class D site.

4.4 Peat sites

The shear wave velocity in the peat bogs within the Hamilton Basin ranged from 28m/s-38m/s across four peat sites as shown in table 4.9. This is significantly slower than the findings of (Dawson et al., 2015) for the Manukau peaty silt which ranges from 60-90m/s. This phenomenon may have also influenced the passive data obtained at Kainui road and Wallace road (small) sites, which are described in subsections 4.4.3 and 4.4.4.

Table 4.9 *Shear wave velocity and frequency ranges from the multichannel analysis of surface waves (MASW) survey at each of the four peat sites surveyed in the Hamilton Basin; Woodlands Road, Kainui Road, Temple View and Wallace Road (small).*

Site	Woodlands road (WR)	Kainui (KN)	Temple View (TPV)	Wallace road small (WRS)
Shear wave velocity (m/s)	31-35	28-30	31-35	38-35
Frequency range (Hz)	5-13	5-12	5-13	5-12

4.4.1 Temple View (TV)

The processed dispersion curve ranges from 0.4 to 13Hz, however, after discovering anomalies with the active dataset the final inversion only includes the passive dataset which ranges from 0.4 to 3.5Hz range (figure 4.17a). This anomaly is an incredibly low shear wave velocity (31-35m/s) across a broad frequency range (5-13Hz) as per table 4.9 above. Due to this, higher frequency sampling was attempted at the site with small 5m and 15m passive arrays, in an attempt to resolve the near surface, where the active method was not obtaining credible results. A plot of the processed raw dispersion curves is in figure 4.14, which shows the alignment of the 5m (red) and 15m (purple) arrays with other three passive arrays at the site. The 5m dispersion curve appears to be a fundamental mode although the velocity is quite low, whereas the 15m array looks like a higher mode; neither assumptions are certain.

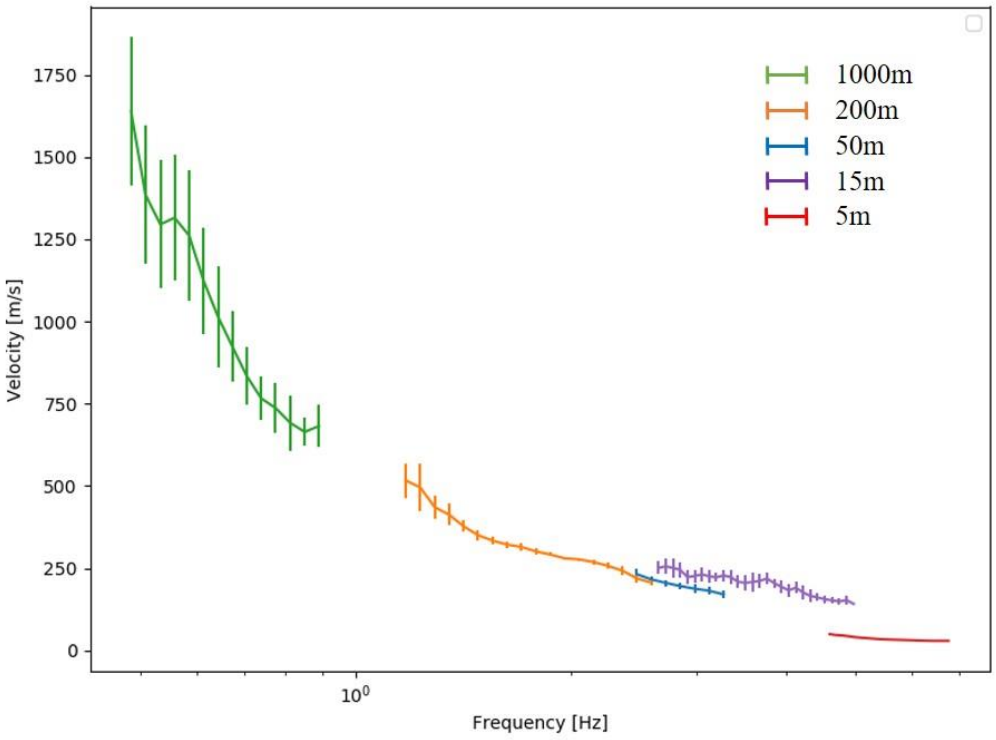

Figure 4.14 *- Raw dispersion curve dataset for all Microtremor Array Measurement (MAM) arrays at the Temple View site. Each colour represents a dispersion curve corresponding to an array diameter; 1000m in green, 200m in yellow, 50m in blue, 15m in purple and 5m in red.*

Another interesting aspect of the results for this site was the obtained ellipticity peaks from H/V analysis, shown in figure 4.15. The large variation in fundamental H/V peak as well as other higher frequency peaks is evident in this figure. The seismometer recordings at a single site are expected to produce similar H/V peak structures (SESAME, 2005).

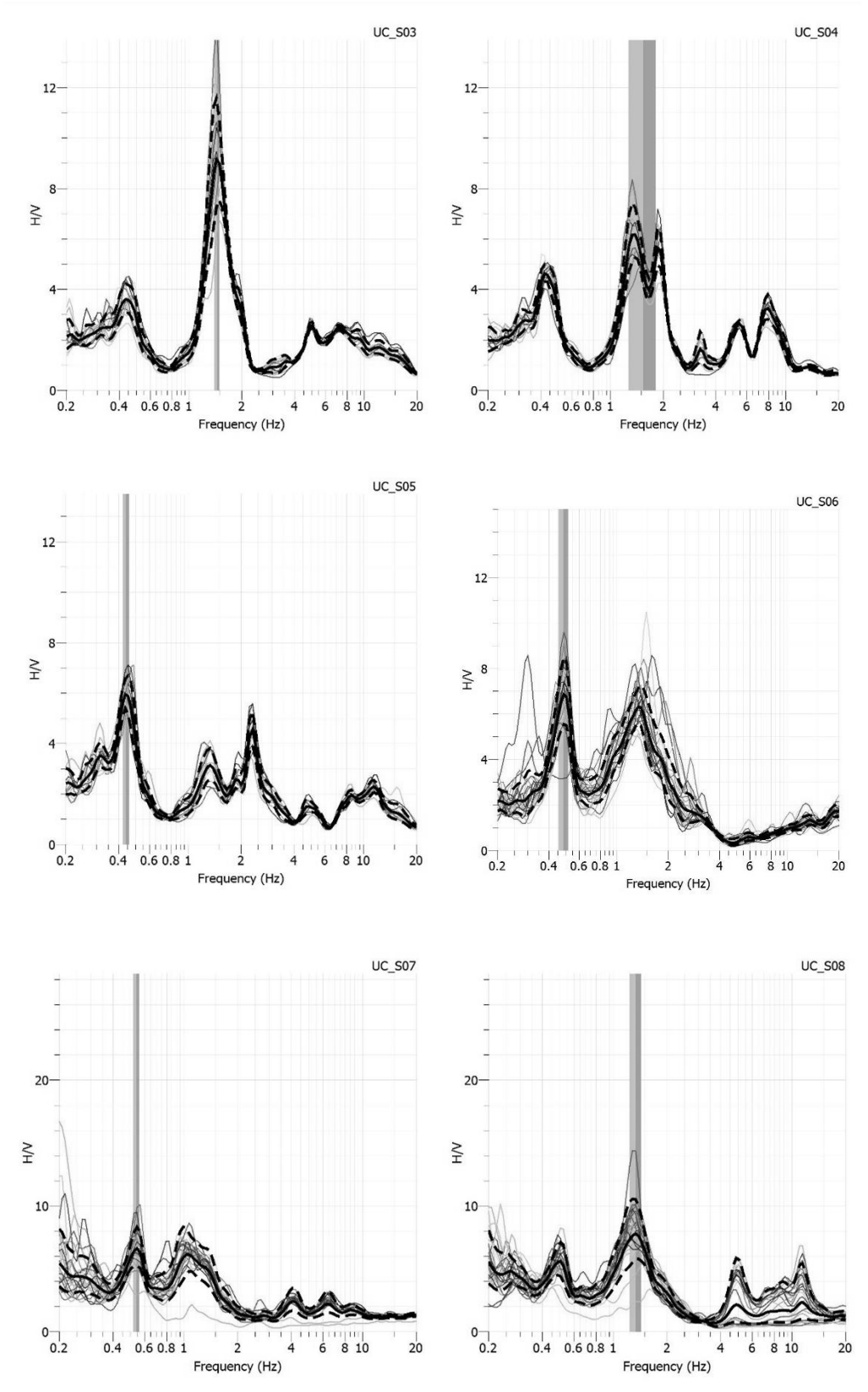

Figure 4.15 *H/V analysis for Temple View site showing large variation in fundamental frequency peak (indicated by the vertical grey line) and other peaks from Microtremor recordings. Seismometers (UCS0) 3 and 4 are from the 50m array, seismometers 5 and 6 are from the 200m array and seismometers 7 and 8 are from the 1000m array.*

Given the unique dataset, many inversions were run for the Temple View site. Inversion 1 includes the active MASW data as well as the 50 m, 200 m and 1000 m array data inverted with unmodified parameterisations taken directly from the layering ratio method. These misfits were very high as per table 4, ranging from 1.23-5.89 and the models were discounted. Another inversion was attempted by constraining the velocity of the peat layer; V_s0 was changed to 0.1m-7m with V_s of 10-90m/s for all layering ratios. This was taken from the dispersion curve velocities and went to 7m based on the probable end of the peat layer being 6m according to surrounding geological data. This is not shown in table 4.10 as the misfits were all >2. Inversion 2 includes the 5m, 50 m, 200 m and 1000 m passive arrays; some of the layering ratios were modified to extend final depth parameter to no more than the maximum wavelength at the site as specified by (Foti, 2017). These misfits, while lower than inversion 1 were still >0.5 as per table 4.10. Inversion 3 includes the 50, 200 and 1000m passive arrays (shown in figure 4.17a) with and without the S06 peak; the lowest misfits from both are shown in table 4.10. The resulting shear wave velocity models (shown in figure 4.17c) had a very low misfit with the peak used in the inversion (0.15-0.19).

Table 4.10 *Misfits between the experimental dispersion curve and theoretical data for each layering ratio used for the Temple View site. Three different dispersion curves were used, Inversion1 – includes 50, 200, 1000m + active data, Inversion 2 – includes 5, 50, 200 and 1000m dispersion curves and Inversion 3 – 50, 200, 1000m dispersion curves*

	1) Active+50+200+ 1200m arrays		2) 5+50+200+1000m arrays		3) 50+200+1000m arrays	
Layering Ratio	No peak	With Peak	No peak	With Peak	No peak	With Peak
LR5.0	2.40	1.36	1.12	0.53	0.24	0.18
LR4.0	2.12	1.23	0.96	0.52	0.21	0.15
LR3.0	2.32	1.34	0.85	0.52	0.37	0.17
LR2.0	2.64	1.41	1.13	0.32	0.39	0.18
LR1.5	3.26	1.46	1.24	0.65	0.43	0.19
LR1.2	5.89	1.80	1.31	0.72	0.45	0.19

With the variation in fundamental frequency, selecting a peak was not straightforward. All recordings for the 5, 10, 50, 200 and 1000m arrays were analysed, which produced 40 H/V curves. The common fundamental peak for all curves was 0.49Hz and the final curve selected has an fundamental frequency of 0.49±0.02Hz. The final curve (figure 4.17b) has two peaks because 35 of the 40 H/V curves had two peaks. One observation is that while the best1000 theoretical Rayleigh wave ellipticity lowest misfit models closely follow the fundamental fundamental frequency, they do not follow the second fundamental frequency above 1Hz (figure 4.17b). The shear wave velocity profiles for all layering ratios in inversion 3 both

without the peak and with the peak are given in figure 4.16. This shows that with no peak used (figure 4.16a), it looks like V_s is incrementally increasing, however this is not an accurate inversion result. In figure 4.16b the V_s profile with the peak used shows a typical stepwise pattern.

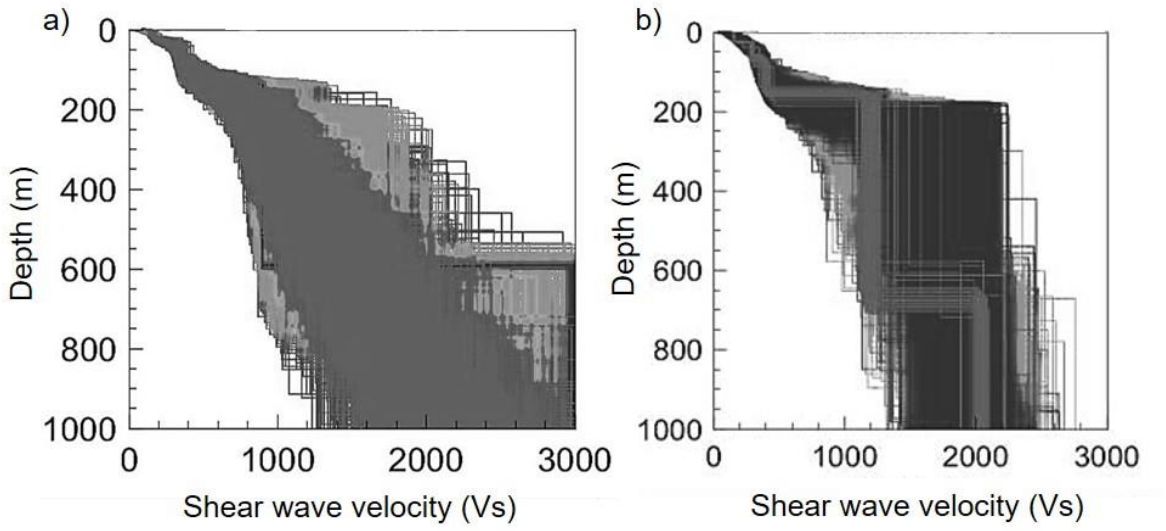

Figure 4.16 *Shear wave velocity profiles for all layering ratios a) without the peak and b) with the peak. The foreground velocity profiles are layering ratio 5, with background velocity profiles decreasing in ratio 4-3-2-1.5.*

The depth to basement also varied between layering ratios (LR); LR1.2, LR1.5, LR2.0 and LR3.0, fit a depth of 250m while LR4.0 and LR5.0 fit a depth of 700m. The maximum wavelength for the site was 3307m therefore the maximum resolvable depth is 1653m and data below 827m ($\frac{1}{2}res$) is considered more reliable; the basement depth is below this limit. The final shear wave velocity profile presented is inversion 3, layering ratio 4, with peak (Figure 4.17), selected due to having the lowest misfit. Unfortunately, this inversion is limited in near surface resolution due to the removal of the active dataset and therefore the 50m plot presented in figure 4.17d is limited in accuracy.

Following the lowest misfit profile in figure 4.17c, there are several impedance contrasts above 50m. At 71m shear wave velocity increases to 402m/s, increasing to 1180m/s at 158m and then to 2039 at 676m. The fundamental period of the site is 2s. The V_{s30} is 166m/s, however, this does not account for the peat layer at the surface of unknown thickness.

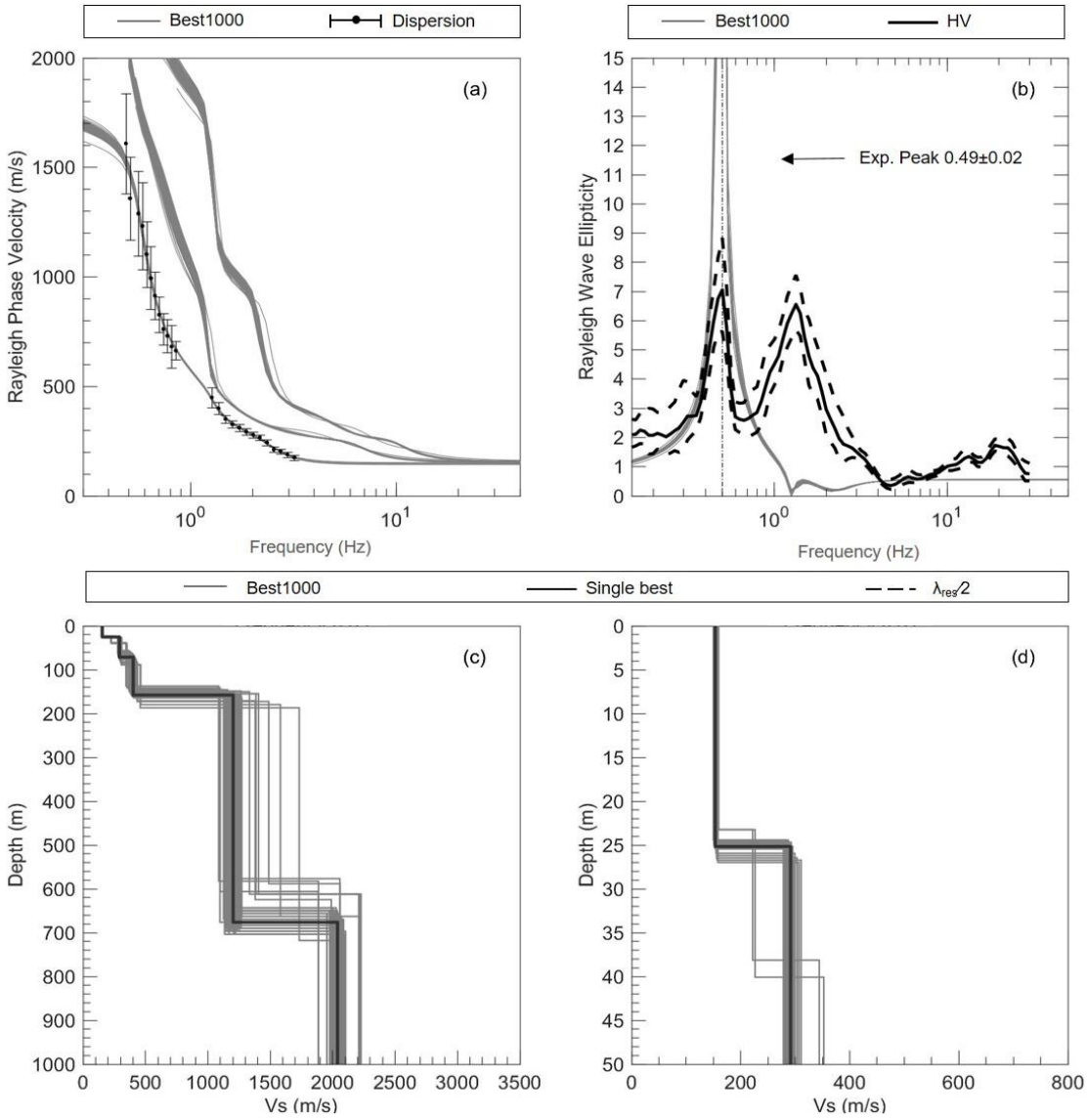

Figure 4.17 *Surface wave inversion results for Temple View. a) Experimental and best1000 theoretical Rayleigh wave dispersion curves. b) Experimental and best1000 theoretical Rayleigh wave ellipticity curves with the fundamental frequency used in the inversion. c) Best1000 shear wave velocity (V_s) models down to basement (in grey) with the lowest misfit profile in black. A 3000m resolution limit applies. d) Best1000 shear wave velocity (V_s) models for the upper 50m (in grey) with the lowest misfit profile in black.*

4.4.2 Gordonton

The HV anomaly observed at the Temple View site was not observed at Gordonton, and HVSR from Gordonton are given in figure 4.18 to show the small variation in Rayleigh wave ellipticity structure between seismometer recordings. This is expected behaviour, and further highlights the anomaly at Temple View. The fundamental peak frequency used in the inversion was 0.19±0.02Hz, which is the second lowest fundamental frequency peak of all surveyed sites.

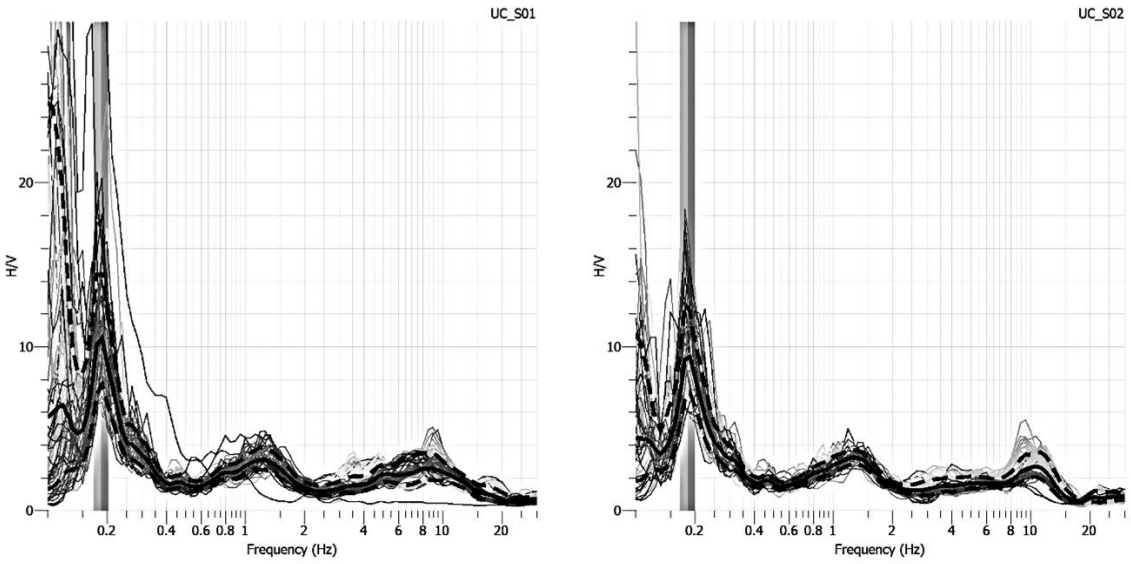

Figure 4.18 *H/V analysis for Gordonton showing little variation in fundamental frequency peak (indicated by the vertical grey line) and in other peaks from Microtremor recordings. Seismometers (UCS0) 1 and 2 are from the 50m array.*

The dispersion data from the active MASW survey on the peatland produced a very low shear wave velocity of 31-35m/s across a frequency range of 5-13Hz. A single inversion was run with the active dispersion combined with the passive to check that the effect on the V_s profile was similar to Temple View and this run produced a misfit of >5, confirming the similarity. The dispersion curve presented in figure 14.19 is from passive acquisition only and spans a frequency range of 0.4-4Hz. The inversion run with the passive dispersion removed produced a lowest misfit of 0.467 when no peak was used compared to 0.166 when the peak was used in the inversion (as per table 4.11).

Table 4.11 Gordonton inversion misfits between the experimental dispersion curve and theoretical data for each layering ratio with and without the fundamental peak frequency

	1) Fundamental mode dispersion curve inversion	
Layering Ratio	No Peak	With Peak
5.0	0.539	0.217
4.0	0.467	0.166
3.0	0.512	0.282
2.0	0.528	0.243
1.5	0.536	0.266
1.2	0.531	0.272

Following the lowest misfit profile in figure 14.19, Vs increases from 128-221m/s in the upper 28m. Increasing from 301-539m/s in the underlying layer to 254m and 634-1122m/s to 1394 where basement is reached (3020m/s).

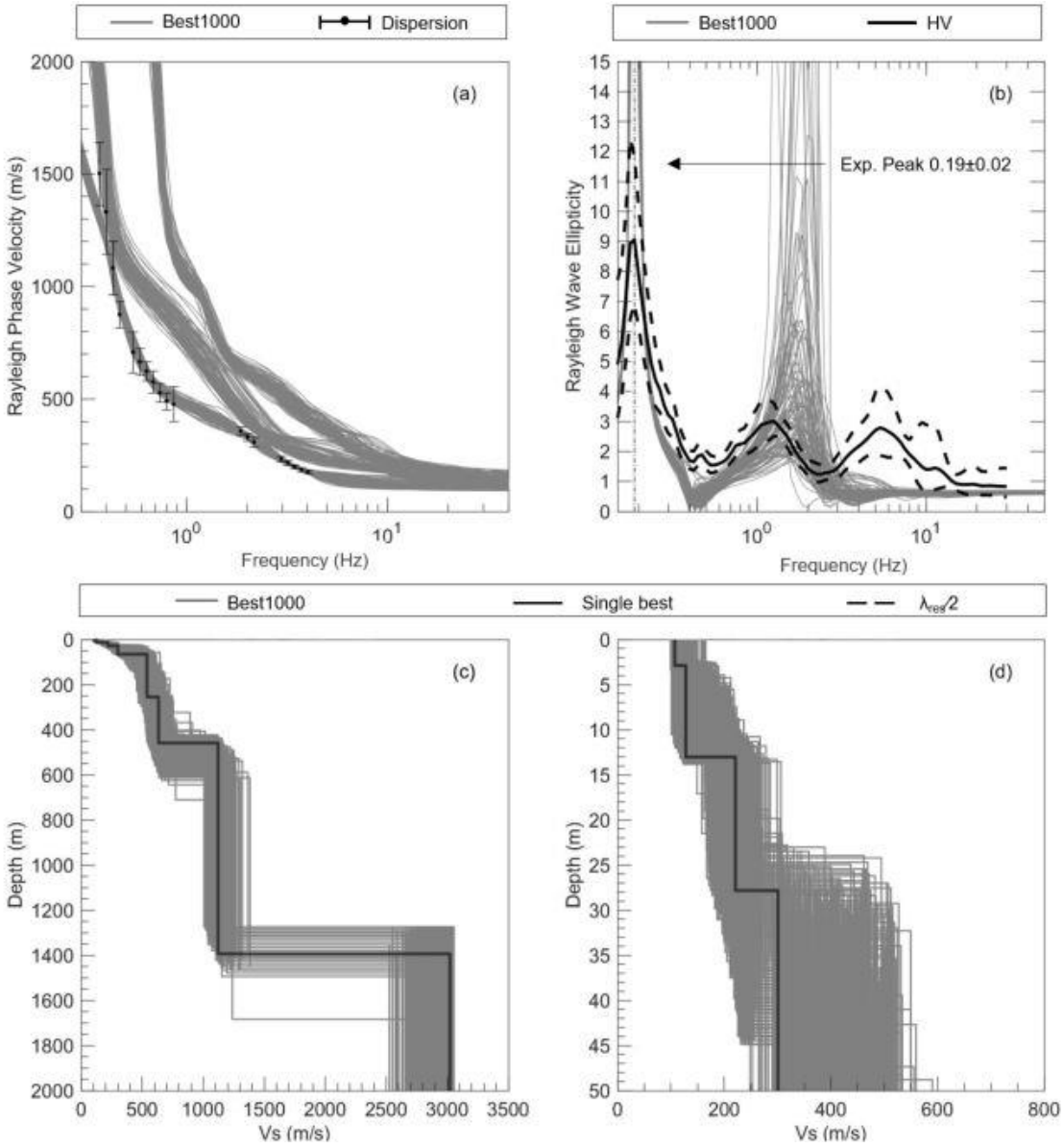

Figure 4.19 *- Surface wave inversion results for Gordonton. a) Experimental and best1000 theoretical Rayleigh wave dispersion curves. b) Experimental and best1000 theoretical Rayleigh wave ellipticity curves with the experimental peak used in the inversion. c) Best1000 shear wave velocity (V_s) models down to basement (in grey) with the lowest misfit profile in black. A 3000m off graph resolution limit applies. d) Best1000 shear wave velocity (V_s) models for the upper 50m (in grey) with the lowest misfit profile in black.*

The V_{s30} for the site is 166m/s and the fundamental period is 5.3s, this is a class E site per the criteria in NZS1170.5.

4.4.3 Kainui Road and Wallace Road (small)

The active data acquired for Kainui Road ranged from 30m/s at 5Hz to 28m/s at 12Hz. At Wallace Road this ranged from 38m/s at 5Hz to 35m/s at 12Hz, as per table 4.9. The resulting

dispersion curves for the site are given in the slowness domain (figure 4.20 below) to show the contrast between the passive data and the active data acquired for both sites.

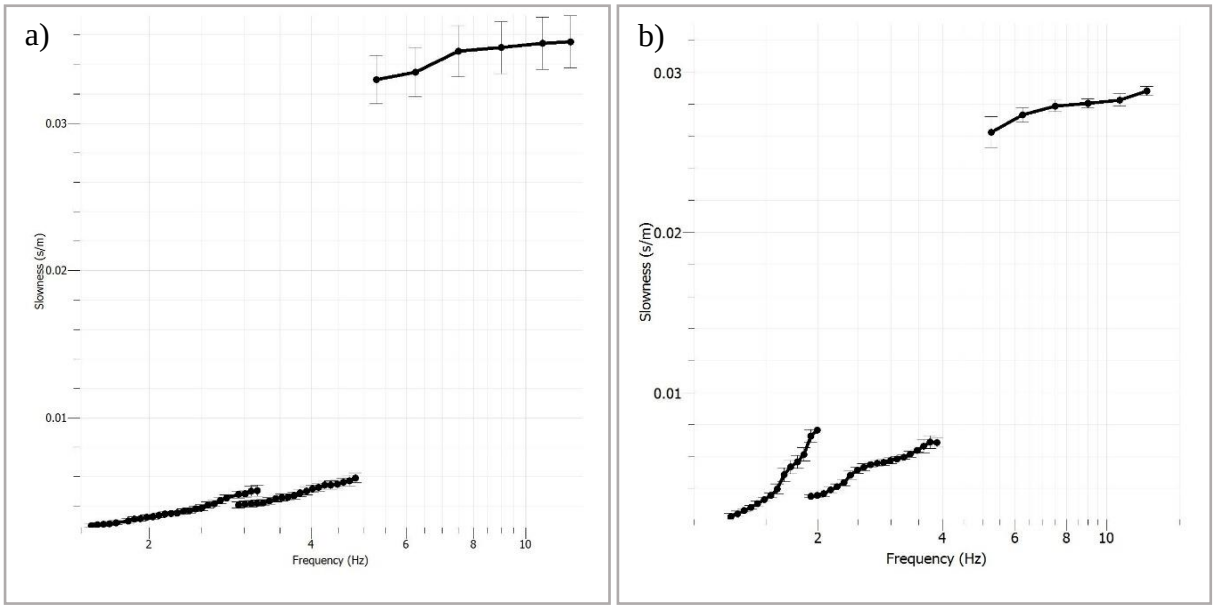

Figure 4.20 *Passive (small standard deviation) and active (large standard deviation), dispersion curves for a) Kainui Road and b) Wallace road (small)*

.

Unlike Temple View and Gordonton which had arrays with maximum diameters of 1000m, the largest arrays at Kainui and Wallace Road were 150m in diameter. For Wallace road (small) in particular this meant that the data acquired through the passive MAM method did not yield results compatible for inversion. The quality of the dispersion data influences the resulting shear wave velocity profile, so with dispersion data this poor from these two sites any inversion was going to be of comparatively poor quality. The processed dispersion curves are given in the appendix B. Results at the Wallace Road large site were not obtainable due to high winds up to 65kmhr which picked up during the day (appendix B) The additional dispersion curves from the larger arrays for the larger sites produced a reliable composite curve for an inversion.

4.5 Summary

The results from the processing and analysis of the acquired surface wave data have been presented in this chapter, resulting in 13 shear wave velocity profiles. Each site has been given a figure with the final shear wave velocity profile, the dispersion curve and fundamental frequency peak used in the inversion as well as 1000 theoretical solutions for each. Uncertainty has been presented by standard deviation in the dispersion and a set of the 1000 lowest misfit solutions. The following chapter discusses these results in detail.

Chapter 5

Result validity and implications for seismic design and site response

5.1 Introduction

As per the aim of this research, thirteen shear wave velocity profiles, their accompanying HVSR peaks, and dispersion curves have been determined and are presented in chapter 4. The geological correlations are combined with statistical analysis in section 5.2. If geological information is available it is used to constrain the inversion, however, given the sparsity of information at depth in the Hamilton Basin, geological parameterisation was not used in any inversion. Instead, section 5.3 details the analysis made to determine whether the obtained velocity profiles make geophysical and geological sense; a recommendation for result validity (Foti, 2017). An analysis of the peat anomalies is given in sub-section 5.4. The general theme of the literature on surface wave analysis for site characterisation is methodology, and how to produce reliable shear wave velocity profiles; this is evident in chapter 2 of this thesis. Section 5.5 includes an overview on the possible site response and amplification implications as well as the limitations of these profiles. Site response analysis is beyond the scope of this research. Section 5.6 includes recommendations on future work.

5.2 Shear wave velocity distribution

Based on the resulting shear wave velocity profiles there are four main groupings of shear wave velocity. Unit 1 is commonly between 100 and 250m/s , unit 2 is commonly 300-650m/s, unit 3 is commonly 690-1200m/s and unit 4 is >1200m/s. These velocity units and inferred age based geological units are given in table 5.1. Separating V_s of the Waitemata and Te Kuiti Groups is difficult because of the poorly known depositional history (Schofield, 1967) and largely unknown distribution and thickness in the Hamilton Basin. These sedimentary groups are present in some well logs, and not others. The Te Kuiti Group is comprised of siltstone and sandstone with some limestone, this differs only slightly to the lithology of the Waitemata

Group, which is alternating siltstones and sandstones (Edbrooke, 2005; Schofield, 1967). Defining the velocity of the 'basement rock' is independent of the NZ1170.5 site classification standards which define a rock site as V_{s30} >360m/s and different to the international classification of engineering bedrock as >760m/s (BSSC, 2015). Basement rock here refers specifically to the greywacke terrane underlying the Hamilton Basin (Edbrooke, 2005). A histogram analysis was used to determine groupings of shear wave velocity (figure 5.1). These groups are particularly definable in the low velocity range due and more varied in the higher velocity range due to the decreasing resolution with depth using the applicable methods.

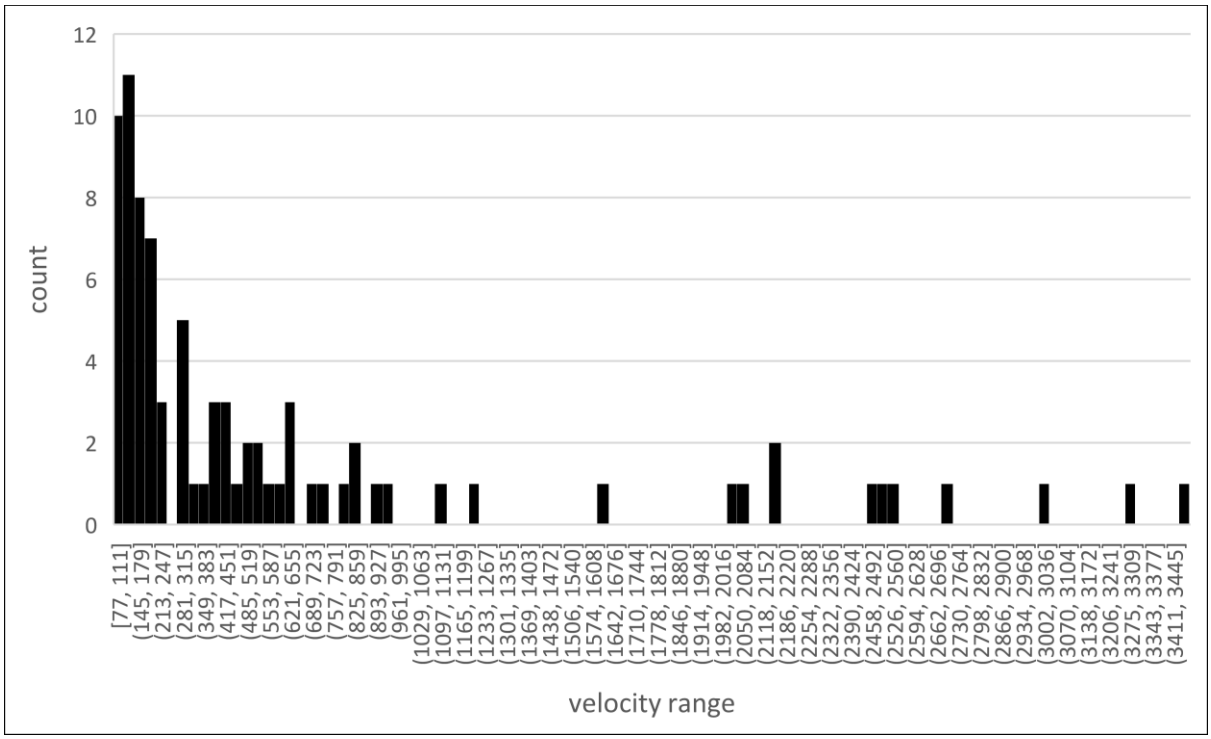

Figure 5.1 *Histogram of shear wave velocity values throughout the Hamilton Basin, taken from the lowest misfit profiles for all 13 sites.*

Table 5.1 *Shear wave velocity units. Determined from the histogram analysis in figure 5.1, from the lowest misfit profiles for 13 sites across the Hamilton Basin. Each velocity unit corresponds to an age based geological unit with a shear wave velocity range.*

Velocity unit	Shear wave velocity (V_s)	Inferred geological unit
1	<250m/s	Late Pleistocene Hinuera Formation
2	300-650ms	Pliocene-Pleistocene pumiceous sediments
3	690-1200m/s	Oligocene-Miocene sedimentary rocks
4	>1200m/s	Jurassic Basement Rock

5.3 Site evaluation

As previously discussed, surface wave inversion is inherently non-linear, and the inversion solution can have polarising V_s profiles with the same misfit for the same experimental dispersion (Foti & Parolai et al., 2011; Foti & Hollender et al., 2017). How to quantify aleatory (randomness) and epistemic uncertainty (model development) is still undecided in the literature, however, the Interpacific Project reported that final uncertainty can range from 5-10% depending on the analyst and dataset quality (Garofalo, 2017). For this study, dispersion uncertainty is represented by standard deviations and velocity profile ambiguity by a set of 1000 solutions of lowest misfit. Resolution limits caution interpretation boundaries and result reliability for each V_s profile. Procedural recommendations presented in chapter 2 were followed (chapter 3) to reduce errors arising from surface wave acquisition, processing and inversion. Geologically blind inversions were performed with multiple parametrisations, dispersion curve selections and where applicable, with multimodal dispersion curves. Each site will have varying uncertainty due to the quality/randomness of the data gathered and it is worth evaluating each site independently.

In comparing the velocity profiles to the available geological information it is worth highlighting that shear wave velocity profiles represent the average geology across the surveyed site (Foti, 2017). Given that the surveys in this research were up to 1100m in diameter and the focus depth was up to 2km, the averaged geology is across a large vertical and horizontal distance. In geology changes can occur in lithology over mm, cm, m or km, the V_s profiles in this research represent changes from m to km. Another constraint in the comparison is that the geology for the upper 9m around Hamilton City is well-detailed while there is less information for the upper 30m. Deeper than 30m and only 8 petroleum logs and seismic lines centred in the north-western basin are available from the 1970's. This information has its own uncertainties outlined in chapter 2.

5.3.1 Saint Peters

The multimodal dispersion at the Saint Peters site (figure 4.1a) was particularly interesting given that this was not observed at any of the other sites in the basin. This may be representative of more complex geology, similar to the inter-bedding in the Canterbury region (Foti, 2017; Teague et al., 2018). While there is interbedding of the silts sands gravels and pumice in the Hinuera Formation and even interfingering between volcanic ashes and ignimbrites in the Walton Sub-group; the deposits are primarily alluvial and reworked. In the Canterbury Region,

the very soft marine formations with low shear wave velocities directly contrast the complex V_s propagation that occurs in the gravel formations, which can be up to 30m thick (Lee et al., 2017). This interbedding creates shear wave velocity reversals, which are not typically expected with the less contrasting geology in the Hamilton Basin. One possibility is the presence of an emplaced ignimbrite, given the larger impedance contrast at 55m in the SP V_s profile from 300-750m/s, which represents a density increase (Figure 4.1c). What can be taken from the literature is that re-worked ignimbrites, particularly the Ontatiti Ignimbrite dominate the low lying hills and underlie the alluvial plains of the Hamilton Basin. The Rocky Hill Ignimbrite, which is a non-welded through to densely welded deposit, is also mapped close to Cambridge and this could be causing the velocity increase at 55m. An impedance contrast of similar magnitude in the near surface occurs at the Kiroa Road site however, no higher mode is observed. This could indicate that the density of the underlying deposit at SP decreases whereas at KR it increases, even though there is a significant contrast to the overlying layer in both instances. An inversion with a velocity reversal could be considered for SP however, geological information would be needed to constrain the inversion and was not available for these results.

Distribution of the Oligocene-Miocene sedimentary deposits is not known this far southeast, as the depositional history of the Waitemata Group in particular is not well understood (Schofield, 1967). It is theorised that sea level retreat occurred out the western side of the present day basin and that erosion of these rocks was quite significant in the area. With the velocity correlation in table 5.2 it could be concluded that these sedimentary rocks are present. However, with the large impedance contrast in the near surface it is likely that the increased velocity at depth is due to this; as velocity increases with depth in an inversion without velocity reversals (Foti, 2017; Socco, 2010). There is a large impedance contrast at 650m, which is the inferred basement depth at this site. While there is no existing confirmation of depth for basement at this site, based on the fundamental period data a slight increase in fundamental period (indicating a depth increase) occurs in the area. The gravity anomaly map depicts a slight decrease in gravity in the area associated with a decrease in elevation of basement rock. The colour guide grades from pink, which is high elevation to red, which is slightly lower (figure 2.8). A grade to light green would indicate a more significant decrease in elevation (expected with a decrease in basement elevation, from 180m at Tamahere, to 650m at Saint Peters). However, an ignimbrite would have a high density, which could influence the gravity at this site. The dispersion curve for the 600m array does have a sparsity of data points with large standard deviations in comparison to other sites, however, it follows the correct dispersion pattern and the low misfit for the dispersion dataset, indicates a good result.

In summary, five impedance contrasts are identified in the lowest misfit shear wave velocity profile for the Saint Peters site; at 17, 55, 160 and 560m depth. With velocity ranging from 108-195m/s in the upper 17m, this is concluded to be the Hinuera Formation. V_s increases to 294m/s below 17m, which is inferred to be the Walton Sub-group (Pliocene-Pleistocene). At 55m V_s increases to 725m/s thought to be due to a thick Ignimbrite within the Walton Sub-group. At 160m V_s increases to 851m/s thought to still be within the same unit. Basement is inferred at 560m where V_s increases to 2490m/s. These depths, associated velocities and geological correlations are presented in figure 5.3.

5.3.2 Ngaroto

There were no kinks or higher modes in the dispersion dataset for this site (figure 4.x) and the overlap between the active and passive dispersion curves was more than sufficient, increasing the reliability of the result (Foti, 2017). The lowest obtained misfit of 0.117 also indicates a good result; however, the variance of the theoretical H/V peak to the experimental in the higher frequency range does seem to cause some variability in the V_s profile between 15 and 40m (figure 4.2d). The experimental H/V peaks suggest an impedance contrast occurs at some depth (0.64Hz) as well as smaller one in the near surface (20Hz) (figure 4.2b). The peak at 20Hz does not satisfy the requirements for a clear peak with a standard deviation of 2.1 (higher than the frequency threshold of $0.05*f_0$) (SESAME team, 2004).

The Walton Sub-group is thought to underlie the survey area (Edbrooke, 2005), however, the Taupo Pumice Alluvium and the Hinuera Formation were very close by and may be resolved in the inversion. Two nearby groundwater logs (<30m from the array) detail sands, clays, pumice and interbedded peat, with increasing pumice content towards 73m depth. This is potentially consistent with the Hinuera Formation over the Walton Sub-group (Schofield, 1967; Edbrooke, 2005), but is also not conclusive. The higher frequency of the fundamental peak indicated a shallower basement and the inversion reflects this with a 190m basement depth for Ngaroto. This is the second shallowest basement result for the Hamilton Basin and no geological data for basement is available this far south.

Three impedance contrasts exist in the lowest misfit V_s profile at 13, 32 and 190m. V_s ranges from 100-175 in the upper 13m, consistent with the Hinuera Formation. A layer from 13 to 190m has a velocity range from 426-535m/s consistent with the Walton Sub-group (Pliocene-

Pleistocene). At 190m, the velocity increase to 2536m/s is inferred as basement. The geological correlation for this site is presented in figure 5.3.

5.3.3 McGregor Road

A different approach was taken for the McGregor Road site by conducting the MASW survey on the small hill close to the middle of the largest array (1200m) but adjacent to the peatland to create an overlap with the active and passive data. The resulting frequency gap between the active and passive dispersion curves ended up ranging from 1.5-5.5Hz. While this gap does decrease the reliability of the inversion results corresponding to the missing frequency band, it is significantly less than if the survey was conducted on peat. This would have confined the active data to a V_s of 35-40m/s, similar to other peat sites. The dispersion curves for the 50 and 200m passive surveys varied from other sites with a sharp increase in velocity over a small frequency range. This anomaly is presented in figure 5.2, with the raw dispersion curves for the McGregor site compared to those for the Kiroa Road site. The high velocity trend is very prominent in this figure.

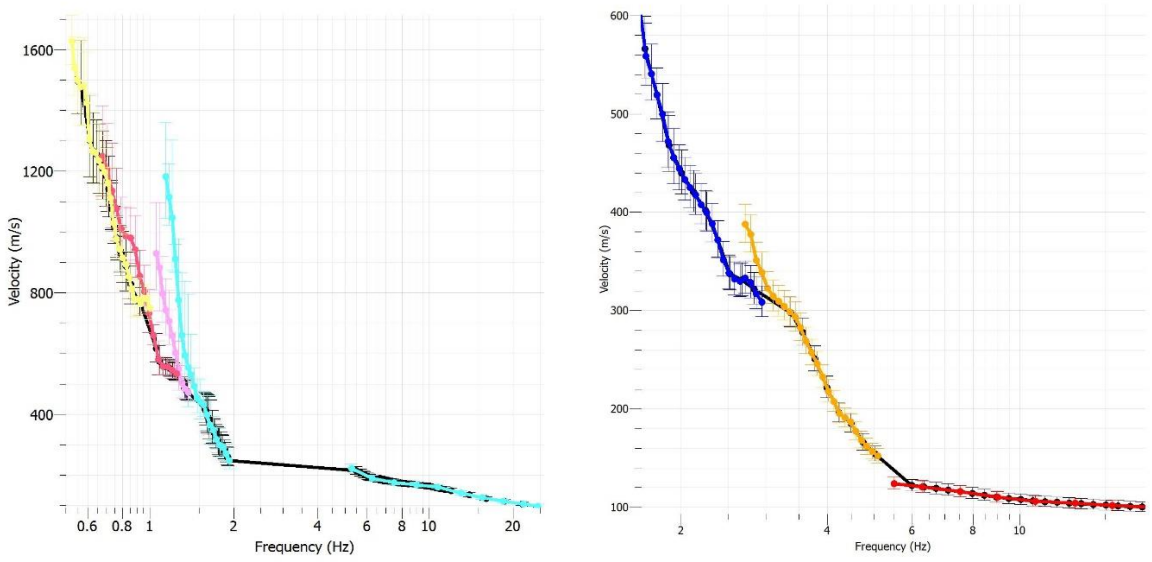

Figure 5.2 *Dispersion curves (uncut and un-resampled), black is the average dispersion. a) the McGregor Road site where cyan is active and passive 50, pink is passive 200, red is passive 600 and yellow is passive 1200 and b) the Kiroa Road site where red is active, yellow is passive 50 and blue is passive 150.*

The 297m result for basement depth could explain the dispersion anomaly in the passive data and the higher overall velocities at this site. The largest impedance contrast occurs at 297m with a V_s of 2065m/s from the single best profile. Considering the largest array at the site was 1000m in diameter, this impedance contrast is well within the resolution limit of 3000m. Therefore, data below 1500m ($\frac{1}{2}res$) is considered increasingly reliable. In hindsight, he 600m array would have been a suitable sizing for the investigation depth for this site. Vs profiles with and without the peak were similar visually in depth and Vs, however, velocity profiles with the peak used in the inversion resulted in lower misfits (0.152wp Vs 0.328np). The close match of the theoretical ellipticity to the fundamental fundamental frequency suggests an adequate resolution of this impedance contrast. MSPAC (modified spatial auto-correlation) method was used to analyse the 50m and 200m passive arrays to resolve the frequency gap missed through HFK analysis. The dispersion curves developed using the MSPAC method were in a very low frequency range (0.6-1.2Hz) and biased towards a lower phase velocity; therefore these curves were not used in the final inversion. The largest array for the McGregor Road site was 1000m, which proved to be quite large given the resolved basement depth of 297m. Despite proving to be larger than required for the investigation depth, the density of data points in the lower frequency range (figure 4.3a) seem to have helped reduce variability in depth and V_s of the basement impedance contrast (figure 4.3c).

The McGregor road site is located in the southwest quadrant of the Hamilton Basin at the base of the Walton subgroup hills in the Rukuhia Peat Bog. The site was expected to be relatively homogenous with an increasing shear wave velocity with depth. The near surface surveyed by active testing on the Walton Subgroup hills, may be layered with ashes underlain by pumiceous sands and grits of the Karapiro Formation then sands and silts with interbedded peat from the Puketaha Formation (Edbrooke, 2005). This is expected to be underlain by sedimentary rocks and basement rock, however, the distribution of the Te Kuiti Group in the area is not known. A ground water log on the steeper hill east of the array details clays and some pumice to 40m, consistent with the Walton Sub-group (Schofield, 1967; Edbrooke, 2005).

The five velocity increases in the shear wave velocity profile indicate five density increases. V_s ranges from 91-191m/s in the upper 19m, it is hard to define what material is represented in the inversion given the geological complexity at the site. The underlying layer from 19m-156m likely represents the Walton Sub-group at 422m/s. The layer from 156m to 297m is inferred as sedimentary rock due to the higher trending velocity (701m/s). At 297m, basement rock is reached with an increase in V_s to 2065m/s. The schematic for this correlation is in figure 5.3.

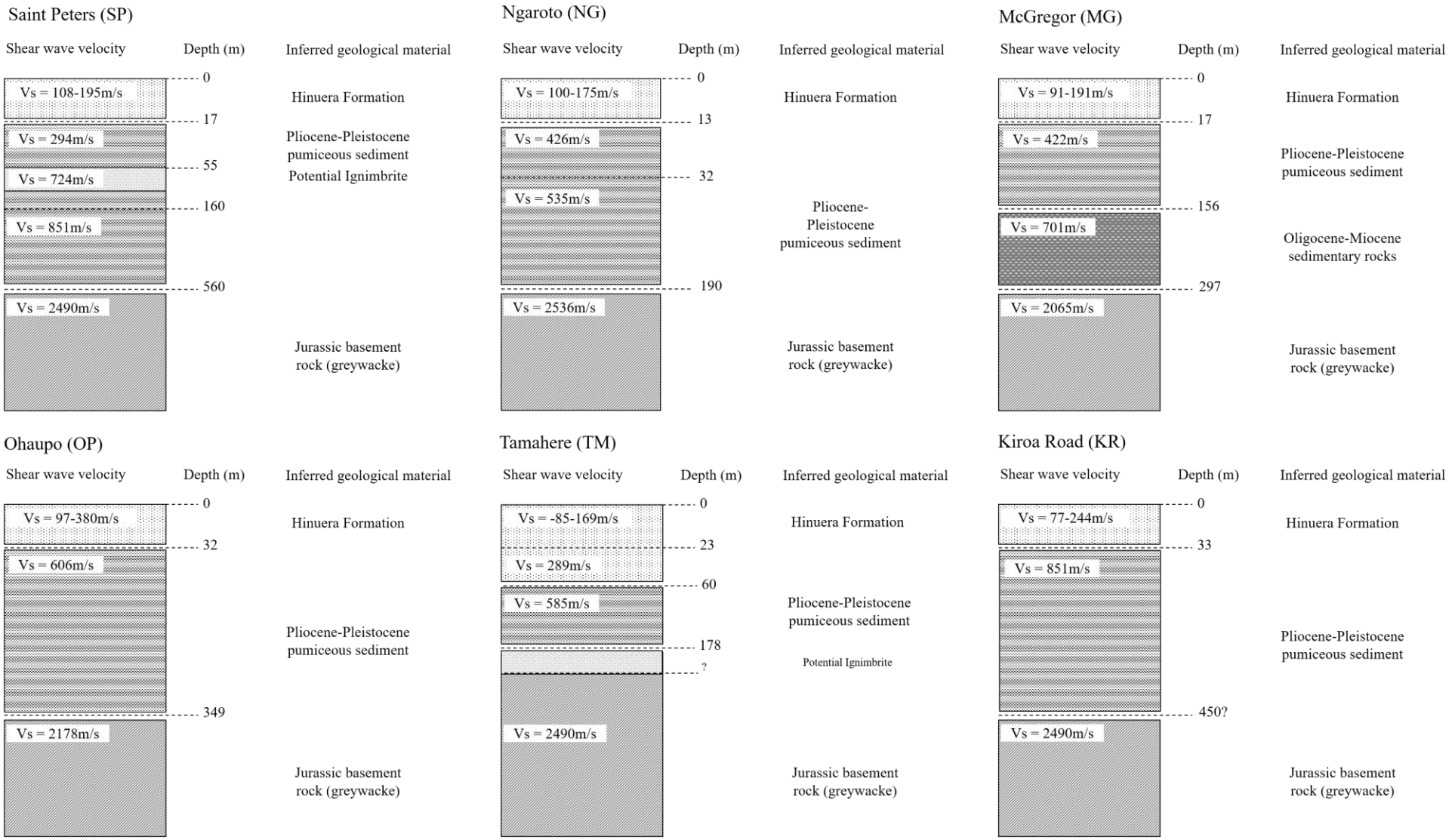

Figure 5.3 *Correlations between the available geological data and the shear wave velocity profiles for six sites in the Hamilton Basin*

5.3.4 Ohaupo

The dispersion data obtained through the analysis of the Ohaupo site is ideal with the overlap between the active and passive data and the smooth decrease in phase velocity with increasing frequency (figure 4.4a).

The map by Edbrooke, 2005 shows the Hinuera Formation at the surface with Taupo Pumice Alluvium (TPA) nearby to the north and Walton sub-group to the west. The proximity of the site to the nearby stream and an abundance of pumice and gravel at the surface suggests this could be TPA. The well log Ohaupo-1 2km from this site indicates that the geological layering is likely Tauranga Group over basement, which occurs at 295m.

The V_s profile shows multiple small impedance contrasts in the near surface (<35m) with a large impedance contrast at 349m. V_s in the very near surface (<5m) starts relatively low at 97m/s increasing to 120m/s then 217m/s up to 16m. The only other sites with a near surface velocity of <100m/s are KR, TM and MG. The layer from 16-349m is inferred as the Walton Sub-group with V_s ranging from 380m/s to 606m/s. At 349m basement starts, indicated by the increase in velocity to 2178m/s. The inferred geological profile for this site is given in figure 5.3.

5.3.5 Tamahere

Similar to the Ohaupo dispersion dataset, the active and passive datasets overlap at Tamahere, consistent with increased reliability (figure 4.5a). At lower frequencies phase velocity in the experimental curve tends to steepen as it increases, compared to the theoretical dispersion. This could suggest a very stiff layer at depth (Foti, 2017). Spatial resolution for identification of basement depth was adequate at the site with data below 225m considered more reliable than data below the resolution limit of 450m. The extracted HVSR peaks for the Tamahere site were similar to Ngahinapouri and varied from all other sites in this study given the presence of one peak rather than multiple. Preliminary conclusions for this were one impedance contrast at this site with a relatively consistent geological unit or units. The fundamental peak at Tamahere was the highest in the basin at 0.67, indicating a shallow depth to basement.

A nearby ground water log (700m from the array) records alternating silts sands and gravels to 50m changing to alternating pumice and silt to 100m. At 100m, a 15m thick layer of Rhyolite overlies basement rock which is reached at 115m. Given this information it is likely that an emplaced ignimbrite is present at the Tamahere site. This is likely the Ongatiti Formation as

this was deposited during the initial stages of the Walton Sub-group deposition (Edbrooke, 2005). The Isostatic Residual Bouguer Anomaly map from FrOG Tech (2011) shows an increase in basement elevation in the Tamahere area, as per figure 2.8. This is consistent with the shallow basement indication from the fundamental HV peak and the known basement depth of 115m from the well log.

V_s ranged from 85-169m/s in the upper 23m, increasing to 289m/s until 60m. This is inferred as the Hinuera Formation, although it is slightly outside the bounds of velocity unit 1 in table 5.1. An underlying layer from 60-178m where V_s is 585m/s is inferred as the Walton Sub-group. At 178m velocity increases to 2525m/s which is the inferred basement depth for the site. Given the dispersion indication of a stiff layer at depth, it is presumed that the Rhyolite present in the well log overlies basement at this site. This information was not used to constrain the inversion given the distance of the well log from the site. The deepening of basement depth from the ground water log to the array location is ~60m and the possible thickness of the rhyolite layer is 15m, this meant that it was not possible to define the rhyolite in the inversion. An inferred stratigraphy from the V_s profile is given in figure 5.3.

5.3.6 Kiroa Road

The largest array at the Kiroa Road site was 150m and for the V_s profile, results deeper than 225m depth (half of the maximum wavelength) may be adversely affected and results shallower than 225m should be considered more reliable (Foti, 2017). The large impedance contrast occurs at the resolution limit, cautioning the interpretation of basement depth at this site. The joint HV inversion, produced a lower misfit of 0.18 compared to 0.31 with no peak. Profiles with no peak lacked a large impedance contrast although other smaller impedance contrasts were similar depths and V_s to the final profile presented (figure 4.6c). There are two peaks in the HVSR, one large peak which represents the fundamental frequency and one smaller amplitude higher frequency peak which does not meet the critera for a clear peak (SESAME, 2004). The f_0 of 0.42 suggested a deepening of basement rock in comparison to the Tamahere site. The 1st higher mode theoretical dispersion curves trend towards the experimental dispersion curve at 3.5Hz indicating a higher mode is likely. This is likely similar to Tamahere, although, no geological information is available in this area to confirm a cause or constrain an inversion.

There is limited geological data for this site, the geological map from Edbrooke, 2005, classifies the surficial lithology as peat. The higher velocity of the active survey and lack of vibration at the site indicates peat was not present at the site although subsurface lenses are still a possibility, particularly in the Hinuera Formation (Schofield, 1967). Seismic line assessment, presented in chapter 2 of this thesis outlines that basement is present at the lower Oligocene-Miocene contact whereas the Miocene-Pliocene contact is at 400m. This infers that there are likely very thin-no sedimentary rocks at this site. This is consistent with the cross section from (Edbrooke, 2005) which runs just south of this site and shows that the Waitemata Group grades out to not present in the far eastern basin (Figure 2.7a).

Shear wave velocity ranges from 77-244m/s to 33m which is inferred as the Hinuera Formation. From 33m to 450m V_s is 851m/s, which is indicative of sedimentary rock (unit 3) in the velocity correlation in table 5.1. This is however not likely based on the indication of geology for this site; the Walton Sub-group, possibly including an ignimbrite, will more likely underlie the Hinuera Formation at this site. The basement depth result from this study which is highly cautioned is 450m with the increase in V_s to 2490m/s. A schematic for the inferred geology at this site is given in figure 5.3.

5.3.7 Ruakura

The anomaly in the HVSR curves presented in chapter 4 (figure 4.7) is interesting for this site, especially as the guidelines from (SESAME, 2004) state that there is no known influence of power lines on H/V curves. Large pylons run through the array at the Ruakura site to the nearby power station, and have a noticeable hum. From the appearance of the peaks in figure 4.7 it looks like the higher frequency peak has an ‘industrial origin’ (SESAME, 2004) which is masking the fundamental peak of the site. Analysis of seismometers further from the pylons (UC_S03 figure 4.7) produced a clear H/V peak at 0.3Hz. Therefore, it looks like in this instance the presence of the pylons has had an effect on the HVSR curves. The misfit from the inversion with the peak was slightly lower than without (0.201 with versus 0.231 without) suggesting that 0.3Hz indeed represents the fundamental frequency of this site. This is relatively consistent with research from (Jeong, 2019) which details a 0.33Hz fundamental peak for the ‘Hillcrest’ area, very close to Ruakura. The dispersion for the site appears smooth and a large overlap between active and passive datasets was obtained increasing reliability (Foti, 2017).

The QMAP from (Edbrooke, 2005) maps the Hinuera Formation as the surficial unit at this site, multiple CPTs and hand augers within the array confirm the Hinuera Formation is present to at least 19m (NZGD). The only other shear wave velocity profile for the Hamilton Basin which is available in the literature is from a liquefaction study using crosshole and downhole measurements of V_s; this is presented in figure 5.4 below. Although the location is not known it is from the Waikato Expressway development which is close to the Ruakura site so it has been compared to the upper 50m V_s obtained from the Ruakura inversion. The two are in relatively good agreeance; V_s increases gradually to 250m/s in figure 5.3a which is where the Walton Sub-group was recorded at 20m, and V_s increases to 261m/s at 22m in figure 5.3b, indicating a lithology change. The CST/DMT profile is much more detailed as it is focused on the very near surface whereas the surface wave analysis is focused on significant depths in comparison and impedance contrasts represent rapid density changes rather than gradually increasing V_s. Not much is known about the distribution of the sedimentary rocks in the area, other than that they are likely present at Ruakura compared to Kiroa Road (Edbrooke, 2005).

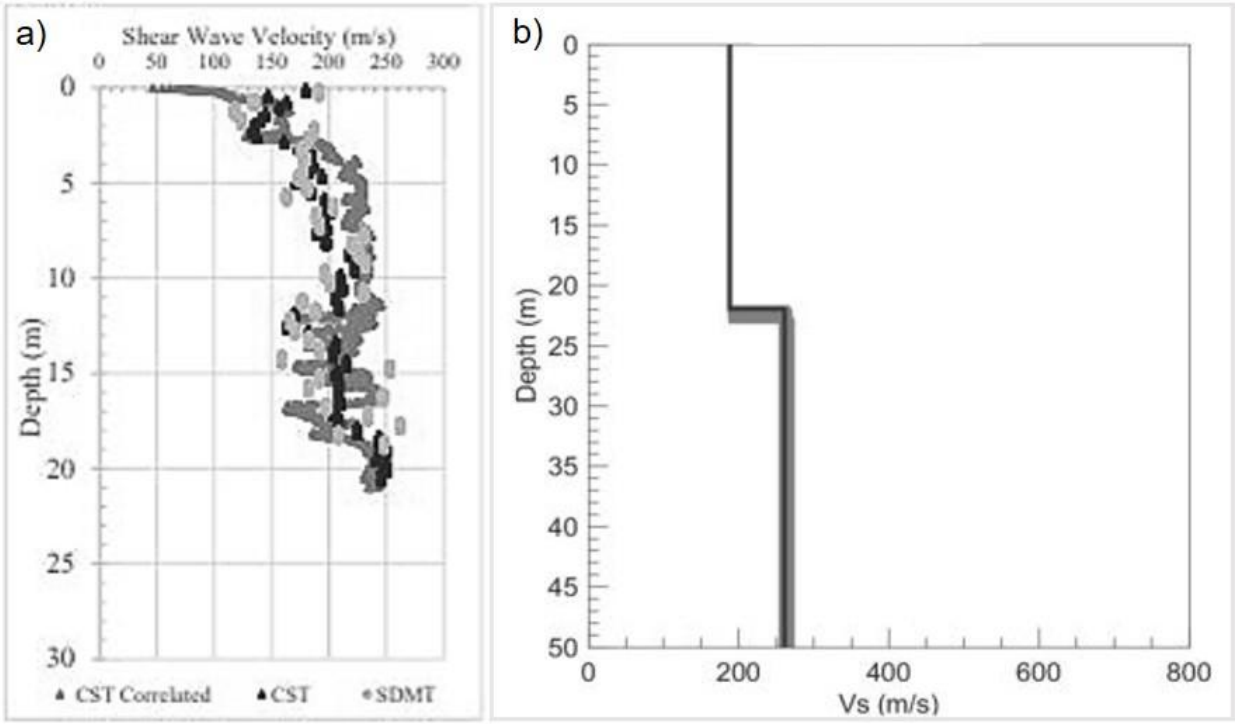

Figure 5.4 *Two shear wave velocity profiles. A) Shear wave velocity profile from SDMT (downhole) and CST (crosshole) testing for the Waikato Expressway development* (Clayton et al., 2017). *B) Shear wave velocity profile from surface wave testing) for the upper 50m at the Ruakura site (this study).*

The Hinuera Formation is expected to 22m where velocity increases from 188m/s to 261m/s. The Walton Sub-group is expected from 22-206m where velocity increases from 261m/s to

389m/s. Where V_s increases to 700m/s at 206m likely represents sedimentary rock (unit 3) with the velocity correlation in table 5.1. Basement is inferred at 492m where V_s increases to 1944m/s. A schematic for the inferred geology is given in figure 5.6.

5.3.8 Hamilton Boys High

The Hamilton Boys High site showed very dissimilar velocity profiles with and without joint HV inversion, however the profiles with the peak matched the dispersion with a lower misfit (0.277 no peak versus 0.17 with peak). The profile presented in figure 4.9c has one large impedance contrast which ranges from 355-480m in depth and 2200-3490m/s with a lowest misfit of 396m at 3282m/s. This range could be down to the larger standard deviation in the dispersion at lower frequencies compared to those above 2Hz. This is common due to the decreasing resolution with depth, where thinner layers cannot be resolved and the velocity/depth boundary becomes less defined (Foti, 2017). Geological ground-truth data for this site include a shallow (9.5 m) borelog ~700 m from the array, and a 19 m deep CPT trace ~200 m from the array. These indicate silt and sand alternations with some pumice to the full depth (19 m), consistent with the mapped Hinuera Formation (Edbrooke, 2005). The basement map of Edbrooke (2009) suggests a basement contact at just above 500 m depth, whilst seismic line interpretation on the petroleum mineral database, suggests the Oligocene/Miocene contact occurs at ~396 m. However, considerable uncertainty is expected in the basement contact and other contacts at depth given the poor quality of the seismic data used for these interpretations.

Based on the correlations between geological materials and velocities as described above, the inferred stratigraphy at this site consists of Hinuera Formation to 22 m (126-163m/s), overlying Walton Subgroup materials to 91 m (340m/s), Oligocene / Miocene sediments to 396 m (489-624m/s), and basement greywacke below 396m (3282m/s). A schematic for this site is presented in figure 5.6.

5.3.9 Elliot Park

Elliot Park is located on the western side of Hamilton City in the suburb of Nawton. The Hinuera Formation is likely present at the site (Edbrooke, 2005). The stratigraphy at the site is

expected to be HF over Walton Sub-group over Waitemata Group, potentially over Te Kuiti Group based on the Waikato-2 petroleum well log. The dispersion curve used in the inversion is smooth with sufficient overlap between the dispersion curves (figure 4.11a).

The fundamental frequency peak for the EP site of 0.49Hz is higher than the 0.28Hz peak frequency for the RK site suggesting a shallower basement depth. The misfits for the inversion with the peak were variable and typically higher than the misfits for no peak, with the exception of layering ratios 3.0 and 4.0 (table 4.7). The profiles for LR3.0 and LR4.0 appeared constrained presenting as single profiles, therefore, the peak frequency is questionable. Considering the nearby Waikato-2 petroleum well log recorded basement at 1015m depth, the fundamental frequency obtained for EP appears high. Acquisition advice was followed, the seismometers were buried and compacted for more than half their height with buckets used overtop. The urban area had traffic nearby but there was only one instance of foot traffic in the park during the survey. The peak does not appear to be industrial in origin and fits the criteria for a clear peak (SESAME, 2004). Another possibility for the higher misfits with the joint HV inversion is that the fundamental peak is beyond the resolution limit in the dispersion curve, given that the largest array at the site was 150m. It is not recommended to undertake a joint inversion when this is the case (Parolai et al., 2005).

The profiles retrieved from the inversion without the peak and appear similar to the expected geology at the site. V_s ranges from 101-183m/s to 25m, consistent with the Hinuera Formation. The Walton Sub-group is correlated to the increase in velocity at 25m to 635m/s. With V_s increasing to 700m/s at 126m, Oligocene/Miocene sediments are expected based on the velocity correlations in table 5.2. A schematic of the velocity profile is presented in figure 5.6.

5.3.10 Ngahinapouri

Ngahinapouri is the westernmost site in the surveyed area. Approximately 7km southwest of Temple View (TV), the Hinuera Formation is likely the surficial geology with the Walton Subgroup hills nearby (Edbrooke, 2005). There is no information on the subsurface geology within 500m of the array locations. Based on the lower velocity trend in the high frequency passive dispersion (figure 4.12a) it was thought that there may be a slightly stiffer near surface layer at the site. The high misfits returned for the inversions with the active data set as a higher mode as well as inversions with the low velocity passive data removed, ruled this out.

Interestingly the theoretical dispersion does not follow the low velocity experimental data (figure 4.12a) however, when this was manually removed there appeared to be not enough data for the inversion process, with arbitrary models produced. The peak increased the reliability of the inversion by assisting with bedrock depth resolution. The high misfits without the peak appear to be down to the lack of low frequency data in the dispersion. The similar shallow layering in profiles with and without the peak suggests good near surface agreement but a basement depth estimate with no peak was ~250m shallower than the basement depth retrieved with the peak. A reliable result was obtained for the final inversion based on the low obtained misfit of 0.13.

The lowest misfit profile has three predominant impedance contrasts at 30m, 123m and 395m. The Hinuera Formation is thought to be the upper layer, with the Walton Sub-group underlying this to 123m and basement is reached at 395m based on the velocity correlations in table 5.1. A schematic of this layering is given in figure 5.6.

5.3.11 Te Rapa

The dispersion curve and HVSR curve do not have any notable anomalies for this site with theoretical results from the inversion closely matching the experimental curves (figure 4.13). Looking at the comparison between the Te Rapa-1 well log and the Te Rapa V_s profile in figure 5.5 on the following page, the profile is generally agreeable with identified lithology changes, except for the basement depth. (Jeong, 2019) found that the fundamental periods changed rapidly in areas where they were the longest, this indicates a rapid shallowing in basement depth. Since the V_s profile represents an averaged geology over the diameter of a kilometre it is possible that the averaged basement depth is less than the well log. The well log is also 1km east of the most eastern point of the largest array. There could also be an unquantified influence of the shale deposits having a higher velocity than the weathered greywacke, however, there is no indication of complex layering in the dataset (unlike Saint Peters).

The inferred geology for the V_s profile is presented in figure 5.6, independent of the geology inferred for the petroleum log in figure 5.4. The Hinuera Formation is correlated to the upper 21m with a V_s of 120-175m/s. The impedance contrast at 21m represents the start of the Walton Sub-group with a V_s of 455-518m/s. The increase in velocity to 932m/s at 287m marks the start

of the sedimentary rocks based on the correlation in table 5.2. Basement is inferred from the impedance contrast at 1212m where V_s increases to 3479m/s.

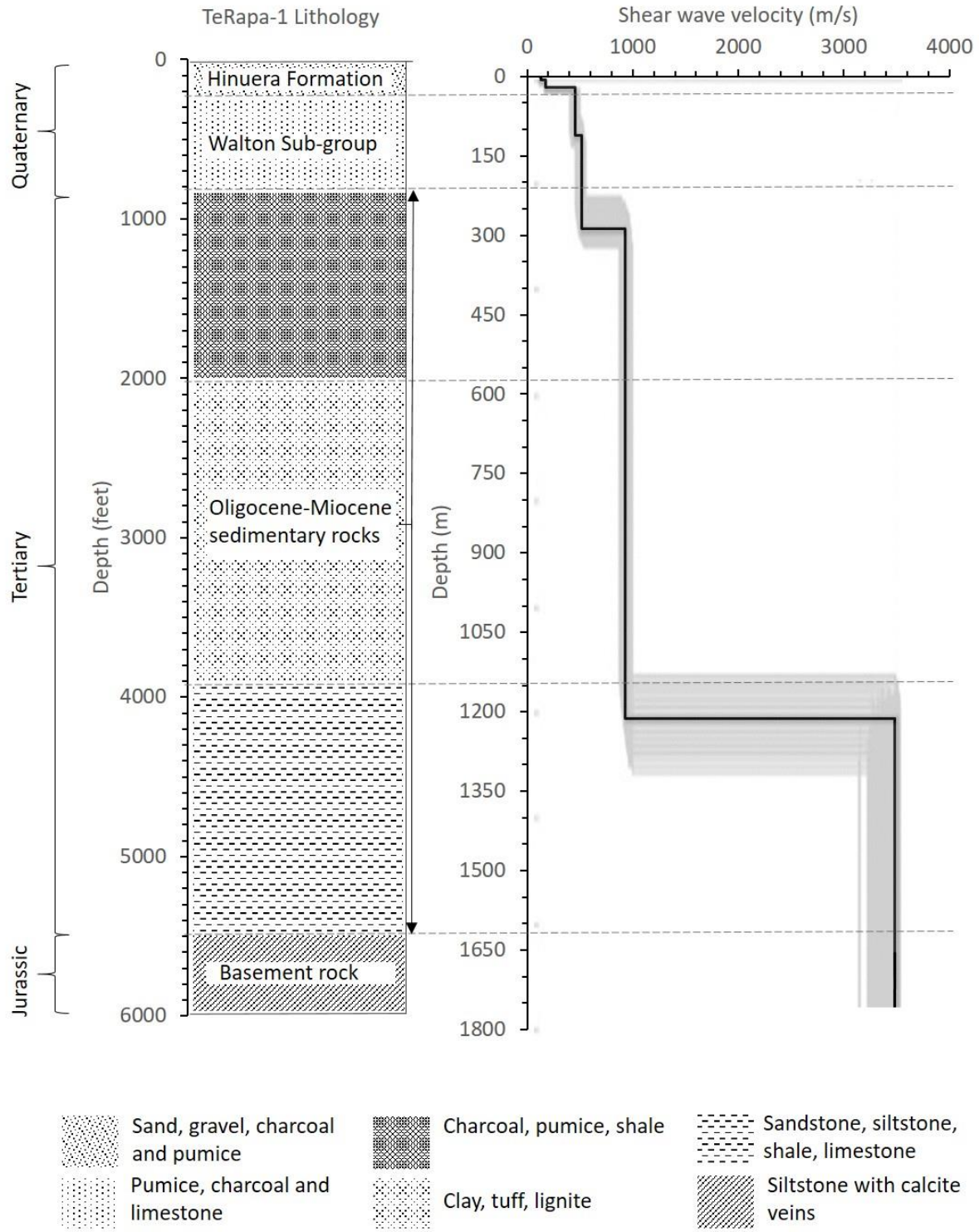

Figure 5.5 *Correlation between the Te Rapa-1 welllog and the shear wave velocity profile for Te Rapa. It should be noted that there are uncertainties in the bore log, hole collapse was mentioned at 800ft/240m.*

5.3.12 Temple View

The Temple View site is located in the north-western quadrant of the study area, just outside of the Temple View suburb. Surface wave testing was conducted on the peatland adjacent to the Walton SubGroup hills (Edbrooke, 2005). Nearby groundwater logs recorded that peat overlies the Hinuera Formation on the flats with the Walton Subgroup sloping underneath, 300m from the largest array.

What is particularly interesting is the anomaly in the H/V dataset, presented in figure 4.15. The wind on the day was recorded from the MetService website as a light 5kmhr wind, which would not have effected the results given that the seismometers were buried for more than half their height (Foti, 2017). If external influences were responsible for the result, the peaks would likely not be so well defined (SESAME, 2004). Instead, the defined peaks vary significantly in fundamental frequency over the diameter of 1km. This anomaly appears consistent with H/V measurements which are effected by strong lateral discontinuities; such as faulting, steep sloping or an irregular basement (SESAME, 2004). The Kukutaruhe Fault Zone identified from geomorphic assesment by (Spinardi, 2017; Moon & de Lange, 2017) is inferred to run along the ridge 400m from the largest array for this site. The position of the Fault with depth is not known, it is possible that the HVSR results are displaying the variation in basement depth across the fault. This anomaly is concluded to not be an effect of peat as this variation in peak frequency was not observed at the other peat sites in this study.

The peat will be discussed in section 5.4, however the inversion without the active (MASW) dispersion curve resulted in lower misfits and the final profile was accepted from this inversion. Without a peak frequency used in the inversion the results did not appear reliable, the inversion with the peak was acceptable. With the variation in peak frequency across the site and the removal of the active dataset the resulting shear wave velocity profile is not as reliable as the previous Te Rapa site. V_s in the upper 25m is 153m/s increasing to 291-402m/s to a depth of 158m, which is consistent with HF over Walton Sub-group expected for the site. At 158m V_s increases to 1202m/s indicating sedimentary rock. The inferred basement depth is 676m however; there are many uncertainties in this result outlined above. Multiple inversions with all peaks could be attempted to find an ideal fit, given a single inversion takes an hour this would take 200 hours and the uncertainties would likely still exist. A 500m array would resolve

some uncertainties with depth and a velocity reversal with the depth of the peat known would resolve some shallow uncertainties.

5.3.13 Gordonton

The consistency of HVSR curves between seismometers for the Gordonton site (figure 4.18) suggests that the variance at Temple View is not related to the peat. The active data however, was affected in the same way as Temple View with a very low shear wave velocity on the peat. With the removal of the active data in the final inversion, the near surface resolution is decreased (<50m depth). This is represented by the variability in the near surface V_s profile (figure 4.19d. There was a lack of overlap between the 200 and 1000m arrays at this site due to land use constraints preventing the deployment of a 600m array. The deployment of a 600m array would have covered the frequency band missing from the dispersion data. This is likely contributing to some of the variation in the deeper velocity profile. The low frequency peak indicated a deep impedance contrast, which was resolved in the inversion as 1394m deep. Gordonton is northeast of Hamilton City, and the survey site was located just east of the township on the peatland. Peat, clay, pumice and sand was recorded to a depth of 48m in a ground water log 200m south of the largest array. This suggests that the Hinuera Formation likely underlies the peat layer at this site. The lowest misfit V_s profile from the inversion has been illustrated in relation to the expected geology at the site in figure 5.6; the upper 50m in particular has a higher uncertainty.

Based on reported values of shear wave velocity, engineering bedrock was expected to be >760ms (Fema, 2012); more specific to the Waipapa Composite terrane, ‘basement rock’, was expected to be in the order of 1500-2500m/s based on results from (Deschenes et al., 2018). The lowest misfit models for all sites had a basement rock velocity that ranged from 1635m/s to 3478m/s. A shear wave velocity result of 3478m/s is quite high, and is commonly associated with seismic bedrock, which is >3000m/s (Stein & Wysession, 2003). Shear wave velocities of >3000m/s appeared in three site results, HB, GD & TR. At HB in particular there is a large variation in velocity (2200-3500m/s) which is most likely due to the inability of the inversion to resolve beyond the resolution limit which causes high variability in bedrock velocity and depth (Foti, 2017). At GD and TR there is little variation in bedrock velocity (2500-3000: GD) (3100-3500:TR), so the high basement velocities are likely down to the depth extent, whereby V_s increases with depth so at large depths there is a large V_s. The surveys at both GD and TR were large so the basement depth is within the array resolution limits.

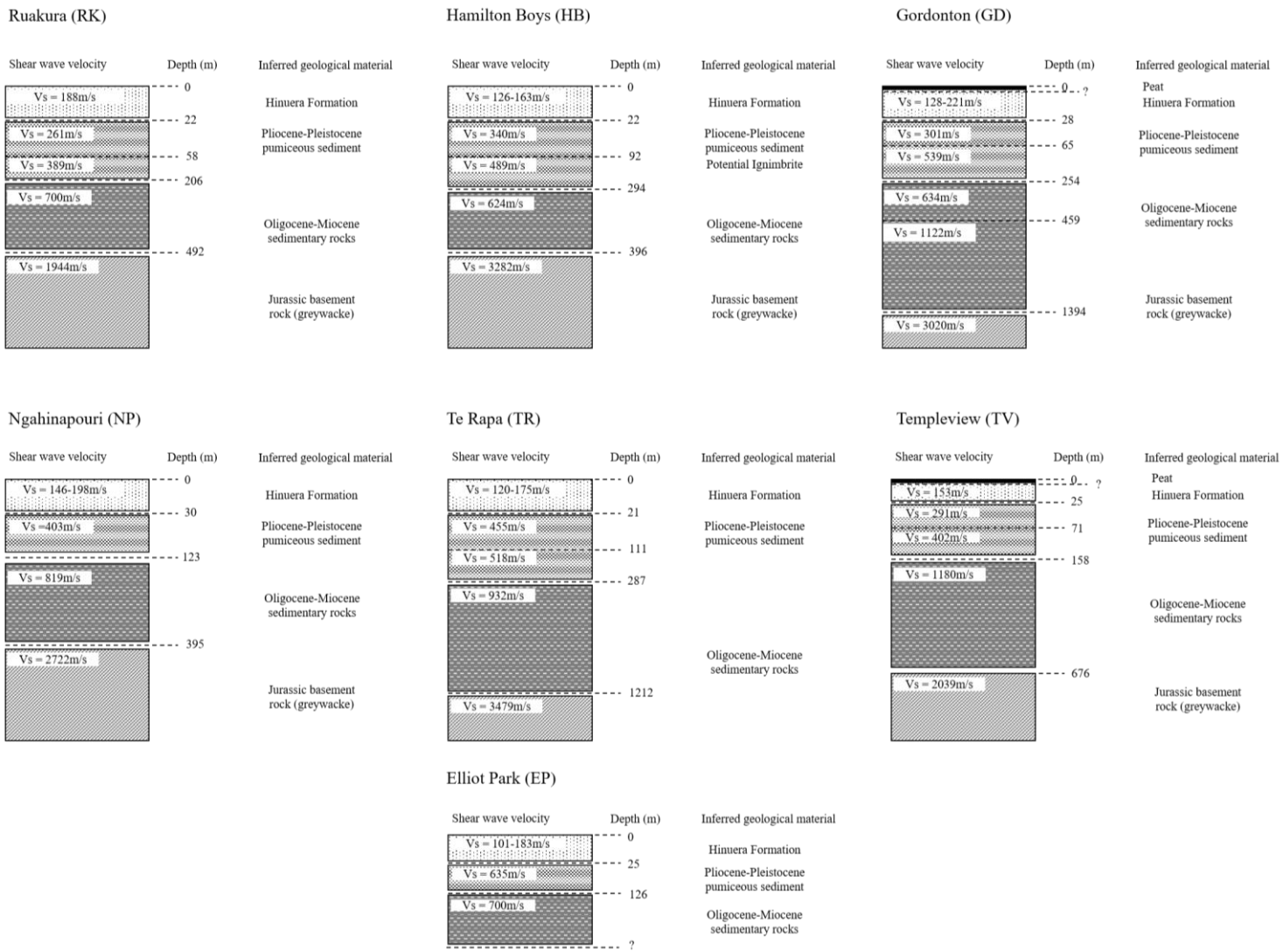

Figure 5.6 *Correlations between the available geological data, and the shear wave velocity profiles for seven sites in the 'northern' Hamilton Basin*

5.4 Peat anomalies

As determined by many authors, peat bogs are an extensive surficial feature in the Hamilton Basin with a depth range in the order of 2-15m (McKenzie, 2004). Peat has a high organic matter content (>75%), a very high water content (>200%). The resulting shear wave velocity of the peat from this study was 28-35m/s across all peat sites surveyed by MASW. However, a shear wave velocity of 28m/s is significantly lower than the 65-90m/s obtained in the Manukau study (Dawson et al., 2015). This low velocity creates significant issues in the inversion due to the large dispersion variation between the active and passive data, particularly in the frequency-slowness domain.

The thickness of the peat in the Hamilton Basin is not well defined. One study for the Rukuhia peat bog estimates thickness to be between 1 and 11m using a steel probe (McKenzie, 2004); in contrast thickness was defined as 10.5m in the Manukau study. Both peats tend to be silty in composition and thus the composition does not explain the difference in V_s. Worldwide, studies on the V_s of peat are limited, one by (Kramer, 2000) measured V_s using a seismic cone and found that V_s ranged from 12-30m/s in peat with a water content of 600%. (Wehling et al., 2003) surveyed V_s using downhole methods and found that V_s ranged from 22-27m/s in peat with a measured water content of 236-588% and 88-129m/s in peat with a lower water content of 152-240%. There is no available data of the water content of the Hamilton Basin peat and the Manukau study peat to see whether there is a comparison.

Another interesting point is that the shear wave velocity of peat is so slow, that it was often aliased when measured with pre-determined array spacing of 2m. This caused the observed dispersion to be spread over a minimal frequency range (e.g. 5-12Hz in figure 5.6), meaning that outside this range the waves had wavelengths much shorter than the array spacing of 2m. This translates to resolvable depth ranges of 2-4m suggesting that the typical dispersive behaviour of surface waves is not occurring and the assumptions made during the inversion are not met (assumes homogenous linear elastic layering). Below in figure 5.7 is two raw ‘shot’ seismographs, one from the Hinuera Formation at the Kiroa Road (KR) site and one from the peat at the Kainui (KN) site. The wave record in the peat looks to be made up of multiple wave types and the Rayleigh wave signal does not dominate the record when compared to figure 5.1a.

There is the possibility that Rayleigh waves are not contributing to the signal, but rather love waves are, as they propagate with a faster velocity.

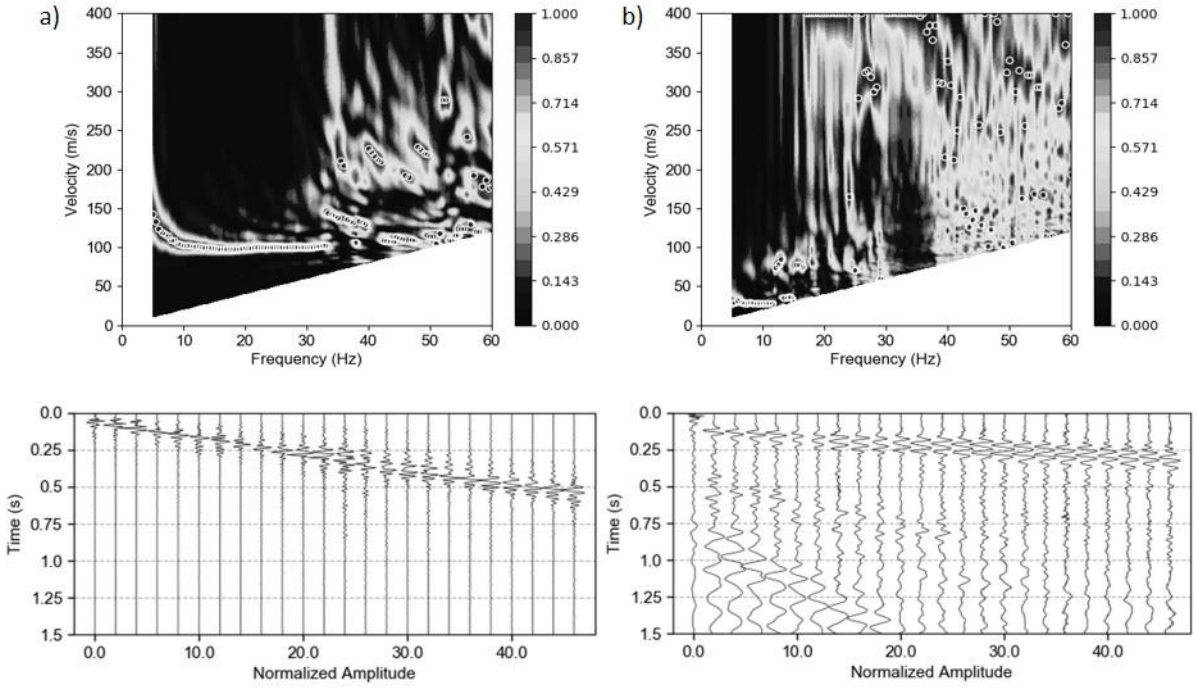

Figure 5.7 *Recorded sledgehammer 'shot' using the Multichannel analysis of surface waves (MASW) method for a) The Kiroa Road site not on peat and b) The Temple View site on peat. Each vertical line represents a geophone position, each one being 2m apart with a total spread of 48m.*

For peat sites with larger investigation depths and array diameters (TV, GD) the active data was ultimately excluded from the inversion producing lower misfits. For these sites results shallower than 50m are considered to have reduced reliability because the active data was not used and the near surface was not resolved. The attempt to use the Microtremor Array Method to survey a higher frequency range with array diameters of 5m and 15m was relatively unsuccessful with higher misfits produced.

The 15m dispersion curve appeared as a higher mode and the 5m dispersion curve while fundamental mode had a low velocity at a much higher frequency than the passive data. Both the passive and active data obtained at sites with array diameters of 50m and 150m (KN, WS) was not usable, the higher frequency range produced misfits >3 for multiple inversion attempts. Interestingly, inversions using the passive curves were also unsuccessful with misfits >3 for the experimental dispersion.

5.5 Fundamental frequency to basement depth relationship

The depth to a large impedance contrast (bedrock-soil) is particularly important for site response studies because the amplification response of the overlying soil column will depend on the thickness of the 'soil' among other parameters (Kramer, 1996). Soil is hyphenated because soil in engineering is unconsolidated material that is not rock which is what is referred to in this case, and in geology soil is a thin layer at the ground surface. A revised fundamental frequency-bedrock depth relationship has been developed for the Hamilton Basin following from (Jeong, 2019). A regression analysis of the basement depth (H) from the lowest misfit V_s profile and the accompanying site $f_{0.}$ was undertaken to determine the relationship. This is based on studies confirming a power law relationship between H and $f_{0.}$ (Ibs-von Seht and Wohlenberg, 1999; Parolai et al., 2002). The regression analysis is presented in figure 5.8 and the derived empirical relationship is given in equation 5.1 below:

$$H=118.8f_0^{-1.396} \qquad (5.1)$$

Where H is the thickness of the soil overlying basement, and f_0 is the fundamental frequency at that site. This builds on the model from (Jeong, 2019) by adding data to a higher frequency range and accounting for spatial variability in V_s.

As shown in figure 5.8 the results of this study are relatively consistent with the model developed by (Jeong, 2019) with some variation in depth at higher frequencies.

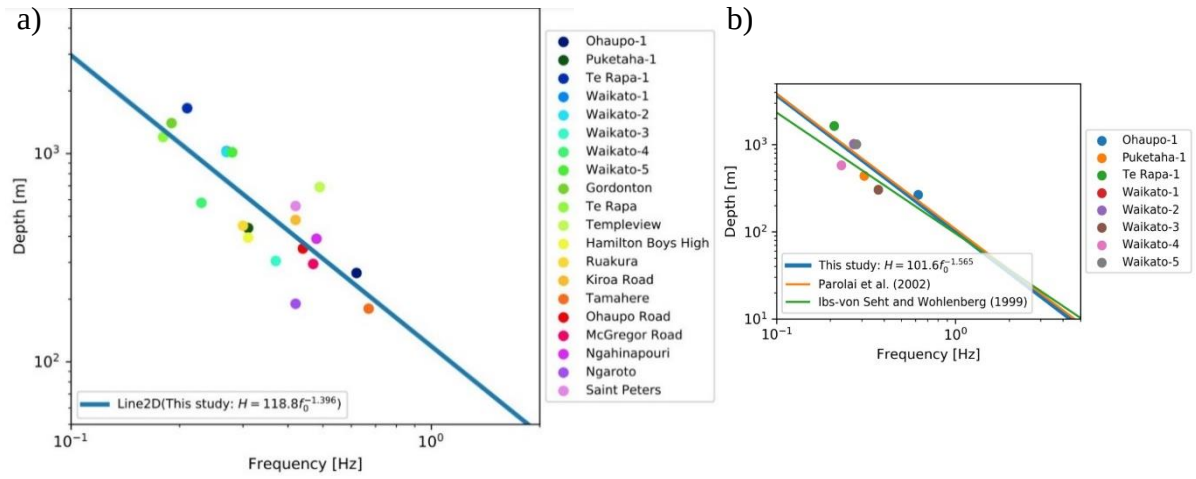

Figure 5.8 *Relationship between bedrock depth (H) and fundamental frequency (ƒo) developed by a) Shear wave velocity inversion and measurement of f_0 from MAM testing b) Model from (Jeong, 2019) developed by using measured H from petroleum logs and measured f_0 from HV testing*

When using both models to estimate bedrock depth it seems that the model by (Jeong, 2019) is consistent with this study in the higher frequency range and predicts a larger depth at lower frequencies. This revised model is still limited in application where frequencies are higher than 1Hz as the data available was up to 0.67Hz, however, addition of data from this study accounts for spatial variability of V_s and higher frequency data. As a result, estimations of H are typically less than 0.7 times true H. This relationship is useful in sedimentary basins with large impedance contrasts, because, it allows for regional scale resolution of the sedimentary layer thickness from surface HVSR analysis (Parolai et al., 2002).

5.6 Seismic response

Dynamic properties are key to modelling soil behaviour (particularly peak ground acceleration and amplification response) when soil is subject to earthquake loading. Soil dynamics commonly include the shear modulus (G) and shear wave velocity (V_s); the two are related by equation (5.2) where ρ is the density of the soil. The V_s profile is essentially the variation of stiffness with depth, in earthquake engineering V_s and thickness are the essential components of velocity profiling (Kramer, 1996).

$$Vs = \sqrt{\frac{Gmax}{\rho}} \tag{5.2}$$

Other soil dynamic properties such as stiffness (from G) and damping are also related to shear wave velocity. A 1D model of V_s structure is often adequate for site response analysis and is what has been developed for the Hamilton Basin (Socco, 2010). Surface wave inversion uses a linear system where it is assumed these dynamic properties do not change with no account for non-linearity; this linear assumption is carried through into response analysis. Transfer functions are used to model site response; when the input motion and stresses at bedrock are known or simulated and multilayer dynamics are known for the overlying soil column (1D profile), the output motion at the surface can be solved. The input V_s profile significantly influences the output surface response (Teague & Cox, 2017), which is why epistemic and aleatory uncertainties were outlined and reduced where possible for the Hamilton Basin profiles. Using the shear wave velocity profiles developed for the Canterbury Region, site response analysis was undertaken by (Teague & Cox, 2017). The authors determined that

response spectra developed using geologically blind inversion profiles were no different to those from geologically informed inversions as long as the profile fit closely to the experimental dispersion. It is therefore recommended that representative profiles used in future site response analysis in the Hamilton Basin are checked against the experimental dispersion to check for close alignment, rather than a randomised selection of the best 50. If randomised selection is used, checking this alignment is still essential, as a set of 1000 solutions has been chosen for each site and some profiles may have a variation of >20% from the lowest misfit profile. The HVSR obtained for each site will also be valuable for response analysis in conjunction with the V_s profile. Rayleigh wave ellipticity peaks from this research range from 3.8 at the lowest to 9 at the highest; which is significant compared to other studies where ellipticity was <4 in Wellington (Kaiser et al., 2019), <5 in Canterbury (Deschenes, 2018) and <7 in Nelson (Mcmahon & Wotherspoon, 2017). Twelve sites in this study have an ellipticity >6 and Gordonton and Hamilton Boys have an ellipticity of 9. This is significant considering actual amplitudes are 80% likely to be larger than Rayleigh wave ellipticity measurements (SESAME, 2004). Large impedance contrasts for the basement-soil contact across the basin may cause large surface resonance. The high Rayleigh wave ellipticity at many sites, also suggests that amplification may be significant in the Hamilton Basin. A factor to consider however, is that the input ground motions may result in something less significant, given the historical low seismicity of the area (Foti, 2017). Soil damping also reduces amplification. Calculations of V_{s30} revealed that there were four class E sites in this study all near or where basement depth was the largest. Gordonton, Te Rapa, Temple View, Elliot Park and Kiroa Road are class E very soft soil sites according to NZS1170.5. All other sites in this study are site class D sites; they represent deep or soft soil; rather than very soft soil (class E).

5.7 Summary

Tentative correlations between velocity groupings and geological units were made in section 5.2 with four main velocity units determined to be associated with four age based geological units. These correlations were applied to each shear wave velocity profile, which was compared against existing geological data and uncertainties were discussed. A revised fundamental frequency to basement depth relationship for the Hamilton Basin was presented and a brief discussion on the potential site response implications of the velocity profiles concludes the chapter

Chapter 6

Research summary

In response to a lack of data on the subsurface velocity structure of the Hamilton Basin, 13 shear wave velocity profiles have been developed, meeting the primary aim of this research.

This study has also

- Met the objectives of
  1) acquiring dispersion data through active (MASW) and passive (MAM) surface wave methods and
  2) obtaining fundamental frequency datasets through the ambient vibration HVSR method
- Produced a revised fundamental frequency to basement depth relationship following on from (Jeong, 2019)
- Characterised the velocity units for four age based geological units in the Hamilton Basin; Late Pleistocene, Pliocene-Pleistocene, Oligocene-Miocene and Jurassic
- Identified site classes in line with NZS1170.5

This chapter will conclude the development of these profiles, limitations, implications as well as recommendations for future work and use of the data for the purpose of seismic response analysis and seismic risk assessment.

6.1 General summary and reflection

This is the first regional scale study on the subsurface velocity structure of the Hamilton Basin and initial investigations conclude a relatively consistent velocity structure exists with comparable potential for amplification. Surface waves were utilised due to their dispersive nature whereby the surface wave velocity is a function of the wavelength. Dispersion datasets obtained through acquisition, processing of both artificially generated surface waves (MASW), and ambient source surface waves (MAM) founded the inversion results in this study. Fundamental frequency data obtained through the HVSR method increased the reliability of the inversions, in most cases decreasing the misfit between the theoretical and experimental

data. Final uncertainty is likely 5-20% depending on data quality and analysis, and is mostly due to the non-linear solution non uniqueness limitations of surface wave inversion. The quality of the data varied in the Hamilton Basin, with anomalies requiring intensive analysis and solution exploration. The polarising issues were the peat sites, higher modes and lack of overlap in the experimental dispersion data in certain frequency bands for some sites (which was also due in part to the peat influence).

Sites with higher modes in the dispersion datasets, have reduced reliability in the depth range corresponding to the higher mode frequency. Geological data to basement depth was required to define, in the inversion, the boundaries of the stiffer layer causing this higher mode. This data was not available. Higher mode propagation was prominent at the Saint Peters site, which had a frequency band in the first order higher mode. At Tamahere and Kiroa Road the higher mode was less evident in the dispersion curves, which instead trended towards a higher mode at different frequencies. This influence is concluded to be down to ignimbrite emplacement due to geological data near the Tamahere site, this also made geological sense based on deposition maps (Briggs et al., 1993), geological age (Edbrooke, 2005) in addition to the density of ignimbrite compared to other geological deposits known in the south eastern basin.

Active data acquired for peat sites was of very low velocity 28-38m/s, and aliased towards higher frequencies. Smaller spacing would have reduced aliasing in the higher frequency range; 0.5m spacing would potentially be suitable (Foti, 2017). For peat sites, the near surface resolution is limited at Temple View and Gordonton, which leads to high uncertainty in the V_s at shallower depths and consequently the V_{s30} and site class calculations. The low velocity high frequency trend in the peat meant that the active and passive dispersion curves did not overlap (particularly evident in the slowness domain) which created high misfits in the inversion results. If the depth of the peat layer was determined, this could be constrained in the inversion. The dispersion data looks confined to the peat layer however, and I would conclude that the near surface resolution would still be poor with the constrained layer. This is because the 50m array would not resolve the upper 30m due to the targeted depth range controlled by the receiver spacing being deeper. It was also determined that passive surveys targeted toward a higher frequency do not yield good results; something expected based on the physics of surface wave inversion. The low shear wave velocity in the Hamilton Basin peat relative to other studies is notable. Based on international literature this is theorised to be due to a high water content, however, this is not conclusive.

For the two sites McGregor Road and Ohaupo, which had a lack of overlap in the dispersion datasets, there is unquantified uncertainty in Vs profile corresponding to the depth range where the dispersion data is not available. Where dispersion datasets were favourable and no fundamental anomalies encountered, final uncertainty is expected to be lower. This is true for, Ruakura, Hamilton Boys High, Elliot Park, Te Rapa, Ngahinapouri and Ngaroto. What is notable in all cases is how the dispersion datasets and the HVSR datasets have related well to the known geology and basement structure.

The revised fundamental frequency to basement depth relationship (f_0, H) has been developed for the purpose of estimating the thickness of the sediment overlying basement rock at a site from HVSR analysis. This geophysical technique is a much more cost effective method for estimating H than in situ investigations such as well logs and boreholes (Parolai et al., 2002). Estimates of H will still have uncertainty, however, with the additional dataset from site specific V_s it is likely less than 0.7-1.5 times true H (Jeong, 2019).

The assumption of a lateral discontinuity at the Temple View site is indicative and not conclusive. While a fault line would make geological sense based on geomorphic data, the rapidly varying basement depth in the area means a slope is also plausible. There is a lack of information on HVSR analysis and lateral discontinuities in the literature with two sentences on the topic in the (SESAME, 2004) H/V guidelines. This assumption requires further investigation to be conclusive. The Ruakura site also had a similar variation in peak frequency between seismometers but it was not varied across the site and tended to be in line with pylons. This is not an effect backed up in the literature (SESAME, 2004). Large impedance contrasts are present at the basement-soil interface across all sites. This indicates the potential for large surface resonance and reverberation of ground motions across the basin during an earthquake. This finding is consistent with the ‘basin effect’ phenomenon expected in sedimentary basins where ground motions are amplified in thick soft soil overlying stiff basement rock. This is additional to the fundamental period data from this study, which found long periods correlated to deeper sites and shorter periods, correlated to shallower sites. This indicates increased duration of shaking in an earthquake and the findings in this study are consistent with the findings from (Jeong, 2019). A summary of the calculated Vs30, site class, fundamental frequency and fundamental period is presented in table 6.1 for all 13 sites. The reader is referred to chapter 4 for the final Vs profiles developed through this research.

Table 6.1 *Summary table for all 13 sites, V_{s30} (m/s), site class (NZS1170.5: 2004), fundamental peak frequency f_0 (Hz) and corresponding site period T_0 (s)*

Site name	Latitude (degrees)	Longitude (degrees)	V_{s30} (m/s)	Site Class	f_0 (Hz)	T_0 (s)
Gordonton (GD)	-37.658795	175.323065	166.2997*	E	0.19±0.02	5.3s
Te Rapa (TR)	-37.749458	175.177178	194.8215	D	0.18±0.02	5.5s
Elliot Park (EP)	-37.783230	175.239750	176.4937	D	0.49±0.03	2s
Temple View (TV)	-37.827408	175.232564	165.9396*	E	0.49±0.02	2s
Hamilton Boys High (HB)	-37.785057	175.296666	181.9176	D	0.31±0.02	3.2s
Ruakura (RK)	-37.779211	175.328247	203.4725	D	0.28±0.03	3.6s
Kiroa Road (KR)	-37.724053	175.369607	173.1582	E	0.42±0.03	2.4s
Tamahere (TM)	-37.816514	175.415889	176.3852	D	0.67±0.01	1.5s
Ohaupo Road (OP)	-37.882900	175.317122	227.8379	D	0.44±0.03	2.3s
McGregor Road (MG)	-37.906643	175.272696	212.93	D	0.47±0	2.1s
Ngahinapouri (NP)	-37.892493	175.212413	195.3065	D	0.47±0.02	2.1s
Ngaroto (NO)	-37.971002	175.274903	234.0463	D	0.67±0.07	1.5s
Saint Peters (SP)	-37.88807	175.4239	214.9304	D	0.42±0.05	2.4s[1]

* Peat site subject to further investigation or site class E if peat layer is >10m thick.

6.2 Concluding remarks

The 13 shear wave velocity profiles developed in this study provide valuable data for site response analysis. Results confirm relatively homogeneous layering occurs across the basin, with the exception of the increasing complexity in the south eastern basin and any peat sites. Higher modes are present in the dispersion datasets in the south east indicating complex wave propagation in areas of expected and recorded ignimbrite deposition. As a result of the significantly low shear wave velocity in peat, profiles presented for peat sites have decreased reliability compared to non-peat sites. The results from this study are comparable to existing geological information in most cases, with uncertainties existing in specific datasets. In any case, large impedance contrasts are present at the soil-basement interface in the 13 measured V_s profiles, confirming the potential for amplification of ground motions during an earthquake.

6.3 Recommendations for future research

Many methods have been utilised to combat the uncertainty arising from surface wave inversion, overall increasing certainty in the obtained shear wave velocity profiles. However, it is ultimately recommended that care is taken when using these V_s profiles for site response studies, particularly with data beyond the resolution limit. It is also recommended that interpretations of the near surface are made cautiously, particularly for peat sites.

Therefore, the main recommendations resulting from this study are:

1- Love wave testing of peat sites could resolve the peat layer (if required); since Rayleigh wave propagation in peat is unlikely other modes of propagation need to be considered
2- Potential velocity reversal inversions should be considered for areas of complex wave propagation, if geological data becomes available
3- To evaluate the dynamic properties which can be obtained through the shear wave velocity results of this research and refine them for site response studies
4- To use shear wave velocity profiles that closely match the experimental dispersion for site response analysis

Limitations should always be considered when utilising these profiles, surface wave inversion in inherently non-linear, ill posed and solutions are non-unique.

References

Aki, K. (1993). Local site effects on weak and strong ground motion. *Tectonophysics*, *218*(1–3), 93–111. https://doi.org/10.1016/0040-1951(93)90262-I

Ballance, P. (2009). *New Zealand geology: an illustrated guide*. Retrieved from https://www.geotrips.org.nz/downloads/Ballance_NZ_Geology-V2.pdf

Bard, P., Duval, A., Koehler, A., & Rao, S. (2004). Guidelines for the Implementation of the H / V Spectral Ratio Technique on Ambient Vibrations Measurements , Processing and Interpretation. *SESAME European Research Project*, (December), 1–62.

Bard, P. Y., Cadet, H., Endrun, B., Hobiger, M., Renalier, F., Theodulidis, N., … Kristekova, M. (2010). From Non-invasive Site Characterization to Site Amplification: Recent Advances in the Use of Ambient Vibration Measurements. *Geotechnical, Geological and Earthquake Engineering*, *17*(January), 105–123. https://doi.org/10.1007/978-90-481-9544-2_5

Bettig, B., Bard, P. Y., Scherbaum, F., Riepl, J., Cotton, F., Cornou, C., & Hatzfeld, D. (2001). Analysis of dense array noise measurements using the modified spatial auto-correlation method (SPAC): Application to the Grenoble area. *Bollettino Di Geofisica Teorica Ed Applicata*, *42*(3–4), 281–304.

Briggs, M., Itaya, T., Lowe, D. J., & Keane, A. J. (1989). Ages of the pliocene—pleistocene alexandra and ngatutura volcanics, western North Island, New Zealand, and some geological implications. *New Zealand Journal of Geology and Geophysics*, *32*(4), 417–427. https://doi.org/10.1080/00288306.1989.10427549

BSSC (Building Seismic Safety Council) 2015. NEHRP recommended provisions for seismic regulations for new buildings and other structures (FEMA 450-1): Part I, Provisions. Federal Emergency Management Agency, Washington, D.C.

Capon, J. (1969). High-Resolution Frequency-Wavenumber Spectrum Analysis. *Institute of Electrical and Electronics Engineers*, *57*(8), 1408–1418.

Cho, Ikuo & Iwata, Takaki. (2018). A Bayesian Approach to Microtremor Array Methods for Estimating Shallow S Wave Velocity Structures: Identifying Structural Singularities. Journal of Geophysical Research: Solid Earth. 124. 10.1029/2018JB015831.

Clayton, P. J., Tilsley, S. C., Bastin, S. H., & Green, R. A. (2017). Case study in the use of paleoliquefaction techniques to investigate liquefaction potential of Waikato soils for the

Hamilton section of the Waikato expressway. *20th NZGS Geotechnical Symposium*, 1–8.

Cornell, C. A. (1968). Engineering seismic risk analysis, Bull. Seismol. Soc. Am. 58, no. 5, 1583–1606.

Waikato Regional Council. (2003). Earthqauke hazard zones. Retrieved from https://www.waikatoregion.govt.nz/assets/PageFiles/2529/earthquake.pdf

Cox, B. R., & Teague, D. P. (2016). Layering ratios: A systematic approach to the inversion of subsurface wave data in the absence of a priori information. *Geophysical Journal International*, (207), 422–438. https://doi.org/10.1093/gji/ggw282

Dawson, H., Wotherspoon, L. M., Nelis, S. B., & Fraser, J. G. (2015). *Dynamic Site Characterisation of the Manukau Lowlands Region of Auckland, New Zealand*. (November).

Deschenes, M. R., Wood, C. M., Wotherspoon, L. M., Bradley, B. A., & Thomson, E. (2018). Development of deep shear wave velocity profiles in the canterbury plains, New Zealand. *Earthquake Spectra*, *34*(3), 1065–1089. https://doi.org/10.1193/122717EQS267M

Eberhart-Phillips, D., Reyners, M., Bannister, S., Chadwick, M., & Ellis, S. (2010). Establishing a Versatile 3-D Seismic Velocity Model for New Zealand. *Seismological Research Letters*, *81*(6), 992–1000. https://doi.org/10.1785/gssrl.81.6.992

Edbrooke, S. W. (2005). Geology of the Waikato area. In *Institute of Geological and Nuclear Sciences 1:250,000 map 4*. Lower Hutt.

Edbrooke, S.W. (compiler) (2005). Geology of the Waikato area: scale 1:250,000. Lower Hutt: Institute of Geological & Nuclear Sciences. Institute of Geological & Nuclear Sciences 1:250,000 geological map 4. 68 p. + 1 folded 142 map

Fema. (2012). *FEMA P-751: 2009 NEHRP Recommended Seismic Provisions: Design Examples*. (September).

Foster, K. M., Bradley, B. A., McGann, C. R., & Wotherspoon, L. M. (2019). A V_{s30} map for New Zealand based on geologic and terrain proxy variables and field measurements. *Earthquake Spectra*, *35*(4), 1865–1897. https://doi.org/10.1193/121118EQS281M

Foti, S. (2005). Surface Waves in Geomechanics: Direct and Inverse Modelling for Soils and Rocks. *Surface Waves in Geomechanics: Direct and Inverse Modelling for Soils and Rocks*, (January 2005). https://doi.org/10.1007/3-211-38065-5

Foti, S., Hollender, F., & Garofalo, F. (2017). *Guidelines for the good practice of surface wave analysis : a product of the InterPACIFIC project*. https://doi.org/10.1007/s10518-017-

0206-7

Foti, S., Parolai, S., Albarello, D., & Picozzi, M. (2011). *Application of Surface-Wave Methods for Seismic Site Characterization*. 777–825. https://doi.org/10.1007/s10712-011-9134-2

FrOG Tech, 2011. Waikato Strucutral GIS and SEEBASE Project: Phase 1 November 2010, FrOG Tech Project Code CWE701 and Phase 2 November 2011, frog Tech Project Code CWE703. Ministry of Economic Development New Zealand Unpublished Petroleum Report PR 4432

Garofalo, F., Foti, S., Hollender, F., Bard, P., Cornou, C., Cox, B. R., … Cornou, C. (2017). Reliability and accuracy assessment of invasive and non-invasive seismic methods for site characterisation: Feedback from the Interpacific project. *Id : hal-01461225*

Geoconsultants, F. (2005). *the Importance of Shear Wave Velocity Information of a Soil Site*. (January 2015).

Graves, R. W., & Pitarka, A. (2010). Broadband ground-motion simulation using a hybrid approach. *Bulletin of the Seismological Society of America*, *100*(5 A), 2095–2123. https://doi.org/10.1785/0120100057

Hall, S. L., Nicol, A., Moore, T. A., & Bassett, K. N. (2006). Timing of normal faulting in the waikato coal measures, New Zealand, and its implications for coal-seam geometry. *New Zealand Journal of Geology and Geophysics*, *49*(1), 101–113. https://doi.org/10.1080/00288306.2006.9515151

Heisey, J. S., Stokoe, K. H., & Meyer, A. H. (1982). *Moduli of pavement systems from SASW*. 10.

Horike, M. (1996). Geophysical exploration using microtremor measurements. Xth WCEE, Acapulco.

Hume, T. M., Sherwood, A. M., & Nelson, C. S. (1975). Alluvial sedimentology of the upper pleistocene hinuera formation, hamilton basin, New Zealand. *Journal of the Royal Society of New Zealand*, *5*(4), 421–462. https://doi.org/10.1080/03036758.1975.10419362

J Kamp, P. J., & Lowe, D. J. (1981). 4. Quaternary Stratigraphy, Landscape and Soils of the Hamilton Basin. *Geological Society of New Zealand*, *29*(B), 14–28. Retrieved from https://researchcommons.waikato.ac.nz/bitstream/handle/10289/10207/Kamp and Lowe 1981 guide Ham Basin.pdf?sequence=2&isAllowed=y

Jeong, S. (2019). *Development of a Waikato Basin T 0 and depth model by the H / V spectral ratio method*. 1–8.

Jeong, Seokho, & Bradley, B. A. (2017). Amplification of strong ground motions at Heathcote Valley during the 2010–2011 Canterbury earthquakes: Observation and 1D site response analysis. *Soil Dynamics and Earthquake Engineering*, *100*(June), 345–356. https://doi.org/10.1016/j.soildyn.2017.06.004

Jongmans, Denis. Ohrnberger, M. W. M. (2005). *Final report WP13: Recommendations for quality array measurements and processing. Deliverable D24.13 of the SESAME project*. (March), 35. Retrieved from http://sesame.geopsy.org/SES_TechnicalDoc.htm

Kaiser, A. E., Bourguignon, S., Hill, M. P., & Bruce, Z. R. (2019). *Updated 3D basin model and NZS 1170 . 5 subsoil class and site period maps for the Wellington CBD : Project 2017-GNS-03-NHRP*. (May).

Kaiser, A., Massey, C., & Holden, C. (2014). *Site amplification, polarity and topographic effects in the Port Hills during the Canterbury earthquake sequence*. (121), 1–33.

Kear, D. (2004). Reassessment of neogene tectonism and volcanism in North Island, New Zealand. *New Zealand Journal of Geology and Geophysics*, *47*(3), 361–374. https://doi.org/10.1080/00288306.2004.9515062

Kear, D., & Schofield, J. C. (1964). Stratigraphic Summary, Nngaruawahia Subdivision. *New Zealand Journal of Geology and Geophysics*, *7*(4), 892–893. https://doi.org/10.1080/00288306.1964.10428141

Kleyburg, M. A., Moon, V. G., Lowe, D. J., & Nelson, C. S. (2013). *Paleoliquefaction in Late Pleistocene alluvial sediments in Hauraki and Hamilton basins , and implications for paleoseismicity*. (Anz), 524–531.

Kramer, S. L. 1996. Geotechnical Earthquake Engineer- ing, 653 pp., Prentice-Hall, Inc.

Lee, R. L., Bradley, B. A., & McGann, C. R. (2017). 3D models of Quaternary-aged sedimentary successions within the Canterbury, New Zealand region. *New Zealand Journal of Geology and Geophysics*, *60*(4), 320–340. https://doi.org/10.1080/00288306.2017.1334671

Leica, T., Gs, V., Captivate, L., Infinity, L., Active, T., Care, C., & Package, C. C. (n.d.). *Leica Viva GS15 Data sheet Engaging software*. 16–17.

Lowe, D. J. (2010). Introduction to the landscapes and soils of the Hamilton Basin. Lowe, D.J.; Neall, V.E., Hedley, M; Clothier, B.; Mackay, A. 2010. Guidebook for Pre-Conference North Island, New Zealand "Volcanoes to Oceans" Field Tour (27- 30 July). 19th World Soils Congress, International Union of Soil Sciences, Brisbane, (Soil and Earth Sciences

Occasional Publication No. 3), 1.24-1.61.

Macau, A., Benjumea, B., Gabàs, A., Figueras, S., & Vilà, M. (2015). The Effect of Shallow Quaternary Deposits on the Shape of the H/V Spectral Ratio. *Surveys in Geophysics*, *36*(1), 185–208. https://doi.org/10.1007/s10712-014-9305-z

McCormack, K. D., Mary Gee, M. A., McNaughton, N. J., Smith, R., & Fletcher, I. R. (2009). U-Pb dating of magmatic and xenocryst zircons from Mangakino ignimbrites and their correlation with detrital zircons from the Torlesse metasediments, Taupo Volcanic Zone, New Zealand. *Journal of Volcanology and Geothermal Research*, *183*(1–2), 97–111. https://doi.org/10.1016/j.jvolgeores.2009.03.005

McCraw, J. D. (1967). the Surface Features and Soil Pattern of the Hamilton Basin. *Earth Science Journal*, *1*(1), 59–74.

McCraw, J. D. (2011). The wandering river: landforms and geological history of the Hamilton Basin. Geoscience Society of New Zealand.

McKenzie, S. (2004). *Subsidence Rates Of Peat Since 1925 In The Moanatuatua Swamp Area*. (June).

Mcmahon, R., & Wotherspoon, L. (2017). *Dynamic Site Characterisation of the Nelson-Tasman Region*. 1–8.

Moon, V., & Lange, W. De. (2017). *Final report on EQC potential shallow seismic sources in the Hamilton Basin project 16/717*. (July).

Nakumara, Y. (1989). *A method for dynamic characteristics estimation of subsurface using microtremor on the ground surface*.

Nazarian, S., Stokoe II, K. H., & Hudson, W. R. (1983). Use of Spectral Analysis of Surface Waves Method for Determination of Moduli and Thicknesses of Pavement Systems. *Pavement Design, Performance, and Rehabilitation*, 38–45.

Nogoshi M, Igarashi T (1970) On the propagation characteristics of microtremors. J Seism Soc Jpn 23:264–280 (in Japanese with English abstract)

NZ Geotechnical Society Inc. 2005. Guideline for the field classification and description of soil and rock for engineering purposes, NZGS Guideline, December 2005.

Okada, H. (2003) The microtremor survey method. Geophys Monograph Series, SEG

Park, C. B., Miller, R. D., Ryden, N., Xia, J., & Ivanov, J. (2005). Combined use of active and passive surface waves. *Journal of Environmental and Engineering Geophysics*, *10*(3),

323–334. https://doi.org/10.2113/JEEG10.3.323

Park, Choon B., Miller, R. D., & Xia, J. (1999). Multichannel analysis of surface waves. *Geophysics*, *64*(3), 800–808. https://doi.org/10.1190/1.1444590

Park, Choon B., Miller, R. D., & Xia, J. (2002). Multichannel analysis of surface waves. *Geophysics*, *64*(3), 800–808. https://doi.org/10.1190/1.1444590

Parolai, S., Picozzi, M., Richwalski, S. M., & Milkereit, C. (2005). Joint inversion of phase velocity dispersion and H/V ratio curves from seismic noise recordings using a genetic algorithm, considering higher modes. *Geophysical Research Letters*, *32*(1), 1–4. https://doi.org/10.1029/2004GL021115

Persaud, M., Villamor, P., Berryman, K. R., Ries, W., Cousins, J., Litchfield, N., & Alloway, B. V. (2016). The Kerepehi Fault, Hauraki Rift, North Island, New Zealand: active fault characterisation and hazard. *New Zealand Journal of Geology and Geophysics*, *59*(1), 117–135. https://doi.org/10.1080/00288306.2015.1127826

Piatti, C., Foti, S., Socco, L. V., & Boiero, D. (2013). Building 3D shear-wave velocity models using surface waves testing: The Tarcento basin case history. *Bulletin of the Seismological Society of America*, *103*(2 A), 1038–1047. https://doi.org/10.1785/0120120089

Rosenblad, B. L., & Goetz, R. (2010). Study of the H / V spectral ratio method for determining average shear wave velocities in the Mississippi embayment. *Engineering Geology*, *112*(1–4), 13–20. https://doi.org/10.1016/j.enggeo.2010.01.006

Schofield, J. C. (1965). The hinuera formation and associated quaternary events. *New Zealand Journal of Geology and Geophysics*, *8*(5), 772–791. https://doi.org/10.1080/00288306.1965.10422116

Schofield, J. C. (1967). Geology of the Hamilton Region. *Earth Science Journal*, *1*(1), 82–88. Retrieved from https://researchcommons.waikato.ac.nz/bitstream/handle/10289/9097/ESJ_0101_82.pdf?sequence=5&isAllowed=y

Selby, M. J., & Lowe, D. J. (1992). The middle Waikato Basin and hills. *Landforms of New Zealand,1*(c), 233–255. Retrieved from http://www.scopus.com/inward/record.url?eid=2-s2.0-0020372511&partnerID=tZOtx3y1

SESAME team (2004) Guidelines for the implementation of the H/V spectral ratio technique on ambient vibrations: measurements, processing and interpretation (Deliverable No. D23.12), WP12. SESAME European research project

Socco, L. V., Foti, S., & Boiero, D. (2010). Surface-wave analysis for building near-surface velocity models — Established approaches and new perspectives. *Geophysics*, *75*(5), 75A83-75A102. https://doi.org/10.1190/1.3479491

Spinardi, F. (2017). *A preliminary evaluation of tectonic geomorphological signals within the Hamilton Basin*. *Master of*. Retrieved from https://hdl.handle.net/10289/11824

Stats NZ. 2018. Hamilton City | Stats NZ. Available at: https://www.stats.govt.nz/tools/2018-census-place-summaries/hamilton-city (Accessed: 10 October 2020).

Stein, S., Wysession, M., & Stein, S. (Ed.) (2003). *Introduction to Seismology, Earthquakes, and Earth Structure*. Blackwell Publishing.

Stirling, M., McVerry, G., Gerstenberger, M., Litchfield, N., Van Dissen, R., Berryman, K., … Jacobs, K. (2012). National seismic hazard model for New Zealand: 2010 update. *Bulletin of the Seismological Society of America*, *102*(4), 1514–1542. https://doi.org/10.1785/0120110170

Stokoe, K.H., Wright, S.G., Bay, J.A., & Roesset, J.M. Characterization of geotechnical sites by SASW method. Proc. 13th International Conference on Soil Mechanics and Foundation Engineering, 22 (9-12). New Delhi, India, 1994; 923-930.

Sutherland, R., 1999. Basement geology and tectonic development of the greater New Zealand region: An interpretation from regional magnetic data. Tectonophysics, 308(3), pp.341–362.

Tarbali, K., Bradley, B., Huang, J., Lee, R., Lagrava, D., Bae, S., … Zhu, M. (2019). Cybershake nz v18.5: New zealand simulation-based probabilistic seismic hazard analysis. *Earthquake Geotechnical Engineering for Protection and Development of Environment and Constructions- Proceedings of the 7th International Conference on Earthquake Geotechnical Engineering, 2019*, 5224–5231.

Teague, D., Cox, B., Bradley, B., & Wotherspoon, L. (2018). Development of deep shear wave velocity profiles with estimates of uncertainty in the complex interbedded geology of christchurch, New Zealand. *Earthquake Spectra*, *34*(2), 639–672. https://doi.org/10.1193/041117EQS069M

Wathelet, M., Jongmans, D., & Ohrnberger, M. (2004). Surface-wave inversion using a direct search algorithm and its application to ambient vibration measurements. *Near Surface Geophysics*, *2*(4), 211–221. https://doi.org/10.3997/1873-0604.2004018

Wathelet M (2005) Array recordings of ambient vibrations: surface-wave inversion. PhD thesis, Universite´ de Lie`ge, Belgium

Wathelet, Marc. (2008). An improved neighborhood algorithm: Parameter conditions and dynamic scaling. *Geophysical Research Letters*, *35*(9), 1–5. https://doi.org/10.1029/2008GL033256

Wehling, T. M., Boulanger, R., Arulnathan, R., Harder, L. F., and Driller, M. W., 2003. Nonlinear dynamic properties of a fibrous organic soil. Journal of Geotechnical and Geoenvironmental Engineering, ASCE, 129(10), 929-939

Wotherspoon, L. M., Bradley, B. A., Thomson, E. M., Hills, A. J., Jeong, S., Wood, C. M., & Cox, B. R. (2015). Development of deep V_s profiles and site periods for the Canterbury region. *New Zealand Society for Earthquake Engineering Conference*, (1997).

Xia, J., R. D. Miller, and C. B. Park, 1999, Estimation of near-surface shear- wave velocity by inversion of Rayleighwave: Geophysics, 64, 691–700.

Zywicki, D. J., 1999. Advanced signal processing methods applied to engineering analysis of seismic surface waves, Ph.D. Dissertation, School of Civil and Environmental Engineering, Georgia Institute of Technology, Atlanta, GA.

Appendix A

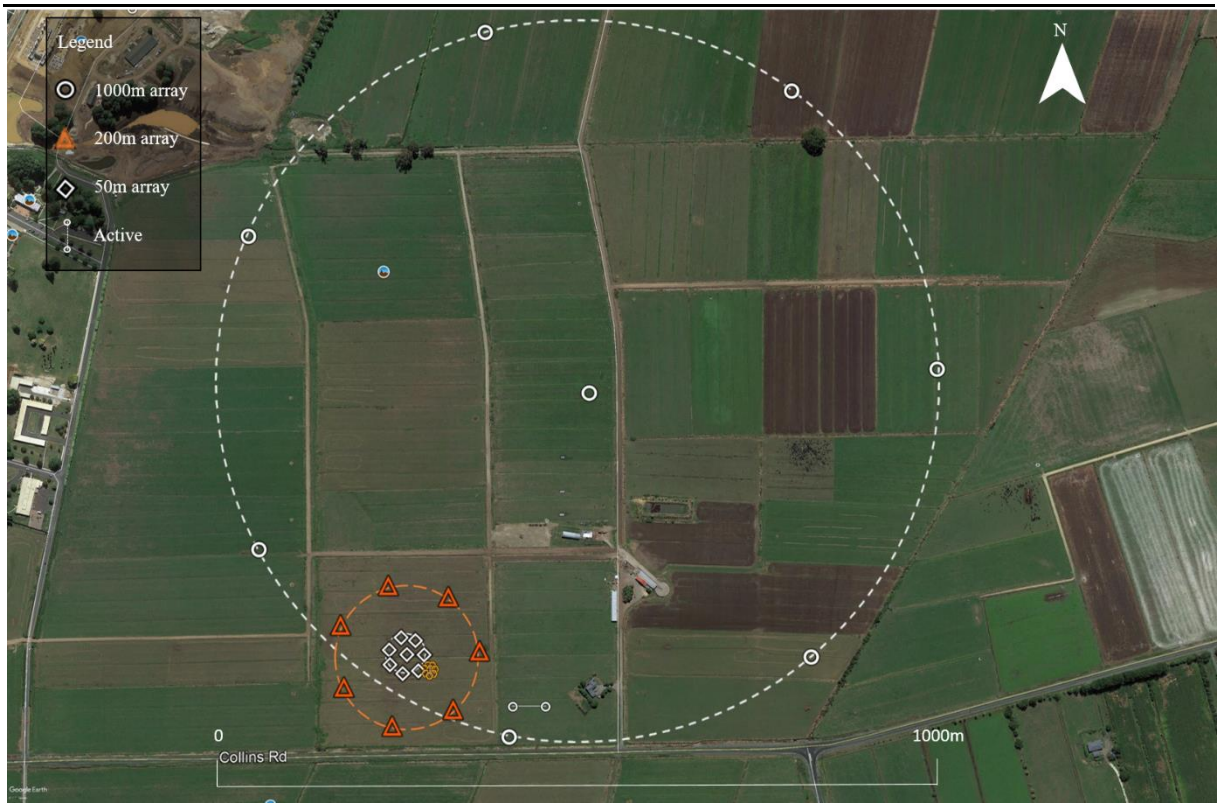

A.1 Temple View array layout

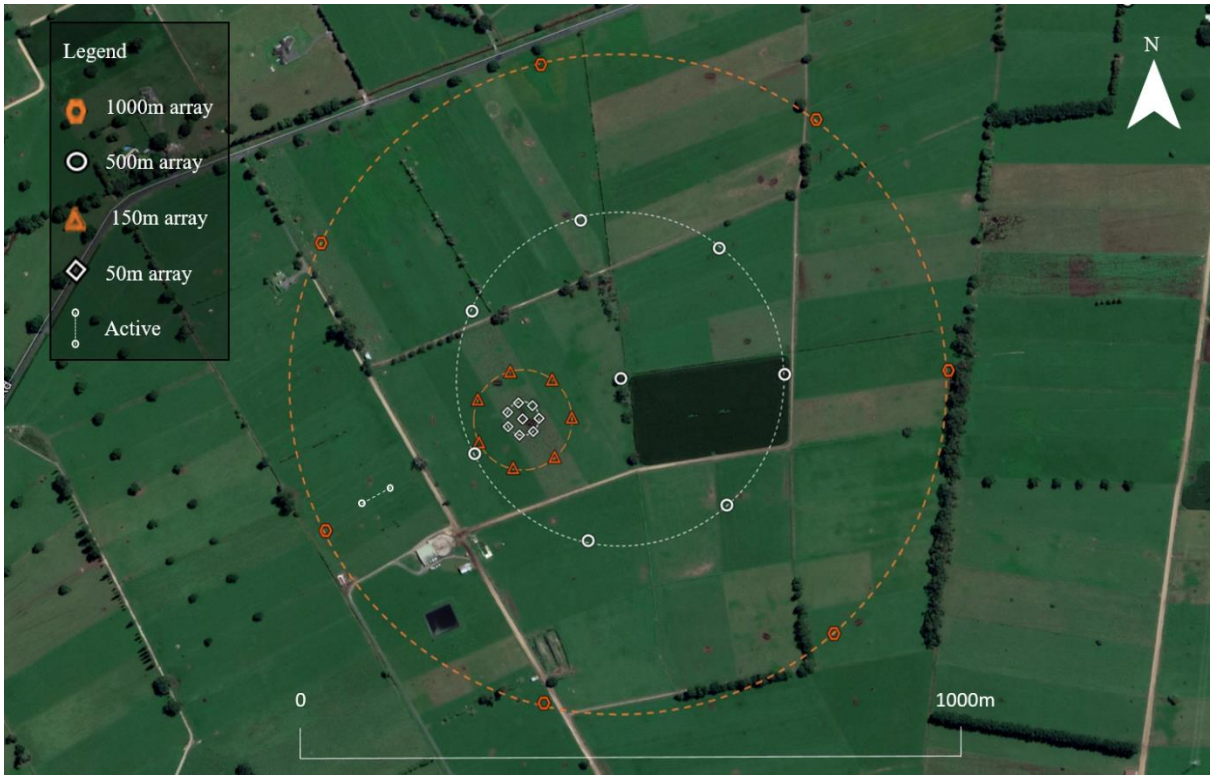

A.2 Gordonton array layout

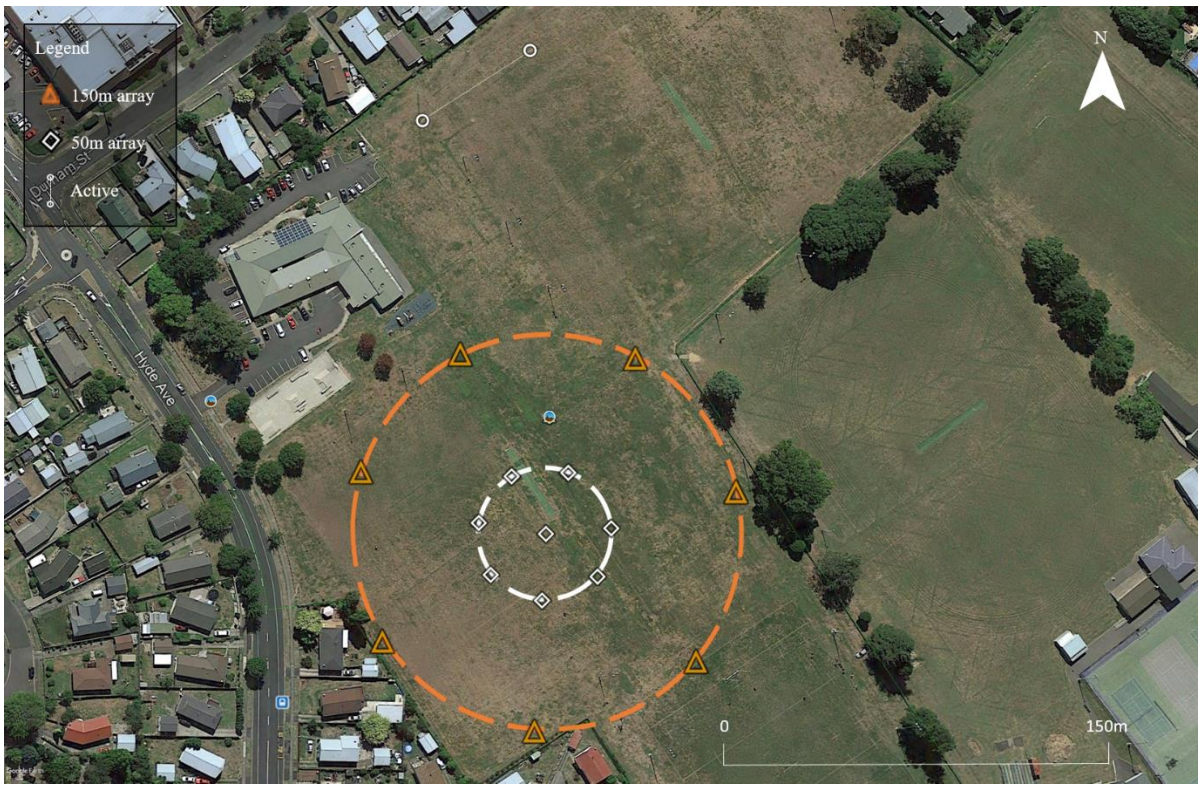

A.3 Elliot park array layout

A.4 Hamilton Boys High array layout

A.5 Kiroa Road array layout

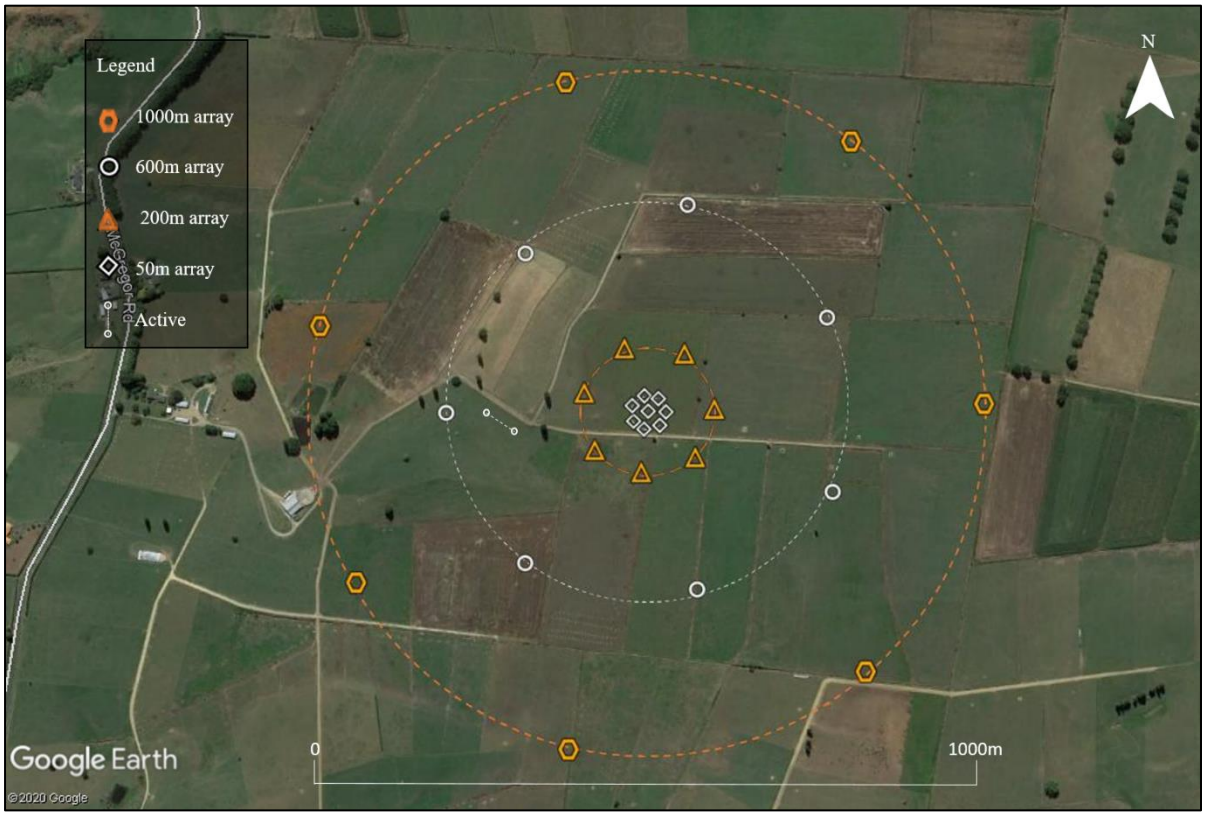

A.6 McGregor Road array layout

A.7 Ngahinapouri array layout

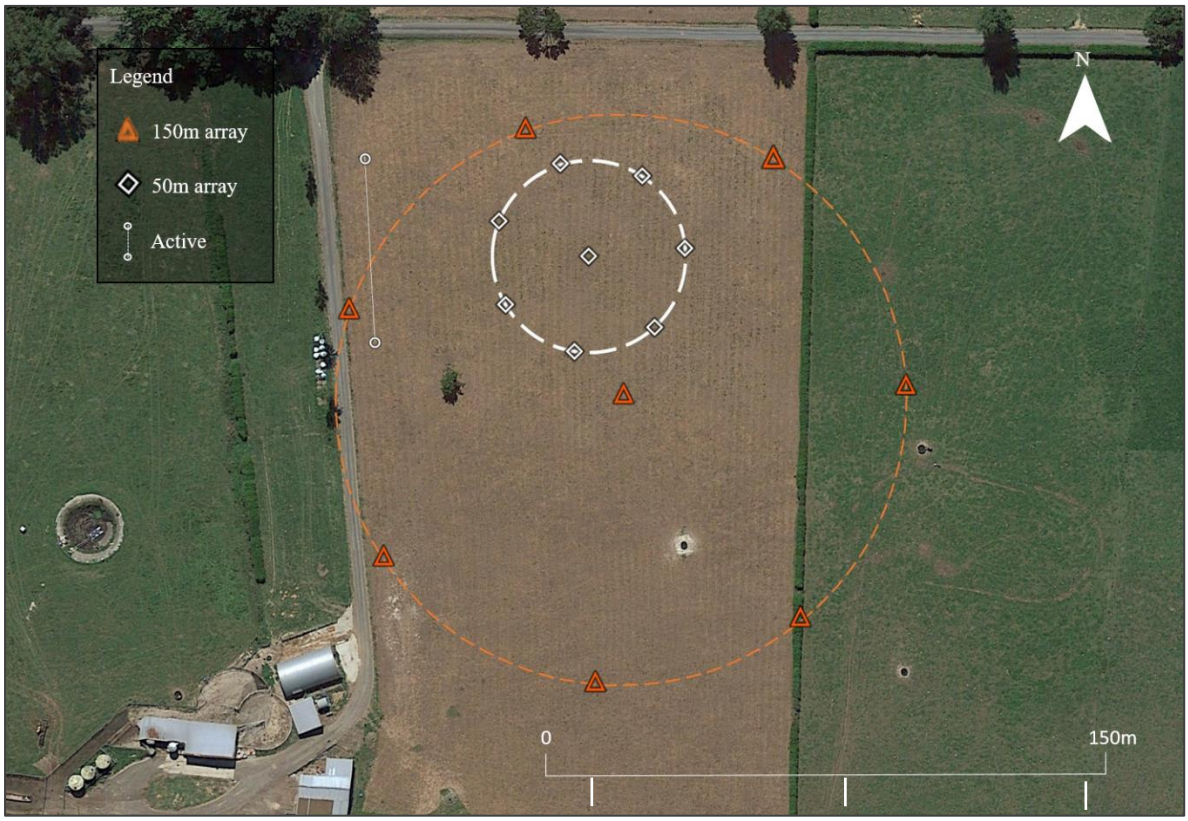

A.8 Ohaupo array layout

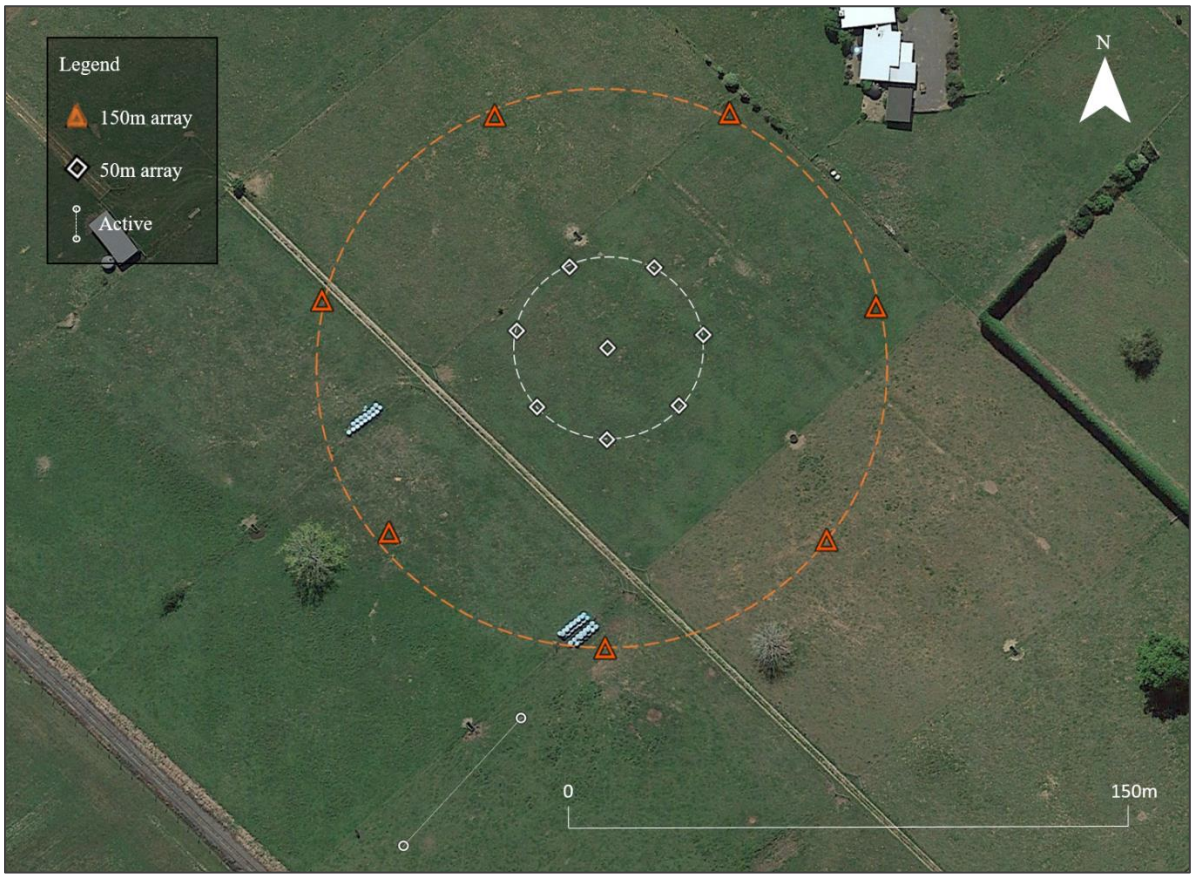

A.9 Tamahere array layout

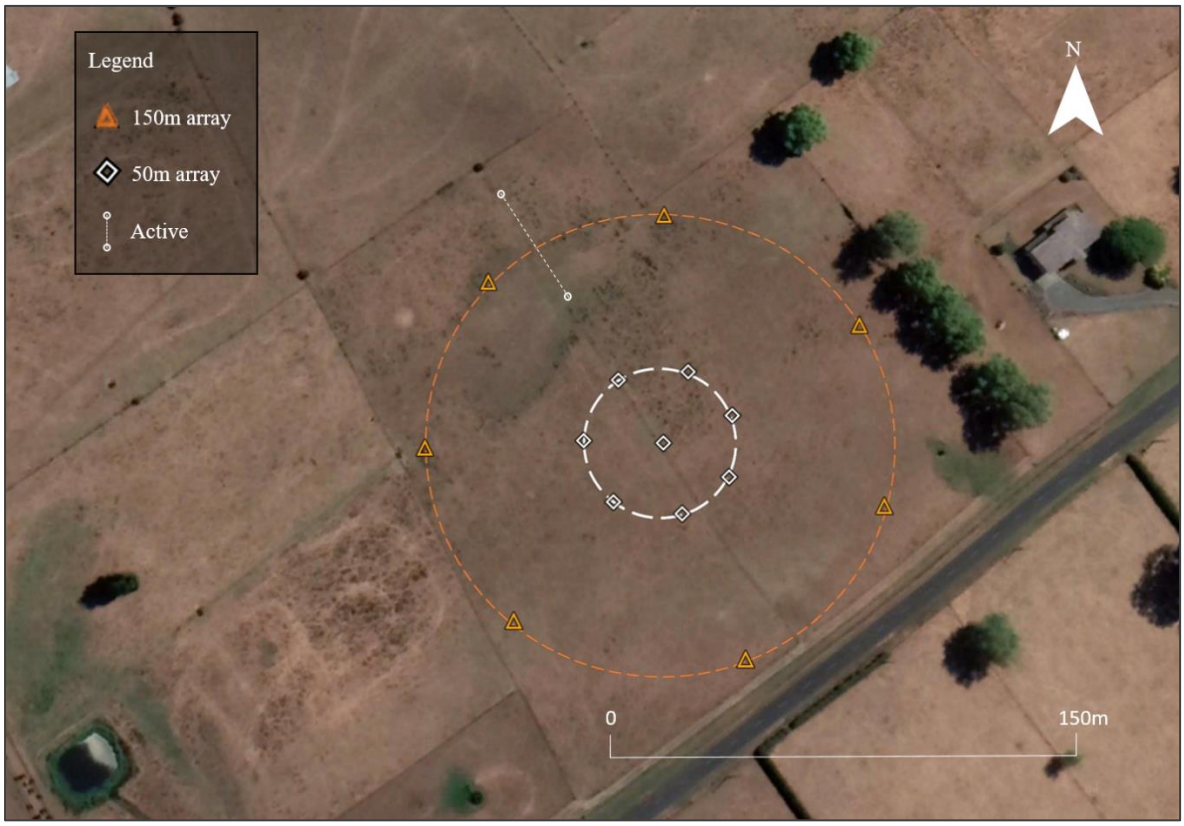

A.10 Ngaroto array layout

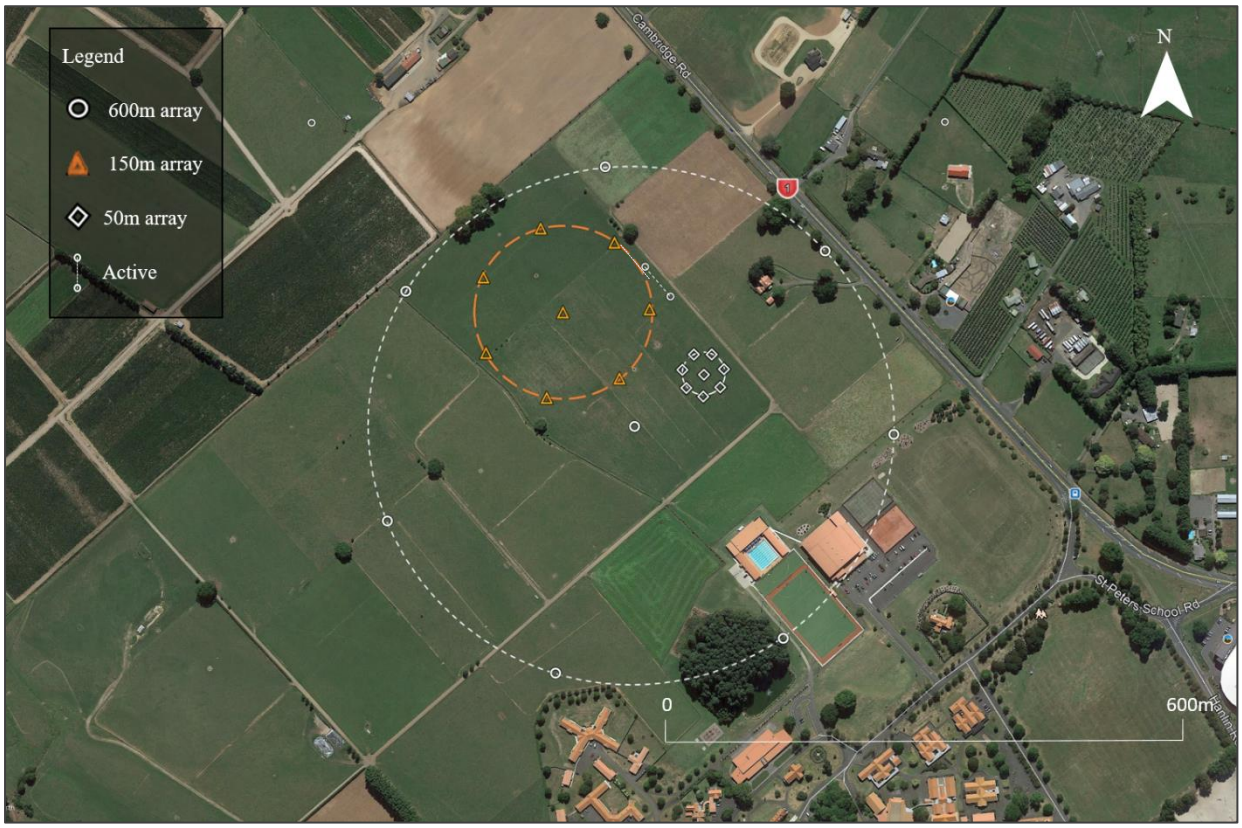

A.11 Saint Peters array layout

A.12 Wallace small array layout

A.13 Te Rapa array layout

Appendix B

B.1 McGregor Road dispersion curve processing

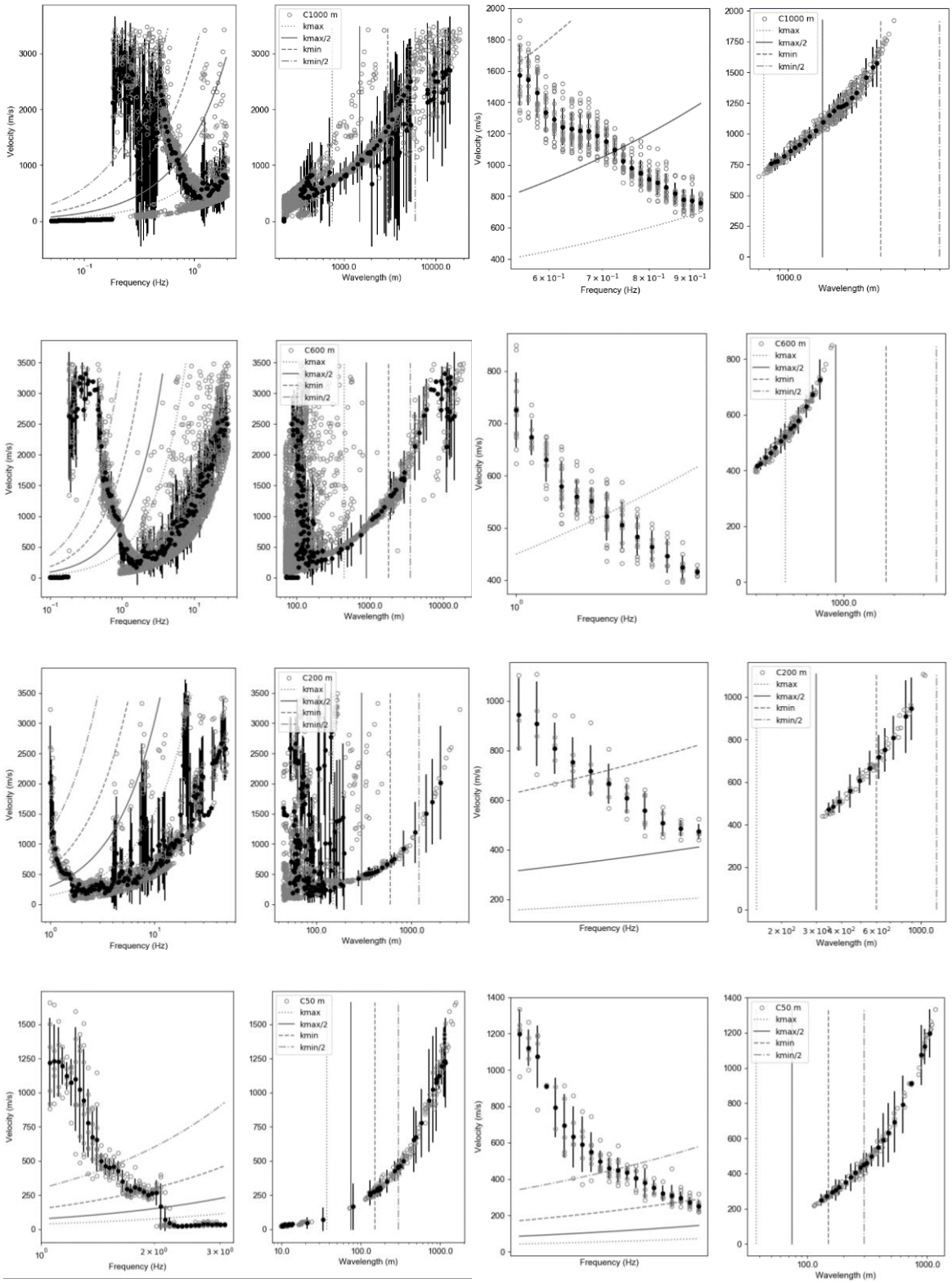

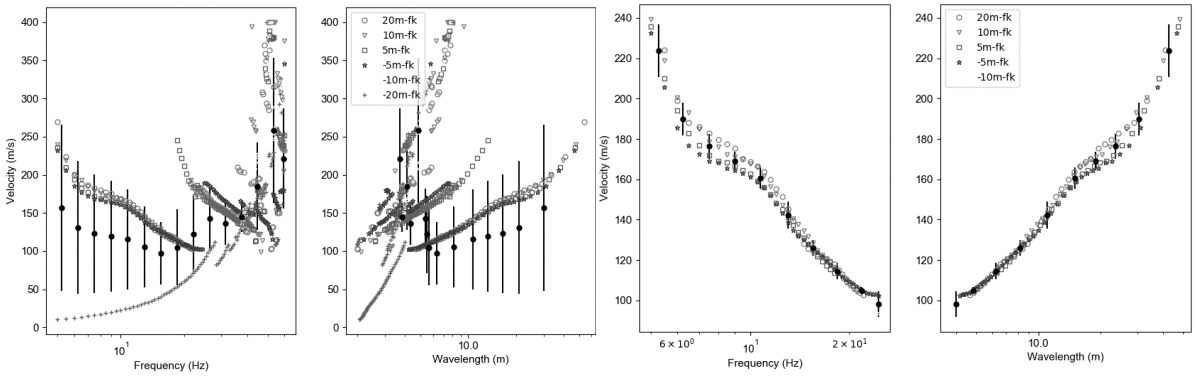

McGregor Road resampled and reduced COV dispersion curve

Frequency (Hz)	Slowness (s/m)	Stddev (s/m)	Weight
0.531644564	0.000631051	3.54E-05	4.418737
0.56317427	0.000675224	6.15E-05	10.62324
0.588729863	0.00069117	7.07E-05	16.39499
0.635902712	0.000791888	6.67E-05	22
0.686855355	0.000833155	7.64E-05	21.6704
0.741890654	0.000931546	9.10E-05	43
0.801335738	0.001044313	0.000106	43.94283
0.865543947	0.001113643	0.000142	37.34089
0.934896933	0.001241808	0.000106	28.73818
1.009806929	0.001425559	0.000108	11.5744
1.178114685	0.001813208	9.07E-05	9.111942
1.374474835	0.002125688	0.000131	5
1.484606659	0.002285258	9.80E-05	5
1.603562959	0.002444827	6.51E-05	5
5.286	0.004482	0.000263	7
6.25	0.0052703	0.000264	8
7.5	0.00567661	0.000284	12
9	0.00591855	0.000296	12
10.75	0.00623315	0.000312	16
13	0.00703764	0.000352	20
15.5	0.00794383	0.000397	20
18.375	0.00874869	0.000437	24
21.75	0.00953359	0.000477	14
24.5	0.01021817	0.000661	2

B.2 Hamilton Boys High School dispersion curve processing

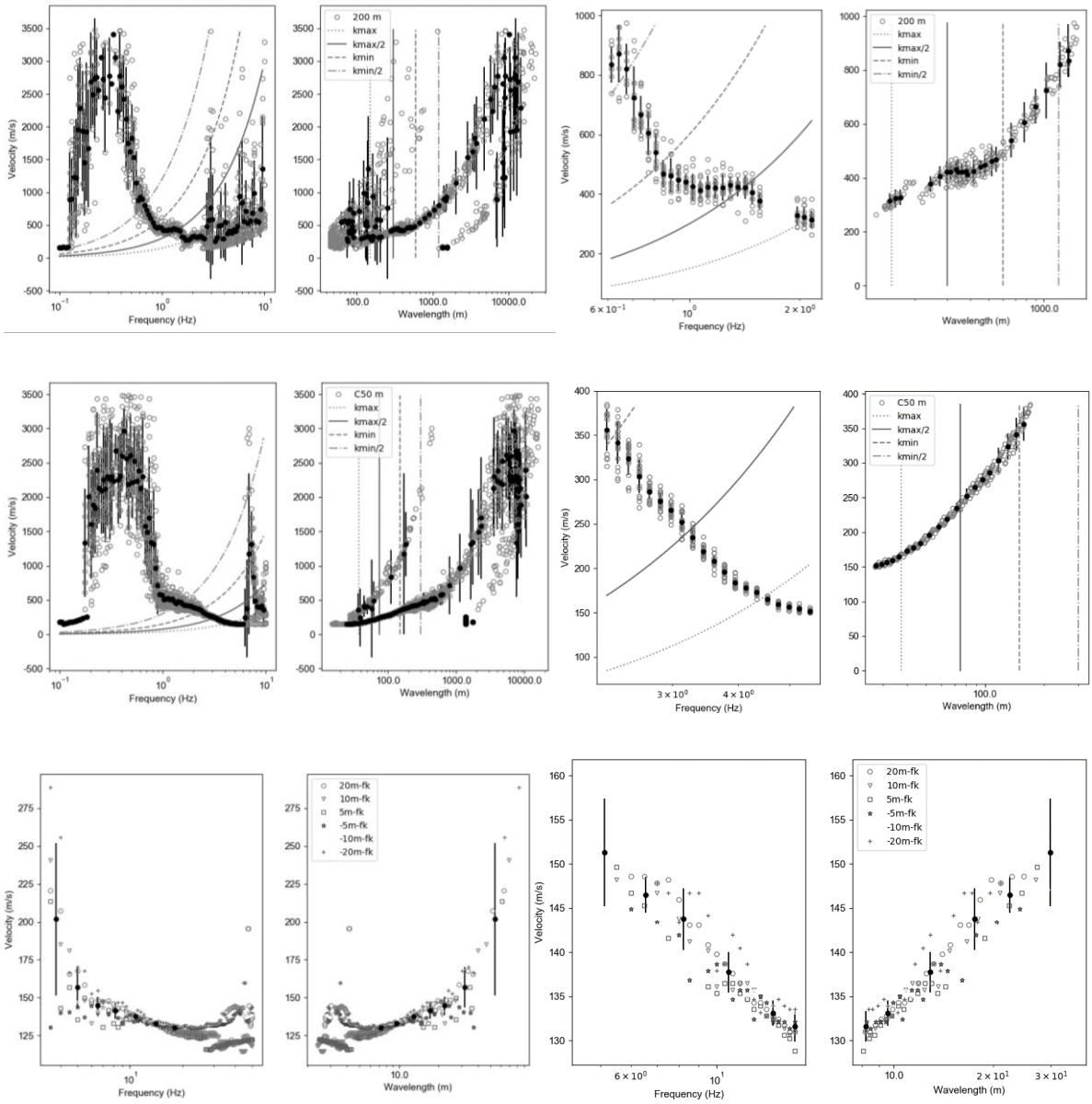

Hamilton Boys High resampled and reduced COV dispersion curve

Frequency (Hz)	Slowness (s/m)	Stddev (s/m)	Weight
0.635902712	0.001170637	0.00013	8.535902
0.686855355	0.00130354	0.000149	8.69941
0.741890654	0.001527225	0.000143	13
0.801335738	0.00182692	0.000225	13
0.865543947	0.002167615	0.000223	12.39524
0.934896933	0.002251401	0.000201	12
1.009806929	0.002343275	0.000196	12.71032
1.0907192	0.002408522	0.000184	12.36654
1.178114685	0.002386569	0.000187	12

1.272512863	0.002349984	0.000185	10.63906
1.374474835	0.002381195	0.000232	11.33814
1.484606659	0.002483875	0.000237	12
1.603562959	0.002717929	0.000217	10.26061
1.732050808	0.002852153	0.000235	10.92351
1.870833935	0.002986377	0.000252	11.58641
2.020737265	0.003100852	0.000288	12
0.686855355	0.001302324	0.000147	8.663413
0.741890654	0.001540202	0.000176	12.51553
0.801335738	0.001829458	0.000224	12.96286
0.865543947	0.002140439	0.000234	12.62796
0.934896933	0.002251629	0.000202	12.03112
1.009806929	0.002336262	0.000172	12.37432
1.0907192	0.002394972	0.000191	12.61063
1.178114685	0.002384687	0.000194	12.11178
1.272512863	0.002365291	0.000204	11.07483
1.374474835	0.002377499	0.000234	11.33785
1.484606659	0.002501067	0.00024	11.59587
1.603562959	0.002712682	0.000219	10.38685
1.732050808	0.002852153	0.000235	10.92351
1.870833935	0.002986377	0.000252	11.58641
2.020737265	0.003098942	0.00029	11.97589
2.750478767	0.003529041	0.000176	19
2.970864938	0.003758566	0.000188	19
3.208909875	0.004140001	0.000207	19
3.466028515	0.004621856	0.000231	19
3.743749165	0.005070097	0.000254	19
4.043722592	0.005538613	0.000277	18.53573
4.367731833	0.005830124	0.000292	19
4.717702792	0.006234791	0.000312	19
5.095715691	0.006434533	0.000322	19
5.504017431	0.006678256	0.000334	6.042084
5.945034951	0.006744638	0.000337	8.24818
6.42138965	0.006811019	0.000341	10.45428
6.935912973	0.006861508	0.000343	12.539
7.491663236	0.006906774	0.000345	14.58384
8.091943809	0.00695204	0.000348	16.62868
8.74032275	0.007030773	0.000352	21.1947
9.440654009	0.007116931	0.000356	26.32012
10.19710034	0.00720309	0.00036	31.44554
11.01415806	0.007285395	0.000364	35.6276
11.89668373	0.007358983	0.000368	37.67522
12.84992307	0.007432572	0.000372	39.72283
13.87954212	0.00750616	0.000375	41.77044
14.99166092	0.007558737	0.000378	23.54948

B.3 Ngahinapouri dispersion curve processing

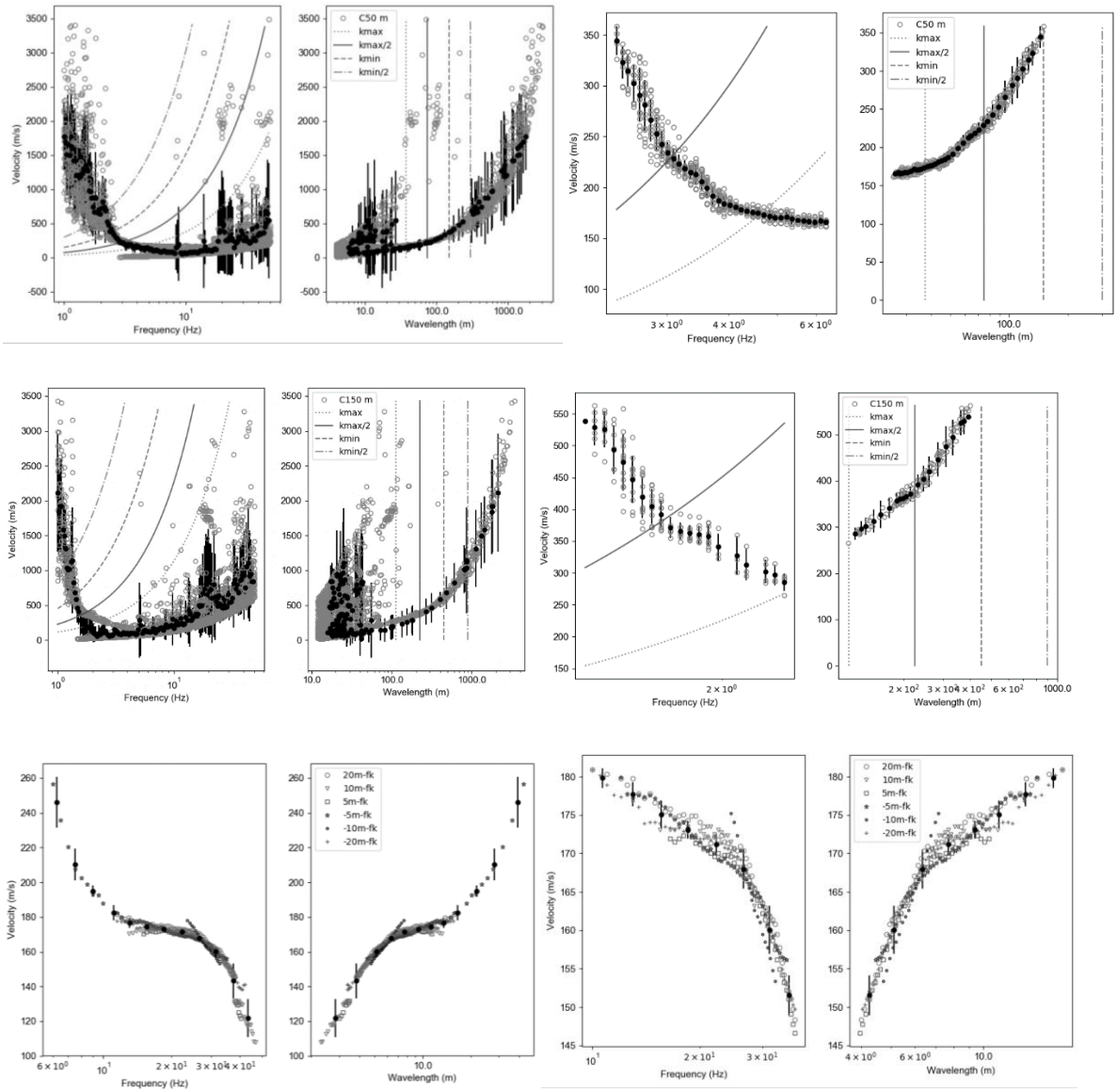

Ngahinapouri resampled and reduced COV dispersion curve

Frequency (Hz)	Slowness (s/m)	Stddev (s/m)	Weight
1.415746946	0.001898262	1.03E-04	6.241622
1.499709216	0.002076323	0.000177	10.05463
1.588650951	0.002344378	0.000189	11.63079
1.682867464	0.002543959	0.000144	10.17464
1.78267158	0.00273727	0.000137	8
1.888394677	0.002783049	1.39E-04	9
2.000387787	0.002967349	0.000196	3.796252
2.119022759	0.003150992	2.58E-04	3
2.244693495	0.00330926	2.10E-04	3.89837
2.668218116	0.003509614	0.000323	15.75882
2.826459425	0.003890021	0.000279	17.42572
2.99408539	0.004243777	0.000213	17

3.171652579	0.004481298	0.000224	15.07553
3.359750566	0.004660191	0.000233	16
3.559003889	0.004920585	0.000246	16.64836
3.66	0.005100042	0.000255	15.38113
3.770074127	0.00529563	0.000265	14
3.993662094	0.00546573	0.000273	16.25983
4.230510166	0.005601555	0.00028	15.06558
4.481404747	0.005690468	0.000285	14
4.747178878	0.005789028	0.000289	14.32353
5.028715006	0.005865111	0.000293	12.48221
5.326947913	0.005895799	0.000295	10.15044
5.642867816	0.005969154	0.000298	10.81352
5.977523661	0.006024791	0.000301	8.899042
11.26566931	0.005580251	0.000279	8.48463
11.93379095	0.005599729	0.00028	11.10617
12.6415362	0.005619207	0.000281	13.7277
13.39125498	0.005642173	0.000282	15.48604
14.18543657	0.00566843	0.000283	16.43039
15.02671788	0.005694686	0.000285	17.37475
15.91789222	0.005719575	0.000286	19.94915
16.86191853	0.005741787	0.000287	25.7175
17.86193125	0.005763998	0.000288	31.48586
18.92125071	0.005785253	0.000289	35.60993
20.04339416	0.005805015	0.00029	37.17068
21.23208743	0.005824777	0.000291	38.73143
22.49127733	0.005847799	0.000292	40.86382
23.82514473	0.005884974	0.000294	45.47814
25.23811845	0.005922149	0.000296	50.09246
26.73488997	0.005969086	0.000298	53.89568
28.32042901	0.006069994	0.000303	53.2146
30	0.006170902	0.000309	52.53353
31.385	0.00624995	0.000312	52
35.65	0.00660091	0.00033	20

B.4 Ohaupo dispersion curve processing

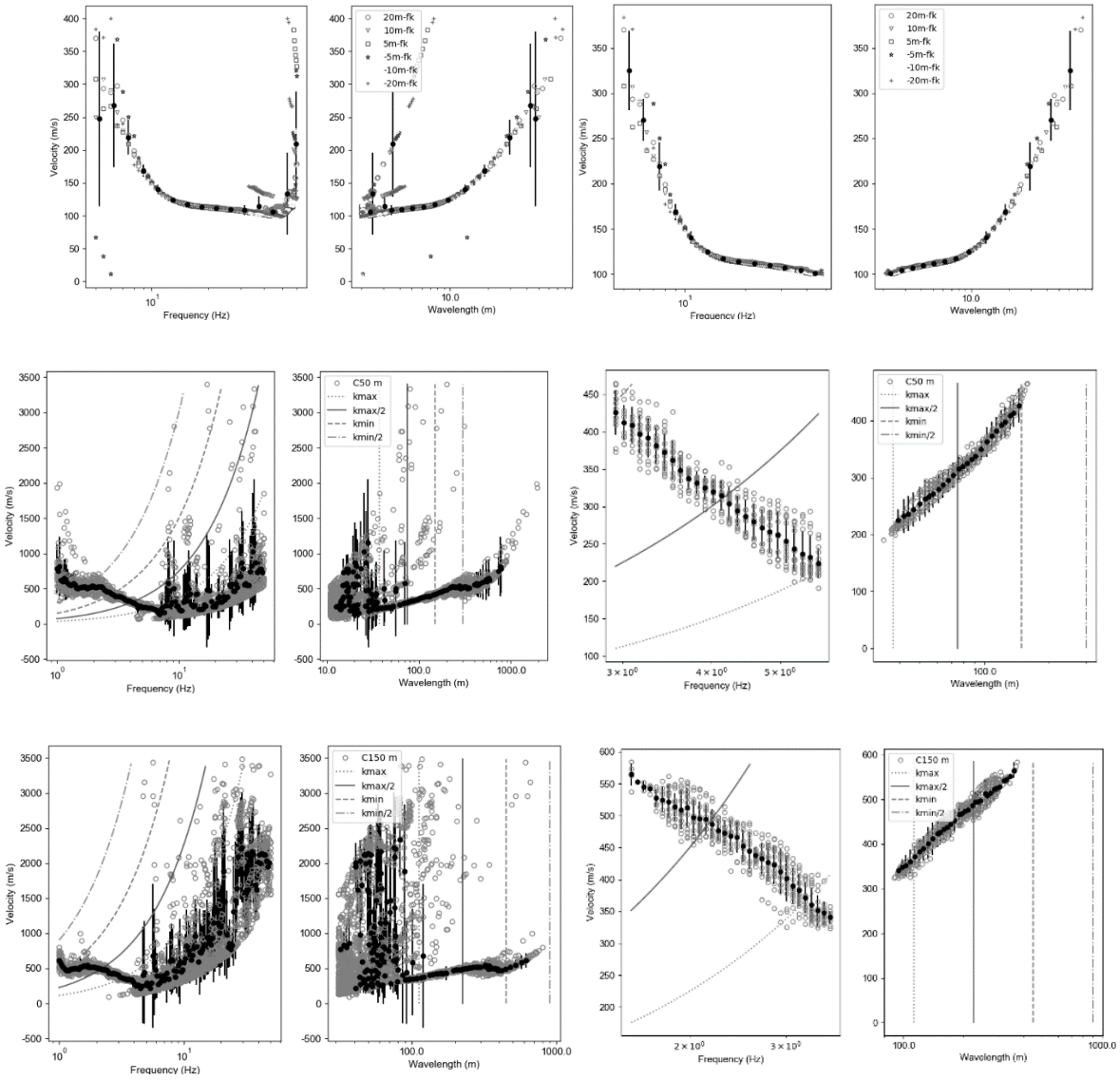

Ohaupo resampled and reduced COV dispersion curve

Frequency (Hz)	Slowness (s/m)	Stddev (s/m)	Weight
1.655936151	0.001835452	9.18E-05	2632297
1.798447691	0.001911344	9.56E-05	9.062648
1.953223918	0.001963887	1.18E-04	15.49888
2.121320344	0.00202496	1.03E-04	14
2.303883318	0.00211281	0.000106	14.78858
2.502157846	0.002212732	0.000124	10
2.71749608	0.002318497	0.000143	16
2.951366541	0.002460206	0.000234	16
3.205364131	0.002651284	0.000177	15
3.481221009	0.002867965	0.00016	14.46977
3.78081841	0.002999676	0.00015	15
4.106199466	0.003173585	0.000197	15

4.459583144	0.003498542	0.000274	14.05649
4.84337938	0.003797178	0.000421	13.82548
5.260205507	0.004188528	0.000506	14
8.632330323	0.005645057	0.000361	18
9.3752374	0.006221762	0.00032	19.37935
10.18207981	0.006773715	0.000342	22.16717
11.0583599	0.007271422	0.000364	24.89288
12.01005353	0.007665022	0.000383	27.49936
13.04365089	0.008051865	0.000403	30
14.16620067	0.008279058	0.000414	30
15.38535823	0.00850625	0.000425	30
16.70943772	0.008637416	0.000432	35.0958
18.14746883	0.008759094	0.000438	40.69511
19.70925835	0.008848476	0.000442	44.05832
21.40545705	0.008928045	0.000446	46.74208
23.24763233	0.009007203	0.00045	49.50551
25.24834708	0.009086	0.000454	52.33925
27.42124536	0.009172595	0.000459	55.81107
29.78114547	0.009270231	0.000464	60.18633
32.34414097	0.009374475	0.000469	61.50287
35.12771045	0.009490626	0.000475	57.30821
38.15083673	0.009616839	0.000481	54.31334
41.43413633	0.009780608	0.000489	55.79603

B.5 Tamahere dispersion curve processing

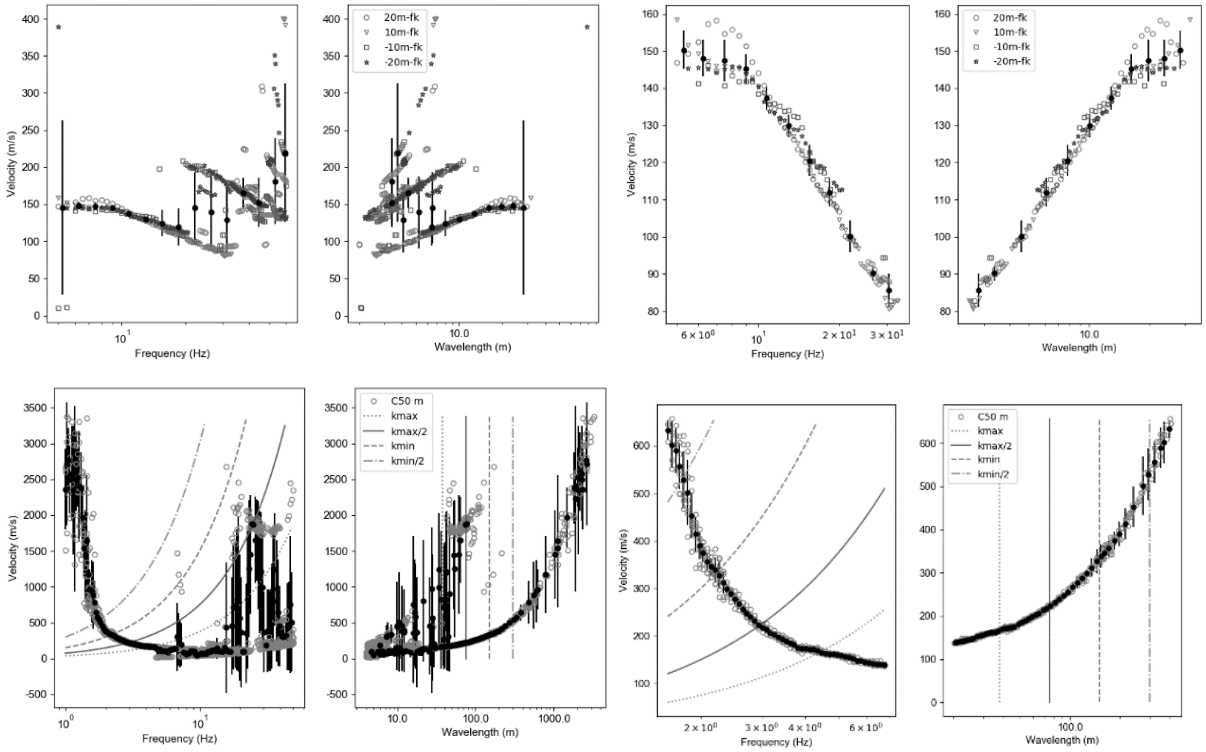

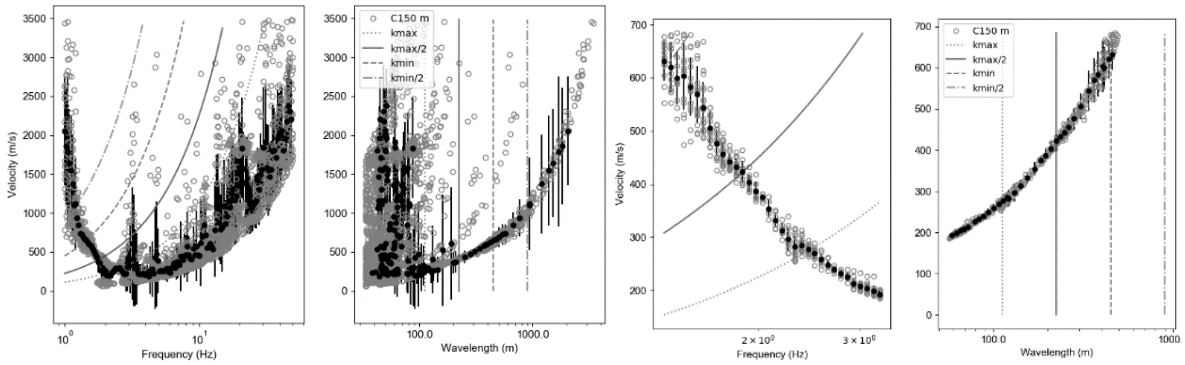

Tamahere resampled and reduced COV dispersion

Frequency (Hz)	Slowness (s/m)	Stddev (s/m)	Weight
1.499709216	0.001697606	1.76E-04	15.87275
1.588650951	0.001821773	0.000158	18.63079
1.682867464	0.002082217	0.000116	19
1.78267158	0.002263173	0.000113	15
1.888394677	0.002392827	0.00012	9.785901
2.377817258	0.003353393	0.000168	8
3.770074127	0.005625471	0.000281	8
4.230510166	0.005826431	0.000291	8
4.747178878	0.006183604	0.000309	6.676468
5.642867816	0.006713216	0.000319	11.1406
5.977523661	0.006731995	0.000337	7.188928
6.332026601	0.006761166	0.000338	8.286063
7.52674168	0.006791055	0.00034	12
8.445976424	0.006856606	0.000343	12
9.477476547	0.007006476	0.00035	13.16374
10.03954765	0.007133227	0.000357	14.46076
11.26566931	0.007387029	0.000369	16.98618
12.6415362	0.007641266	0.000382	19.41147
13.39125498	0.007804175	0.00039	19.83301
14.18543657	0.008000832	0.0004	19.50854
17.86193125	0.008828264	0.000441	23.10392
18.92125071	0.009105912	0.000455	22.6086
20.04339416	0.009456314	0.000473	19.64081
21.23208743	0.009806717	0.00049	16.67303
22.49127733	0.010143029	0.000507	15.12734
23.82514473	0.010461134	0.000523	15.41923
25.23811845	0.010779238	0.000539	15.71112
28.32042901	0.011367567	0.000575	16
30	0.011638281	0.000596	16
30.469	0.01171117	0.000601	16

B.6 Kiroa Road dispersion curve processing

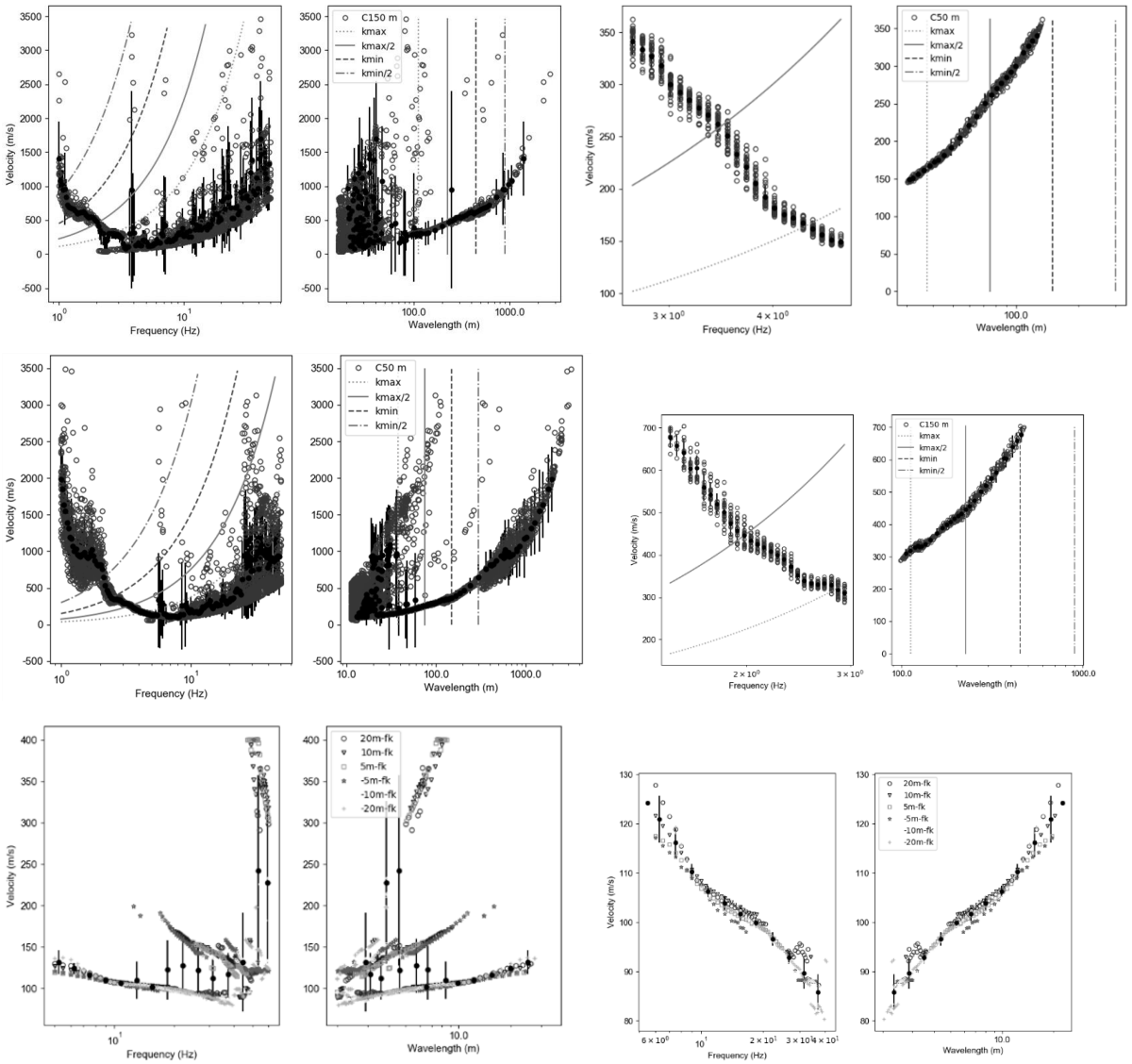

Kiroa Road resampled and reduced COV dispersion curve

Frequency (Hz)	Slowness (s/m)	Stddev (s/m)	Weight
1.484607	0.00148	7.40E-05	5.897119
1.603563	0.001659	8.30E-05	10.98723
1.732051	0.001843	9.72E-05	19.92208
1.870834	0.002102	0.000125	22.14173
2.020737	0.002296	0.000116	20.20626
2.182652	0.002437	0.000122	19.08264
2.35754	0.002651	0.000133	18.33515
2.750479	0.003024	0.000151	22.46379
3.466029	0.003452	0.000173	6
3.743749	0.003938	0.000197	6
4.043723	0.004634	0.000232	5
4.367732	0.005257	0.000263	5.150609
4.717703	0.005964	0.000298	5.913549
6.42139	0.008322	0.000416	9.994243

6.935913	0.008462	0.000423	13.38769
7.491663	0.008601	0.00043	16.78113
8.091944	0.008798	0.00044	17.40404
8.740323	0.008999	0.00045	17.83595
9.440654	0.009166	0.000458	19.61415
10.1971	0.009311	0.000466	22.21695
11.01416	0.009438	0.000472	24.51095
11.89668	0.009524	0.000476	26.13328
12.84992	0.00961	0.00048	27.7556
13.87954	0.009702	0.000485	28.7444
14.99166	0.009795	0.00049	29.62083
16.19289	0.009878	0.000494	30
17.49037	0.009952	0.000498	30
18.89181	0.010048	0.000502	29.4001
20.40554	0.010194	0.00051	27.28651
22.04057	0.010341	0.000517	25.17292
23.8066	0.010516	0.000526	25.38825
25.71414	0.010693	0.000535	25.8111
27.77453	0.010872	0.000544	28.77637
30	0.011052	0.000553	33.79457
31.514	0.011167	0.000558	37
36.911	0.011664	0.000583	28

B.7 Saint Peters dispersion curve processing

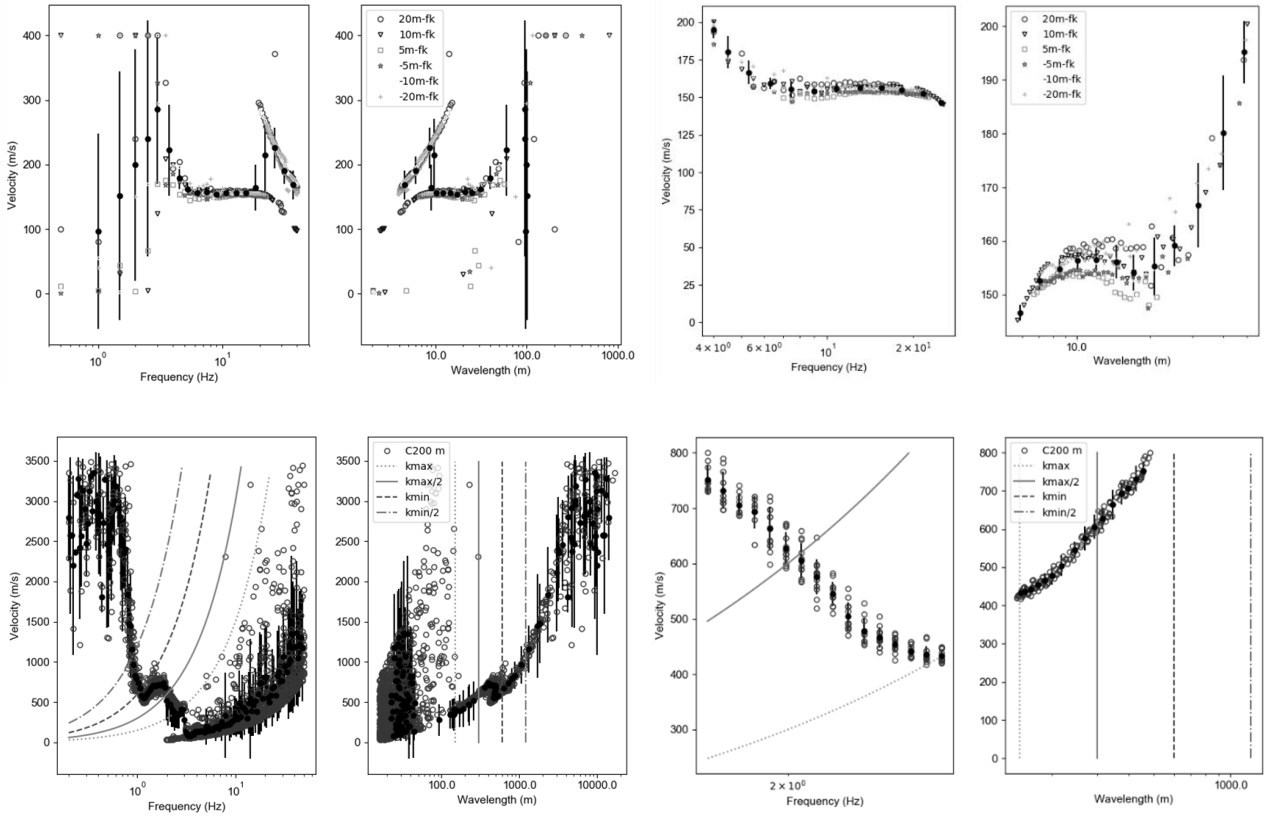

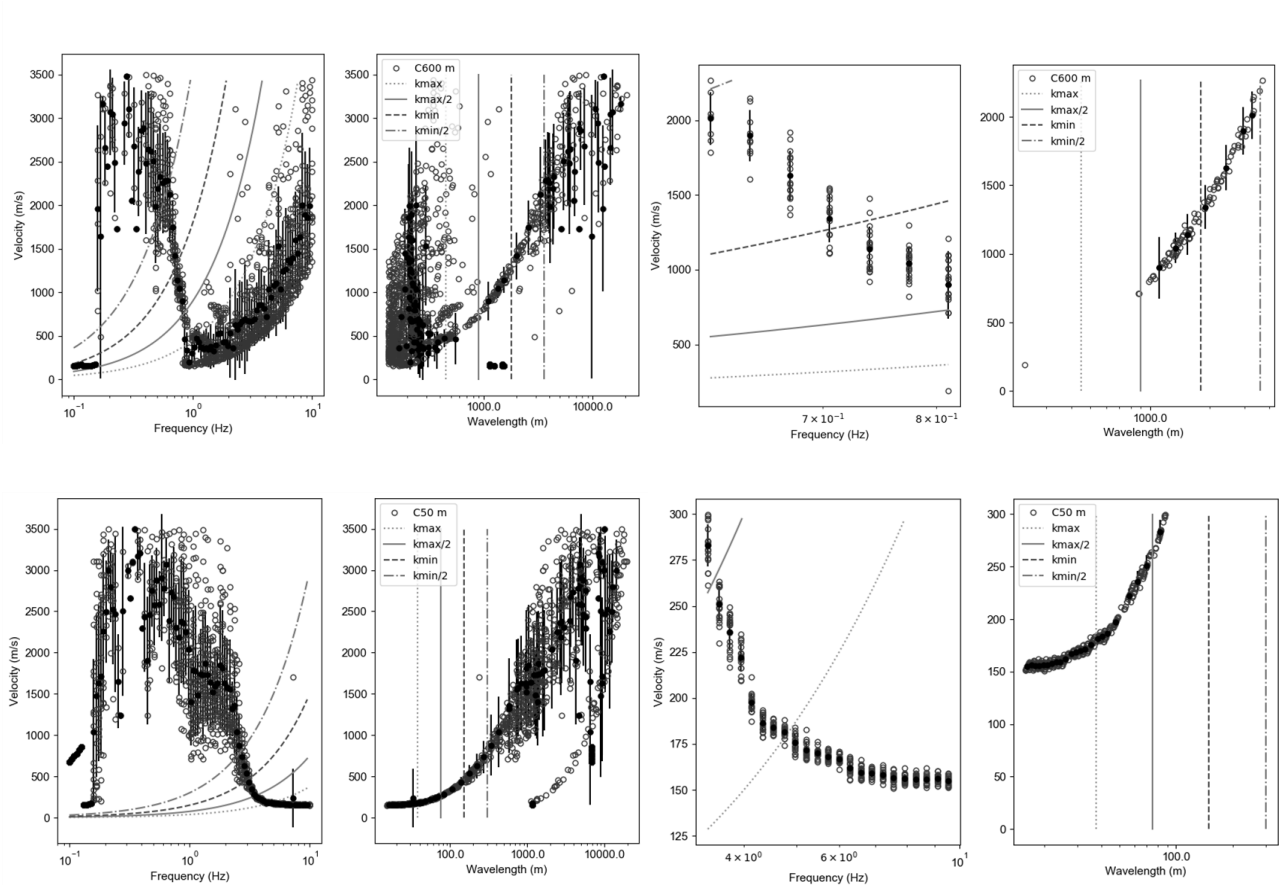

Saint Peters resampled and reduced COV dispersion curve

Frequency (Hz)	Slowness (s/m)	Stddev (s/m)	Weight
1.732051	0.001381	6.91E-05	10.49065
1.870834	0.001467	7.80E-05	9.013342
2.020737	0.00162	8.18E-05	12.58489
2.182652	0.001788	9.31E-05	12.50524
2.35754	0.00205	0.000103	11.42505
2.546441	0.002184	0.000109	12
2.020737	0.00162	8.18E-05	12.58489
2.182652	0.001788	9.31E-05	12.50524
2.35754	0.00205	0.000103	11.42505
2.546441	0.002184	0.000109	12
4.043723	0.004811	0.000241	17.53573
4.367732	0.005396	0.000269	21.63828
4.717703	0.005543	0.000287	23.28948
5.095716	0.005799	0.000293	25.9977
5.504017	0.005947	0.000302	27
5.945035	0.006049	0.000312	26.17925
6.42139	0.006247	0.000309	27.81669
6.935913	0.006329	0.000314	31.34568
7.491663	0.006411	0.000318	34.8242
8.091944	0.006434	0.000318	35.85923
8.740323	0.00645	0.00032	36.68597
9.440654	0.006454	0.000319	38.61415
10.1971	0.006431	0.000322	22.21695

11.01416	0.006404	0.00032	24.76643
11.89668	0.006397	0.00032	27.19992
12.84992	0.006389	0.000319	29.6334
13.87954	0.006392	0.00032	30
14.99166	0.006396	0.00032	30
16.19289	0.006414	0.000321	30.53842
17.49037	0.006443	0.000322	31.48737
18.89181	0.006478	0.000324	29.75387
20.40554	0.00652	0.000326	24.86885
22.04057	0.006583	0.000329	18.96794
23.8066	0.006729	0.000336	9.199153

B.8 Elliot Park dispersion curve processing

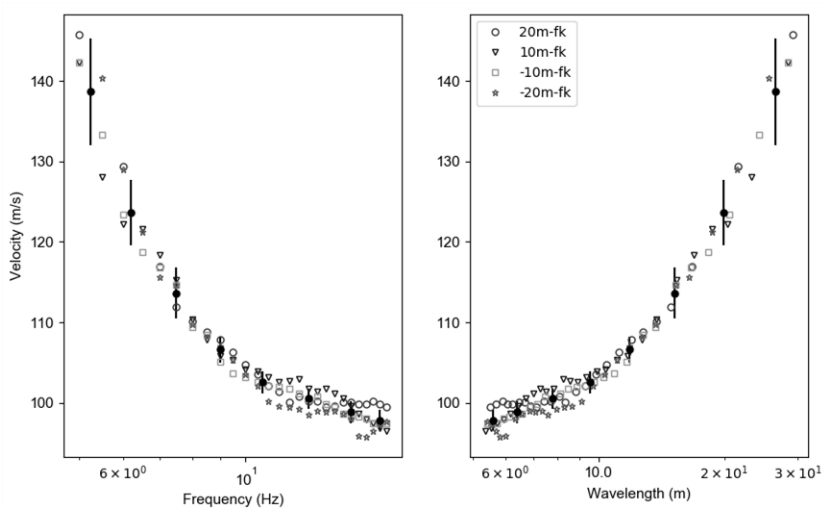

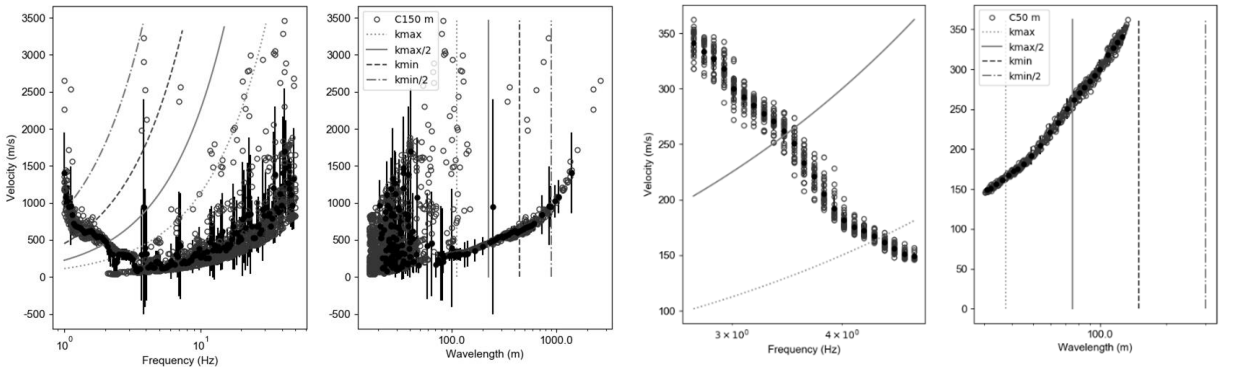

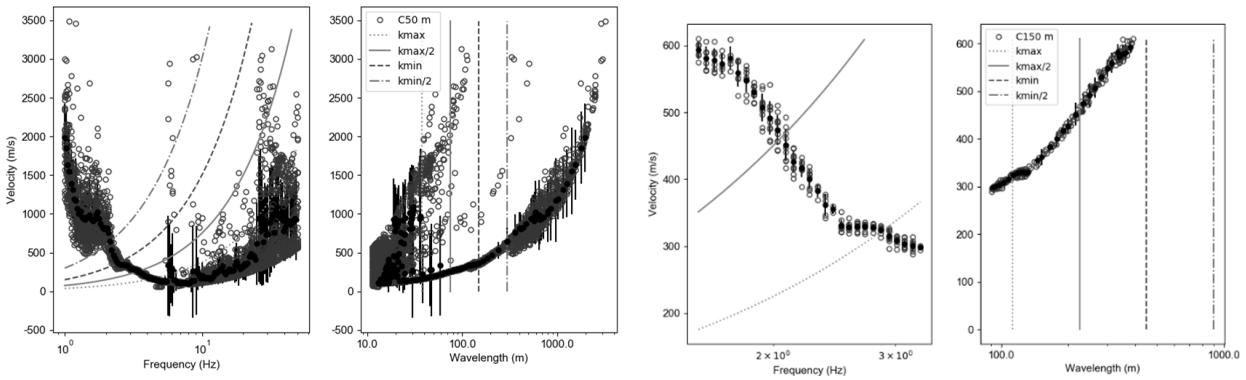

Elliot Park resampled and reduced COV dispersion curve

Frequency (Hz)	Slowness (s/m)	Stddev (s/m)	Weight
1.5626	0.001686	8.43E-05	6
1.615448	0.001724	8.62E-05	6.536672
1.673941	0.00174	8.70E-05	6.131744
1.78047	0.001787	8.94E-05	5.971574
1.888005	0.001904	9.52E-05	10.20625
1.987252	0.002049	0.000103	11
2.036745	0.002124	0.000107	10.90564
2.079709	0.002208	0.000117	10.11129
2.712	0.002935	0.000147	24
2.724673	0.002946	0.000147	23.72891
3.399667	0.003774	0.000189	26
3.408169	0.003784	0.000189	26
3.82117	0.004908	0.000259	26
3.87944	0.005101	0.000271	26
3.941371	0.005293	0.000278	26
4.009155	0.005483	0.000276	26
4.556103	0.006365	0.000318	25.24084
5.576346	0.007524	0.000376	6.346315
5.9443	0.007864	0.000393	6.736784
5.990287	0.007894	0.000395	6.881304
6.434955	0.008188	0.000409	8.278732
7.425767	0.008736	0.000437	10.80427
7.976993	0.008999	0.00045	11.98274
7.985068	0.009003	0.00045	12
9.463116	0.009485	0.000474	13.1296
11.49453	0.009822	0.000491	17.40948
14.17203	0.010032	0.000502	20
17.5	0.01022	0.000511	12

B.9 Gordonton dispersion curve processing

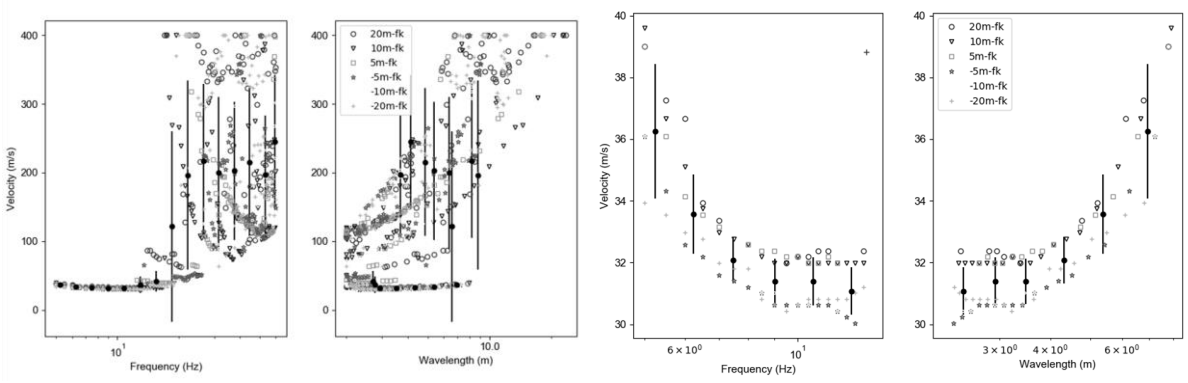

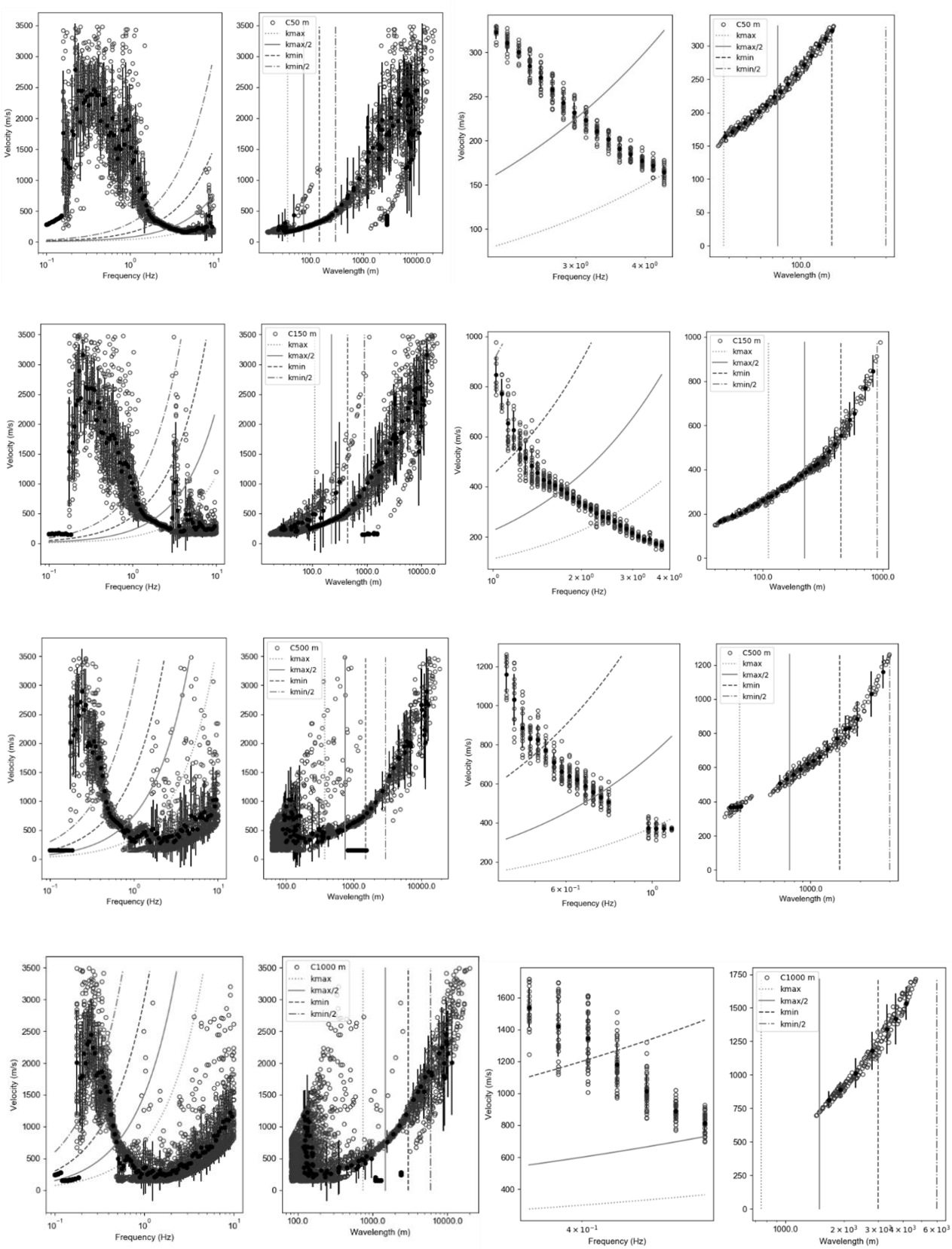

Gordonton resampled and reduced COV dispersion curve

Frequency (Hz)	Slowness (s/m)	Stddev (s/m)	Weight
0.432531	0.000925	0.000102	35.48262
0.467189	0.001144	7.64E-05	34.72404

0.504623	0.001261	0.000195	23
0.545056	0.001416	0.00018	46
0.58873	0.001506	0.000134	46
0.635903	0.001606	0.000105	46
0.686855	0.001742	0.000147	46
0.741891	0.001901	0.000147	20.919
0.801336	0.002047	0.00016	20
1.009807	0.002478	0.000248	59.50499
1.090719	0.002514	0.000247	66.48504
1.178115	0.002554	0.000259	77.66131
1.272513	0.00255	0.000243	75.25561
1.374475	0.002501	0.000197	76.51713
2.182652	0.003259	0.000226	22.28003
2.35754	0.003452	0.00022	34.44348
2.546441	0.003698	0.000199	40.18751
2.750479	0.004059	0.000232	41.49858
2.970865	0.004455	0.000271	38.18392
3.20891	0.004815	0.000334	28.69478
3.466029	0.00519	0.000352	32.77844
3.743749	0.005714	0.000418	37.27324
4.043723	0.005745	0.000287	17.92855

B.10 Temple View dispersion curve processing

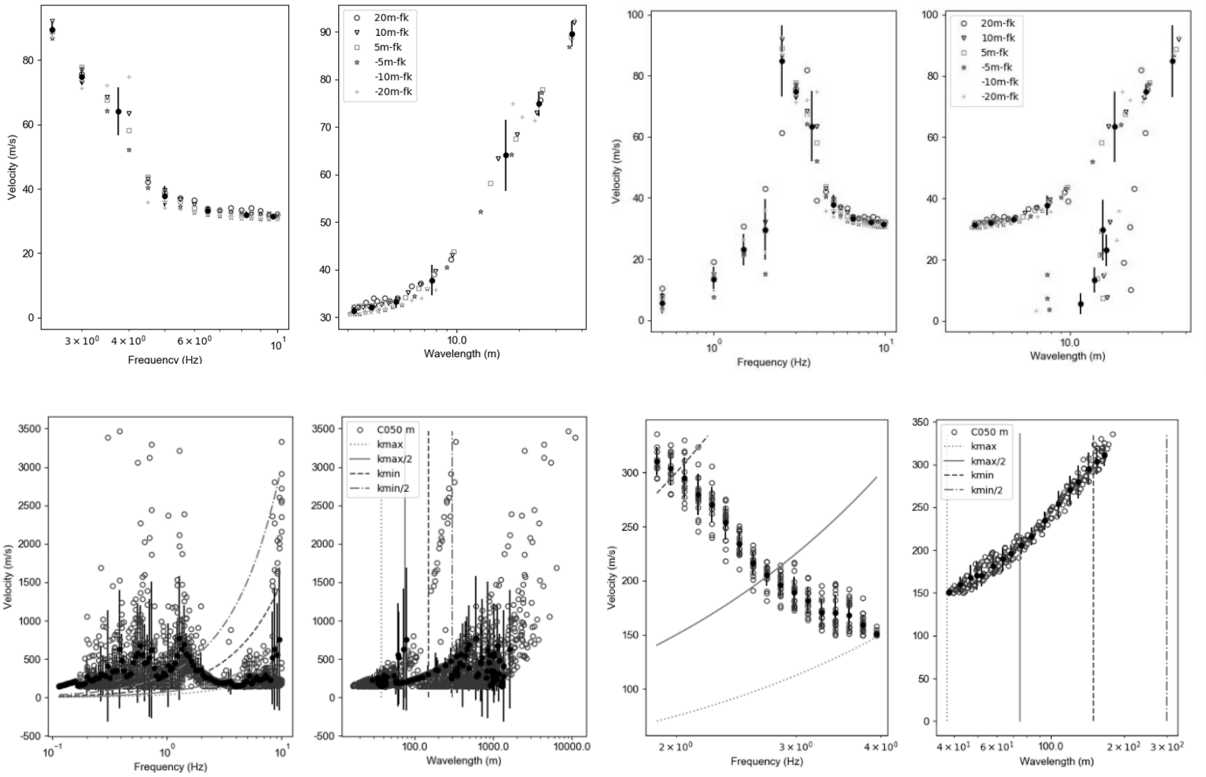

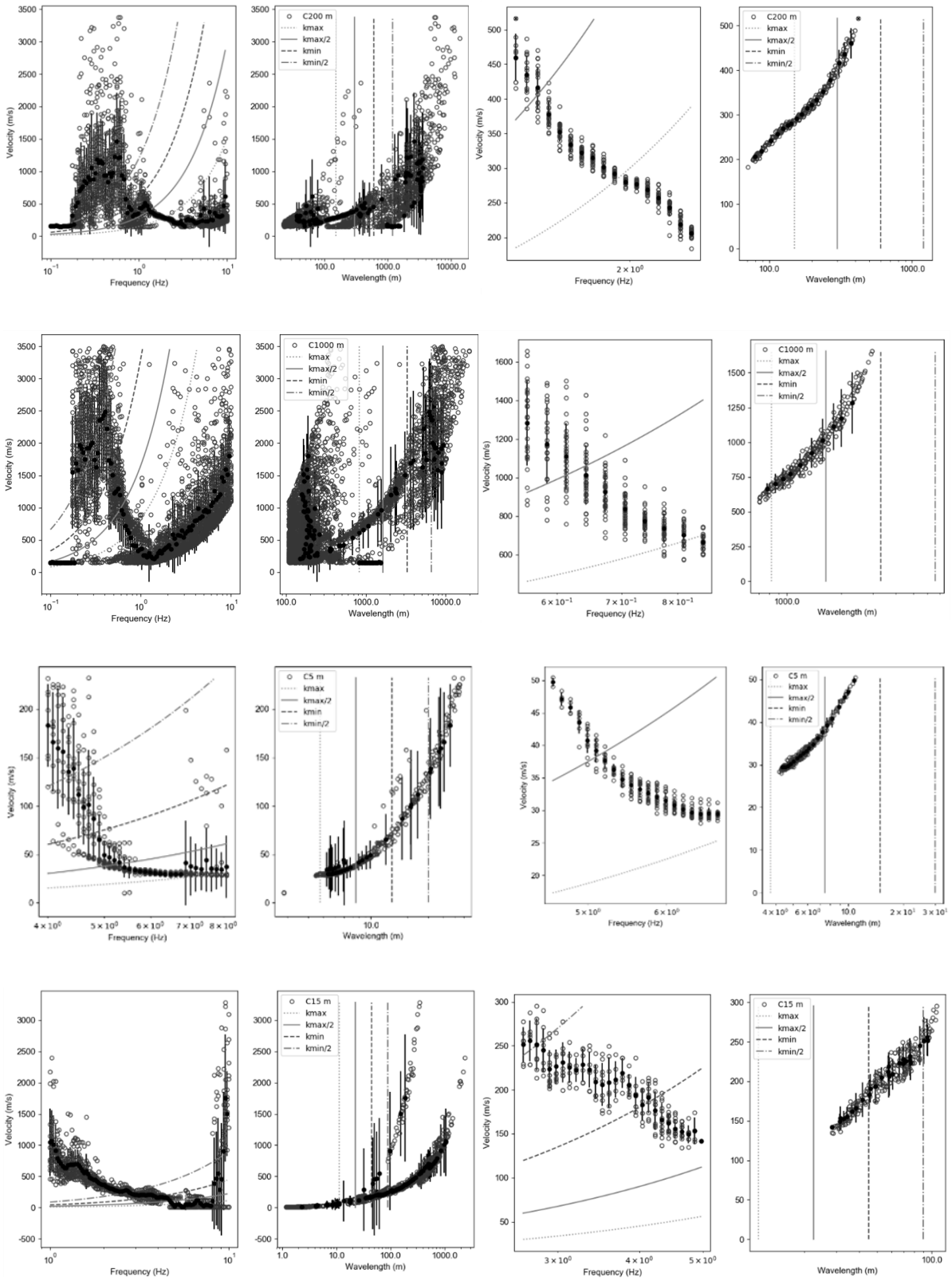

Temple View resampled and reduced COV dispersion curve

Frequency (Hz)	Slowness (s/m)	Stddev (s/m)	Weight
0.4863	0.000622	8.82E-05	20
0.5094	0.000737	0.000103	28
0.6428	0.001007	1.45E-04	35
0.6734	0.001095	1.30E-04	35

0.7055	0.00121	0.00012	34
0.7391	0.001315	0.000122	35
0.7743	0.001371	0.000141	30
0.8111	0.001469	0.000212	22
0.8498	0.00151	9.53E-05	22
1.1768	0.001953	0.00019	17
1.2328	0.002059	0.000311	19
1.2915	0.002311	0.000197	18
1.3531	0.002436	0.000197	21
1.4175	0.002651	0.000124	23
1.485	0.002857	0.000131	23
1.5557	0.002997	9.93E-05	23
1.6298	0.003106	9.47E-05	24
1.7073	0.00318	0.000102	24
1.7886	0.003319	9.16E-05	24
1.8738	0.003428	6.66E-05	24
1.963	0.003571	5.53E-05	24
2.0565	0.003609	5.34E-05	24
2.1544	0.003719	0.000102	24
2.257	0.003892	0.000143	24
2.3645	0.004131	0.000235	23
2.584701	0.004609	0.000243	18
2.595	0.00463	0.000243	18
2.712697	0.004865	0.000246	18
2.848393	0.005118	0.000284	18.99406
2.997133	0.005362	0.000349	16.80547
3.154634	0.005599	0.000384	14.80188
3.2745	0.005895	0.000428	14
4.772453	0.021649	0.001082	4.732373
4.849186	0.022431	0.001122	6.57793
4.862504	0.022605	0.001131	6.985348
4.910328	0.023231	0.001163	8.448319
4.961626	0.02404	0.001209	9.999448
5.023131	0.02484	0.00125	11
5.103153	0.025627	0.001281	11
5.183473	0.026414	0.001321	11
5.263351	0.027203	0.00136	11
5.339885	0.027996	0.0014	11.32023
5.41289	0.028793	0.00144	11.99531
5.521614	0.029556	0.001478	12.98481
5.669484	0.03027	0.001514	14.29917
5.818221	0.030989	0.001549	15.58738
5.925398	0.031522	0.001576	15.8897
5.964502	0.031717	0.001586	16
6.096673	0.032467	0.001623	16
6.243583	0.033203	0.00166	16
6.435403	0.033874	0.001694	15.39803
6.7533	0.033971	0.001699	13

B.11 Ngaroto dispersion curve processing

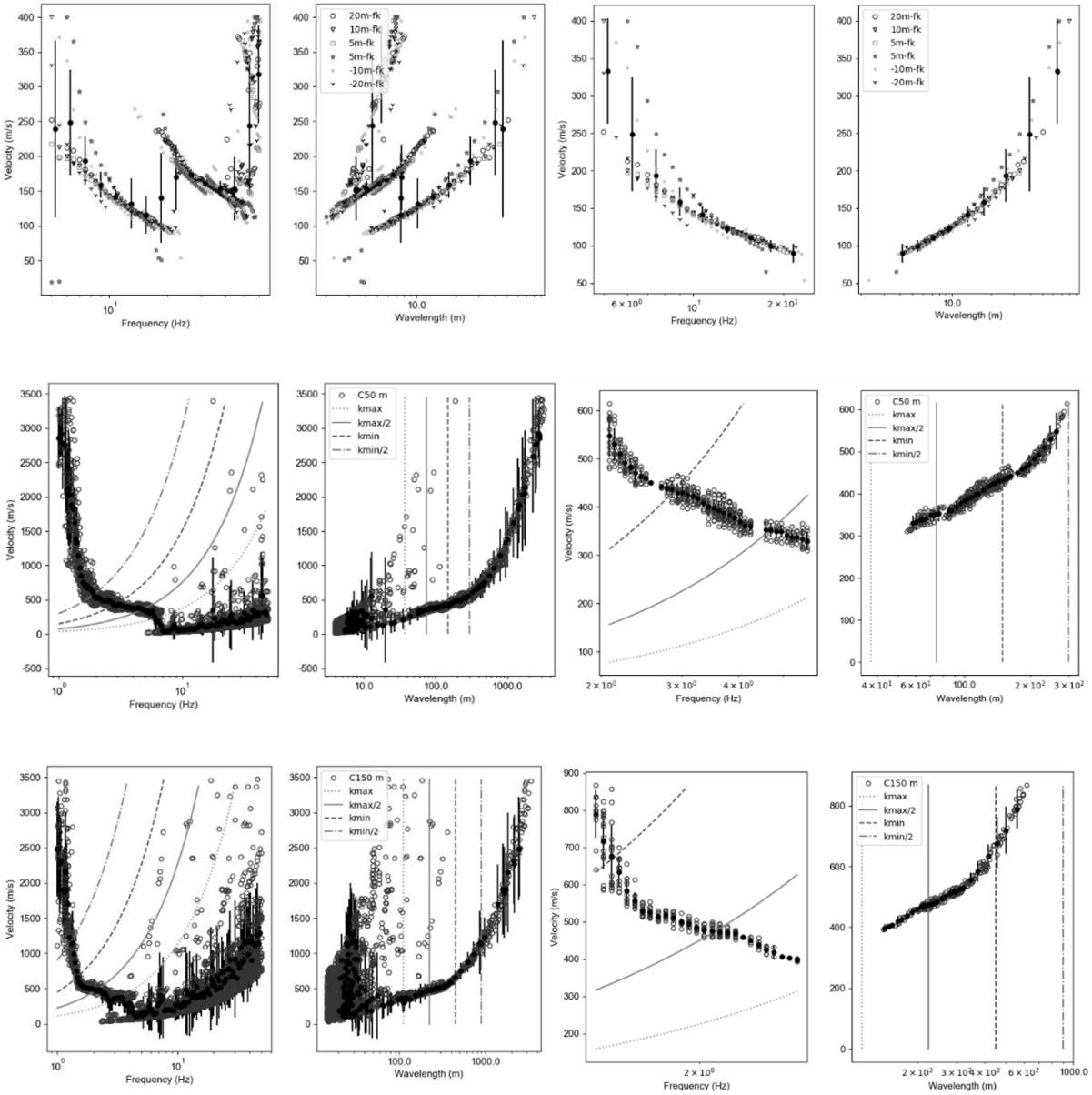

Ngaroto resampled and reduced COV dispersion curve

Frequency (Hz)	Slowness (s/m)	Stddev (s/m)	Weight
1.415747	0.001307	0.000128	13.20811
1.499709	0.001537	0.000143	14.26029
1.588651	0.001769	9.02E-05	23.47684
1.682867	0.001901	9.29E-05	22.69858
1.782672	0.00193	9.33E-05	16.07451
1.888395	0.002007	9.74E-05	18.4282
2.000388	0.002077	0.000101	21.6315
2.119023	0.002112	0.000104	30.40703
2.244693	0.002137	0.000104	22.81243
2.994085	0.00233	0.000116	11
3.171653	0.00237	0.000119	13.03776
3.359751	0.002457	0.000123	13.94416

3.559004	0.002528	0.000126	18.64836
3.770074	0.002598	0.000134	18.54597
3.993662	0.002698	0.000135	16.51966
4.23051	0.002782	0.000139	8.32762
4.481405	0.002824	0.000146	5.160877
5.977524	0.004036	0.000965	10.59451
6.332027	0.004384	0.001022	12.4291
6.707554	0.004697	0.000943	14.32511
7.105352	0.00501	0.000864	16.22112
7.526742	0.005324	0.000789	18
7.973123	0.005664	0.000762	18
8.445976	0.006003	0.000736	18
8.946873	0.006342	0.00071	18
9.477477	0.006589	0.000649	19.7456
10.03955	0.006826	0.000583	21.69113
10.63495	0.007063	0.000518	23.63666
11.26567	0.007377	0.000482	25.00826
11.93379	0.00771	0.000452	26.24806
12.64154	0.008043	0.000421	27.48787
13.39125	0.00834	0.000417	28.18555
14.18544	0.00861	0.000431	28.50168
15.02672	0.008881	0.000444	28.81782
15.91789	0.009213	0.000554	28.53633
16.86192	0.009628	0.000794	27.44205
17.86193	0.010043	0.001034	26.34777
18.92125	0.010465	0.001405	22.59957
20.04339	0.010891	0.001837	17.61499
21.23209	0.011317	0.002269	12.63041

B.12 Wallace small dispersion curve processing

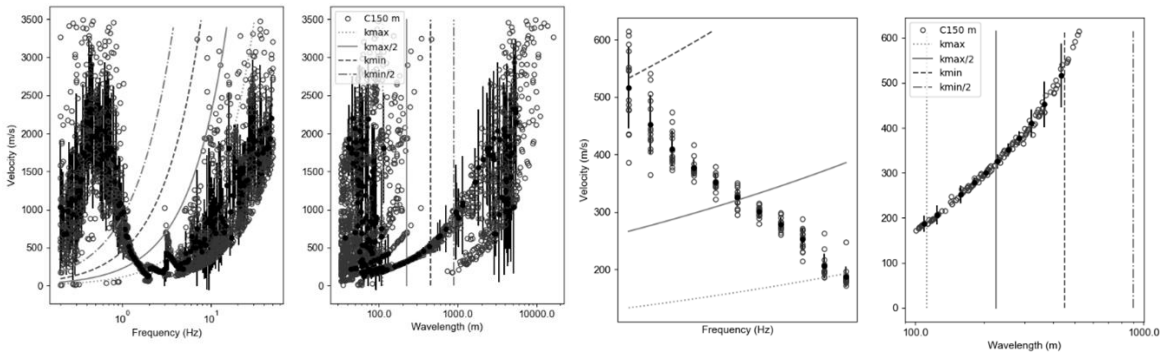

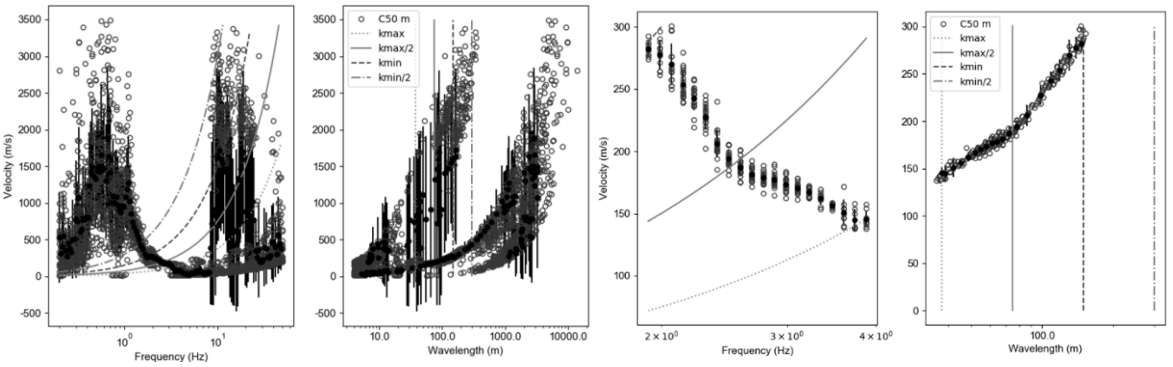

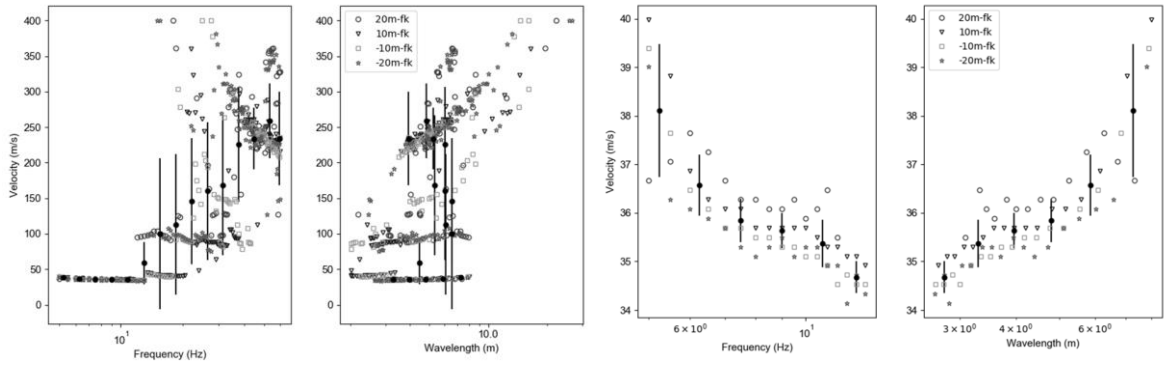

B.13 Wallace Large – Not Obtainable